Flow Characteristics in Multi-Layered Vegetated Channels

A Thesis Submitted

In partial fulfilment of the requirement for the degree of

Doctor of Philosophy

Submitted By

Jyotirmoy Barman

(196104010)

DEPARTMENT OF CIVIL ENGINEERING

INDIAN INSTITUTE OF TECHNOLOGY GUWAHATI

GUWAHATI – 781039, INDIA

March 2024

DECLARATION

I, Jyotirmoy Barman, declare that this thesis titled, "Flow Characteristics in Multi-Layered Vegetated Channels" is part of my research for the degree of Doctor of Philosophy. All the work presented in this thesis are my own and the results generated are of the original research.

I confirm that

- The work contained in this thesis is original and was done wholly or mainly while in candidature for the research degree at this institute under the guidance of my supervisor.
- The work reported herein has not been submitted to any other Institute for any degree or diploma.
- Wherever I reported material from other sources, I have duly cited and acknowledged their respective authors and sources.
- I also affirm that no part of the thesis is plagiarized to the best of my knowledge.
- I take complete responsibility for the results and inferences reported in the thesis.

Date: Jyotirmoy Barman

Department of Civil Engineering

Indian Institute of Technology Guwahati

Guwahati – 781039, Assam, India

Dr. Bimlesh Kumar

Professor

bimk@iitg.ac.in

0361-258 2420

CERTIFICATE

This is to certify that the thesis entitled "Flow Characteristics in Multi-Layered Vegetated Channels" submitted by Jyotirmoy Barman, in partial fulfilment of the requirements for the award of the degree of Doctor of Philosophy, to the Indian Institute of Technology Guwahati, is a record of bonafide research work under my supervision. I certify that this thesis is worthy of consideration for the award of the degree of Doctor of Philosophy of the Institute. To the best of my knowledge, no part of the work reported in this thesis has been presented for the award of any degree at any other institution.

Date:

Place: IIT Guwahati

(Dr. Bimlesh Kumar)

PUBLICATIONS

JOURNALS

1. Barman, J., Kumar, B., & Balachandar, R. (2024). Hydrodynamics in Channels with Partial Vegetation Cover: Investigating the Effects of Homogeneous and Heterogeneous Vertical Vegetation Distribution. ***Advances in Water Resources***, 104642. https://doi.org/10.1016/j.advwatres.2024.104642
2. Barman, J., Roy, M. & Kumar, B. (2023). Velocity estimation in compound channels with different bank slopes using Renyi and Tsallis entropy. ***Stochastic Environmental Research and Risk Assessment.*** https://doi.org/10.1007/s00477-023-02423-2
3. Barman, J., & Kumar, B. (2023). Flow in multi-layered vegetated compound channels with different bank slopes. ***Physics of* Fluids**, 35(3), 036601 https://doi.org/10.1063/5.0142400
4. Barman, J., & Kumar, B. (2022). Turbulence in a compound channel with the combination of submerged and emergent vegetation. ***Physics of Fluids***, *34*(4), 045114. https://doi.org/10.1063/5.0086739
5. Barman, J., & Kumar, B. (2022). Flow behavior in a multi-layered vegetated floodplain region of a compound channel. ***Ecohydrology***, *15(4), e2427.* https://doi.org/10.1002/eco.2427

CONFERENCES

1. Barman, J., & Kumar, B. (2023). Experimental analysis of multi-layered vegetated compound channel at different bank slopes. ***M.S. Yalin Memorial Colloquium 2023: Flow-sediment-biota Interactions in Fluvial system: recent research trends***, January 26-27, 2023, Palermo (Italy)
2. Barman, J., & Kumar, B. (2022). Higher Order Correlations in Muti-layered Partially Vegetated Channel. In ***AGU Fall Meeting*** 2022, 12-16 December, 2022 (online poster presentation)
3. Barman, J., Taye, J., & Kumar, B. (2021, April). Turbulence Scale in Compound Channel. In ***EGU General Assembly Conference*** *Abstracts* (pp. EGU21-10900) (online presentation).

ACKNOWLEDGEMENTS

The journey of completing my Doctoral Dissertation has been a bitter sweet experience, with lots of highs and lows. It would have been impossible without the support and guidance of several people. They gave me the motivation I needed to keep going, and without their support, I would not have succeeded.

First of all, I am highly indebted to my supervisor Prof. Bimlesh Kumar for his guidance and supervision in completing my research work. During my PhD, he gave me the freedom to work and engaged me in new ideas. His unconditional support and motivation gave me strength and lifted my spirit whenever I got stuck. And thus, I am looking forward to work with him in the future.

I would also like to thank members of my doctoral committee; Prof. Ajay Kalamdhad (chairman), Dr. Arindam Dey, Dr. Raghvendra Gupta, Dr. Rishikesh Bharti and Prof. Sisir Kumar Nayak for their insightful comments, encouragement, and valuable time throughout the research. I would like to acknowledge Department of Civil Engineering at IIT Guwahati, for providing me the required resources and a fruitful work environment.

I would like to extend my genuine gratitude to Dr. Jyotismita Taye, Dr. Abhijit Lade, Dr. Bandita Barman and Dr. Anurag Sharma for their valuable inputs on various complex topics. I will always cherish my MTech and PhD days spent in the laboratory with Dr. Jyotismita Taye and Dr. Abhijit Lade. I would also like to thank Sukhjeet Arora, Harish Patel, Mrinal Roy, Vedant Jha, Licha Amma, Mampi who gave their time and assisted me in my experiments. I would also like to thank Prof. Ram Balachandar for his valuable inputs on vegetated flow.

I would like to specially thank Bazal Da (Bazal Hoque) for helping me in my experimental work. His management skills and network of vendors helped me in continuing my experiment even during the COVID 19 lockdown. I sincerely appreciate his tremendous assistance throughout the process, which was made possible by his impulsive and consistent support.

As it is commonly said “All work and no play make Jack a dull boy”. My 4 years of PhD journey wouldn't have been possible without my friends who always stood by my side during my highs and lows. I will miss the evening time and outings spent with my ‘Khokha group’ friends Saurabh, Rahul, Anurag and Mrinal. I am also grateful to Mriganabh, Smitom, Saubhik, Indraneel, Apoorva, Priya, Sanghamitra, Dipsikha and Angana for being there for me and will

cherish the time spent with you all. I would also like to thank my school, BTech and MTech friends who helped me in this journey and provided support and motivation. I would also like to specially thank Paramita for staying by my side and supporting consistently and selflessly during my research journey.

Last but not the least all this wouldn't have been possible without the love and support of my parents and family. I shall always be grateful of their selfless support both directly and indirectly. I would also like to thank my cousins and all relatives for their love and support. I also want to thank everyone who, directly or indirectly have helped me to complete my journey.

ABSTRACT

Riparian vegetation plays a crucial role in determining the flow behavior in the channel. The effect of flow on the slope and main channel varies based on the size, type, and density of floodplain vegetation in a compound channel. Though vegetation distribution in different water bodies is non-uniform, most studies mainly concentrate on uniformly distributed vegetation with fixed vegetation height. Laboratory studies were conducted to address this issue as it was not explored properly. Experiments were performed by taking partially vegetated rectangular channels and compound channels. Rectangular channels were considered to compare flow between homogeneous height/single-layered partially vegetated channels and heterogeneous height/multi-layered partially vegetated channels. Compound channels of three bank angles, namely 31^0, 45^0 and 90^0 were considered with vegetated floodplains.

In the partially vegetated channels, although the average frontal area of both submerged cases is equal, flow characteristics differ in the main channel. It is because of the variation in height of vegetation in the fully submerged multi-layered case compared to the single-layered case. As the vegetation emergence and density increase, the flow characteristics near the interaction zone between the floodplain and the main channel undergo significant enhancements. In fully emergent cases, a dip phenomenon is noticeable near the water surface within the main channel. This dip phenomenon is characterized by the presence of positive velocity gradients near the wall and negative velocity gradients near the surface. Furthermore, the dip phenomenon induces negative streamwise Reynolds shear stress near the surface, indicating the prevalence of outward and inward interactions in fully emergent cases. The quadrant analysis for different vegetation distribution cases showed the dominance of sweep and ejection events near the channel bed of the main channel.

While investigating 31^0 bank angle compound channels, the flow properties are more pronounced for uniformly distributed vegetation than non-uniform distribution. The multi-layered vegetation showed higher velocity, turbulent intensity, and turbulent kinetic energy than single-layered vegetation on slopes and main channel sections. Turbulent anisotropy was studied in detail to get further insight into flow behavior in different vegetation setups with a combination of submerged and emergent vegetation in compound channels. The anisotropic invariant map (AIM) and invariant function *F* reveal that the main channel section of 67 percent

emergent vegetation case has a greater tendency to approach two-dimensional turbulence than other non-uniform vegetation setups.

The role of bank angles in compound channels was also compared by considering two sets of 45^0 and 90^0 bank angle. The flow characteristics like velocity, Reynolds shear stress (RSS), and turbulent kinetic energy (TKE) do not vary much in the cross-section in the absence of vegetation. However, with vegetation, the slopes and nearby region are affected the most as it acts as an intermediary region between the main channel and floodplain. The analysis of the Anisotropic Invariant Map (AIM) shows the dominance of the transverse component in the slopes compared to the main channel and floodplain. The velocity in and around slopes is higher for steep slopes (90^0) compared to a gradual slope (45^0) compound channel. The streamwise RSS and bursting events also show higher magnitude near the channel bed in and around the sloping region. It indicates the instability of the steep banks compared to gradual bank slopes. The increase in floodplain vegetation emergence also affects the slopes. The magnitude of RSS and TKE in the slopes is higher with greater vegetation emergence in the floodplain. It shows the higher vulnerability of the slopes in the presence of higher vegetation emergence. From the hydraulic engineering perspective, this study will be helpful in the field of understanding the failure of banks and ways to maintain their stability.

Contents

LIST OF FIGURES

LIST OF TABLES

NOTATIONS

D_{50}	Median grain diameter
τ_c	critical bed shear stress
u_{*c}	critical shear velocity
θ	Bank angles
Q	Flow discharge
L_n	Width of the notch
(C_d)	Coefficient of discharge
H	water head over the notch
g	acceleration due to gravity
u, v, w	Instantaneous velocities in streamwise (X), transverse (Y), and vertical (Z) directions.
u', v', w'	Instantaneous fluctuations in streamwise (X), transverse (Y), and vertical (Z) directions.
$\overline{u}, \overline{v}, \overline{w}$	Average velocities in streamwise (X), transverse (Y), and vertical (Z) directions.
$\sqrt{\overline{u'u'}}$	Turbulence intensity in streamwise direction
$\sqrt{\overline{v'v'}}$	Turbulence intensity in transverse direction
$\sqrt{\overline{w'w'}}$	Turbulence intensity in transverse direction
$-\rho\overline{u'w'}$	Reynolds shear stress in streamwise direction
$-\rho\overline{u'v'}$	Reynolds shear stress in transverse direction
a	Average frontal area
h_{veg}	Average vegetation height
d	Diameter of single vegetation
ΔS	Average spacing between elements
Re	Reynolds number
Re_d	Stem Reynolds number
U	Average velocity in the channel
$\overline{U}$	Depth-averaged velocity
d	Diameter of reed
ν	Kinematic viscosity
Fr	Froude number
y	Characteristic length
z	Vertical distance from the bed surface
h	Depth of flow
k	Von Karman constant
z^+	Non-dimensional vertical height
Δz	Virtual bed level depth
z_0	Zero velocity level
$I_{i,H}$	Indicator function
$S_{i,H}$	Stress fraction
T	Total sampling time of velocity pulse
H	Hyperbolic hole region

b_{ij}	Non-dimensional Reynolds anisotropic tensor
δ_{ij}	Kronecker's delta
$\lambda_1, \lambda_2, \lambda_3$	Eigenvalues
I_1, I_2, I_3	First, second and third invariants respectively
ξ	Nature of anisotropy
η	Degree of anisotropy
TKE	Turbulent Kinetic Energy
F	Invariant function

1 Introduction

1.1 Overview

Vegetation in river channels is an integral part of the river system. Vegetation in open channel flow affects the flow behavior and sediment transport as it obstructs the natural flow of the river. Majority of the rivers are covered with vegetation in the bed and in the banks. Understanding the flow and turbulent behavior in a vegetated channel is very important for the study and management of fluvial processes.

The presence of vegetation in water bodies can be discussed from two contrasting perspectives. Firstly, the flow resistance increases in the presence of aquatic vegetation, decreasing the conveyance capacity, which leads to the removal of vegetation to increase the flow passage (Kouwen 1992; Masterman and Thorne 1992; Wu *et al*. 1999). A case study on Dongting lake, China, concludes that the presence of aquatic vegetation decreases suspended sedimentation ultimately increasing the thickness of sediment deposition and reduces the conveyance capacity over one flood season (Zhang *et al*. 2020). The excessive growth of some vegetation, like water hyacinth obstructs the flow passage, creating problems for waterways and affecting water quality (Urantinon, 2017; Zarkami *et al.*, 2020). Secondly, aquatic vegetation provides food sources and habitat for fishes and other aquatic beings (Edgar 1990; Kemp *et al*. 2000). It also plays a crucial role in regulating the concentration of oxygen, carbon and nutrients through their uptake and biological transformation (Carpenter and Lodge, 1986; Stamati *et al.*, 2010; Wang *et al.*, 2010; Pierobon *et al.*, 2013; Soana *et al.*, 2021). Furthermore, the presence of aquatic vegetation has a direct impact on the natural flow structure (Nepf, 1999; Jarvela, 2002; Ghisalberti and Nepf, 2006; Chen *et al.*, 2011; Vandenbruwaene *et al.*, 2011; Meire *et al.*, 2014; Yamasaki *et al.*, 2021), thereby indirectly influencing the transportation and diffusion of pollutants and sediments (Okamoto *et al.*; 2012; Le Bouteiller and Venditti, 2015; Huai *et al.*, 2019). It helps to reduce the concentration of heavy metals in water bodies as they use the metals for their growth (Wang and Freemark, 1995; Zayed *et al.*, 1998; Mohan and Hosetti, 1999; Vincent *et al*., 2001). Aquatic vegetation plays a crucial role in shaping hydrodynamic behavior, maintaining ecological equilibrium, and influencing flow characteristics (Wilcock *et al.*, 1999; Lee and Shih, 2004; Turker *et al.*, 2006; Cao *et al.*, 2011; Zhu *et al*., 2016). The existence of vegetation canopies in rivers is considered a vital aspect of water management and river environment, emphasizing the need to preserve flow structures in vegetated channels

(Poggi *et al*., 2004; Ghisalberti and Nepf, 2006; Tanino and Nepf, 2008; Nepf, 2012; Dupuis *et al.*, 2017; Caroppi *et al.*, 2021). Vegetation offers numerous benefits, such as enhancing bank stability, reducing erosion, mitigating floods, providing aesthetic value, and acting as a natural filter for pollutants (Kemp *et al.*, 2000; Gholami and Khaleghi, 2013; Bertoldi *et al.*, 2015; Rowiński *et al.*, 2018; Tisserant *et al.*, 2021; Rauch *et al.*, 2022). Overall, there are benefits and drawbacks of aquatic vegetation, and appropriate management is necessary to maintain a proper fluvial system.

1.2 Vegetation categories

Before studying the flow characteristics in vegetated channels, the study of different types of vegetation is necessary. The different types of vegetation are shown in figure 1.1. Based on the height of vegetation, it is divided into submerged and emergent vegetation. As the name suggests, submerged vegetation is found inside the water body, i.e., the height of the vegetation is lower than the flow depth (For example, hydrilla, coontail, muskgrass, pondweed etc.). Submerged vegetation can have a positive impact on water quality by removing Nitrates and Phosphates from the river and other water bodies (Velasco *et al*. 2003). Emergent vegetation protrudes out of the water body, i.e., the flow depth of the channel is less than the height of vegetation (For example, cattails, flowering rush, wild rice species, etc.). Another form of vegetation classification is based on the stiffness of plants. It is classified into flexible and rigid vegetation. The flexible vegetation height varies with different flow conditions, whereas the rigid vegetation height remains constant regardless of the prevailing flow conditions. Flexible vegetation, such as grass-like plants, tends to be submerged due to their relatively small average height. Shrubby vegetation is considered rigid, which could have both submerged and emergent configurations. During a flood event, a channel has the potential to completely bend rigid vegetation, causing it to break and lie on the bed (Ferro, 2006). The bending stiffness in vegetation can be expressed as EI, where E is the streamwise modulus of elasticity of the vegetation element and I is the moment of inertia of the cross-section of the element itself (Kouwen *et al.*, 1969; Kowobari *et al.*, 1972). More the bending stiffness, less will be the flexibility of the plant. The present thesis considers experiments with only rigid vegetation.

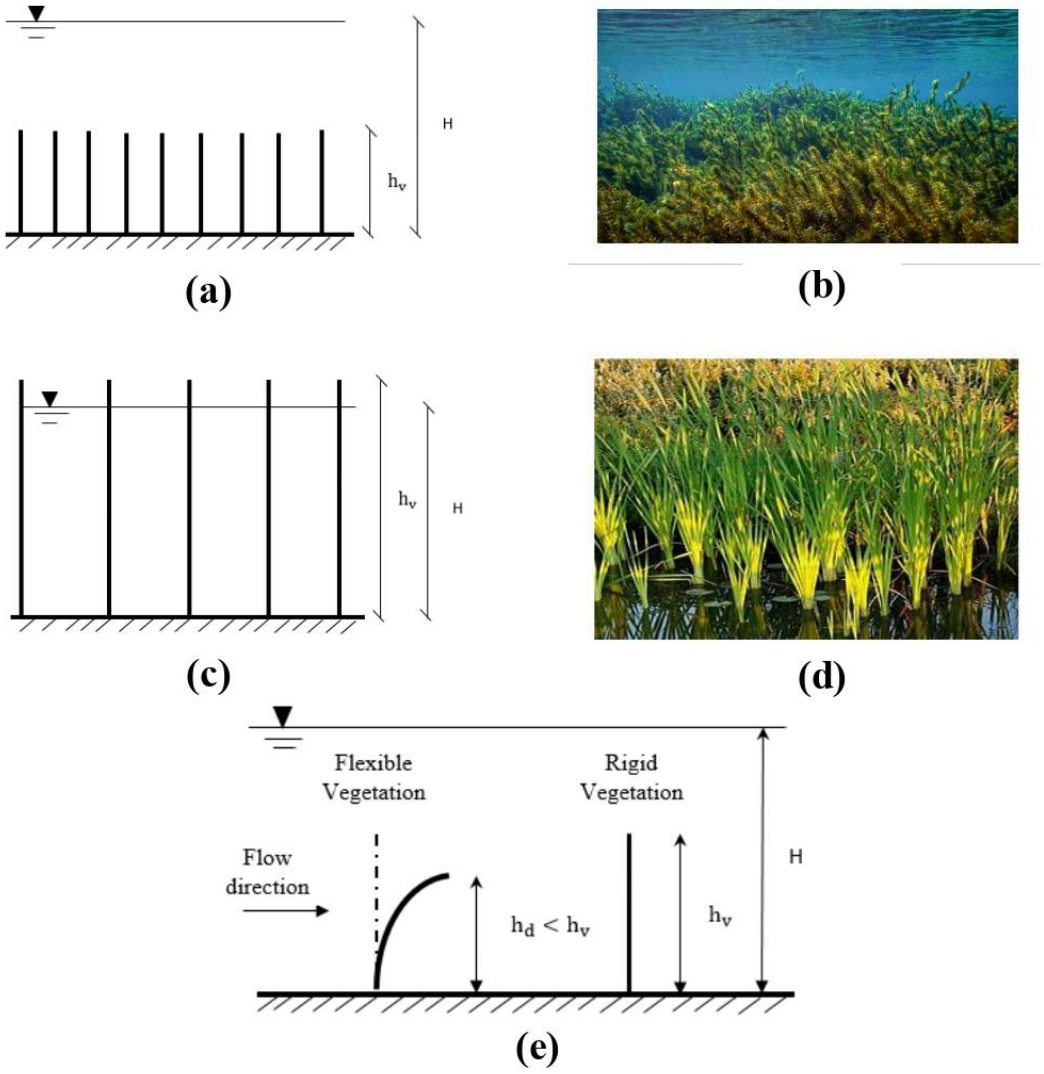

Figure 1.1 (a) Submerged Vegetation (b) Picture of hydrilla (Courtesy: consciouslifestylemag.com) (c) Emergent vegetation (d) Picture of cattails (Courtesy: fotosearch.com) (e) Flexible and Rigid vegetation

1.3 Flow Characteristics in Vegetated Channels

The study of the hydrodynamics of channels in the presence of vegetation is a complicated problem. Resistances offered by vegetation will vary based on the height, density and nature of vegetation which makes it more complicated. Kouwen (1988) explored the resistance provided by herbaceous and algal vegetation. A significant number of researches were conducted regarding resistances by woody (Righetti and Armanini, 2002; Järvelä, 2004; Box *et al.*, 2021; Nicosia and Ferro, 2023); submerged (Stephan and Gutknecht, 2002; Carollo *et al.*, 2005; Baptist *et al.*, 2007; Ferro, 2019; Cui *et al.*, 2023) and rigid and emergent vegetation

(Ishikawa *et al.*, 2000; Kothyari *et al.*, 2009b; Tanino and Nepf 2008; D'Ippolito *et al.*, 2019). Studies have also been carried out to see the relationship between flow characteristics and drag resistances offered by vegetation (Nepf, 1999; Nezu and Sanjou, 2008; Devi *et al.*, 2016). Because of its complexity, studies are now focusing on the structure of turbulence and sediment transport and deposition due to vegetation (Nepf and Ghisalberti, 2008; Ghisalberti and Nepf, 2009; Meire *et al.*, 2014; Liu and Nepf, 2016; Kitsikoudis *et al.*, 2020; Wu *et al.*, 2023).

Laboratory studies have been conducted in the past in order to get a better understanding of sediment transport. These studies aimed to observe the impact of artificial vegetation with rigid stems (e.g., Fairbanks, 1998; Kothyari *et al*., 2009; Follett and Nepf, 2012; Fu *et al*., 2020) as well as flexible stems (e.g., Nepf and Vivoni, 2000; Wilson *et al.*, 2003; Ghisalberti and Nepf, 2006; Wang *et al.*, 2015; Mu *et al.*, 2019) on both steady and unsteady turbulent flow structures. Flume studies were conducted by numerous researchers to understand the flow turbulence using artificial and natural vegetation (Meijer & Van Velzen, 1999; Stephan & Gutknecht, 2002; Järvelä, 2002; Righetti & Armanini, 2002; Devi *et al.*, 2016). Various materials have been used to depict vegetation which includes wooden cylindrical dowels or rods (Stone and Shen, 2002; Poggi *et al.*, 2004; Liu *et al*., 2008; Truong *et al.*, 2019; Shi *et al.*, 2023), flexible strips or blades (Nepf and Vivoni, 2000; Ghisalberti and Nepf, 2006; Nezu and Sanjou, 2008; Chen *et al.*, 2011) and natural vegetation (Stephan and Gutknecht, 2002; Järvelä, 2005; Carollo *et al*., 2005; Devi *et al.*, 2016; Chembolu *et al.*, 2019). Though use of artificial vegetation is easy to analyse the flow, it fails to present the real hydrodynamics as compared to natural vegetation.

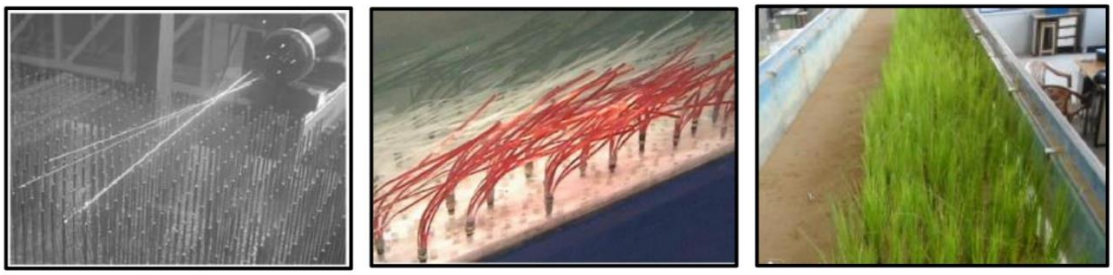

(a) (b) (c)

Figure 1.2 Artificial vegetation with (a) rods (Courtesy: Poggi *et al.* 2004) (b) flexible strips (Courtesy: Ghisalberti and Nepf, 2006) and natural vegetation with (c) rice (Courtesy: Devi *et al.*, 2016)

Studying and analyzing the mean velocity profile is considered the foremost and one of the most important parameters for understanding hydrodynamics. The velocity profile varies when vegetation is present, and it differs from the logarithmic nature, which is seen in the free stream. The velocity profile in emergent vegetation is mostly uniform except near the channel bed,

where a high gradient is observed (Nepf and Vivoni, 2000; Devi *et al.*, 2019), whereas for the submerged flexible vegetation, it is an S-shaped profile (Kouwen *et al.*, 1969; Ikeda and Kanazawa, 1996; Carollo *et al.*, 2002). However, the velocity profile in submerged vegetation follows a logarithmic nature from the top vegetation to the flow surface (Carollo *et al.*, 2002; Nepf, 2012).

Apart from mean flow, turbulence structure, vortex flow, and erosion pattern in a vegetated channel have also been studied in detail. Researchers have focused on studying atmospheric flows within and above terrestrial vegetation to comprehend the turbulent structure of rough flows involving vegetation as roughness elements, such as forests and bushes (Wilson and Shaw, 1977; Finnigan, 1985; Raupach and Shaw, 1982). This flow behavior in terrestrial vegetation is attempted to understand the turbulent structure in aquatic vegetation channels (Tsujimoto *et al.*, 1992; Shi *et al.*, 1996; Nepf, 1999; López & García, 2001; Nezu and Sanjou, 2008; Righetti, 2008; Caroppi *et al.*, 2021). Fairbanks (1998) understood the local scour patterns due to horseshoe vortex in rigid vegetation. Flow in submerged vegetation with sufficient vegetation density could lead to the formation of Kelvin-Helmholtz (KH) vortices due to the formation of a shear layer at the top of vegetation (Nepf and Ghisalberti, 2008; Termini, 2015). These KH vortices might generate a waving motion called *monami* when it passes over the top of flexible vegetation (Nepf and Ghisalberti, 2008; Nepf, 2012). The formation of wakes and vortices in vegetated channels can play a significant role in sediment movement (Vandenbruwaene et al., 2011; Nepf, 2012).

The arrangement of vegetation in the laboratory flume can be either fully covered (Järvelä, 2002; Nepf and Ghisaberti, 2008; Termini, 2019; Xu and Nepf, 2020) or partially covered (Truong *et al.*, 2019; Caroppi *et al.*,2021; Shi *et al.*, 2023) along the width of the flume. In the submerged vegetation fully covered channel, only vertical momentum exchange occurs between the vegetation and the free flow region. On the other hand, a partially vegetated channel mainly simulates a river channel ecosystem where alongwith vertical momentum exchange, horizontal exchange of momentum also occurs between the vegetated and main channel regions. Laboratory studies were also conducted considering compound channels which are an extension of partially vegetated channels with slopes (Dupuis *et al.*, 2017; Mehrabani *et al.*, 2020; Rao *et al.*, 2022). The present thesis considers partially vegetated (objective 1) and compound channel (objectives 2 and 3) vegetation arrangements.

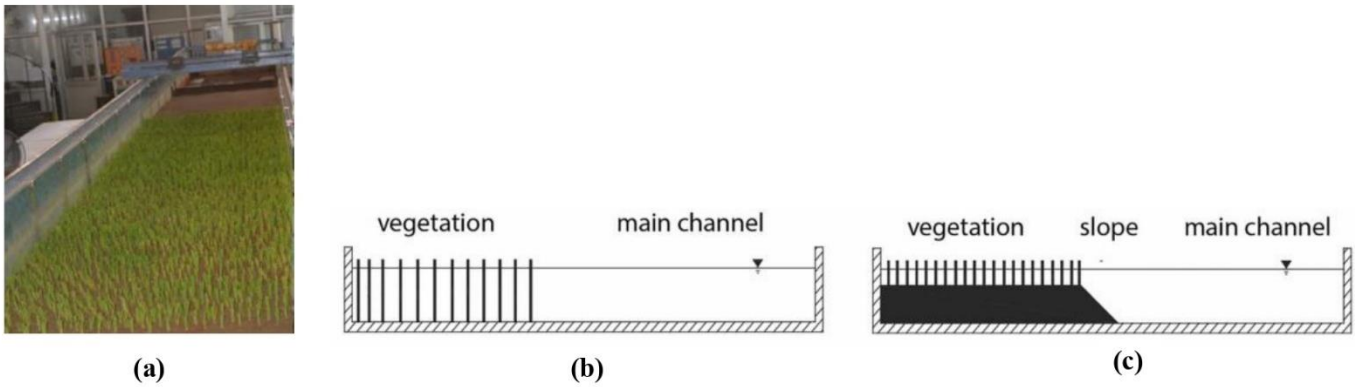

Figure 1.3 (a) Snapshot of the fully covered experimental flume (Courtesy: Chembolu *et al.*, 2019). Cross-section of (b) partially vegetated and (c) compound channel (Courtesy: Truong and Uijttewaal, 2019)

Kouwen *et al.* (1969) performed laboratory experiments to study the velocity profile using styrene strips as vegetation. They observed that the velocity profile followed logarithmic law above the vegetation layer, which was constant inside it.

Ikeda and Kanazawa (1996) studied the three-dimensional vortices which arise above flexible vegetation. They observed an inflection point in the velocity profile near the top of vegetation, which makes the flow unstable, and ultimately discrete vortices are formed. These vortices consist of a pair of counter-rotating vortices in both horizontal and lateral sections. The vortices have an elliptical shape and are also inclined downward toward the front.

Carollo *et al.* (2002) studied the flow velocity profile in submerged flexible vegetation in the laboratory using Acoustic Doppler Velocimeter (ADV). The shape of the velocity profile follows an S-shaped profile which agrees with Kouwen *et al.* (1969). Furthermore, they also found three different zones in the velocity profile when it passes through submerged flexible vegetation. Zone I corresponds to the lower region of canopies where the velocity gradient increases and velocity is less; Zone II represents the middle portion and from which a logarithmic profile can be fitted. It contains the inflection point, which can be found at the top of vegetation; Zone III is characterized by positive velocity gradients, which decrease to zero on the free water surface. They also found that velocity increases inside the vegetation with decreasing stem concentration, whereas it decreases above it.

Nepf and Ghisalberti (2008) studied mean velocity profiles, turbulent structure and dispersion in submerged vegetation. The submerged canopies with sufficient vegetation density can generate shear layer at the top of the vegetation, ultimately creating Kelvin- Helmholtz (KH)

instability. Due to this instability, coherent vortices are formed, which travels with the flow. When these vortices pass above a flexible vegetation, it produces a wavy motion called *monami*. Sometimes, the presence of KH vortices may not guarantee a *monami* due to the high flexural rigidity of the elements. KH vortices penetrate a certain scale into the canopy dividing it into two layers. The upper layer comprises of KH vortices which are more energetic and have bigger scale size as compared to the lower wakes which are formed in the lower part of canopies due to canopy elements.

Nezu and Sanjou (2008) conducted experiments considering submerged vegetation canopy and concluded that the mechanism of flow in the terrestrial and aquatic canopy is the same. They also studied the turbulent kinetic energy (TKE) budget, which shows that turbulent diffusion plays a crucial role in the TKE budget. Furthermore, ejection and sweep events are formed due to the shear instability between the vegetation top and the free-flow region. These events play a dominant role in shaping the turbulent structure and coherent movement within aquatic flows.

Devi and Kumar (2016) studied flow nature in submerged flexible vegetation patches with conditions of downward seepage. They concluded that flow velocity and Reynolds shear stress increase in the case of downward seepage condition compared to no seepage condition.

Dupuis *et al.* (2017) investigated the development of mixing layer in the compound channel by performing experiments considering uniform height rigid vegetation for submerged and emergent vegetation in a compound channel. They concluded two mixing layer widths in the floodplain (δ_f) and main channel (δ_m) on either side of the mean velocity inflection point. The growth rate of both the widths differ according to the submergence of the vegetation in the floodplain. They also concluded that wooded floodplain provides more secondary currents than grassed floodplains.

Huai *et al.* (2019) studied the velocity flow profile in submerged flexible vegetation using a vegetation zone of $8\,m$ length. They used a large vegetation zone to observe the longitudinal development of the velocity profile. The experimental set up used here is an upgrade as compared to Okamoto and Nezu (2013), as it could capture the complexity of real field to some extent. They wanted to see the equilibrium stage after which profile shape is no longer dependent on distance. The whole vegetation zone is divided into three stages based on the velocity profile: diverging flow stage, developmental stage and completely developed stage. They also observed that Reynolds shear stress and turbulent intensities are maximum at the top

of the vegetation and decrease as it reaches the top and bottom of the channel. The ejection events are also seen to be dominated above the vegetation, whereas sweep events dominate below the canopies.

Proust and Nikora (2019) analyzed the transverse currents in a compound channel by releasing different flow discharges in the floodplain and the main channel in the upstream portion of the flume. The floodplain of the experiments was covered with dense artificial grass. Three developed secondary current cells were observed in both uniform and non-uniform flow, with transverse currents flowing in the direction of the floodplain. These secondary current cells were induced by turbulence anisotropy. When there is a transverse mean flow in the direction of the primary channel, these cells are replaced by a single cell.

Termini (2019) analysed the turbulent kinetic energy (TKE) budget in a flume covered with real flexible vegetation. It was found that the vegetation density plays a crucial role in determining various TKE budget terms. The ejection and sweep events determine the turbulence structures between the vegetated and free-flow zone, which remains consistent with Nezu and Sanjou (2008). The analysis of the TKE budget terms in the vegetated region has shown three layers along the vertical: wake layer, mixing layer and above mixing layer. The turbulent intensities are observed to maximum value in the mixing layer.

Truong *et al.* (2019) studied the transverse momentum exchange in a partially vegetated compound channel considering emergent vegetation. They analysed large horizontal coherent structures (LHCSs) which induces the transverse momentum exchange in the interface of vegetated and main channel. They concluded that in a gently sloping compound vegetated channel, the characteristics of the shear layer are primarily influenced by the vegetation rather than the disparity in water depth. The moving of the LHCSs along the vegetation interface is linked to the occurrence of sweeps, ejections, as well as stagnant and reverse flows, which collectively forms a cycloid motion.

Xu and Nepf (2020) studied TKE in emergent vegetation considering real plant (*Typha latifolia* and *Rotala indica*). They demonstrated that the shape of a plant determines the flow nature in the channel. The *Typha latifolia* had non-uniform vertical distribution, and its frontal area varies. The flow parameters were also non-uniform in the canopy region with a higher frontal area. On the other hand, the *Rotala indica* had a uniform vertical distribution of frontal area which ensured vertically uniform flow parameters.

Mehrabani *et al.* (2020) performed experiments in compound channels considering prismatic and non-prismatic cross-sections. They considered two non-prismatic channels with convergence angle of 7.25^0 and 11.3^0. They found that the convergence of floodplain in the upstream of the compound channel created a transverse current that was directed from the floodplain to the main channel. This transverse current ultimately leads to helical secondary cells forming, which causes sediment, pollutants and nutrient movement. The lateral shear stress is also observed to be higher in the case of the non-prismatic channel compared to the prismatic compound channel.

Caroppi *et al.* (2021) compared flow when it encountered flexible and rigid vegetation in a partially vegetated channel. They used reconfiguring plants for flexible vegetation and rigid cylinders for rigid vegetation. They concluded that penetration of large-scale vortices and lateral momentum transport is greater for flexible vegetation compared to the rigid cylinders. They also observed that the use of natural vegetation in the laboratory gives an accurate understanding of the flow nature in real field situations.

Li *et al.* (2022) performed experiments considering partially vegetated channel where they used wooden circular cylinders to replicate emergent vegetation. In their newly proposed eddy viscosity model, they discovered that the primary cause of the momentum exchange is turbulence brought on by coherent structures. They also concluded that the proposed model agrees with measured profiles obtained from experiments.

Shi *et al.* (2023) conducted laboratory experiments to study coherent structures and secondary flows in a partially submerged vegetated channel. They concluded that the longitudinal velocity profile in the interface of vegetation and the main channel follows an S-shaped profile in a narrow channel (breadth of channel/flow depth<5). Secondary currents which are induced by the riparian vegetation are responsible for the S-shaped profile. This profile, in turn, creates two distinct vertical mixing layers that promote the development of coherent structures through shear-induced forces. These structures generate correlations between longitudinal and vertical velocity fluctuations.

1.4 Heterogeneity in vegetated channels

The distribution of vegetation in river channels and floodplains is heterogeneous. So, conducting field studies is more applicable to understanding the flow behavior and its interaction with vegetation. Though some researchers have performed experiments in the field,

it is limited due to the flow complexity (Sukhodolov and Sukhodolova, 2010; Lacy and Wyllie-Echerverria, 2011; Sukhodolov *et al*., 2016; Vershoren, 2017; Przyborowski and Loboda, 2021; Caroppi *et al*., 2022). On the other hand, laboratory studies are less complex, and it also has the provision to change the condition according to the requirement. Laboratory studies related to heterogeneous vegetation have been fast-growing since the last decade. However, it is limited compared to homogeneous vegetation. Laboratory experiments are conducted considering varying heterogeneous conditions like heterogeneity in height, types and spacing of vegetation to study the flow behavior. Devi *et al*. (2016) and Li *et al.* (2022) attained heterogeneity in spacing by mixing the vegetation densities in the test section. Chembolu *et al.* (2019) achieved heterogeneity by changing the vegetation type in the test section. They studied the flow behavior in mixed vegetation and compared it with a single vegetation type. Heterogeneity in height is obtained either by naturally growing vegetation in the laboratory (Stephan and Gutknecht, 2002; Shucksmith *et al.*, 2010) or experimented with different vegetation layers or heights (Li *et al.*, 2014; Hamed *et al.*, 2017; Horstman *et al.*, 2018; Tang *et al.*, 2021). Furthermore, river channels are characterized by the presence of both submerged and emergent vegetation, forming a mixed combination within their ecosystems. Figure 1.4 shows a typical example of floodplain region near the Brahmaputra River during the rainy season. Flow structure in channels with varying heights is very complex due to varying flow resistance provided by vegetation (Liu *et al.*, 2010; Li *et al*., 2014; Hamed *et al.*, 2017; Horstman *et al*., 2018; Tang *et al.*, 2021). The flow characteristics change when it encounters different types of vegetation in the measured area. The drag resistance and other turbulent characteristic shows non-uniform traits throughout the vegetation area (Chembolu *et al.*, 2019). Flow resistance also shows variation when the concentration of vegetation in a particular area changes. Increasing the stem concentration increases the resistance and decreases the velocity (Carollo *et al.*, 2005). As a result of this, sediment deposition takes place (Sharpe and James, 2006). Studies have shown that higher stem density in a region increases the depositional nature of sediments (Bos *et al.* 2007; Devi *et al.* 2016). Sediment deposition is also affected by spacing between vegetation patches. Different numerical and analytical models of heterogeneous vegetation also indicate the difference in treatments compared to homogeneous vegetation (Huai *et al.*, 2014; Anjum and Tanaka, 2020).

Figure 1.4 Snapshots from the Brahmaputra River, India (26°12'24.5"N 91°35'49.7"E)

Nepf and Vivoni (2000) conducted laboratory experiments to see the flow behavior from the emergent to the submerged phase. This was done by changing the flow depth with respect to vegetation height. The laboratory model is divided into two distinct zones of aquatic canopy: the lower canopy, called the longitudinal exchange zone and the upper canopy, called the vertical exchange zone. Exchanges in neighbouring water occur by longitudinal advection in the lower canopy and emergent vegetation, whereas vertical exchange takes place in the upper canopy.

Stephan and Gutknecht (2002) studied the roughness caused by aquatic plants with different relative submergence, which was attained by running the experiments for 7-10 days for each plant type. They found that the turbulent intensities are independent of relative submergence because plants are flexible and adapt their shape with the flow initiating wavy motion of plants without damping turbulent intensities.

Carollo *et al.* (2007) conducted experiments on submerged flexible vegetation at three different concentrations (280, 377, 440 stems/dm^2). They found that with increasing relative vegetation roughness (bent vegetation height/flow depth), the turbulent intensity profile gets shifted towards the free surface. Also, with increasing vegetation concentration, turbulent intensity is damped because there is a reduction of momentum exchange between the vegetation zone and the free-flowing zone.

Shucksmith *et al.* (2010) conducted flume study and observed the growth of 2 types of vegetation (*Phragmites australis* and *Carex*) over a period of 26 weeks. During this time, they studied turbulent characteristics and longitudinal mixing and how it changes with passing time. They found that longitudinal mixing in submerged vegetation is more than emergent vegetation due to greater vertical velocity shear in submerged vegetation. The wake zone considered in submerged vegetation is significant, which indicates that longitudinal mixing is a function of degree of submergence.

(a) (b)

Figure 1.5 Vegetation growth at the end of (a) 2 weeks and (b) 26 weeks (Courtesy: Shucksmith *et al.* 2010)

Liu *et al.* (2010) performed experiments considering array of short and long vegetation in the flume. They compared single-layered (uniform height) vegetation with double-layered (non-uniform height) vegetation and concluded that double-layered vegetation flows are more complex than single-layered vegetation. Multiple inflection points were observed in velocity profiles in the case of double-layered vegetation as opposed to a single inflection point in single-layered vegetation.

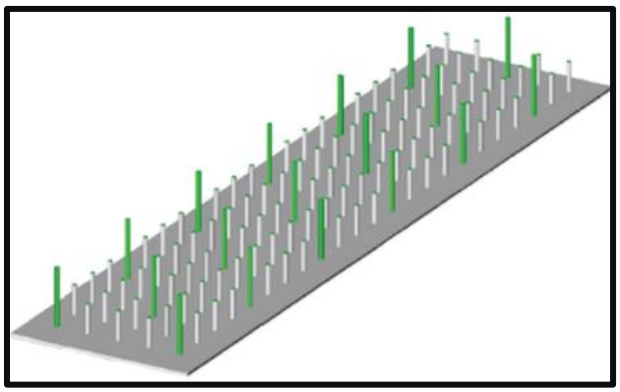

Figure 1.6 Double -layered vegetated zone (Courtesy: Liu *et al.* 2010)

Y. LI *et al.* (2014) tried to explain the heterogeneous vegetation by combining emergent and submerged vegetation. They found that number of inflection points in streamwise velocity profile are more as compared to single type of vegetation. The turbulent intensities are mostly invariant in the bottom layer of the combined vegetation area, which is contrary to the flow in submerged vegetation type. The turbulent intensities mostly fluctuated at the top of the canopy of submerged vegetation.

Huai *et al.* (2014) proposed an analytical model to predict velocity profiles in double-layered vegetation. They arranged the vegetation in a uniform pattern with tall and short dowels precisely behind each other. They also performed experiments and found that the proposed analytical model is in good agreement with experimental findings.

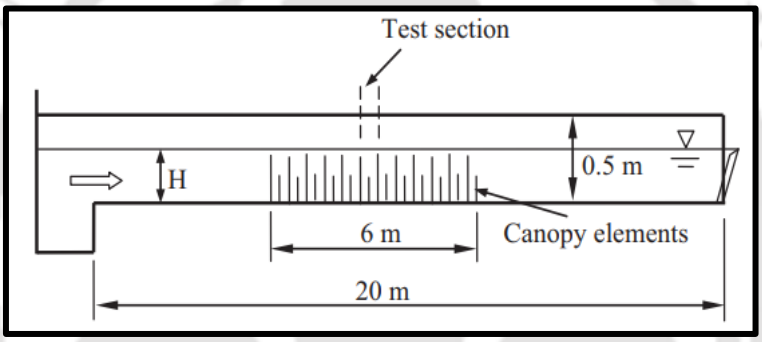

Figure 1.7 Laboratory flume set up for double -layered vegetated zone (Courtesy: Huai *et al.* 2014)

Devi *et al.* (2016) attained heterogeneity in spacing by mixing the vegetation densities in the test section. In the upstream half of the test section, the spacing between vegetation was kept at 10 *cm* centre to centre, whereas in the downstream half, the spacing was kept at 5 *cm* centre to centre. There is a decrease in flow characteristics like velocity, Reynolds shear stress and turbulent intensities when higher vegetation density is placed downstream of flow. The domination of sweep events also decreases in the higher vegetation density part, which indicates less deposition as compared to low density portion.

Hamed *et al.* (2017) conducted experiments investigating the heterogeneity of vegetation height using a particle image velocimeter (PIV). They observed that flow characteristics like Reynolds stress and turbulent kinetic energy are more pronounced in heterogeneous canopies than in homogeneous canopies. The momentum exchange is also higher in the case of the heterogeneous canopy at the top of the canopy.

Horstman *et al.* (2018) replicated a real mangrove vegetation distribution in the laboratory flume and compared results with uniform height vegetation. They used the pneumatophore of *Avicennia marina* (var. *australasica*) and rigid dowel for the experiments. They found that as compared to homogeneous distribution, heterogeneous distribution appears to reduce the strength of the canopy shear layer significantly. They also concluded that turbulent stresses and bed shear stresses were smaller in pneumatophore canopies compared to uniform-height dowel canopies with similar densities.

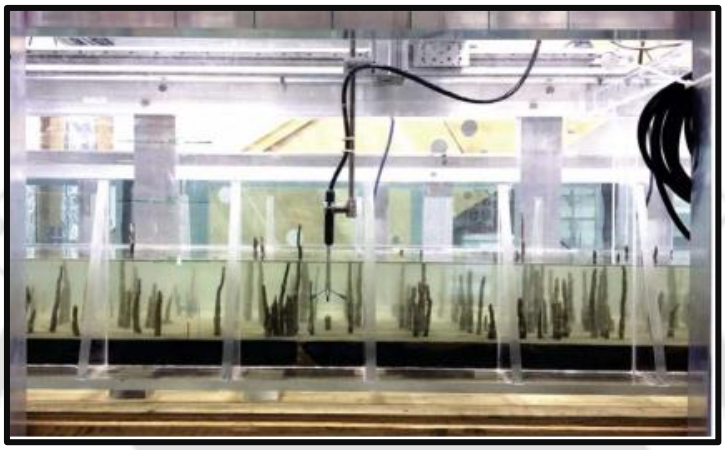

Figure 1.8 Side view of the data collection area in the flume for the high-density pneumatophore experiment (Courtesy: Horstman *et al.* 2018)

Chembolu *et al.* (2019) observed the flow behavior by conducting laboratory experiments taking three vegetation (bladed, leafy and cylindrical) and mixing them in a staggered pattern. They found that there is a reduction of velocity in the mixed heterogeneous patches as compared to homogeneous flexible bladed stems. Moreover, due to spatial heterogeneity in mixed patches, different zones of increasing and decreasing turbulence was observed.

Figure 1.9 Snapshots of different homogeneous and heterogeneous vegetated zone layout with uniform vegetation height (Courtesy: Chembolu *et al.* 2019)

Ahmad *et al.* (2020) performed numerical simulations using a computational fluid dynamics (CFD) code FLUENT on a double-layered floodplain vegetated compound channel. The turbulence closure was achieved by implementing a RANS technique based on Reynolds stress model. They observed quite S-shaped velocity profile when the short vegetation was submerged, whereas during low floods or when both short and long vegetation are emergent, velocity profile seems to be uniform or almost logarithmic.

Anjum and Tanaka (2020) used a $k-\varepsilon$ turbulence model to understand the flow behavior when it encounters double-layered vegetation. The turbulence model was developed using 3-D numerical code FLUENT (ANSYS). The experimental validation was performed using the data from Liu *et al.* (2010). They found that the $k-\varepsilon$ model was efficient in modeling the turbulent characteristics through double-layered vegetation.

Tang *et al.* (2021) analyzed different flow characteristics in a double-layered partially vegetated channel. They found that Reynolds stresses behave differently in different locations because of the combined effect of short and long vegetation in the vegetated portion. In order to more accurately reflect the circumstances found in nature, they also provided a modified hydraulic radius for calculating Mannings' coefficient in double-layered vegetated flows.

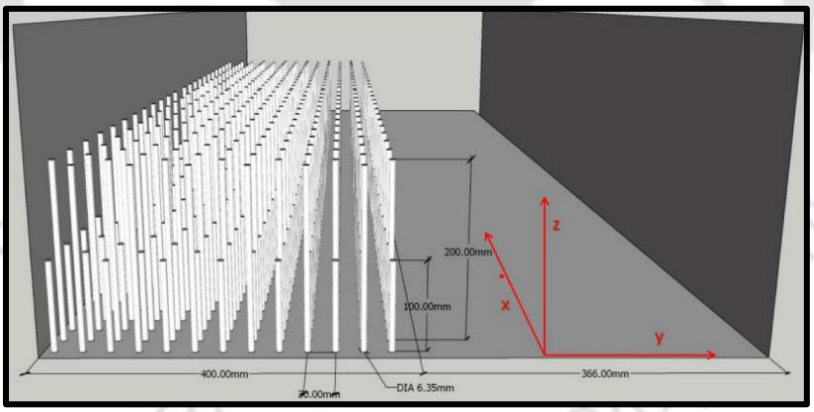

Figure 1.10 Schematic diagram of partially-placed, double-layered vegetation (Courtesy: Tang *et al.* 2021)

Li *et al.* (2022) achieved heterogeneity in vegetation by alternating the density in the vegetated zone and keeping the vegetation height uniform. They performed flume experiments considering the vegetation to be covered partially. They observed that a longer adjustment distance is required for reaching the quasi-equilibrium region for the heterogeneous case (mixture of dense and sparse vegetation) compared to the homogeneous case where the vegetated zone is covered with the same density. The heterogeneous canopy was also observed

to have higher Reynolds stress at the interface between the vegetation and the main channel, indicating higher momentum exchange.

Hu and Zhang (2022) developed a new analytical method to analyze the transverse distribution of streamwise velocity in a compound channel containing both submerged and emergent vegetation. They modified the Shiono and Knight Method (SKM) and used a two-layer model to obtain more accurate results. They found that the developed model is consistent with the experimental data after using proper boundary conditions. They observed that the dimensionless eddy viscosity coefficient has a clear effect on the main channel, whereas the depth-averaged secondary flow coefficient has only a definite effect in the slope sub-region.

Tang *et al.* (2023) investigated two vegetation scenarios to simulate water flow in a shallow lake with vegetated channels. These scenarios included a channel with partially covered rigid emergent vegetation, and a channel with mixture of emergent-submerged vegetation. They concluded that in the combined case scenario, inflection point was observed near the bed and at the top of submerged vegetation within the flexible vegetation canopy. They also observed distinct and transverse coherent vortices at the top of the submerged vegetation and the interface between emergent and submerged vegetation respectively.

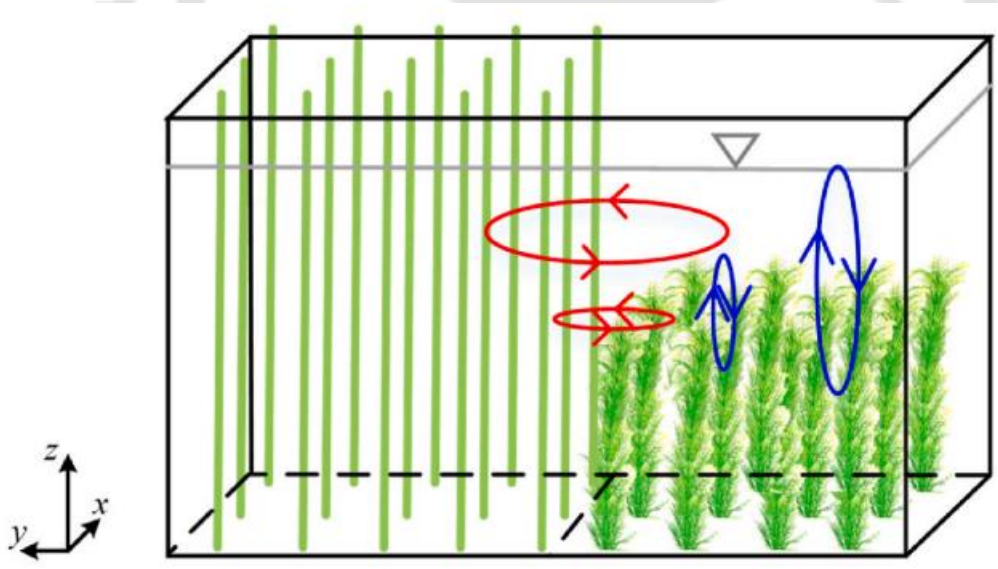

Figure 1.11 Formation of horizontal and vertical coherent vortices in a mixture of emergent-submerged vegetation (Courtesy: Tang *et al.* 2023)

1.5 Need for Research

The impact of vegetation on flow behavior and morphological changes in conveyance channels is well-documented in the literature. However, the distribution of vegetation in river channels is typically heterogeneous, with varying densities, types, and vegetation heights. This heterogeneity creates non-uniform resistances to flow, posing challenges for flow analysis. In particular, the effects of varying vegetation height and density on flow in partially vegetated channels require further investigation, as this area of study has not been thoroughly explored. Additionally, the complexities that arise with the presence of vegetation with varying height and density in a compound channel make it an untapped topic for investigation. Therefore, it is essential to conduct experiments to study the impact of heterogeneous vegetation in a compound channel and to understand the flow behavior in combined emergent and submerged vegetation. The role of bank angles in a compound channel, considering varying vegetation height, is also an area that requires exploration. This research will help advance the understanding of how to recreate a natural flow in vegetated channels, moving us one step closer to accurately predicting the impact of vegetation on flow dynamics.

1.6 Objectives

The main objectives of this research are as follows:

1. Hydrodynamics of partially vegetated channel with multi-layered vegetation.
   - Comparing flow behavior between homogeneous/single-layered and heterogenous/multi-layered height vegetation in partially vegetated channels.
   - Exploring the role of vegetation emergence and density on the overall flow in the channel.
2. Flow behavior in a multi-layered vegetated floodplain region of a compound channel.
   - Analyzing the effect of floodplain vegetation on the slopes and main channel of the compound channel with 31^0 bank angle.
   - Comparing single-layered and multi-layered floodplain vegetation in 31^0 compound channel.
3. Flow in multi-layered vegetated compound channels with different bank slopes.
   - Study the role of bank slopes in the overall flow structures in the channel considering multi-layered floodplain vegetation.
   - Understanding the role of vegetation emergence and its impact on the channel, considering 45^0 and 90^0 bank angle compound channels.

1.7 Organization of Thesis

Given below is a brief description of each chapter:

Chapter 1 "Introduction" provides a comprehensive outline highlighting the significance of vegetation within aquatic environments. Detailed descriptions of laboratory experiments concerning vegetation by different researchers are discussed. A detailed description of previous researches concerning homogeneous and heterogeneous vegetation height are discussed. The problem statement and research gap are thoroughly examined, followed by a discussion on the study's objectives.

Chapter 2 "Methodology" describes the experimental methodology with details of experimental design, vegetation procurement, the overall experimental program, and the methods employed for data collection. Furthermore, comprehensive information regarding the instruments utilized in the experimental study is also presented.

Chapter 3 "Hydrodynamics of partially vegetated channel with multi-layered vegetation" presents the flow difference when it interacts single-layered and multi-layered vegetation in partially vegetated channels. For multi-layered vegetation distribution, three vegetation heights are considered. The effect of vegetation density and emergence are observed in this section.

Chapter 4 "Flow behavior in a multi-layered vegetated floodplain region of a compound channel" discusses the importance of uniform and non-uniform vegetation in spacing and height in compound channels. The effect of floodplain vegetation on the slopes and main channel is also discussed in this section.

Chapter 5 "Flow in multi-layered vegetated compound channels with different bank slopes" discusses the role of bank angles in compound channels considering multi-layered vegetation in the floodplain region. This section compares the flow characteristics of two bank angles with their impact on the slopes.

Chapter 6 "Conclusion and Recommendations" summarizes the key findings from the current research work. Additionally, this chapter offers recommendations based on these findings and explores potential future scope of the work.

2 Methodology

Experimental studies on laboratory flume give a proper understanding of the flow behavior of a channel. The conditions of an experimental set up can be altered according to the need of the researcher, which gives an advantage over field study. The following sections provide the methods and procedure of the experiments.

2.1 Experimental Setup and Procedure

Experiments were carried out on a laboratory flume of 17.2 m long, 1 m wide and 0.72 m deep (Figure 2.1). At the upstream of the flume, a tank of length 2.8 m, width 1.5 m and depth 1.5 m was provided to regulate straight flow into the main channel. The water was gradually released with the help of a valve from the overhead storage tank to the inlet tank and ultimately to the main flume. Since it is a recirculating flume, the water is drained into an underground tank and pumped again to the upstream overhead storage tank. Flow depth and discharge in the flume were regulated with the help of the tail gate and rectangular notch, both situated at the downstream of the flume.

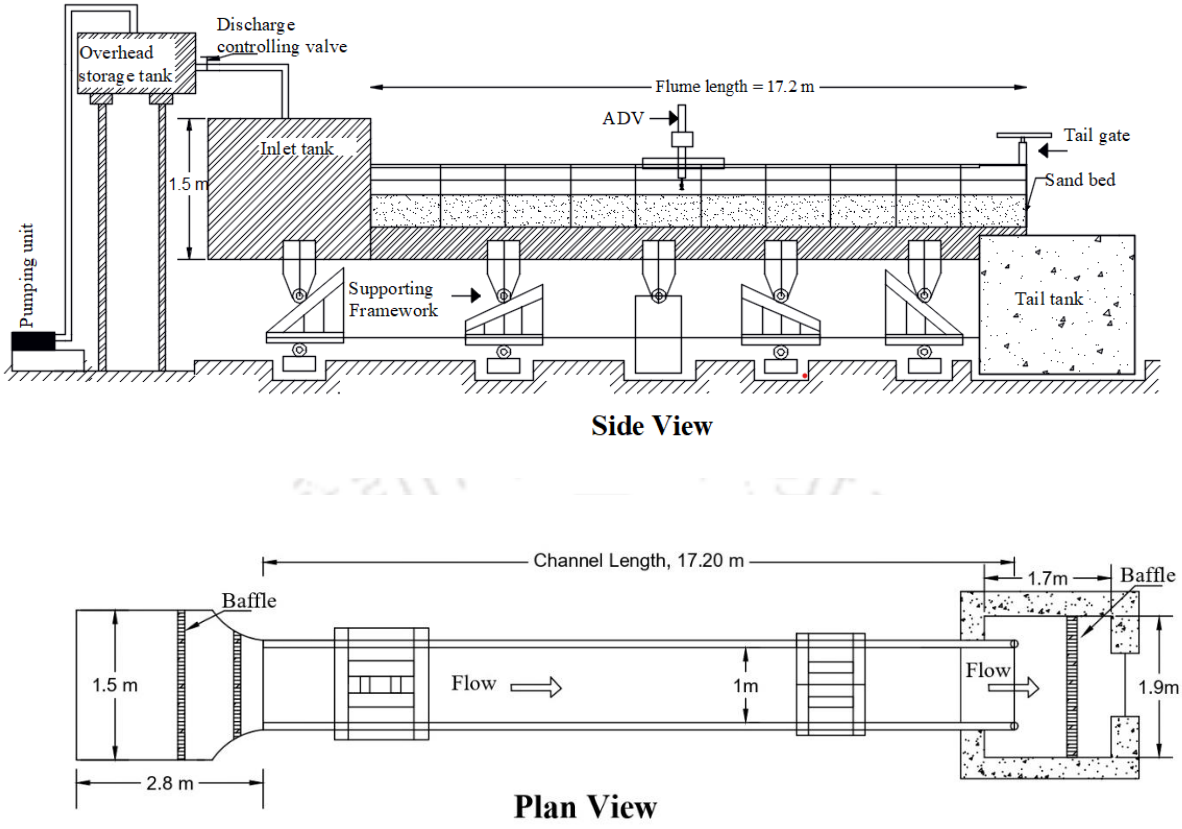

Figure 2.1 Side view and plan view of the experimental flume present at IIT Guwahati.

2.2 Bed Material

The experiments were conducted using river sand with a median particle diameter (D_{50}) of 1.1 mm. The sand was uniform (Figure 2.2) with a geometric standard deviation of 1.03. The sand can be defined as uniform as the geometric standard deviation (σ_g) is less than 1.4 (Marsh *et al.* 2004). It can be calculated as:

$$\sigma_g = \frac{D_{84} - D_{16}}{D_{50}} \tag{2.1}$$

where, $D_{84}(D_{16})$ is the grain size for which 84% (16%) of the sample has a finer grain content by weight. The dry angle of repose of the sand used for experiments was 31.1°. The sand bed is movable, and the flow depth and velocity measurements were acquired once the initial movement of sediment stopped and a steady condition is attained.

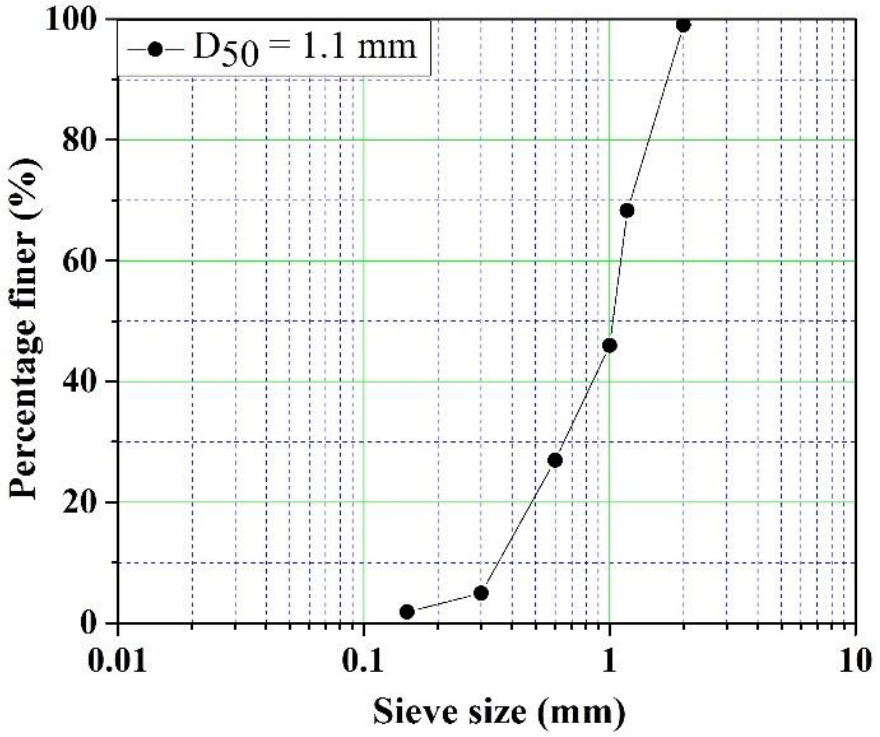

Figure 2.2 Grain size distribution of sediment.

2.3 Bed Preparation

Each experiment begins with the preparation of a plain channel bed. The sand was evenly distributed above the fine mesh over the 15.2 m length of the channel. A cutter on a trolley was used to prepare the plain bed as shown in figure 2.3. The gradual levelling of the sand bed began at the channel's downstream end and extra sand was carefully taken out from the channel. The water was emptied from the channel after the completion of each experiment. After allowing the exposed channel bed to dry naturally, the top layer of the sand bed was disturbed using trowels, and then the plain bed was prepared for the subsequent experiment. Experiments for objective 1 were conducted in the plain bed where vegetation partially covers the flume width. The details of vegetation distribution for objective 1 are discussed in detail in section 2.9.1. For objectives 2 and 3, compound channels were constructed on the plain bed which is discussed in the next section.

Figure 2.3 Snapshots of (a) metal cutter and (b) flat sand bed.

2.4 Preparation of compound channels

The compound channels are divided into 3 regions across the cross-section: Floodplain, Sloping and main channel region. Figure 2.4 demonstrates a rough illustration of a compound channel. The thesis considers three compound channels of 3 bank angles (θ): 31^0, 45^0 and 90^0. The compound channels were constructed after levelling the sand bed (section 2.3) by using angled cutters of 31^0, 45^0 and 90^0. The slopes of the compound channels were made rigid with an aluminum sheet and kept at a fixed angle. This was done so that the slopes did not break away because of the force of the flow. In the thesis, compound channels were constructed for objectives 2 and 3. The width of the floodplain region of all the rectangular and compound channels for all objectives is considered to be $0.5\,m$. For objective 1, experiments were

performed in the rectangular channel of figure 2.3. The distribution of vegetation for all the objectives is discussed in section 2.9. For the 2nd objective, a compound channel of 9 m length was constructed in the rectangular flume with $\theta = 31^0$. For the 3rd objective, compound channels of 10 m lengths were constructed in the flume with $\theta = 45^0$ and $\theta = 90^0$. Positions were marked from the downstream to upstream of the channel (figure 2.11 (a, b)) for better representation and understanding of the experiments, as will be seen while discussing vegetation distribution for all objectives.

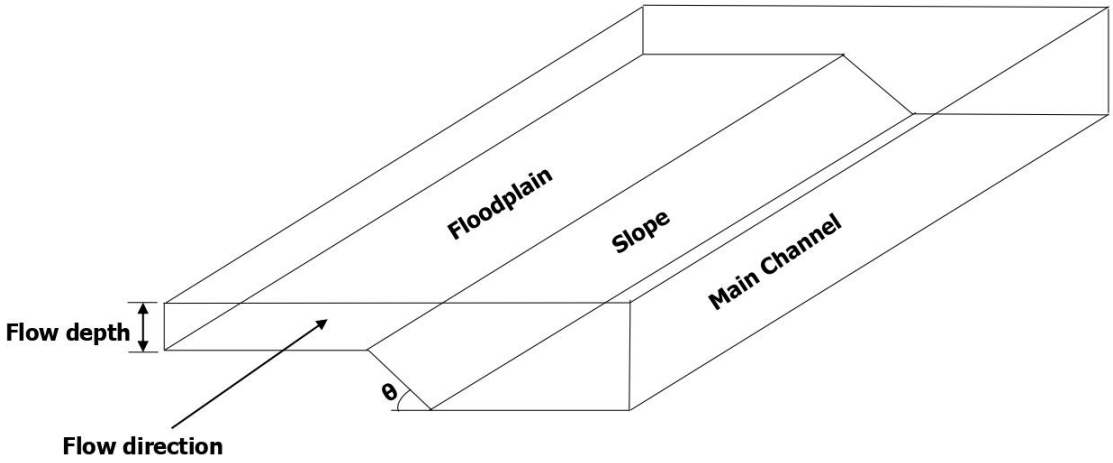

Figure 2.4 A rough illustration of a compound channel

2.5 Vegetation Collection

The present study considers two types of vegetation: Vetiver grass (*Chrysopogon zizanioides*) and Perennial reed (*Phragmites karka*). Vetiver grass can grow up to 5 ft tall, and the roots grow from 7 ft to 13 ft in depth. The vetiver grass is known for its very strong root system, so it is used in controlling bank erosion in many parts of the world. Various studies concerning vetiver grass and its uses in bank protection have been discussed by researchers (Focks and Algera, 2006; Islam *et al.*, 2013; Hamidifar *et al.*, 2018). The perennial reed is a reed species that resembles bamboo. It has a cylindrical stem whose culms grow up to 10 m. Both vegetation types used in the experiments are erect and rigid. It reduces analyzing complications when the flow encounters mixed vegetation. Furthermore, to compare vegetation effect with different heights, it is necessary to consider vegetation which can remain intact after encountering with high discharge flow which is only possible by considering rigid vegetation. The vetiver grass is used only for submerged vegetation, as will be seen in section 4 (objective

2). The perennial reed is used as both submerged and emergent vegetation, as will be seen in section 3 (objective 1) and 5 (objective 3).

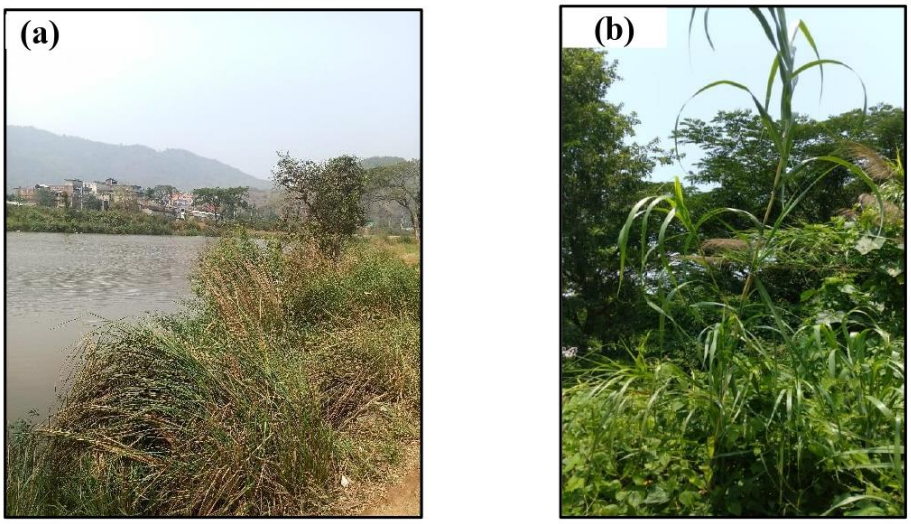

Figure 2.5 Snapshots of (a) Vetiver grass and (b) Perennial Reed from the sites of collection

2.6 Main Flow Discharge

A rectangular notch at the downstream collecting tank's end was used to measure the main channel discharge (Q) (Figure 2.6). The water passes through wooden baffles to give a smooth flow over the notch. The notch (L_n) has a 0.5 m width. The rectangular notch's coefficient of discharge (C_d) was found to be 0.82. The experiment's flow discharge was calculated as

$$Q = \frac{2}{3} C_d \sqrt{2g} L_n H^{\frac{3}{2}} \tag{2.2}$$

where g denotes acceleration due to gravity, and H denotes water head over the notch.

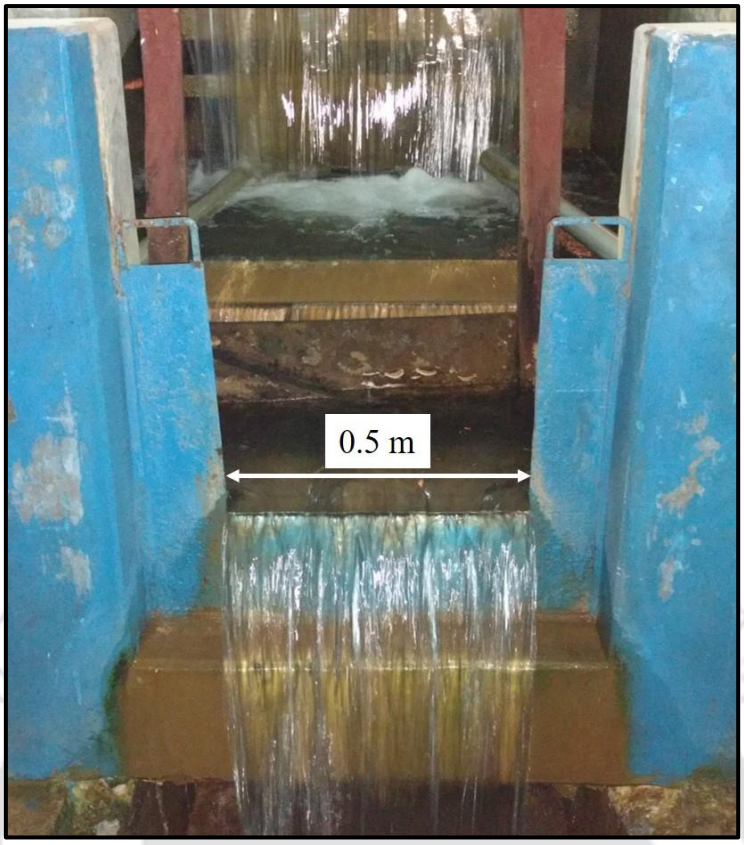

Figure 2.6 Discharge measurement at rectangular notch.

2.7 Flow depth measurement

The flow depth was measured using a digital point gauge in relation to the bed level (Figure 2.7). The liquid crystal display (LCD) on the point gauge has a least count of 0.01 millimeters. Before beginning the experiments, the instrument was reset to zero at the channel bed. The flow depth is measured after the flow is fully developed in the channel. The flow development in the present study for different objectives is discussed in section 2.9. The point gauge can move both longitudinally (along the flume length) and transversely (along the flume breadth) with the help of a movable trolley. In the thesis, the flow depth in the rectangular channel for objective 1 was $0.165\ m$ so that flow characteristics above the submerged vegetation region could be properly captured. For objective 2 and 3, floodplain (FP) depth of $0.1\ m$ and main channel (MC) depth of $0.2\ m$ with a $FP/MC = 0.5$ were considered. In river channels, this is the maximum ratio that is majorly found and previous researchers also considered $FP/MC \leq 0.5$ (Tominaga and Nezu, 1991; Dupuis *et al.*, 2017; Shan *et al.* 2018; Li *et al.*, 2021; Naghavi *et al.*, 2022).

Figure 2.7 Digital point gauge.

2.8 Velocity Measurement

For all objectives, the Nortek® Vectrino+ Acoustic Doppler Velocimeter (ADV) from Nortek AS in Norway was used to measure the instantaneous velocities at different locations of the flume. The ADV uses the Doppler shift principle to measure velocity. The Doppler effect refers to the apparent change in the wave's frequency brought on by the relative motion of the wave's source and the observer. The Vectrino+ used in the study is equipped with a single transmitter and four beam receivers (Figure 2.8). At the center is the transmitter, which sends out brief pairs of sound waves, hears their echoes, and then calculates the frequency shift of the returned sound. The transmitted waves are reflected by the sediment suspended in water because their average speed is equal to that of the water. The four sensors pick up the returned waves. The current study uses a fixed stem downward-looking probe as a velocimeter. The three flow velocities that the ADV measures—the X, Y, and Z directions—are then geometrically combined to yield the three orthogonal velocity components. The red rubber band used to denote the X-direction should always point in the direction of flow. During data gathering, the beam's proper alignment should be guaranteed. The Nortek ADV used in the experiment can capture velocity data $50\ mm$ from the central transmitter. That is why all data were collected near the channel bed to $50\ mm$ below the free surface. The velocimeter emits frequency of 10MHz and can sample data at rates up to a maximum of $200\ Hz$.

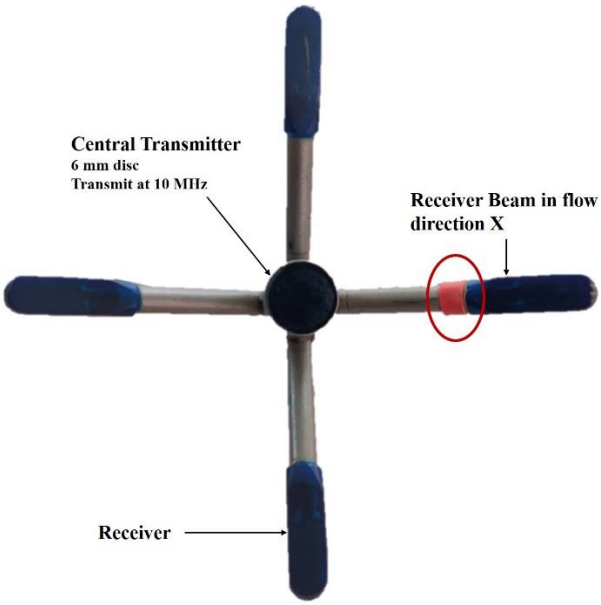

Figure 2.8 ADV transmitter and receivers.

At a specific location, the velocity measurement provides the current velocities u, v, and w in the streamwise (X), transverse (Y), and vertical (Z) directions, respectively. These instantaneous velocities $(u, v, \text{and } w)$ can be decomposed into time-averaged velocities $(\overline{u}, \overline{v}, \text{and } \overline{w})$ and fluctuating components of velocities $(u', v' \text{and } w')$ as $u = \overline{u} + u'$, $v = \overline{v} + v'$, and $w = \overline{w} + w'$, respectively. The time-averaged velocities are calculated as:

$$\bar{u} = \frac{1}{n}\sum_{i=1}^{n} u_i \ , \ \bar{v} = \frac{1}{n}\sum_{i=1}^{n} v_i \quad \text{and} \quad \overline{w} = \frac{1}{n}\sum_{i=1}^{n} w_i \tag{2.3}$$

The Vectrino plus created by Nortek®, captures the velocity signals in a computer system. The software records the correlation in percentage (%) and the signal-to-noise ratio (SNR) in decibels (dB).

Figure 2.9 Snapshot of Acoustic Doppler Velocimeter (ADV) capturing velocity measurement.

The ADV signal output consists of doppler noise, signal aliasing and other disturbances. The output is also affected by velocity shear in the near-bed of the channel. That's why, the collected data from ADV requires to be filtered. Islam and Zhu (2013) created a filtering code for separating the spikes by employing bivariate Kernel density estimation. The linear interpolation method is used to replace the removed spikes. This filtering method works better in high contamination regions than other filtering methods like Goring and Nikora (2002), Wahl (2003), Cea *et al.* (2007), etc. The present research involves taking data in vegetated regions, which are considered to be highly contaminated. So, the filtering method by Islam and Zhu (2013) is apt for the present research. Figure 2.10 shows the velocity power spectra of unfiltered and filtered time series at vegetated portion of an experimental case. It is observed that the filtered graph (red) aligns well with the Kolmogorov -5/3 law.

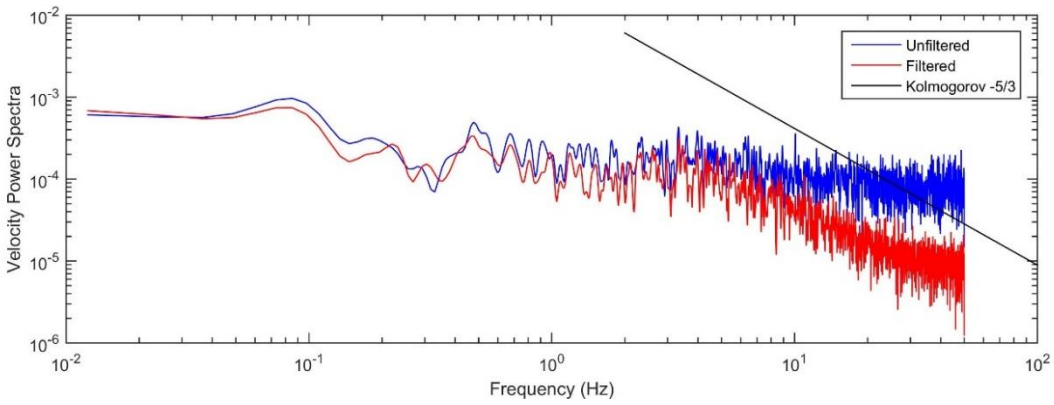

Figure 2.10 Velocity power spectra of unfiltered and filtered time series in vegetated portion

The accuracy of ADV data for the present study was checked by taking 15 readings of velocity data near the channel bed at $z/h = 0.1$. Table 2.1 displays the standard deviation and uncertainty where $\overline{u}, \overline{v}$ and $\overline{w}$ are the mean velocities and $\sqrt{\overline{u'u'}}, \sqrt{\overline{v'v'}}$ and $\sqrt{\overline{w'w'}}$ are the root mean square of fluctuating components of velocity. The $-\overline{u'w'}$ and $-\overline{u'v'}$ are the streamwise and transverse Reynolds shear stress respectively. The uncertainty of different flow characteristics is very low which shows that the instrument is accurate. The uncertainty percentage in the present study compliments other researchers like Rolland (1994), Hurther (2001) and Blanckaert (2010) who found uncertainty as less than 4% in the streamwise velocity, 15% for turbulent shear stress and 20% for turbulent normal stresses. In the present study, the ADV collected data with 100 Hz frequency for 2 minutes. The total number of samples acquired for a single reading is 12000. Garcia *et al.* (2005) assumed implicitly that 6000 samples were enough to describe turbulence. In the presence of vegetation, Dupuis *et al.* (2017) considered a sample time of 2 minutes for single velocity reading. Moreover, Horstman *et al.* (2018) and Tang *et al.* (2021) considered a sample time of 1 minute for velocity data in mixed vegetation (submerged and emergent) cases. Horstman *et al.* (2018) observed that 60 secs or 1 minute is long enough to obtain consistent flow characteristics.

Table 2.1 Accuracy of the ADV data

	u(m/s)	v(m/s)	w(m/s)	$\sqrt{\overline{u'u'}}$ (m/s)	$\sqrt{\overline{v'v'}}$ (m/s)	$\sqrt{\overline{w'w'}}$ (m/s)	$-\overline{u'w'}$ (m^2/s^2)	$-\overline{u'v'}$ (m^2/s^2)
Standard deviation	$2.42 * 10^{-3}$	$6.93 * 10^{-4}$	$3.58 * 10^{-4}$	$1.008 * 10^{-3}$	$3.38 * 10^{-4}$	$2.32 * 10^{-4}$	$1.008 * 10^{-3}$	$3.38 * 10^{-4}$
Uncertainty	0.0037	0.0013	0.00061	0.001565	0.000506	0.00038	$1.03 * 10^{-5}$	$1.9 * 10^{-5}$

2.9 Experimental Program

The experimental program consists of three sections. In section 2.9.1, the experimental program for objective 1 was performed in rectangular channels where different flow characteristics are compared when it encounters single-layered and multi-layered vegetation for two density distributions. Section 2.9.2 (objective 2) compares single-layered and multi-layered vegetation in compound channels. Section 2.9.3 (objective 3) focuses on the role of bank slopes of compound channels considering multi-layered floodplain vegetation.

2.9.1 Partially vegetated rectangular channel with single-layered and multi-layered vegetation

The vegetation in the flume is distributed over half the width ($0.5\ m$) of the flume to achieve a partially vegetated channel. Figures 2.11 (a, b) show the plan view distribution of vegetation in the flume. Perennial reed (*Phragmites karka*) was used for both submerged and emergent vegetation. It is erect and rigid. The vegetation was collected from the field as it is readily available. The perennial reeds used in the experiments were around $11 - 12\ mm$ in diameter. The reed was used as both submerged and emergent vegetation so that different emergence cases could be compared with less complexity. Two sets of experiments were considered for Partially Vegetated (PV) experiments. The length of the vegetation zone in both sets is $6\ m$ and is long enough to capture the flow effect of different vegetated cases in the floodplain and main channel regions. In the first set, the spacing in two vegetation line is $0.1\ m$ in the longitudinal and lateral directions, as seen in Figure 2.11 (a). This distribution for submerged vegetation can be considered to be in the sparse distribution according to Nepf (2011), where $ah_{veg} < 0.1$. Here, h_{veg} represents average vegetation height and a represents the frontal area given by $a = \frac{d}{\Delta S^2}$, where d is the diameter of single vegetation and ΔS is the average spacing between elements. In the second set, the vegetation patch distance in the lateral direction is $0.05\ m$ and densely packed compared to the first set (figure 2.11 (b)). In this case, $ah_{veg} \approx 0.1$, which falls under the transitional canopy (Nepf (2011)). Four different vegetation arrangements were considered in each set based on the submergence/emergence level. These include: 6 cm uniformly distributed vegetation, 3-6-9 cm multi-layered vegetation, 34% emergent vegetation and 100% emergent vegetation. For convenience, the experiments in the sparse vegetation (Figure 2.11 (a)) are denoted as PV 6 for equal height submerged vegetation, PV 3-6-9 for multi-layered vegetation, PV 34E for 34% emergent vegetation, and PV 100E for fully emergent vegetation cases. The term PV 3-6-9 means that height of vegetation is 3 cm, 6 cm and 9 cm which is spread throughout the submerged vegetated zone. Furthermore, PV 34E means that 34% of the whole vegetation is emergent. This was achieved by replacing the 3 cm height vegetation from 3-6-9 submerged with an emergent vegetation. The same process is repeated for PV 100E where all the vegetation is emergent in nature. In the same way, the second set of experiments from Figure 2.11 (b) are named by adding the 'D', which represents dense like PV D 6, PV D 3-6-9, PV D 34E, and PV D 100E. Illustrations of the plan view of the vegetation distribution of Set 1 and Set 2 are shown in Figure 2.12 for 1 m length in the downstream region. It is important to highlight that the vegetation distribution illustrated in

Figure 2.12, representing a 1 m section, is replicated throughout the 6 m vegetation zone. The representation of vegetation height for different dot colors is blue for 6 cm, yellow for 3 cm, green for 9 cm, and black for emergent vegetation (20 cm). The 'cross' sign in red represents the velocity measurement sections in the vegetated portion of the channel. Previous researches which considered heterogeneous vegetation height mainly focussed on double-layered vegetation (Huai *et al.*, 2014; Ahmad *et al.*, 2020; Tang *et al.*, 2021; Rao *et al.*, 2022). The present research considered triple-layered vegetation (PV 3-6-9 and PV 34E) to get a wider range of heterogeneity in height. The analysis of different flow characteristics for this vegetation set-up is discussed in detail in section 3.

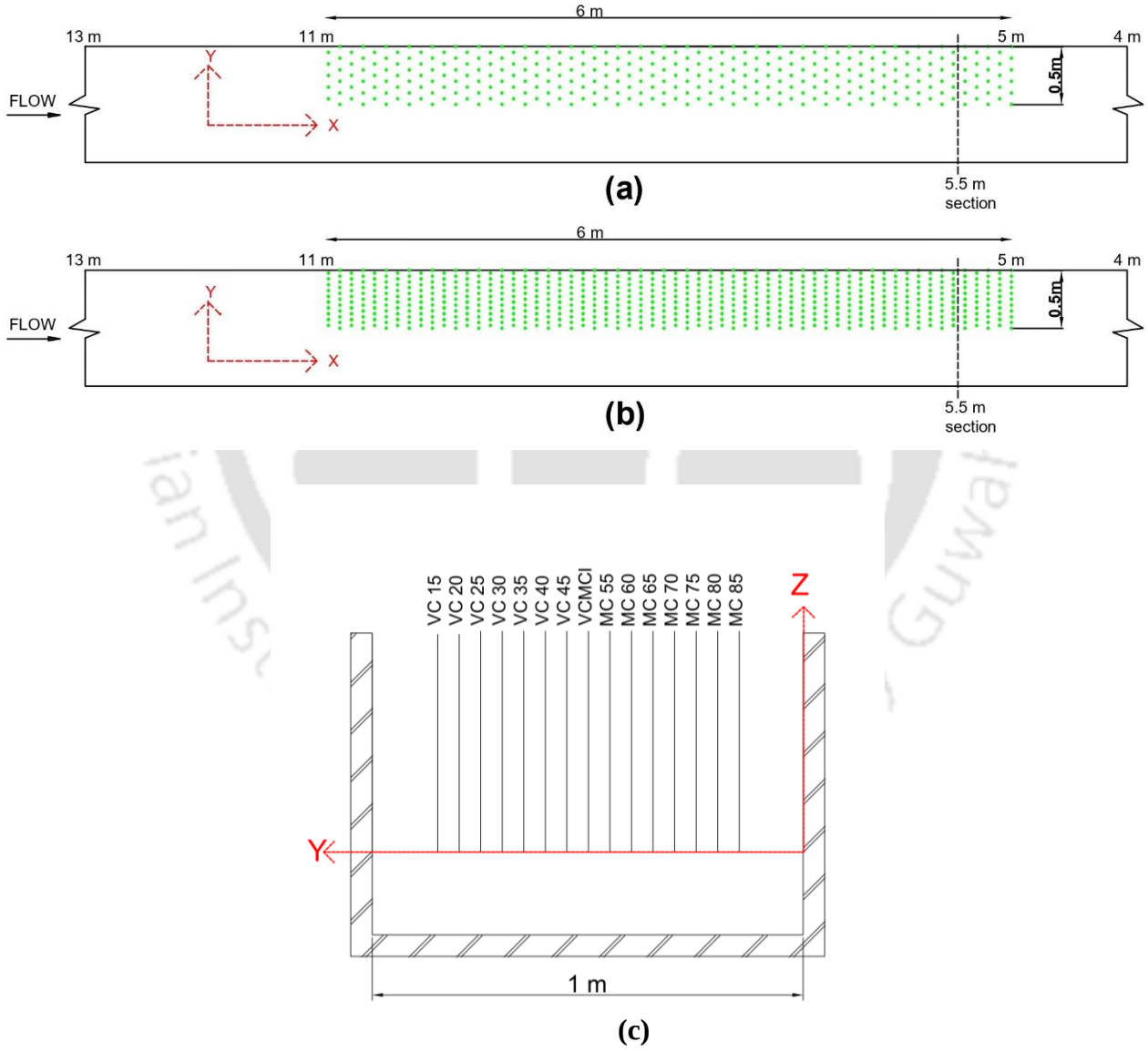

Figure 2.11 Plan view for vegetation (a) set-up1 and (b) set-up 2. (c) Velocity measurement locations at 5.5m cross-section for both set-ups

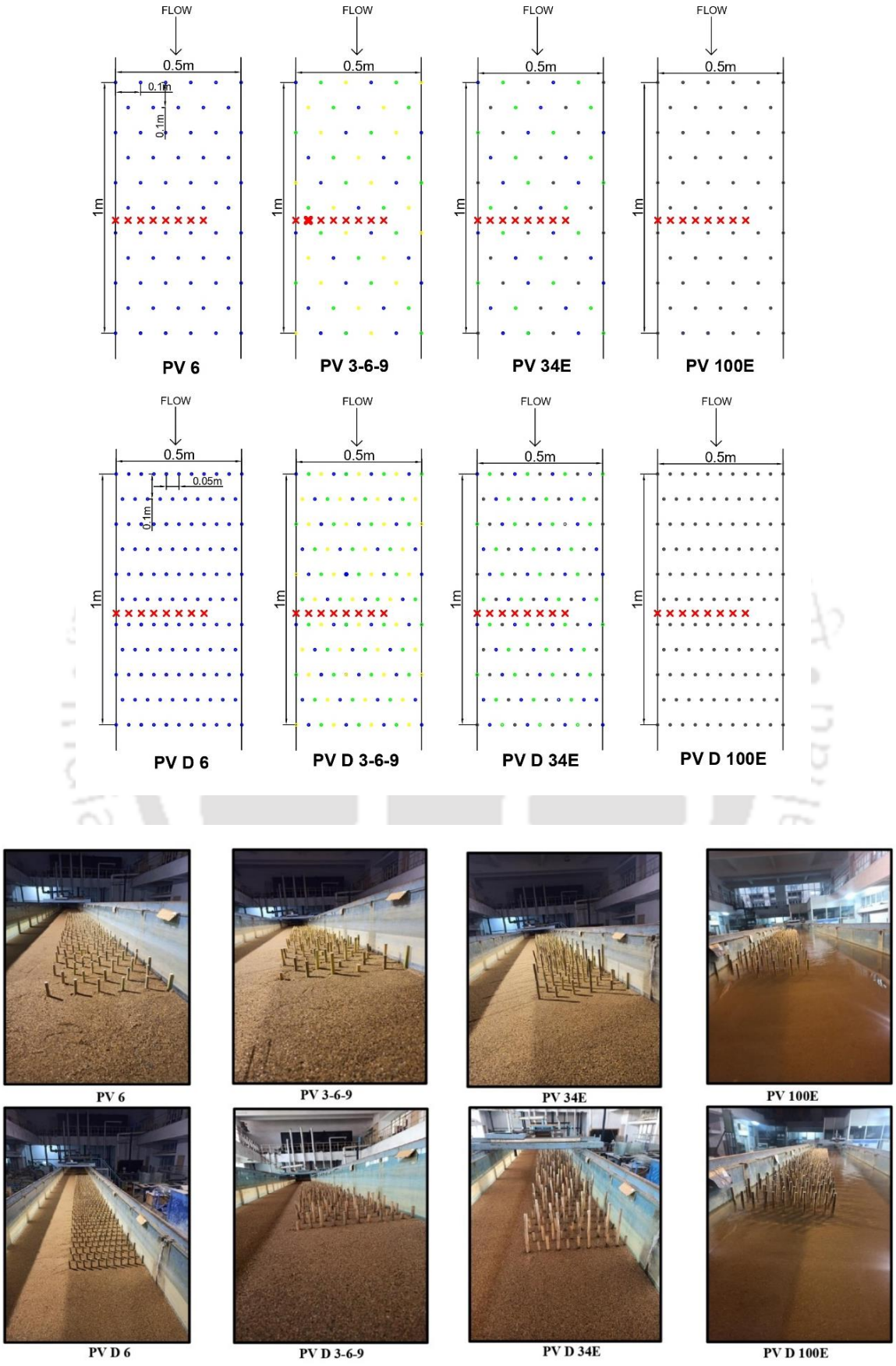

Figure 2.12 Plan view vegetation distribution and snapshots of experimental cases for Setups 1 and 2

Two separate discharges of 35 lps and 42 lps were considered for the first set and 35 lps for the second set. The flow depth in the channel measurement cross-section (5.5 m) was kept at 0.165 m for all the cases. The Reynolds number (Re) for the two discharges in the upstream region before it encountered the vegetation were 29461 and 35351, respectively. Inside the vegetated zone, the stem Reynolds number is calculated as: $Re_d = \frac{\bar{U}d}{\nu}$ where $\bar{U}$ is the depth-averaged velocity inside the vegetated zone, d is the diameter of the reed and ν is the kinematic viscosity. The stem Reynolds number (Re_d) for different vegetated cases lies in the range of 1000-1700 for Set 1 and 800-1400 for Set 2. In natural vegetation, stem-scale turbulence is observed at $Re_d > 200$ (Naden *et al.*,2006). Furthermore, $Re_d > 200$ has also been used in laboratories by many researchers (Liu *et al.*, 2008; Ricardo *et al.*, 2014; Liu *et al.*, 2021). The Froude number defined as $Fr = \frac{\bar{U}}{\sqrt{gy}}$, where y represents characteristic length. The Froude number is found to be less than 1 in the vegetated and main channel regions in both the sets for both discharges. The flow is fully turbulent and in a sub-critical condition.

For both setups (Figure 2.11 (a, b)), the instantaneous velocities at various sections of the 5.5 m cross-section were measured using an Acoustic Doppler Velocimeter (ADV) which was discussed in detail in section 2.8. The full development of flow at 5.5 m cross-section was ensured by adjustment length given by Zeng and Li (2014). They found after performing experiments in the presence of vegetation that flow development occurs within 2 m from the starting of vegetation zone. Yan *et al.* (2016) conducted experiments to observe the flow development in partially vegetated channels. They found that the adjustment length x_a for submerged vegetation is $0.7L_P$ and for emergent vegetation is $0.6L_P$, where L_P represents length of the vegetated zone. These adjustments lengths by Yan *et al.* (2016) are also consistent with Moltchanov *et al.* (2011) for submerged vegetation and Rominger and Nepf (2011) for emergent vegetation. In the present study, using Yan *et al.* (2016) adjustment length (x_a) formula, fully developed flow was attained at 4.2 m for submerged vegetation and 3.6 m for fully emergent vegetation from the beginning of vegetation. These adjustment lengths are ahead of the present study (5.5 m) suggesting fully developed flow at the measured cross-section of 5.5 m. In case of heterogeneous vegetation cases (3-6-9 submerged and 34% emergent) for Set 1 and Set 2, flow variations will occur inside the vegetation because of variable vegetation height. These variations are analysed in this study to understand the effect of variable vegetation height in and around vegetated and main channel interface. Moreover, for mixed vegetation cases of submerged and emergent vegetation, Horstman *et al.* (2018) and

Tang *et al*. (2021) collected readings at $3\,m$ and $2.7\,m$ from starting point of vegetation respectively. In the present study, the flow development was analyzed by measuring velocities in the middle of the main channel, from the upstream region at $10.5\,m$ to the downstream region at $5.5\,m$ (Figure 2.11(a, b)), as depicted in Figure 2.13(a). The results indicate that the velocity profile from $7\,m$ to $5.5\,m$ remains almost constant, implying the flow development in the measurement cross-section of $5.5\,m$ for the present study. In that $5.5\,m$ cross-section, measurements were taken at 15 verticals at a space of $50\,mm$, as shown in Figure 2.11 (c). At each vertical location, 25-30 measurements were obtained. The abbreviation VC represents the vegetated channel, and MC is the main channel. The number associated with VC and MC represents the distance (cm) from the left wall, as seen from the upstream of the channel. The abbreviation VCMCI denotes the vegetated channel and main channel interaction. It is situated in the mid-region of the flume width where the vegetated channel ends and the main channel starts. The details of the experimental cases for partially vegetated rectangular cases are given in Table 2.2. Furthermore, the convergence analysis of PV D 34E and PV D 100E at VC 45 and MC 55 sections were checked as shown in Figure 2.13(c, d). The convergence reading near the bed at $z/h \approx 0.1$ were considered by taking 12000 samples. The velocity and RSS were made non-dimensional by dividing with average streamwise velocity and streamwise RSS after 12000 samples respectively. It is observed that the velocity converges after 7000 samples and its error is less than 2%. On the other hand, the streamwise RSS in Figure 2.13(d) starts properly converging after 8000 samples for both PV D 34E and PV D 100E cases. Its error percentage is less that 10% after 8000 samples. Cassan *et al.* (2015) checked the convergence of velocity and RSS in a vegetated channel by considering 25 Hz and 56 sec. They found that the data convergences at 1400 samples with error less than 2% for longitudinal velocity and less than 10% for Reynolds stress. This shows that consideration of 12000 samples for the present study with $100\,Hz$ and $120\,s$ sampling rate are enough for achieving converged second-order flow statistics.

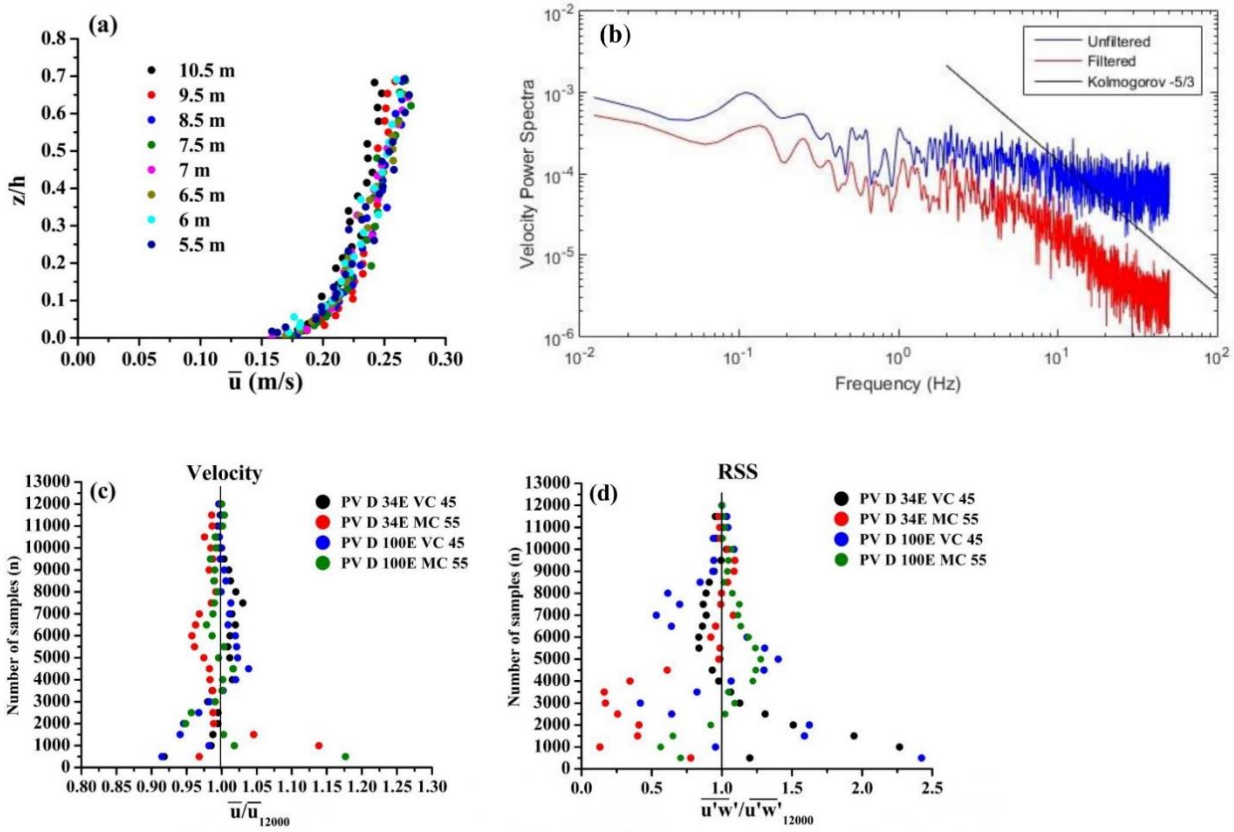

Figure 2.13 (a) Velocity change in the main channel from upstream to downstream region. (b) Velocity power spectra of unfiltered and filtered time series at $z/h \approx 0.03$ of PV 6 for $35lps$. Convergence analysis of (c) velocity and (d) streamwise RSS

Table 2.2 Description of various experimental cases for Section 2.9.1

	Discharge (litres/sec)	Experimental cases	Notation of Experimental cases	Vegetation height (h_{veg})	Vegetation density (N) (reeds/m^2)
1	35	Homogeneous height	PV 6	$6\ cm$	116
	42	Homogeneous height	PV 6	$6\ cm$	116
	35	Fully submerged heterogeneous height	PV 3-6-9	$6 \pm 3\ cm$	116
	42	Fully submerged heterogeneous height	PV 3-6-9	$6 \pm 3\ cm$	116
	35	Partially emergent heterogeneous height	PV 34E	$6, 9, 20\ cm$	116

	42	Partially emergent heterogeneous height	PV 34E	$6, 9, 20\ cm$	116
	35	Fully emergent homogeneous height	PV 100E	$20\ cm$	116
	42	Fully emergent homogeneous height	PV 100E	$20\ cm$	116
2	35	Dense homogeneous height	PV D 6	$6\ cm$	231
	35	Dense fully submerged heterogeneous height	PV D 3-6-9	$6 \pm 3\ cm$	231
	35	Dense partially emergent heterogeneous height	PV D 34E	$6, 9, 20\ cm$	231
	35	Dense fully emergent homogeneous height	PV D 100E	$20\ cm$	231

2.9.2 Single-layered and multi-layered floodplain vegetated compound channel

A compound channel of $9\ m$ length was constructed for objective 2 in the rectangular flume from 13m to $4\ m$ which was discussed in section 2.4 and shown in Figure 2.14. Vegetation was distributed in the floodplain region in a staggered manner from $11\ m$ to $5\ m$ in the flume. For this objective, vetiver grass and perennial reed were used for submerged and emergent vegetation respectively (Figure 2.15). Two sets of experiments were conducted on the compound channel. In Set 1, the vegetation zone was uniformly distributed, which implies that the distance between vegetation patches is equal throughout the vegetated zone. In Set 2, it was non-uniformly distributed, meaning that the distance between vegetation patches varies in the vegetated zone. No-vegetation cases where the flow was allowed to move without vegetation in the floodplain zone were performed for both discharges. In Set 1, the spacing between two vegetation patches was $10\ cm$ center to center (c/c) from $11\ m$ (Upstream) to $5\ m$ (Downstream) in the flume. It consists of 3 experimental cases according to the height of vegetation in the floodplain: a single-layered (6cm submerged) and two multi-layered vegetation cases (3-6-9cm submerged and 34% emergent). The multi-layered vegetation comprises three layers of vegetation height of $3\ cm$, $6\ cm$, and $9\ cm$ in one case and 34%

emergent vegetation where the heights of vegetation were $6\,cm$, $9\,cm$ and $15\,cm$. For convenience, the experiments in the uniform setup are denoted as U 6 for uniform single-layered vegetation, U 3-6-9 for uniform multi-layered vegetation and U 34E for 34% emergent vegetation. The Set 2 experiments were divided into three vegetation zones with different spacing between vegetated patches in these zones as shown in Figure 2.14(b). Flow occurs from the sparsely vegetated portion upstream to the denser region downstream of the flume. This was done to achieve non-uniformity in spacing in the vegetated floodplain. The spacing between two vegetation patches in these three vegetated zones from upstream to downstream was $20\,cm$, $15cm$, and $10cm$, respectively. The cases performed for Set 1 were repeated for Set 2, i.e., single-layered and multi-layered submerged vegetation. In addition to that, 2 new experiments were added namely: 67% emergent and 100% emergent cases. For convenience, the experiments for non-uniform setup are named as: NU 6, NU 3-6-9, NU 34E, NU 67E and NU 100E. Detailed explanation of the experiments and distribution of vegetation is shown in Figures 2.14 and 2.15 and Table 2.3.

Velocity readings were collected by ADV in the compound channel at upstream (9.5m), middle (7.5m) and downstream (5.5m) section of vegetation zone (Figure 2.14 (a) and (b)). Readings were taken at six critical regions across the cross-sections, as shown in Figure 2.14 (c). The notations at each section are denoted as follows: FP 20 means floodplain at 20cm from the left wall of the flume as seen from upstream, FP 35 is floodplain at 35cm from the left wall, SFPI denotes Slope Floodplain Interaction, SM denotes slope mid, SE is Slope end, and MC denotes the main channel of the compound channel. The average flow depth in the floodplain and main channel was considered to be $0.1\,m$ and $0.2\,m$ respectively.

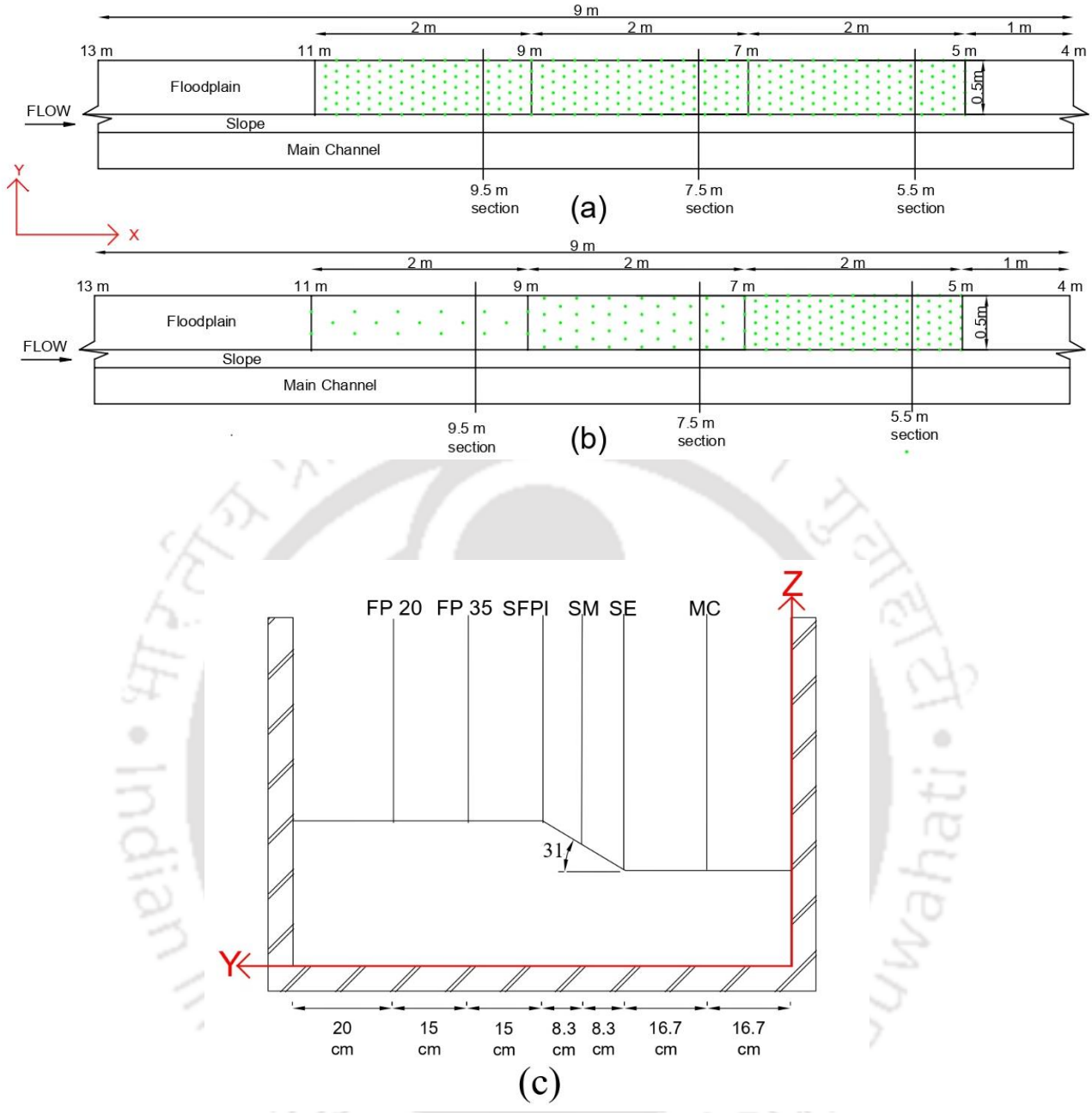

Figure 2.14 Vegetation set up of (a) Set 1 and (b) Set 2. (c) Velocity reading at 9.5m, 7.5m and 5.5m test sections for Set 1 and Set 2

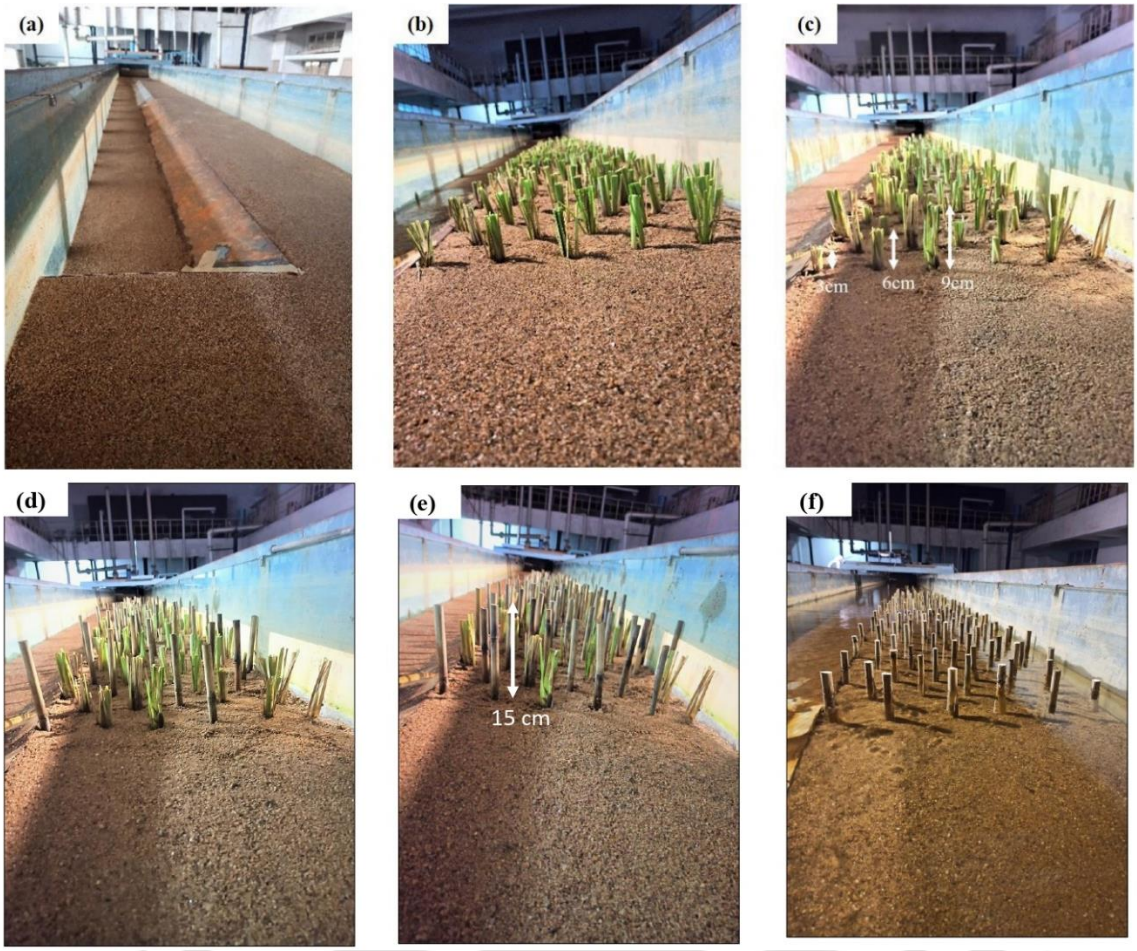

Figure 2.15 Snapshots of 31^0 bank angle compound channels (a) no-vegetation (b) 6cm uniform vegetation (c) 3-6-9cm submerged vegetation (d) 34 percent emergent vegetation (e) 67 percent emergent vegetation (f) 100 percent emergent vegetation

Table 2.3 Description of different experimental cases for Section 2.9.2

Set	Discharge (litres/sec)	Experimental cases	Notation of Experimental cases	Vegetation distribution type
	20	No-vegetation	NV	Nil
	35	No-vegetation	NV	Nil
1	20	6cm uniform vegetation	U 6	Uniform single-layered
	20	3-6-9cm Submerged	U 3-6-9	Uniform multi-layered

	20	34 percent emergent vegetation	U 34E	Uniform multi-layered
	35	6cm uniform vegetation	U 6	Uniform single-layered
	35	3-6-9cm Submerged	U 3-6-9	Uniform multi-layered
	35	34 percent emergent vegetation	U 34E	Uniform multi-layered
2	20	6cm uniform vegetation	NU 6	Non-Uniform single-layered
	20	3-6-9cm Submerged	NU 3-6-9	Non-Uniform multi-layered
	20	34 percent emergent vegetation	NU 34E	Non-Uniform multi-layered
	20	67 percent emergent vegetation	NU 67E	Non-Uniform multi-layered
	20	100 percent emergent vegetation	NU 100E	Non-Uniform single-layered
	35	6cm uniform vegetation	NU 6	Non-Uniform single-layered
	35	3-6-9cm submerged	NU 3-6-9	Non-Uniform multi-layered
	35	34 percent emergent vegetation	NU 34E	Non-Uniform multi-layered
	35	67 percent emergent vegetation	NU 67E	Non-Uniform multi-layered
	35	100 percent emergent vegetation	NU 100E	Non-Uniform single-layered

2.9.3 Multi-layered floodplain vegetated channel with varying bank slopes

Compound channels of $10\,m$ lengths were constructed in the flume for objective 3. The compound channels were constructed from $3\,m$ (downstream) to $13\,m$ (upstream) of the flume (figure 2.16). Two sets of experiments were considered for the study. In Set 1, the bank angle of the compound channel was considered to be 45^0 while for Set 2, 90^0 bank angle was considered as seen in Figure 2.16 and Figure 2.17. The bank angles (45^0 and 90^0) chosen for the study is greater than the angle of repose of the sand (31.1^0). The floodplain width of both sets of compound channels was considered to be $0.5\,m$ to get the same flow effect from the floodplain region for various experimental cases. The slopes in both cases were fixed using the aluminium sheet, as seen in Figure 2.17.

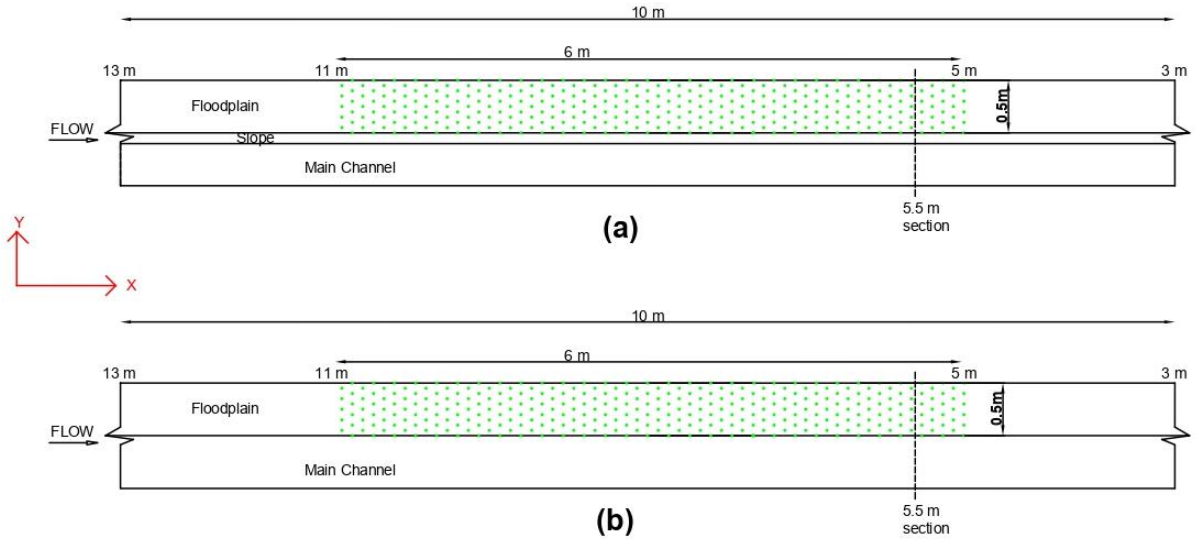

Figure 2.16 Plan view for vegetation (b) Set-up $1/45^0$ bank slope and (c) Set-up $2/90^0$ bank slope compound channel

Figure 2.17 Snapshots of Experimental cases for Set-up 1/ 45^0 bank slope and Set-up 2/90^0 bank slope compound channel

The vegetation used in the floodplain of the experiments for this objective is perennial reed (*Phragmites karka*). The vegetation is rigid and erect in nature. The same vegetation was used for both submerged and emergent vegetation to compare different experimental cases with less complications. Perennial reeds of cylindrical shape were employed in the experiments. By using the same diameter (1.1 cm) for all plants, it is possible to focus entirely on the effects of vegetation height on the channel's overall flow. The length of the vegetation zone considered in the floodplain region is 6 m (figure 2.16) which is the same as observed in sections 2.9.1 and 2.9.2. The distance between vegetation patch lines is 0.1 m along the width and length of the vegetation zone, as shown in Figure 2.18. The whole vegetation zone is staggered in nature. Multi-layered vegetation is considered for the study, meaning that the height of vegetation patches changes throughout the floodplain vegetation zone. In Set 1/45^0 bank slope of the compound channel, three experimental cases with different vegetation arrangements were considered. The cases are no vegetation (NV), multi-layered submerged vegetation (3-6-9 submerged), and multi-layered partially emergent cases (34% emergent). The same cases were repeated for Set 2/90^0 bank slope of the compound channel. The snapshots of the experimental

cases are shown in Figure 2.17. The distribution of multi-layered vegetation is shown in a rough illustration for 1 m vegetation length in Figure 2.18(a, b). The vegetation distribution that is shown in Figure 2.18 for 1 m is followed for the whole vegetation zone of 6 m. The distribution of vegetation in this section is similar to that observed in Figure 2.12 from section 2.9.1 for Set 1. However, the difference between the two cases is that experiments from section 2.9.1 were performed in rectangular channels, whereas in this section, experiments were performed in compound channels with different bank angles. Experimental cases for Set 1 are named 45 NV, 45 3-6-9 and 45 34E for simplicity. Similarly, for Set 2, cases are named as 90 NV, 90 3-6-9 and 90 34E. Two discharges of 35 lps and 42 lps were considered for each set. The Reynolds number (Re) in the compound channel for 35 lps and 42 lps for both setups is around 30000 and 35000, respectively. The flow is also in sub-critical condition as the Froude number is less than 1 for all cases. The flow depths (FD) in the floodplain (FP) and main channel (MC) were considered to be 0.1 m and 0.2 m, respectively, for all the experimental cases. The different experimental case details are shown in Table 2.4.

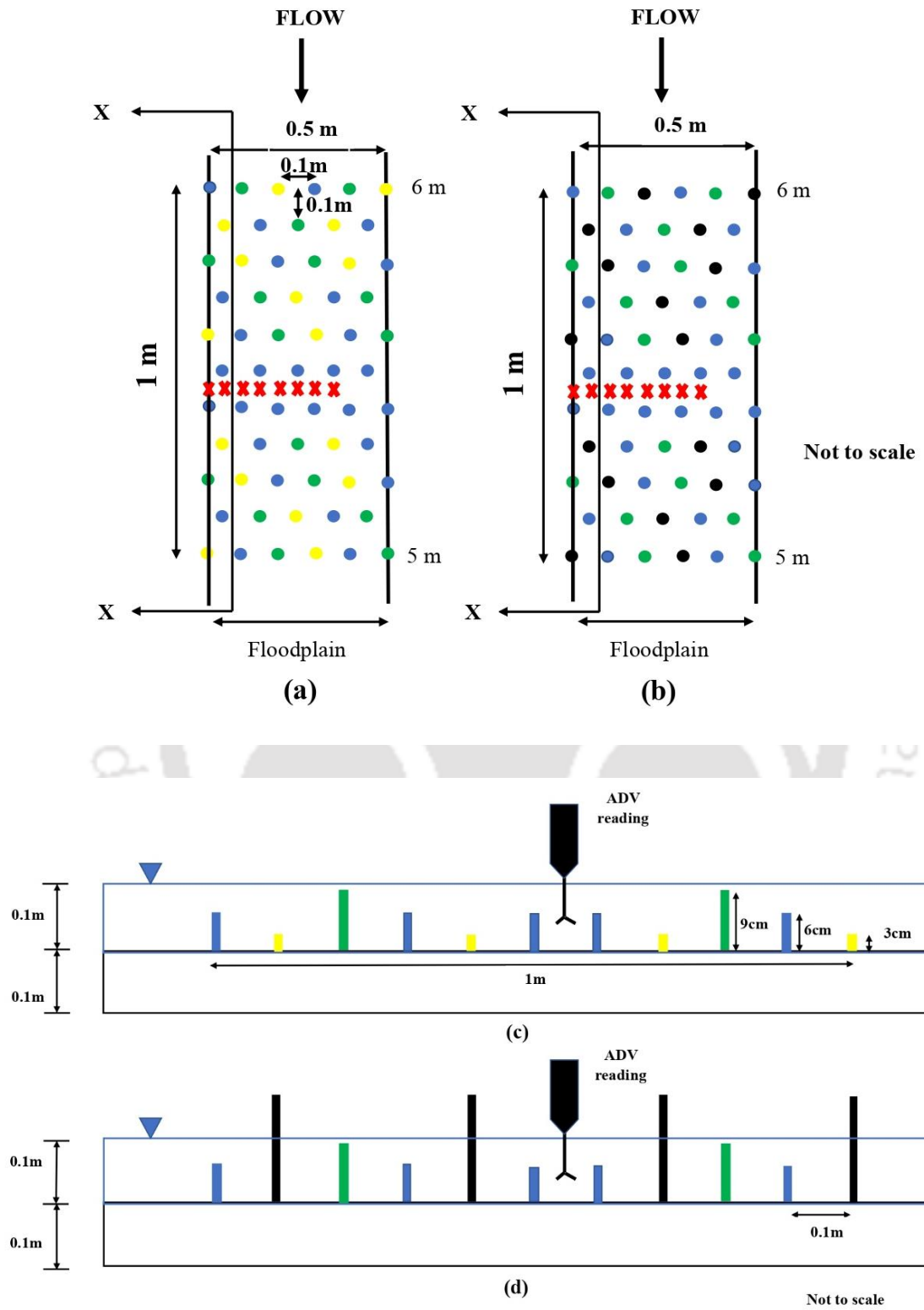

Figure 2.18 A rough illustration of plan view of vegetation arrangements in the floodplain for (a) 3-6-9 submerged and (b) 34% emergent vegetation for both set ups. Side view or X-X section of vegetation in the floodplain for (c) 3-6-9 submerged and (d) 34% emergent vegetation for both set ups.

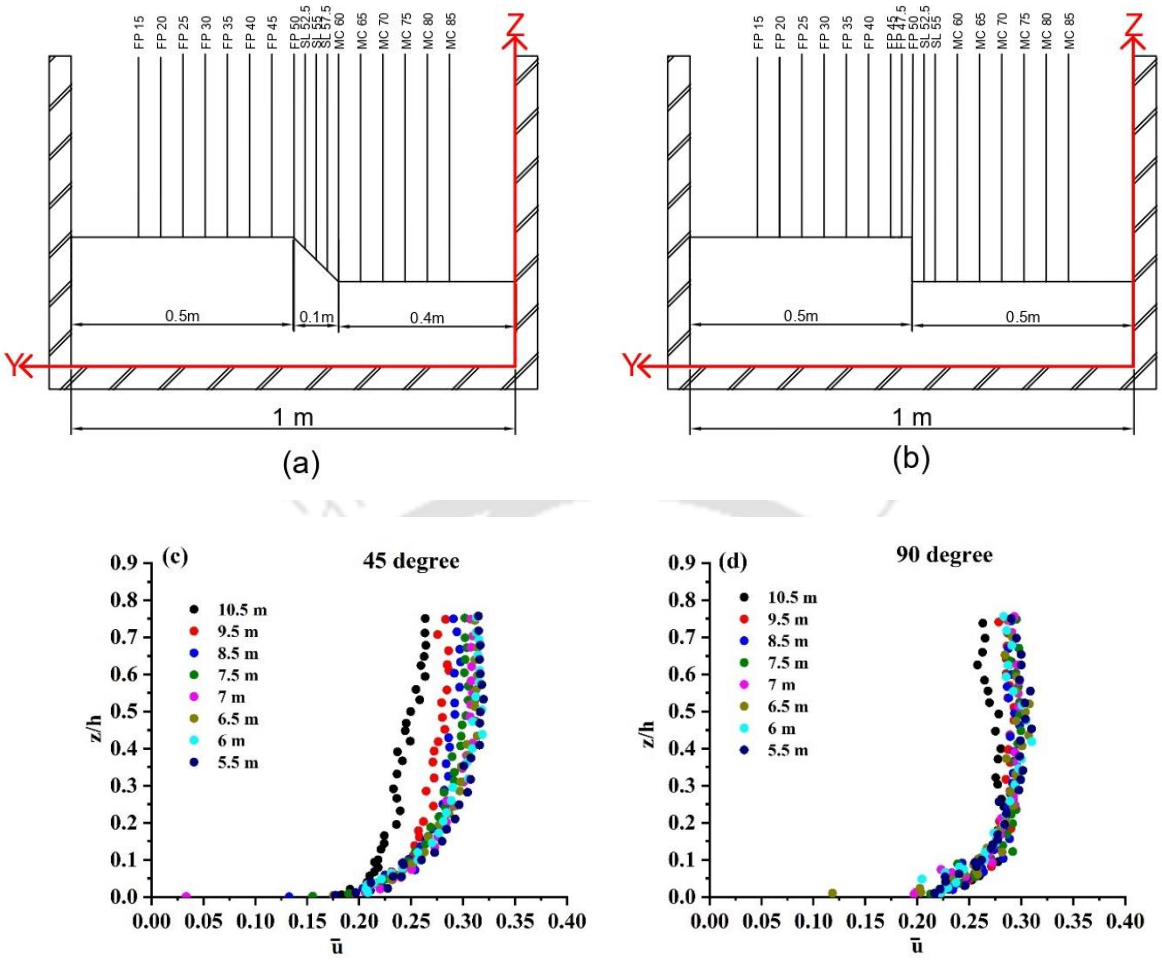

Figure 2.19 Different sections in the 5.5 m cross-section where ADV reading was captured for (a) Set-up 1/45^0 bank slope and (b) Set-up 2/90^0 bank slope compound channel. Velocity change in main channel from upstream (10.5 m) to downstream (5.5 m) for (c) Set-up 1/45^0 bank slope and (d) Set-up 2/90^0 bank slope compound channel.

The velocity reading was captured by Acoustic Doppler Velocimeter (ADV) after the initial sediment movement was stopped and the flow was fully developed in the channel. The velocity reading for both setups was performed at 5.5 m cross-section, which is situated in the downstream of the vegetated zone (figure 2.16(a, b)). Reading in the 5.5 m cross-section was also collected for rectangular partially vegetated channel in section 2.9.1 and 31^0 compound channel in section 2.9.2. Figure 2.19 (c) and 2.19 (d) shows the change of velocity profile in the middle of main channel from upstream (10.5 m) to downstream (5.5 m) for the 45^0 and 90^0 bank slope compound channel respectively. It is observed that velocity profile remains almost constant after 7 m section for both bank angles. This suggests that the flow is fully developed in the measurement section (5.5 m) of the present study for both bank angles. The

velocity reading at 5.5 m cross-section was captured at 17 vertical sections for both setups, as shown in Figure 2.19 (a, b). The distance between the two vertical sections is 5 cm apart in the floodplain and main channel. However, in and around the slopes, the distance is 2.5 cm as it acts as the flow interaction region between the main channel and the floodplain of the channel. The notations in Figure 2.19 (a, b) are: FP stands for floodplain; SL is slopes and MC is the main channel. The number adjacent to the abbreviation denotes the distance in 'cm' from the left wall as seen from upstream of the flume. It is crucial to note that even though SL 52.5 and SL 55 are located at Set 2's main channel (figure 2.19(b)), they are referred to as "SL" so that Set 2 and Set 1 can be compared without any misunderstanding. At each vertical section, more than 20, 25, and 30 readings were captured at the floodplain, slopes, and main channel respectively. The red cross sign in Figure 2.18 (a, b) shows the sections in the floodplain where ADV reading was captured for 3-6-9 and 34E cases for both setups. The vegetation preceding and succeeding the red cross sign is blue (6 cm) for all the vegetation cases (figure 2.18). This was done to ensure that the identical condition is seen in all experimental scenarios right before and after the velocity measurement locations.

Table 2.4 Description of various experimental cases for Section 2.9.3

Set	Bank Slope	Re	FP depth (m)	MC depth (m)	Discharge (lps)	Experimental cases	Notation of experimental cases
1	45^0	30000	0.1	0.2	35	No vegetation	45 NV
		30000	0.1	0.2	35	Multi-layered fully submerged	45 3-6-9
		30000	0.1	0.2	35	Multi-layered partially emergent	45 34E
		35000	0.1	0.2	42	No vegetation	45 NV
		35000	0.1	0.2	42	Multi-layered fully submerged	45 3-6-9
		35000	0.1	0.2	42	Multi-layered partially emergent	45 34E
2	90^0	30000	0.1	0.2	35	No vegetation	90 NV
		30000	0.1	0.2	35	Multi-layered fully submerged	90 3-6-9
		30000	0.1	0.2	35	Multi-layered partially emergent	90 34E
		35000	0.1	0.2	42	No vegetation	90 NV
		35000	0.1	0.2	42	Multi-layered fully submerged	90 3-6-9
		35000	0.1	0.2	42	Multi-layered partially emergent	90 34E

3 Hydrodynamics of partially vegetated channel with multi-layered vegetation[1]

3.1 Introduction

The flow mechanism of river channels spanning both the main channel and floodplain regions is better understood by laboratory research that takes into account the partial vegetation cover of the flume width. The main channel flow is influenced by vegetation in the floodplain region during the high flood season (Dupuis *et al.*, 2017; Proust and Nikora, 2019; Mehrabani *et al*., 2020; Modalavalasa et al., 2023). The interaction between the floodplain and main channel regions is known to exhibit high turbulence due to the significant momentum exchange taking place (Nezu and Onitsuka, 2001; Truong *et al.*, 2019; Caroppi *et al.*, 2021; Shi *et al.*, 2023; Yan *et al.*, 2022). However, the strength of the momentum exchange depends upon factors like distribution, submergence level and density of vegetation. This chapter investigates the role of vegetation height and density on flow characteristics in partially vegetated channels. The study considers single-layered and multi-layered vegetation with three different vegetation heights for multi-layered vegetation to obtain a wider range of height heterogeneity. In previous studies, only two different heights were considered for heterogeneous vegetation (Huai *et al*., 2014; Ahmad *et al.*, 2020; Tang *et al*., 2021; Rao *et al.*, 2022). Previous studies have analyzed transverse Reynolds shear stress (RSS) and quadrant analysis as means to comprehend the intricate interaction between vegetated and main channel regions in partially vegetated channels (Nezu and Onitsuka, 2001; Truong *et al.*, 2019; Truong and Uijttewaal, 2019; Koken and Constantinescu, 2021; Caroppi *et al.*, 2021; Taborda *et al.*, 2022; Shi *et al.*, 2023). However, these studies did not thoroughly examine streamwise RSS, which is crucial for understanding turbulence in the vertical plane. This chapter analyzes both streamwise and transverse RSS to explain the role of vegetation emergence and density in determining overall flow. It will specifically investigate the influence of vegetation emergence and density within the vicinity of the intersection between the vegetated channel and the main channel. Additionally, the chapter also expands on quadrant analysis to understand bursting events in

[1] Barman, J., Kumar, B., & Balachandar, R. (2024). Hydrodynamics in Channels with Partial Vegetation Cover: Investigating the Effects of Homogeneous and Heterogeneous Vertical Vegetation Distribution. Advances in Water Resources, 104642. https://doi.org/10.1016/j.advwatres.2024.104642

regions of heterogeneous vegetation height, expanding upon previous studies that considered only uniform vegetation height (Afzalimehr *et al.*, 2011; Devi and Kumar, 2016; Truong *et al.*, 2019; Li *et al.*, 2020; Wang *et al.*, 2022; Shi *et al.*, 2023). By conducting the above-mentioned analysis, a deeper understanding of the flow dynamics present in areas with submerged and emergent vegetation can be achieved.

3.2 Velocity distribution

The arrangement of vegetation and its geometry, coupled with the submergence level determine the flow nature in the partially vegetated channel. Figure 3.1 displays the contours of streamwise mean velocity ($\bar{u}$) for the partially vegetated scenarios with varying vegetation heights and emergence levels. To make comparisons across different test cases, the velocity values are non-dimensionalized by the average velocity (U) in the channel. The black vertical dotted line demarcates the vegetated channel (VC) from the main channel (MC). The horizontal dotted line in Figures 3.1(a) and 3.1(b) show the vegetation height (VH). The heights of different vegetation cases and velocity measuring locations for this chapter were explained in detail in section 2.9.1. In the heterogenous height/mulit-layered cases (Figures 3.1(c, d)), the vegetation height in the cross-section of the floodplain region is shown at different locations by short dashes and the notation 'VH'. The velocity distribution in a partially vegetated channel with uniform vegetation of height $0.06\ m$ on the floodplain is depicted in Figure 3.1(a). It is observed that velocity in the vegetated region of PV 6 (Figure 3.1(a)) is low for $z/h \lesssim 0.3$ due to the presence of the cylinder wakes, after which it increases towards the surface of water. It is crucial to acknowledge that the observed pattern of velocity distribution arises from the interaction between the vegetation and water flow. The presence of vegetation induces the formation of wakes behind the vegetation elements, thereby influencing the velocity distribution within the VC. Other researchers have noted a similar behavior (Kouwen *et al.*, 1969; Ikeda and Kanazawa, 1996; Carollo *et al.*, 2002; Nepf, 2012). This drag is influenced by frontal area of the vegetation which is also observed in Figure 3.1. The location of velocity increase in PV 6 remains consistent across the cross-sectional area of the floodplain region due to the uniformity of vegetation height within the channel. As the vegetation in PV 100E is emergent in Figure 3.1(b), the resistance from the vegetation elements completely characterizes the floodplain region. The velocity profile in VC of PV 100E is uniform throughout the flow depth. It is observed that velocity in the VC of PV 100E is lower compared to PV 6 as the height and frontal area in PV 100E is higher, providing more obstruction capacity in the VC.

Figures 3.1(c) and 3.1(d) show the velocity contours under the influence of multi-layered cases in the VC. The location of velocity increase in the VC is in accordance with the change in the height of the vegetation in the region. It is observed from PV 3-6-9 (Figure 3.1(c)) that velocity starts to increase at a lower z/h ratio when the vegetation height is short ($0.03\ m$), whereas it starts to rise at higher location for longer vegetation ($0.09\ m$). The same behavior is also observed in the case of PV 34E (Figure 3.1(d)), with greater obstruction in the VC with the emergent vegetation height ($0.2\ m$). The vegetation height also affects the flow velocity in the MC, as seen in Figure 3.1. The velocity in the MC is highest for PV 100E followed by PV 34E. The MC velocity in PV 3-6-9 is slightly higher than PV 6 even though the average frontal area for both cases is same in the VC. This can be attributed to the varying height of vegetation near the VCMCI location (VC 45), which impacts the flow velocity in the MC. In the case of PV 6, VC 45 is obstructed by $6\ cm$ height vegetation, whereas it is $9\ cm$ for PV 3-6-9 case. The higher frontal area in the intersection of VC and MC allowed for slightly higher velocity in the main channel. This finding was supported by examining the velocity profile of homogeneous height/single-layered (PV 6 and PV D 6) and multi-layered (PV 3-6-9 and PV D 3-6-9) at the middle of the MC, as depicted in Figures 3.2(b, d). At MC 75 location from Figure 3.2(b), there is an increase of 5.6% in depth-averaged velocity for PV 3-6-9 compared to PV 6. This percentage increases to 15.8% when the density in the VC increases (Figure 3.2(d)).

Figures 3.2(a) and 3.2(c) shows comparison of velocity profiles in the middle of the floodplain (location VC 25) for Set 1 and Set 2 of vegetation arrangements. It is observed that velocity profiles for PV 6, PV 3-6-9 and PV 34E at section VC 25 for both density arrangements show an increase in value from the top of vegetation towards the water surface. However, velocity profile of PV 100E and PV D 100E is uniform throughout the flow depth in the VC as the vegetated zone is fully emergent. The role of vegetation density in the MC is also observed in Figures 3.2(b) and 3.2(d), where there is a depth-averaged velocity increase of more than 25% for PV D 34E compared to PV D 3-6-9 (Figure 3.2(d)), whereas it is under 25% in case of Set 1 (Figure 3.2(b)). The velocity profiles of 100% emergent vegetation (green colour) at the MC 75 location from Figures 3.2(b) and 3.2(d) show that the location of maximum velocity is at $z/h \approx 0.3$. It is observed that as $z/h > 0.3$, the velocity in the 100% emergent case decreases slightly as it approaches the water surface. This velocity dip phenomenon in the MC zone was observed in simulated data by Choi and Kang (2006) and measured data by Shimizu and Tsujimoto (1994) while considering submerged vegetation. However, the dip phenomenon is not observed for submerged vegetation conditions in the present study. This absence of dip

phenomenon for submerged vegetation was also confirmed by Naot *et al.* (1996a) and Nezu and Onitsuka (2001). The dip phenomenon is only observed in fully emergent cases for both sets in the present study. Kirkgöz and Ardiçlioğlu (1997) showed velocity dip in open channel flow near the sidewall. However, in the present study the fully emergent vegetation acts as a sidewall which creates the dip phenomenon.

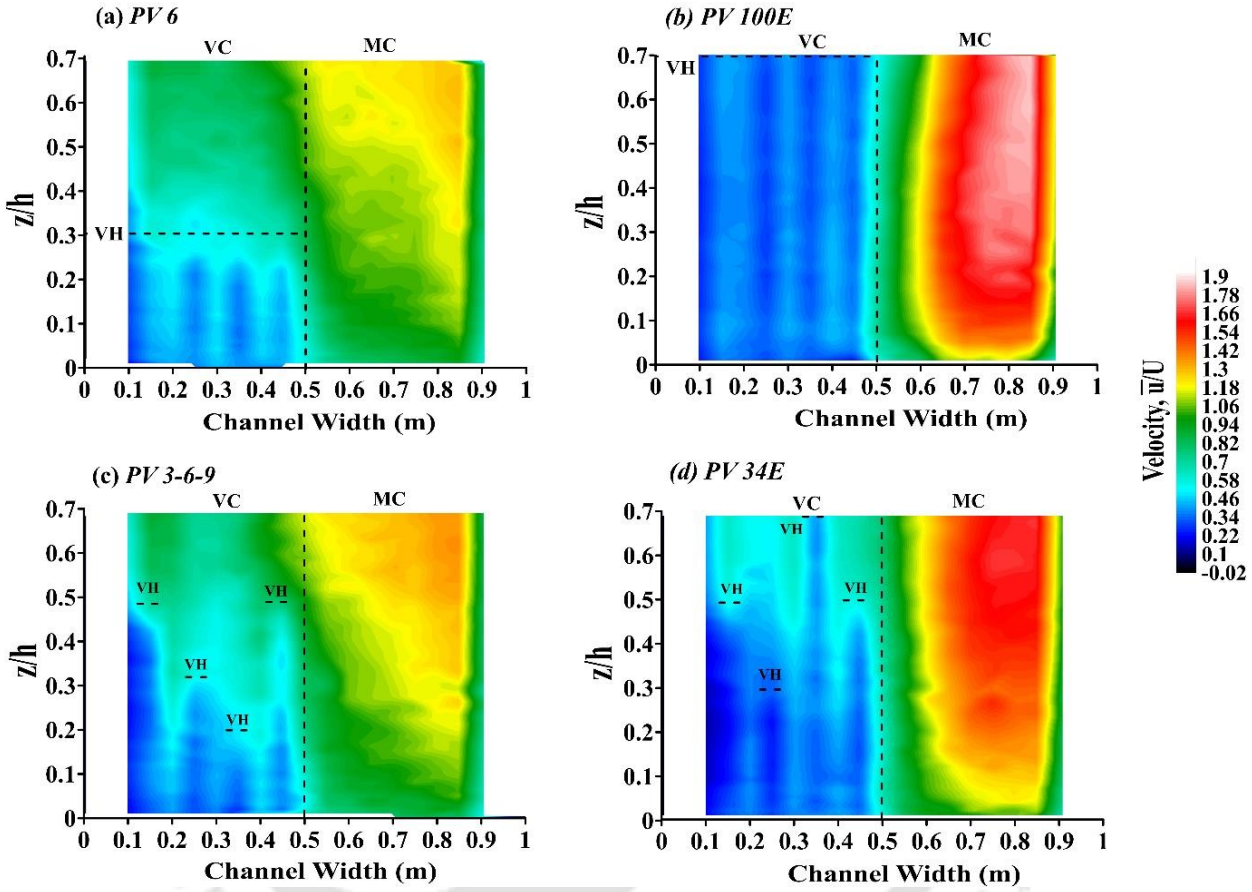

Figure 3.1 Velocity contours of partially vegetated cases of Set 1 for 35 *lps*

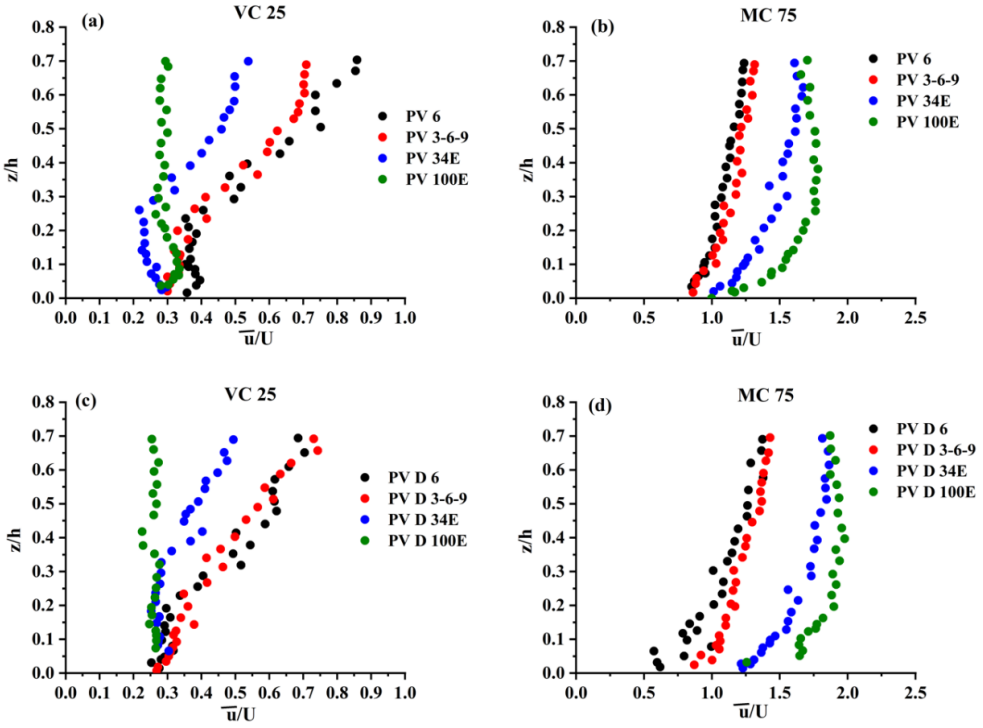

Figure 3.2 Velocity profile of partially vegetated cases at VC 25 and MC 75 sections for 35 lps

Figures 3.3(a) and 3.3(b) shows streamwise velocity profiles of fully emergent cases at different locations of MC for both sets. The maximum velocity location progressively shifts towards the water surface while moving from the MC 55 to the MC 85 section. It is observed that because of the dip phenomenon, positive gradient is observed near the channel bed and negative velocity gradient is observed near the water surface. The dip phenomenon in the main channel of emergent cases is prominent because of secondary circulations observed in the main channel of PV 100E and PV D 100E in Figure 3.3(c, d). Furthermore, in the vegetated zone of PV 100E and PV D 100E, negative transverse velocity dominates over vertical velocity showing the flow to move from the vegetated region to the main channel. This shows that the flow is two dimensional for emergent cases where only horizontal interaction is observed between the floodplain and main channel. Though hints of circulation are observed in the present study, further experimentation need to be done with different vegetation emergence and dense measurement spacing for proper qualitative assessment. Choi and Kang (2006) also mentioned that the dip phenomenon is important for streamwise RSS ($\overline{u'w'}/U^2$) near the VCMCI section as seen in Figure 3.4(b, f). It is observed that the magnitude of negative RSS decreases as one moves away from VCMCI section. The presence of these negative RSS near

the VCMCI section and its link to different bursting events will be discussed in detail in the subsequent sections.

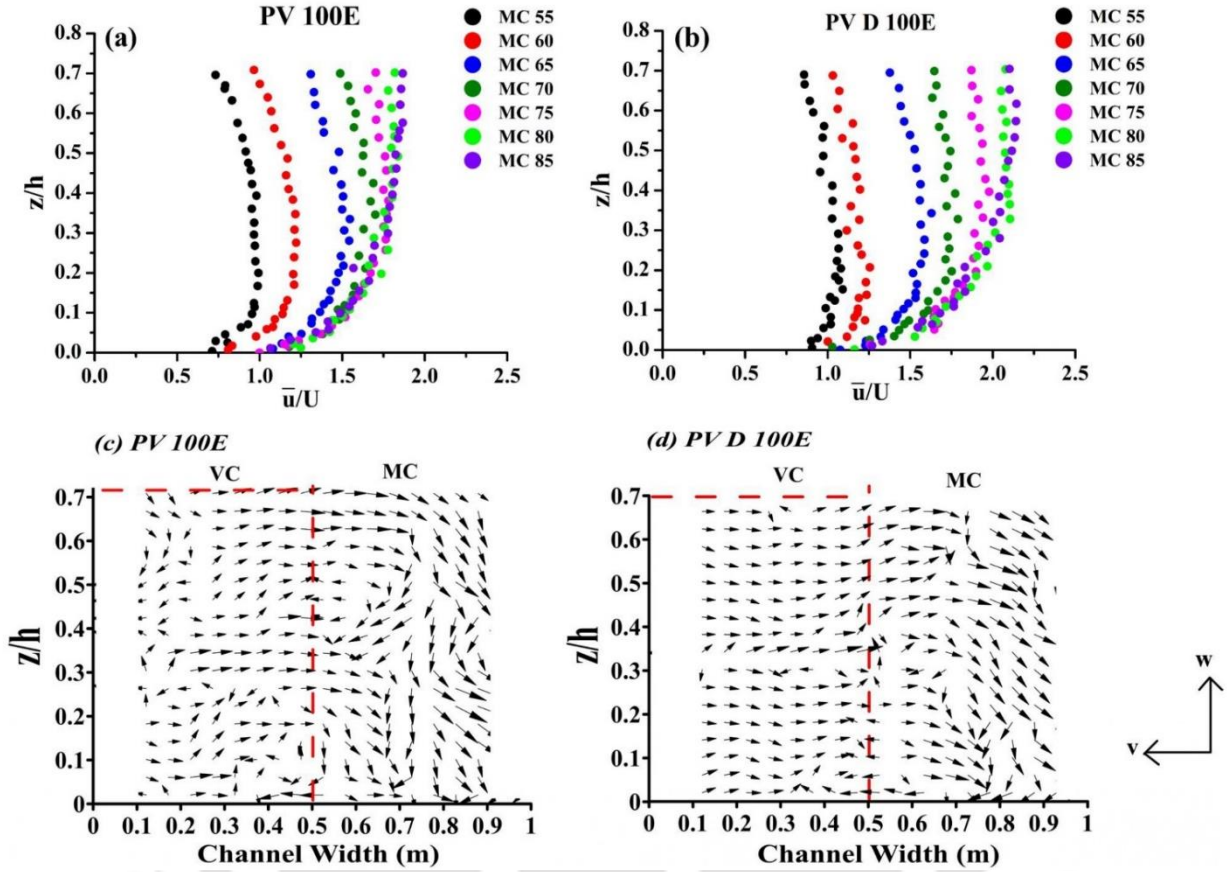

Figure 3.3 Transformation of velocity profile from MC 55 to MC 85 in the main channel of (a) PV 100E and (b) PV D 100E. Secondary flow direction for (c) PV 100E and (d) PV D 100E at the 5.5 m

3.3 Momentum exchange at the downstream cross-section of the vegetated channel

Figure 3.4 presents the normalized streamwise Reynolds shear stress (RSS) in the 5.5 m cross-section of the channel for different submergence and density conditions. The RSS in the uniform vegetation setup (Figure 3.4(a) and 3.4(b)) have uniform values at nearly the same location in the vegetated portion. The RSS for PV 6 in Figure 3.4(a) has larger values in the region $z/h = 0.3 - 0.6$ across the floodplain cross-section because of uniform vegetation height of $0.06\ m$. The same scenario is observed for PV 100E in Figure 3.4(b), where RSS is very low in the VC as all vegetation is above the water surface. However, the RSS in the VC of PV 3-6-9 (Figure 3.4(c)) reaches maximum at different locations compared to the PV 6 case. The reason is the combined influence of variable vegetation height in the vegetated portion of PV 3-6-9 which provides variable flow obstruction. The RSS reaches the highest magnitude

near the top of submerged vegetation. That is why the location of maximum RSS varies in PV 3-6-9 and PV 34E. The RSS behind $0.03\,m$ height vegetation in PV 3-6-9 indicates higher values at a lower height compared to $0.06\,m$ and $0.09\,m$ height vegetation. This pattern in the RSS is also observed in PV 34E (Figure 3.4(d)). The RSS for PV 34E is comparatively lesser compared to the PV 6 and PV 3-6-9 cases because of higher flow obstruction in the floodplain region of PV 34E case. The magnitude of RSS in the MC is also influenced by vegetation arrangement in the VC. The percentage of emergent vegetation in the vegetated portion is directly proportional to the magnitude of RSS in the MC. The RSS magnitude of PV 34E and PV 100E from $0.7 - 0.85\,m$ channel width at $z/h \lesssim 0.2$ is more compared to submerged cases of PV 6 and PV 3-6-9. This magnitude is enhanced with an increase of vegetation density in the VC as observed in Figures 3.4(f) and 3.4(h). Emergence of vegetation in the VC ensured negative RSS near the VCMCI location in the MC, which is evident from Figure 3.4(b, d). The negative RSS in the vicinity of VCMCI section shows the presence of outward and inward interactions. The magnitude of negative RSS is high for PV 100E as compared to PV 34E, which shows that vegetation emergence percentage is directly proportional to the magnitude of negative RSS in the MC. The penetration of negative streamwise RSS in the VC increases with high vegetation density and emergence as observed for PV D 100E in Figure 3.4(f). The negative streamwise RSS in PV D 100E shows high magnitude inside the VC till $0.2\,m$ from VCMCI and is observed to enter deep inside the floodplain region.

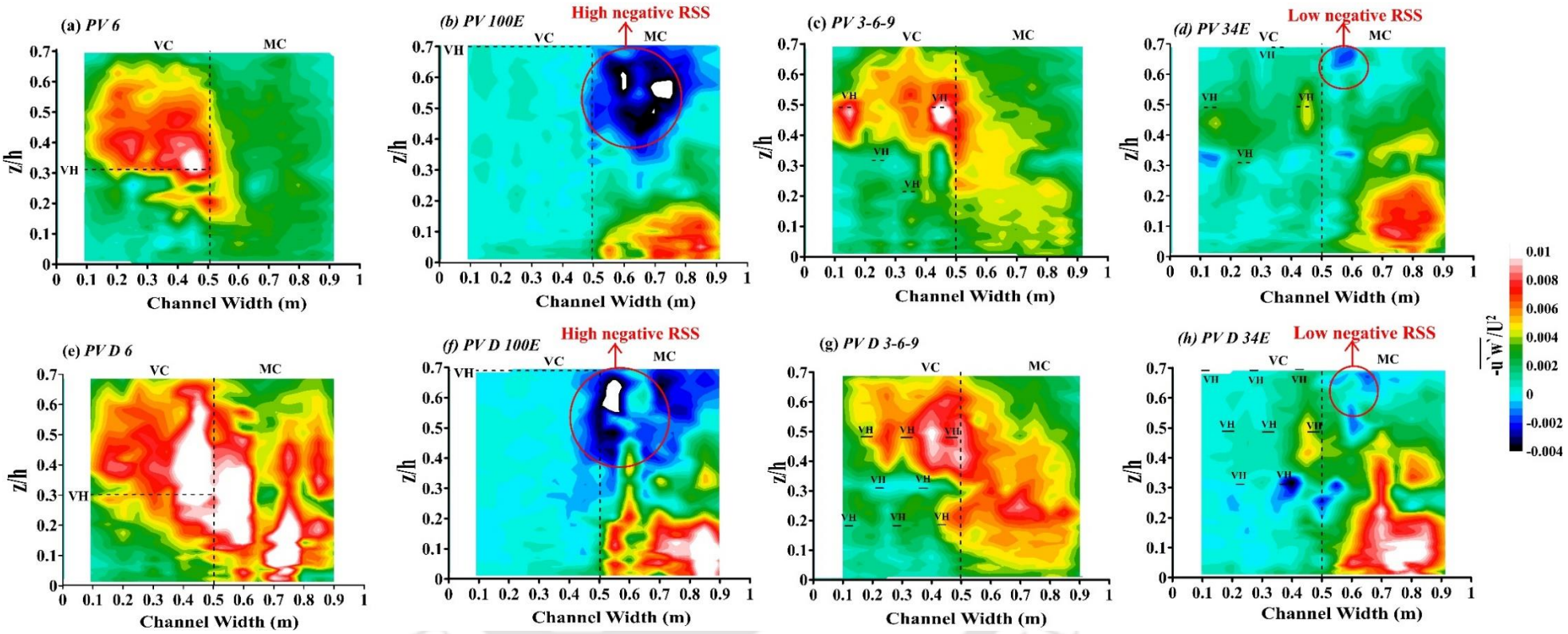

Figure 3.4 Streamwise RSS for different partially vegetated cases at 35 *lps* for Set 1 and Set 2

The momentum exchange across the VCMCI section for different vegetation emergence and density in the horizontal plane could be better understood by studying the transverse RSS. The region near the VCMCI section gets affected the most as can be observed in Figures 3.5 and 3.6. The normalized transverse RSS ($\overline{u'v'}/U^2$) is negative and its magnitude is higher from $0.4\,m - 0.6\,m$ channel width for all the vegetation arrangements in Figure 3.5. The white portion in Figures 3.5(b) and 3.5(d) depicts that the value of normalized transverse RSS is very high. This means that the momentum near the VCMCI section is towards the floodplain region (Truong *et al.* 2019). With increase in vegetation emergence, the magnitude of negative RSS also increases. The increase of white patch in Figures 3.5(f) and 3.5(h) indicates that as vegetation density in the floodplain region increases, the contribution of high transverse RSS in the MC also increases. This observation further suggests the presence of horizontal vortices within this particular region. These vortices are strongest in case of 100% emergent vegetation followed by 34% emergent vegetation. Nezu and Onitsuka (2001) also concluded that with the increase in vegetation density and Froude number, transverse RSS peaks near the junction of vegetated and main channel zone. With increase in distance from the VCMCI section towards the MC, the transverse RSS mostly adopts positive values which shows that the momentum is opposite to that observed near the VCMCI section. Furthermore, this positive RSS is observed with increased vegetation density and emergence in the floodplain region. The contribution of transverse RSS in the cross-section of the channel for all vegetation arrangements is also depicted in Figure 3.6. The normalized transverse RSS is shown for the mid-depth portion of the channel. The region near vegetation-main channel interaction is observed to be affected the most throughout the cross-section. These peaks in transverse RSS near VCMCI section for partially vegetated channels were also observed by other researchers like Nezu and Onitsuka (2001), Koken and Constantinescu (2021) and Caroppi *et al.* (2021). The present study shows that the peak of transverse RSS is directly proportional to the vegetation density and emergence in the VC. That is why the peaks in PV D 34E and PV D 100E are the highest among all the cases. The influence of transverse RSS at the mid-depth in the VC is almost similar for all vegetation cases. However, its impact on the VCMCI and MC is dependent on the vegetation arrangement in the floodplain region. Another point that is to be noted is that some of the maps in Figures 3.4 and 3.5 appears to be noisy mainly in the VC. The reason is that the measurement distances are not dense enough to capture a continuous flow description in the VC. A single vertical velocity measurement between two stems were captured which makes the Figures 3.4 and 3.5 to be noisy. However, the underlying idea of the analysis is to show the influence of

different vegetation arrangements on the overall cross-section of the channel for better visualization of the flow dynamics. As this section showed the role of vegetation emergence and density in the overall downstream cross-section, Section 3.3 will concentrate the analysis in the VCMCI section (Figures 3.7, 3.9 and 3.10) or in the adjacent sections (Figures 3.8 and 3.12).

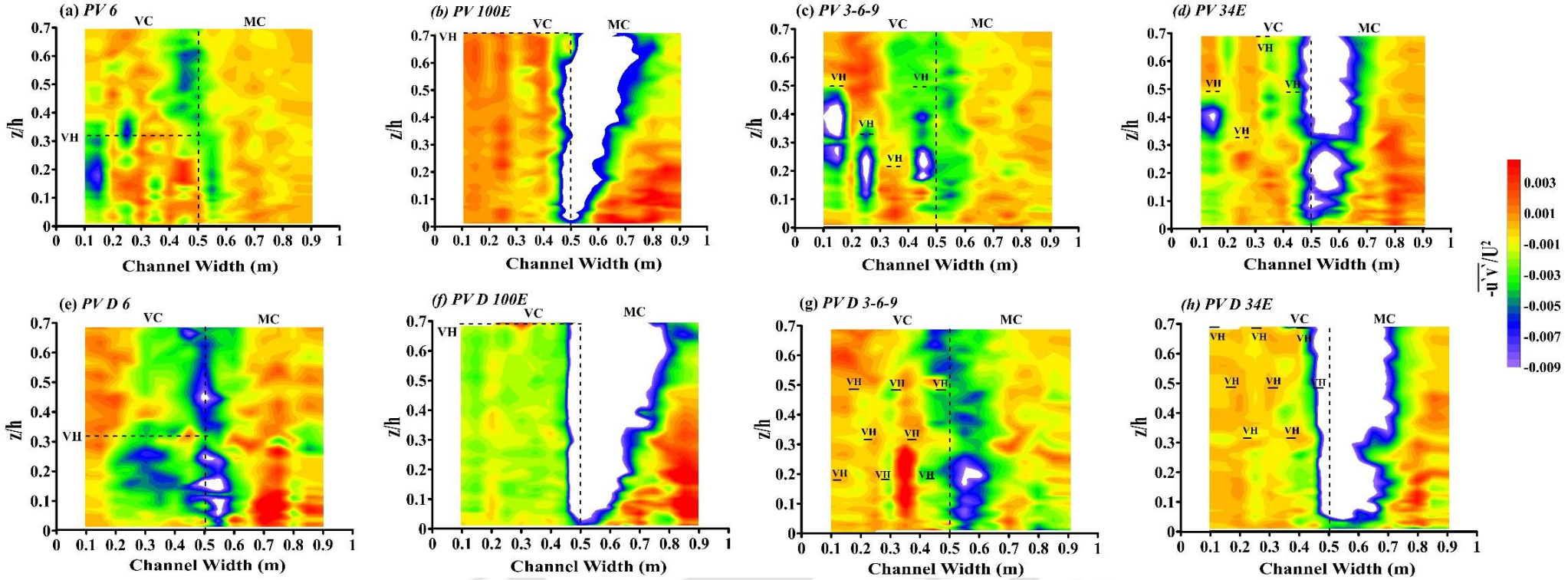

Figure 3.5 Transverse RSS contouring of different partially vegetated cases at 35 *lps* for Set 1 and Set 2

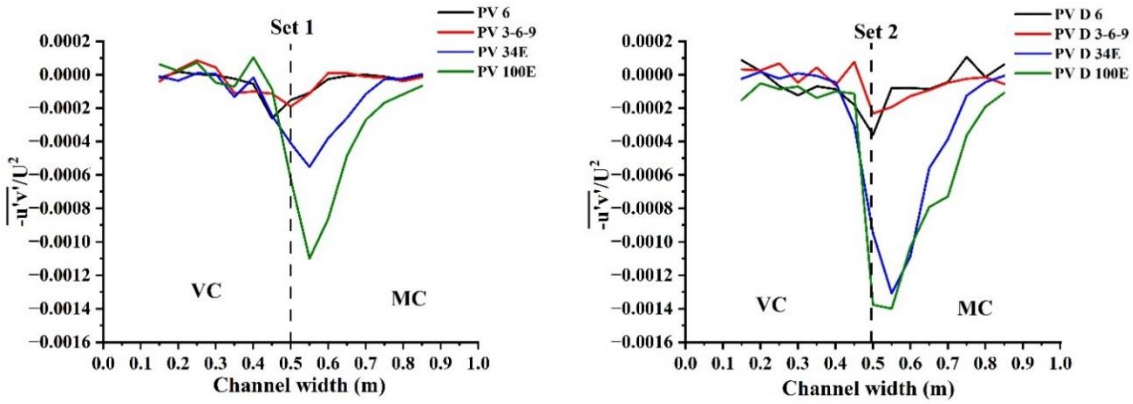

Figure 3.6 Transverse RSS ($\overline{u'v'}/U^2$) at mid-depth portion of 5.5 m cross-section for Set 1and Set 2

3.4 Flow dynamics in and around vegetated channel-main channel interface

Previous researchers like Lightbody and Nepf (2006), Nepf (2012) and Huai *et al.* (2021) have considered spatial averages to remove spatial heterogeneity. They mentioned that in case of emergent vegetation, when diameter (d) of vegetation elements is less than spacing between vegetation (s) i.e., $d < s$, the dominant turbulence length scale is d which is also the case in the present study. However, this section focusses on the flow analysis at the VCMCI location of the 5.5 m cross-section to get a better clarity of the role of vegetation height. The implications of varying vegetation height on the interface of vegetation and main channel are shown in Figure 3.7. The magnitude of RSS for single-layered (PV 6 and PV D 6) and multi-layered (PV 3-6-9 and PV D 3-6-9) submerged vegetation height reaches maximum values at different heights ($z/h \approx 0.3$ and $z/h \approx 0.5$). The reason is because of the local effect of different heights of vegetation in front of VCMCI section as seen in the plan view of Figure 2.12. As the emergence in the VC increases (34%), the streamwise RSS distribution (blue color) in both sets exhibits significantly lower values throughout the flow depth, as compared to the case of multi-layered submerged vegetation (red color). Despite the fact that the height (9 cm) in front of the VCMCI section remains the same for both cases, this observation indicates that the momentum exchange occurring in the VCMCI section is influenced by the overall vegetation emergence rather than being solely dependent on the local effects of individual vegetation elements. However, this point mainly works when the average frontal area varies which is observed for 34% emergent vegetation. In the case of the same average frontal area in the VC, the maximum RSS is almost the same as observed in submerged single-layered (black color) and multi-layered (red color) vegetation distribution in Figure 3.7. Furthermore, Shi *et al.* (2023) observed negative RSS in the near-bed in the VCMCI section for submerged vegetation.

However, no such negative RSS is observed for submerged vegetation in the present study, as depicted in Figure 3.7. The present study considered sparse and transition canopy for submerged vegetation which does not show negative RSS. However, with fully emergent cases (green color) for both sets, negative RSS is observed near the surface, as seen in Figure 3.4(b, f). This shows the presence of inward and outward interactions near the water surface and it transitions to ejection and sweep events as it approaches the channel bed.

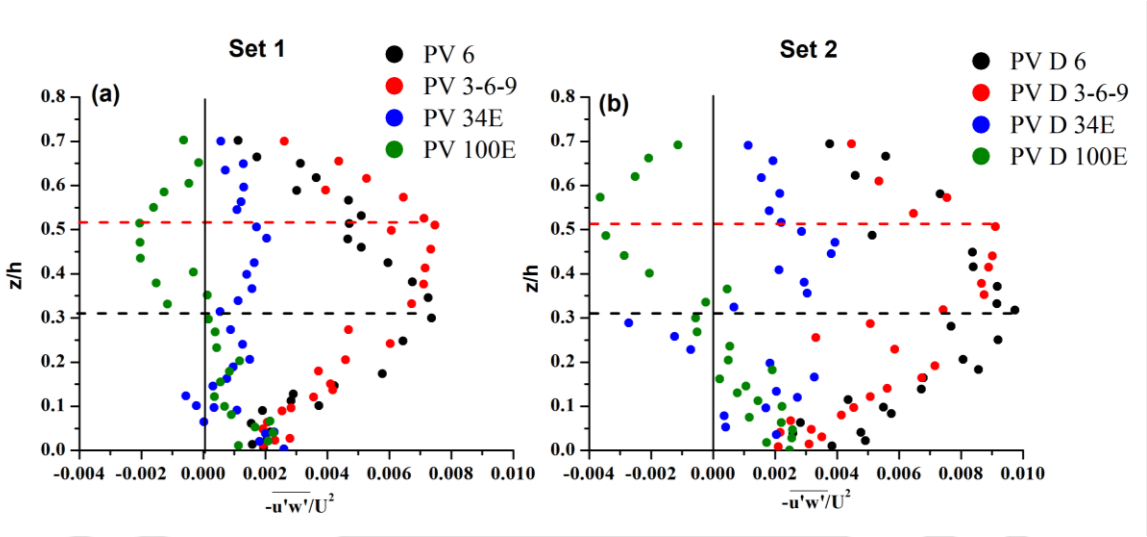

Figure 3.7 Streamwise RSS for (a) Set 1 and (b) Set 2 at VCMCI location

The strength of these bursting events near the VCMCI section at MC 55 for both emergent cases is shown in Figure 3.8. The streamwise and transverse Reynolds shear stress ($-\overline{u'w'}$ and $-\overline{u'v'}$) can be divided into four quadrants based on the signs of the fluctuating components streamwise (u'), vertical (w') and transverse ($-v'$) velocity (Lu and Willmarth, 1973 and Shi *et al.*, 2023). The four quadrants and their events are 1st quadrant, outward interaction ($u' > 0$, $w' > 0$) and ($u' > 0$, $-v' > 0$); 2nd quadrant, ejection ($u' < 0$, $w' > 0$) and ($u' < 0$, $-v' > 0$); 3rd quadrant, inward interaction ($u' < 0$, $w' < 0$) and ($u' < 0$, $-v' < 0$); 4th quadrant, sweep ($u' > 0$, $w' < 0$) and ($u' > 0$, $-v' < 0$). The contribution of different events to total streamwise RSS ($\overline{u'w'}$) at a particular point is calculated as follows (Raupach, 1981):

$$\langle u'w' \rangle_{i,H} = \lim_{T\to\infty} \frac{1}{T} \int_0^T u'(t)w'(t) I_{i,H}[u'(t)w'(t)]dt \quad (3.1)$$

Where $I_{i,H}$ denotes indicator function which is defined as:

$$I_{i,H}[u'(t)w'(t)] = \begin{cases} 1, \ if \ (u'w') is \ in \ quadrant \ i \ and \ |u'w'| \geq H(\overline{u'u'})^{0.5}(\overline{w'w'})^{0.5} \\ 0, otherwise \end{cases} \quad (3.2)$$

The stress fraction is defined as:

$$S_{i,H} = \frac{\langle u'w' \rangle_{i,H}}{\overline{u'w'}} \tag{3.3}$$

Here, H represents the hole size which is called the hyperbolic hole region. If $H = 0$, it considers all the fluctuating components of u' and w'. With the increase in hole size, only the strong events are considered. In Figure 3.8, two points are selected near the water surface ($z/h = 0.6$) and channel bed ($z/h = 0.1$) at MC 55 to understand the strength of the bursting events. As the hole size increases, the value of $S_{i,H}$ decreases and ultimately becomes zero after a certain H. The outward (Q1) and inward interactions (Q3) are positive and dominate at $z/h = 0.6$ compared to ejection (Q2) and sweep (Q4) as seen in Figure 3.8 (a, b). The value of Q1 is slightly greater than Q2, which implies the movement of the parcel of water upwards in that region. In the near-bed at $z/h = 0.1$, Q2 and Q4 are positive and have higher values compared to Q1 and Q3. This is true for all cases as seen in Figure 3.4, where near the channel bed streamwise RSS is high and positive in and around the VCMCI section. It shows the prevalence of Q2 and Q4 near the channel boundary in the vertical plane, which helps increase the sediment transport in the region.

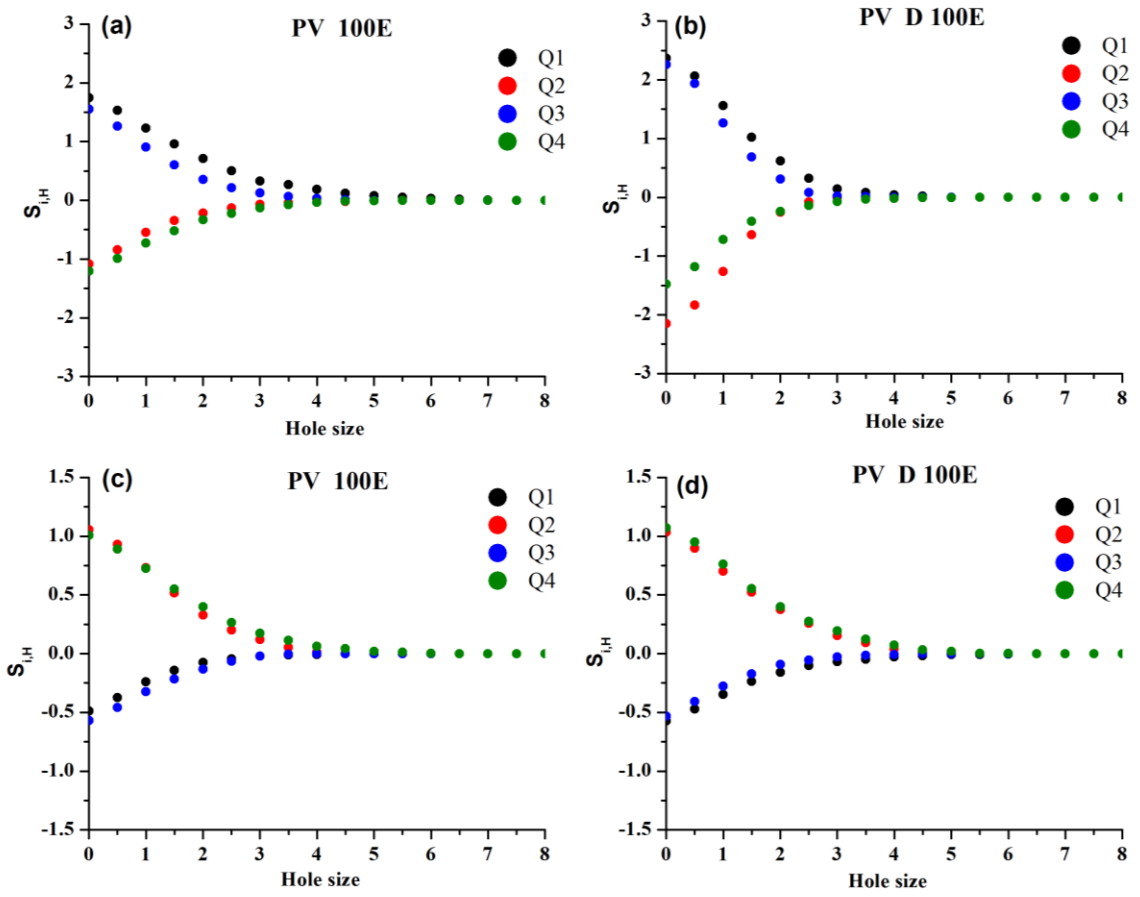

Figure 3.8 Quadrant hole function at MC 55 for PV 100E and PV D 100E at (a)-(b) $z/h = 0.6$ and (c)-(d) $z/h = 0.1$

The turbulence across VCMCI in the horizontal plane for different vegetation emergence and density could be understood better by analysing quadrant distribution between u' and v'. Figures 3.9 and 3.10 shows the distribution of u' vs v' at VCMCI section in the near bed-region ($z/h \approx 0.1$) for Set 1 and Set 2 respectively. The points for different vegetation cases in the near-bed region ($z/h < 0.2$) at the VCMCI section behaves the same way as observed in Figures 3.9 and 3.10. However, for a proper comparison, $z/h \approx 0.1$ is selected for comparing experimental cases. It is observed that in submerged vegetation cases for Set 1 (PV 6 and PV 3-6-9), the contribution of different events is almost symmetrical. As the emergence level increases (PV 34E and PV 100E), the contribution slightly aligned towards the ejection-sweep direction. This was also confirmed by Truong and Uijttewaal (2019) where they observed the dominance of ejection and sweep events in the VCMCI section in presence of emergent vegetation. As the density in the vegetated region is increased as observed in Figure 3.10 for submerged vegetation (PV D 6 and PV D 3-6-9), the bursting events are almost evenly

distributed which is contrary to Shi *et al.* (2023). The reason for this is that they considered a denser vegetated canopy whereas in the present study, sparse and transitional canopy is considered for submerged vegetation. This point shows the dependence of density in the floodplain region for the strength of coherent structures. Furthermore, the dominance of sweep and ejection are highest for PV D 34E and PV D 100E as shown in Figure 3.10. The alignment of the points towards ejection and sweep is more pronounced as density and emergence level of vegetation increases as seen in PV D 34E and PV D 100E. This shows that alongwith density of vegetation, horizontal coherent structures also depend on the emergence of vegetation in the floodplain region. Higher density and emergence of vegetation results in strong movement of the fluid parcel near the VCMCI section, which aids in sediment transport.

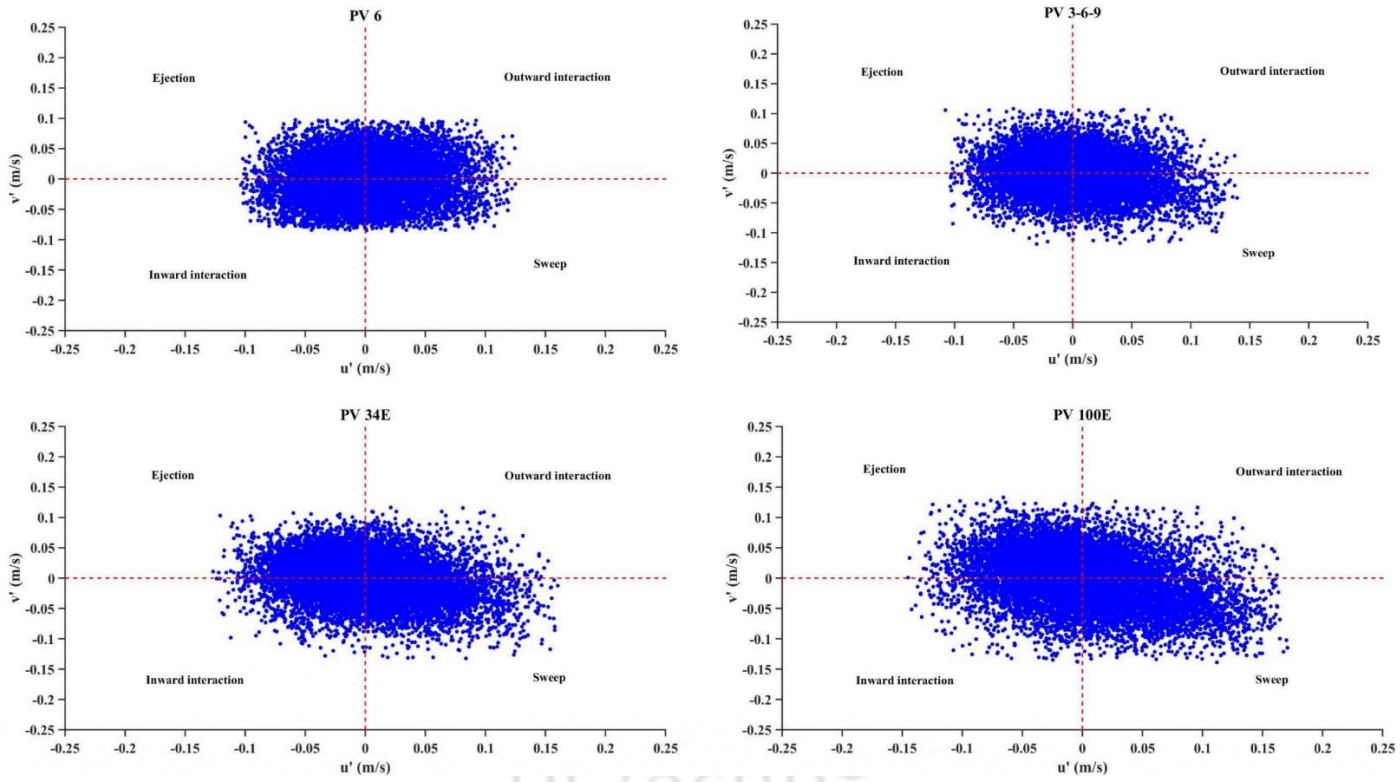

Figure 3.9 Quadrant distribution of different partially vegetated cases at VCMCI for Set 1 in the near-bed region of $z/h \approx 0.1$

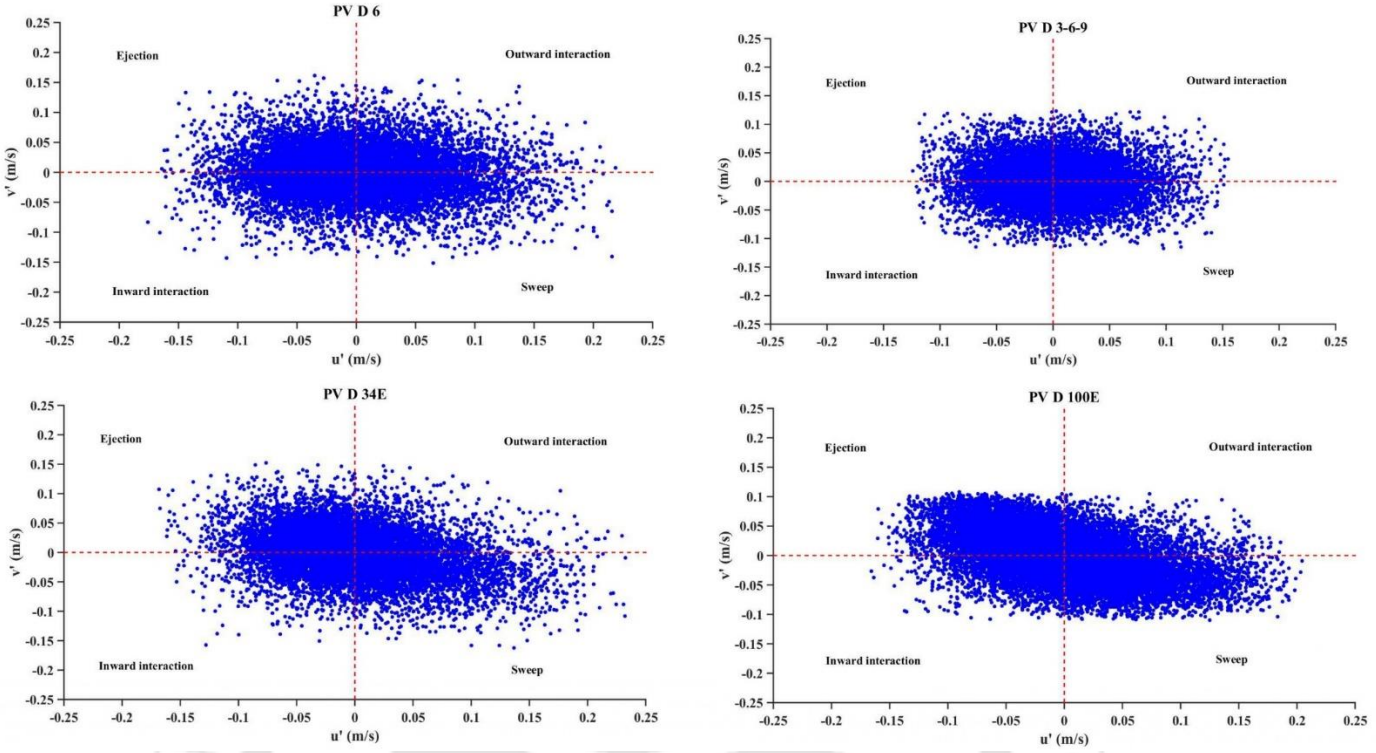

Figure 3.10 Quadrant distribution of different partially vegetated cases at VCMCI for Set 2 in the near-bed region of $z/h \approx 0.1$

Researchers have observed the dependence of turbulent kinetic energy (k) on vegetation density and height. Hamed *et al.* (2017) observed higher TKE in heterogeneous height vegetation compared to homogeneous height as one moves towards downstream of vegetated zone. Li *et al.* (2022) studied the behavior of TKE in the mix vegetation of sparse and dense canopies. They also found that the TKE reaches the peak near the interface of vegetation and main channel. Figure 3.11 shows the convergence analysis of partially emergent (PV 34E and PV D 34E) and fully emergent (PV 100E and PV D 100E) cases in the near-bed ($z/h = 0.1$) and near-surface ($z/h = 0.5$) region at VC 45 and MC 55 sections. The TKE is observed to converge at around 6000 samples for Set 1, whereas it converges from around 8000 samples in Set 2 at an error percentage range of $\pm 5\%$. Though the rate of converging is different in both the sets as observed from the figure, it properly converges at 12000 samples which is considered in the study. Figure 3.12 shows the difference of TKE magnitude between vegetated and main channel region near the VCMCI for partially and fully emergent vegetation cases. The k in Figure 3.12 is calculated as: $k = 0.5(\overline{u'^2} + \overline{v'^2} + \overline{w'^2})$, where u', v' and w' are fluctuating velocities in streamwise, transverse and vertical directions respectively. The presence of transitional and dense canopy shows substantial change in energy as one move from floodplains to the main channel. For Set 1 in Figure 3.12(a, b), TKE dominates at MC 55

compared to VC 45 after a certain height ($z/h > 0.4$ and $z/h > 0.3$). However, for Set 2 in Figure 3.12(c, d), the TKE in MC 55 is greater throughout the flow depth compared to VC 45 section. The average percentage increase at MC 55 compared to VC 45 for emergent cases is under 25% for Set 1. On the other hand, it is more than 50% for Set 2. The low TKE magnitude in the vegetated region can be attributed to the fact that presence of vegetation breaks the eddies leading to decrease of eddies length, ultimately increasing energy dissipation without TKE production (Grinvald and Nikora, 1988; Koziol, 2011). The TKE magnitude further decreases with higher vegetation emergence and density in the floodplain region as observed in PV D 100E. High turbulent fluctuations is observed in Set 2 (Figure 3.12(c, d)) compared to Set 1 which results in high TKE magnitude at MC 55 section. The jump in TKE at MC 55 from VC 45 is highest for PV D 100E case as the degree of obstruction is highest which led to higher diversion of turbulent fluctuations in the main channel. As one moves further away from the VCMCI section in the main channel, there is a gradual decrease of TKE magnitude from the channel bed to the surface which is depicted as dashed lines (MC 80 and MC 85) in Figure 3.12. These TKE profiles follows a trend which is observed in open-channel experiments by researchers like Nezu and Nakagawa (1993), Rowiński et al. (2002) and Koziol (2011). These profiles show that turbulent fluctuations, specially streamwise (u') and transverse (v') have greater prominence near the water surface in the vicinity of VCMCI section and it decreases as one move away from it. The prominence of u' and v' near the VCMCI was also observed while analysing transverse RSS in Figures 3.5 and 3.6.

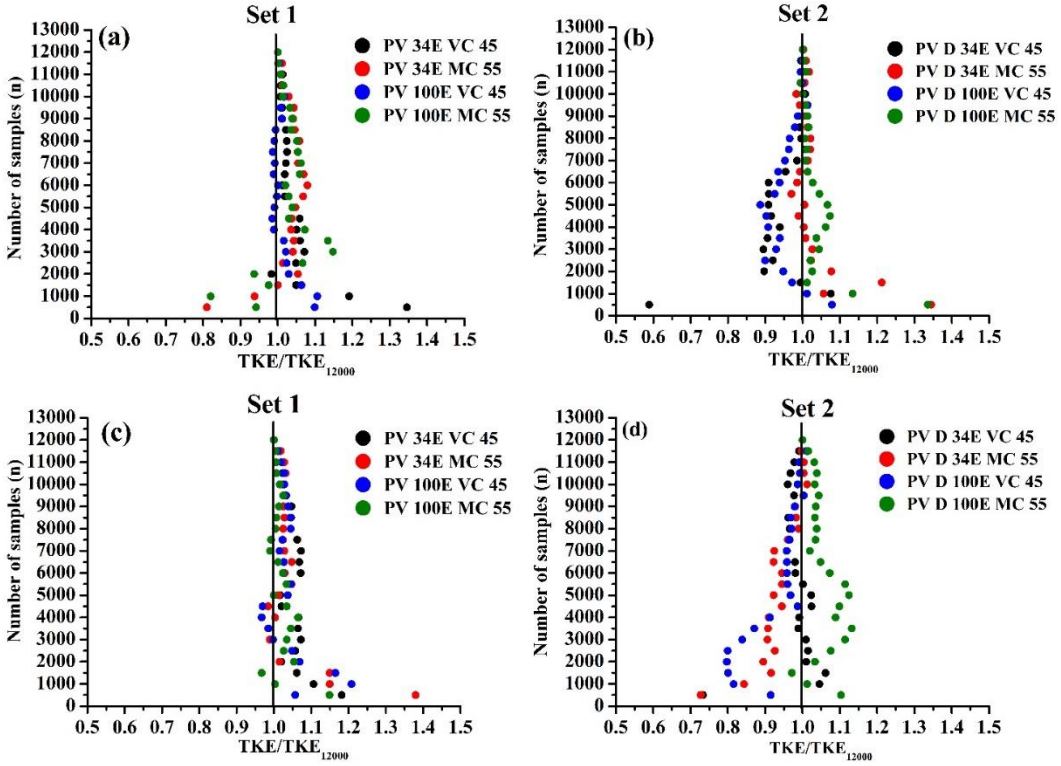

Figure 3.11 Convergence analysis of turbulent kinetic energy for Set 1 and Set 2 for (a, b) $z/h = 0.1$ and (c, d) $z/h = 0.5$ at VC 45 and MC 55 sections.

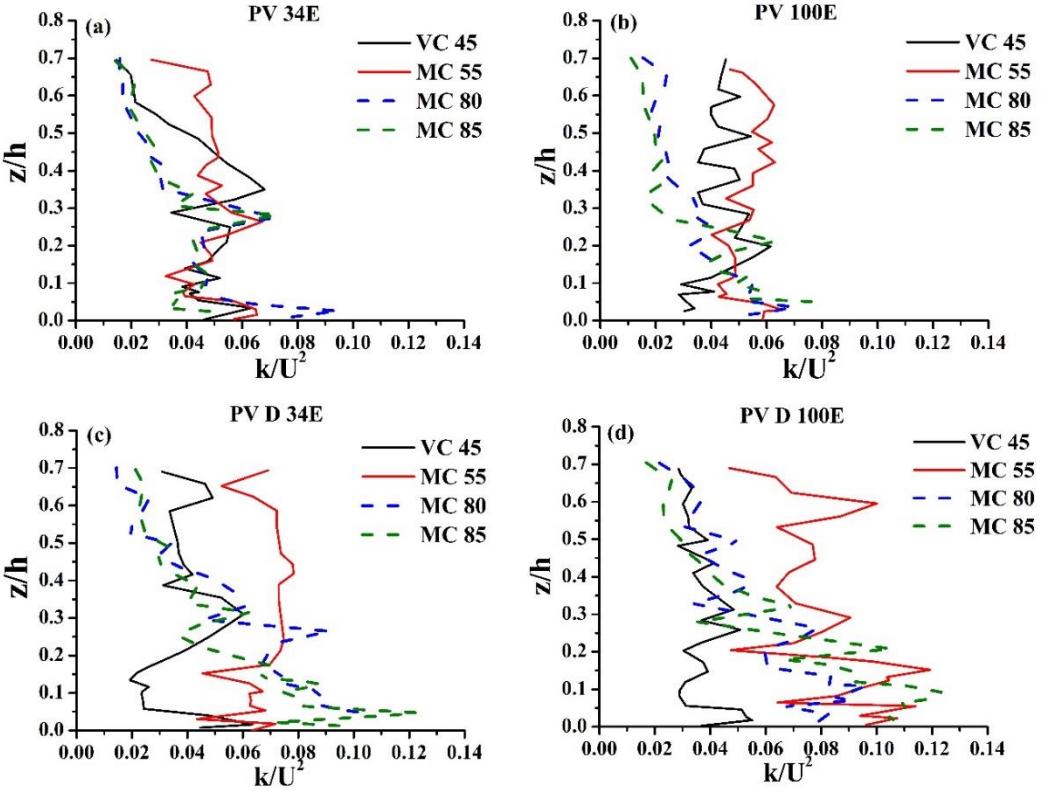

Figure 3.12 Turbulent Kinetic Energy (TKE) profiles at VC 45, MC 55, MC 80 and MC 85 for (a, b) Set 1 and (c, d) Set 2 for 35 lps

3.5 Conclusion

This study was done to understand the role of vegetation height and density in channels which is partially covered with vegetation. Measurements were conducted both in the vegetation portion and main channel regions to understand the role of different submerged/emerging vegetation with two different densities. In the floodplain regions with homogeneous/single-layered vegetation height, the velocity distribution is similar at different sections, as the vegetation is equally distributed across the cross-section. However, in cases where the vegetation height is heterogeneous/multi-layered, the velocity distribution in the vegetated portion changes according to the height of the vegetation. The study showed that when the average frontal area of the vegetated zone is the same, the flow nature in and around the vegetated channel-main channel interface depends on the local resistance provided by the vegetation elements near the VCMCI section. This was observed when analysing the flow in submerged multi-layered (PV 3-6-9 and PV D 3-6-9) and single-layered (PV 6 and PV D 6) vegetation where velocity and Reynolds shear stress (RSS) varies for both cases, although the average frontal area in the vegetated zone is same. Furthermore, when the vegetated zone partially emerges (34%), flow characteristics in both the VCMCI section and the main channel are mainly governed by the overall vegetation distribution rather than depending on individual vegetation elements near the interface.

The VCMCI section and its adjacent areas hold significant importance in fluid dynamics and sediment transport due to continuous momentum exchange. This momentum exchange becomes particularly prominent in fully emergent cases, where a distinct velocity dip is observed near the water surface within the main channel. This dip phenomenon was not observed in other cases as the submerged vegetation distribution considered for the study was either sparse ($ah_{veg} < 0.1$) or transitional ($ah_{veg} \approx 0.1$). Because of this dip in fully emergent cases, negative streamwise RSS was observed in the upper region of the main channel. This indicates the dominance of inward and outward interactions near the surface in the vicinity of VCMCI section. The RSS and turbulent kinetic energy (TKE) were also observed to be significant near the VCMCI section for all the cases. The RSS and TKE in the vicinity of VCMCI are enhanced with increased emergence, as observed in PV 34E and PV 100E cases. The increase in density in addition to vegetation emergence increases the magnitude of TKE and RSS across VCMCI section as observed in cases of PV D 34E and PV D 100E. The transverse RSS analysis showed that the strength of horizontal vortices increases with increase

of vegetation emergence in partially vegetated channels. Quadrant analysis considering the vertical (u' vs w') and horizontal (u' vs v') plane showed that ejection and sweep events dominate near the channel bed ($z/h < 0.2$) in the vicinity of VCMCI sections in the main channel region. This ejection and sweep events play a crucial role in facilitating sediment movement. The magnitude of these events increases as density and emergence of vegetation increases in the floodplain, increasing the chances of sediment transport.

4 Flow behavior in a multi-layered vegetated floodplain region of a compound channel[2,3]

4.1 Introduction

The study of flow considering multi-layered vegetation can be extended to a compound channel to move closer to a real or practical field. During the high flood season, the floodplain gets submerged, where vegetation contributes to the flow behavior in the channel. A case study on a tributary of Conodoguinet Creek, Pennsylvania, USA, concludes that there is more erosion and bank migration in the non-forested area than the forested area (Allmendinger *et al.*, 2005). Previous studies on the compound channels mainly focused on the single-layered vegetated floodplain (Yang *et al.*, 2007; Dupuis *et al.*, 2017; Proust and Nikora, 2019; Caroppi *et al.*, 2021). The analytical approach in compound channel was also investigated by many researchers (Shiono and Knight, 1991; Tang and Knight, 2008; Pu, 2019; Pu *et al.*, 2020). However, these researches did not consider the variation of vegetation height in the floodplain of the compound channel. Ahmad *et al.* (2020) and Tang *et al.* (2021) explained flow dynamics in double-layered vegetation on a compound and partially vegetated channel respectively. However, their studies did not incorporate the variation of double-layered vegetation with single-layered or uniformly distributed vegetation. Laboratory experiments regarding multi-layered vegetated floodplain compound channels are mostly unexplored due to the sheer complexity of handling vegetation with varying heights and densities. In addition to that, researchers have to also deal with flow interaction between the floodplain and the main channel region where constant momentum exchange takes place, making its study more interesting. Previous researchers complimented this floodplain-main channel interaction on a single-layered floodplain but did not explore it in the multi-layered vegetated region (Knight and Shiono, 1990; Tominaga and Nezu, 1991; Truong *et al.*, 2019; Proust and Nikora, 2019). The momentum exchange depends on vegetation density, height, submergence level, and

[2] Barman, J., & Kumar, B. (2022). Turbulence in a compound channel with the combination of submerged and emergent vegetation. Physics of Fluids, 34(4), 045114. https://doi.org/10.1063/5.0086739

[3]Barman, J., & Kumar, B. (2022). Flow behavior in a multi-layered vegetated floodplain region of a compound channel. Ecohydrology, 15(4), e2427. https://doi.org/10.1002/eco.2427

vegetation type. This changed vegetation distribution can affect the flooding and erosion pattern, making its study important.

This chapter attempts to observe the flow behavior in multi-layered vegetation in the floodplain region of the compound channel. Heterogeneity in spacing and height is used to study the flow nature and its impacts on the slopes and main channel. Despite the fact that many researches have performed experiments on vegetation in compound channels, detailed investigation of flow behavior in multi-layered vegetation in the floodplain zone has been scarce. This chapter also attempts to address the flow nature differences between single-layered and multi-layered vegetation in a compound vegetated channel, which have never been investigated before. Although vegetation height and distribution are more random in the real field, the study is considered by using three layers of vegetation to reduce complexity during analysis. The experimental set up and different vegetation arrangement were discussed in detail in section 2.9.2.

4.2 Velocity

Floodplain vegetation density influences the flow behavior in the entire cross-section of the channel. This effect can be seen in the main channel of the compound channel, as seen in figure 4.1. Velocity for uniform set up in the main channel does not show any particular consistent trend throughout the flow depth (Figures 4.1 (a, c)). It is almost equal for $z/h > 0.4$. The introduction of different vegetation density zones showed a trend where the velocity profile at $5.5\ m$ main channel section is highest whereas at $9.5m$ it shows the lowest velocity magnitude for both discharges (Figures 4.1 (b, d)). It is seen that there is more than 20% increase of depth-averaged streamwise velocity in the main channel section from $9.5m$ section to $5.5m$ section. The role of vegetation density can also be seen in figure 4.2, where velocity profiles at various uniform and non-uniform setup sections are shown. The $5.5m$ cross-section was chosen to compare vegetation density in that region ($7m$ to $5m$) is the same for both the setup as discussed in section 2.9.2 in figures 2.14 (a, b). In all the sections from SFPI to MC section, velocity in uniform vegetation set up is higher compared to non-uniform vegetation set up. However, the velocity at the MC section for uniform setup starts to diverge or increase from non-uniform set up at $z/h > 0.5$. The velocity is almost the same for both vegetation setup at $z/h = 0 - 0.5$. The flow in the vegetation zone in a non-uniform setup travel from a sparsely vegetated zone to a densely vegetated zone, whereas in uniform case, the whole vegetation zone is densely populated from $11m$ to $5m$ (Figure 2.14 (a, b)). This decreases the velocity in

the floodplain zone of uniform cases, increasing the velocity in the slope and main channel sections. Figure 4.2 also shows the importance of vegetation height to divert the flow towards the main channel. The velocity in the U 3-6-9 case is greater than the U 6 case at SFPI, SM, and SE throughout most of the flow depth. In the MC section, velocity in both U 6 and U 3-6-9 are almost comparable. The reason for greater velocity in slope and main channel sections for multi-layered vegetation (U 3-6-9 and NU 3-6-9) for most cases is the resistance it gets from $9cm$ length vegetation in the SFPI section. This shows that though 33% of the vegetation is $3cm$ in length, the resistance in flow is mainly provided by 9cm length vegetation. The $9cm$ vegetation provides more frontal area and flow obstruction. This ultimately decreases the flow velocity in the floodplain region and increases the velocity in the slope and main channel sections. This point can be seen in figure 4.2, where the velocity of NU 3-6-9 (pink color) case is less than the NU 6 case (blue color) at the SFPI section and becomes more significant at SE and MC sections.

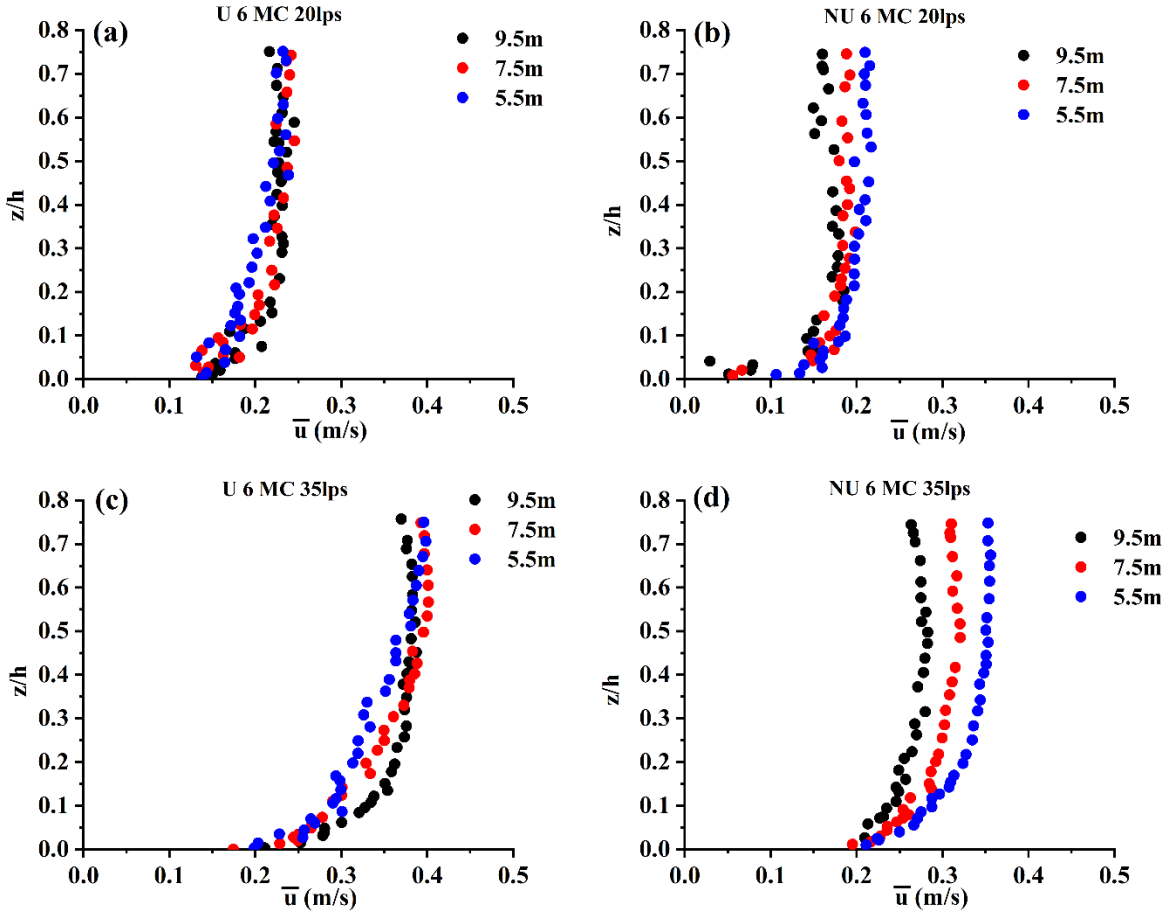

Figure 4.1 Velocity in the main channel of U 6 and NU 6 case from upstream (9.5m) to downstream (5.5m) for (a, b) 20lps and (c, d) 35lps

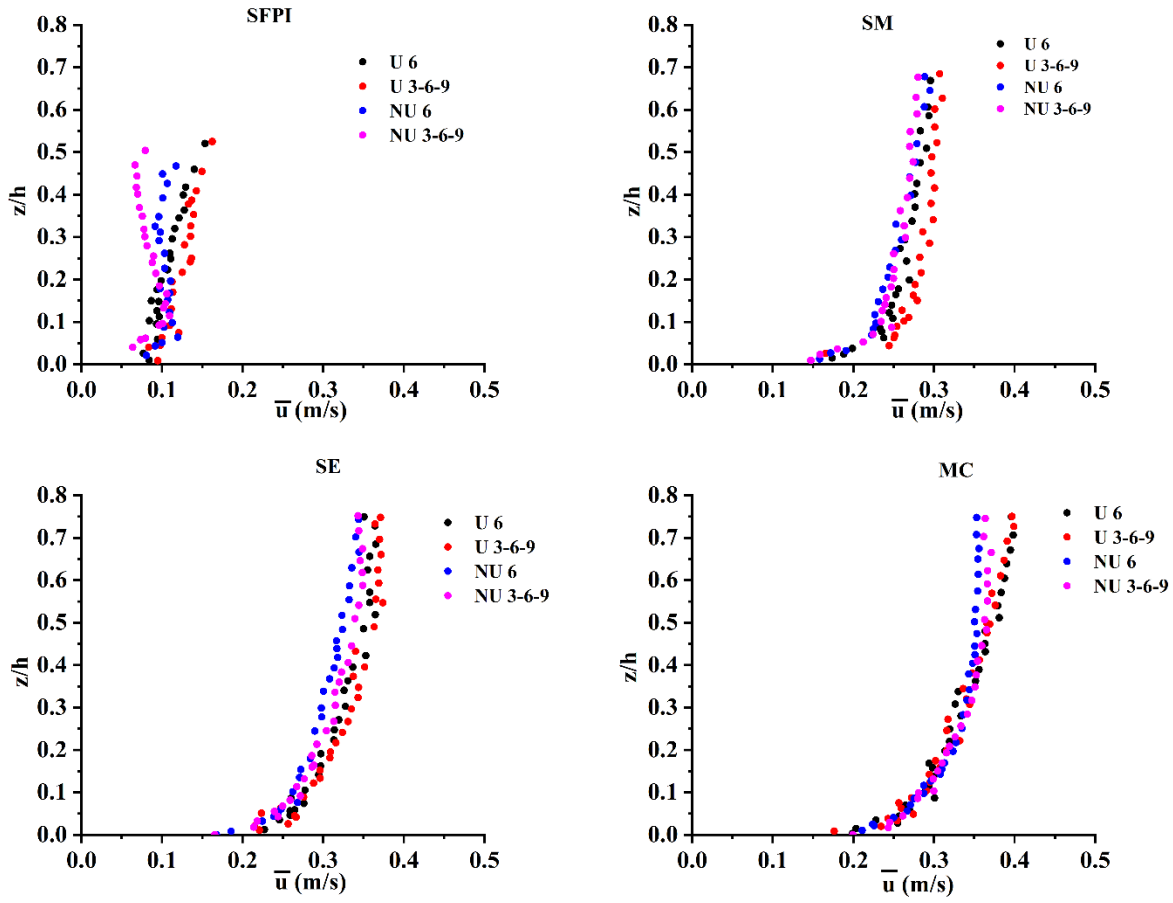

Figure 4.2 Velocity profile in different locations of different vegetation cases for 35 lps at 5.5m cross-section

4.3 Reynolds shear stress

The Reynolds shear stresses (RSS) help to get a better glimpse of the momentum transfer between different layers in streamwise, spanwise and vertical directions. There is a constant momentum transfer between the floodplain and the main channel region in the compound channel because of differences in velocities and flow depth across the cross-section (Dupuis *et al.*, 2017; Proust and Nikora, 2019). Figures 4.3 and 4.4 shows streamwise and transverse RSS ($-\overline{u'w'}$ and $-\overline{u'v'}$) for different vegetation cases at 5.5m cross-section for 35lps. In all cases, irrespective of discharge and uniformity conditions, the RSS is more pronounced in the slope and the main channel sections. For higher flow depths of $z/h > 0.4$, the streamwise RSS in uniform set up (U 6 and U 3-6-9) is greater than in non-uniform cases, primarily at SE and MC sections (Figure 4.3 (e, f)). However, no particular trend is observed for $z/h < 0.4$ at both SE

and MC sections. The reason might be because of flow irregularities in the lower depth of the channel. The uniform setup increases the velocity in the slope and main channel sections, as seen in figure 4.2. As a result, the difference in velocity between the floodplain and main channel increases, ultimately increasing the momentum exchange compared to the non-uniform setup. The pointwise RSS profile of SE and MC (Figure 4.3 (e, f)) shows that the RSS increases from $z/h \sim 0.75$ to $z/h = 0.2$, after which it decreases till the channel bed. The maximum magnitude of RSS in multi-layered vegetation (U 3-6-9 and NU 3-6-9) reaches more than $0.0003 m^2/s^2$ which is greater than the single-layered vegetation (U 6 and NU 6). Negative streamwise RSS is observed for all cases, mainly in the floodplain and SFPI regions. This point shows the presence of a strong circulation system in the region. However, the magnitude of negative RSS at the SFPI section of NU 3-6-9 case is higher than all other cases. An important point to be noted is that the negative streamwise RSS at the interface of vegetated-main channel in Chapter 3 is only observed in case of emergent cases (Figure 3.4 (b, d)) and was absent from submerged vegetation cases (Figure 3.4 (a, c)). However, in this chapter, negative streamwise RSS is also observed at the SFPI for submerged vegetation (U 6 and U 3-6-9) at the same vegetation spacing and discharge as in Chapter 3. The reason is that, in this chapter, in addition to the effect of vegetation, the cross-section is also non-uniform (compound channel), creating varying flow depth and ultimately increasing the momentum exchange across floodplain and main channel. The magnitude of this momentum exchange also depends on the bank slopes which will be discussed in detail in Chapter 5. The SFPI and SM sections are also subjected to high transverse RSS ($-\overline{u'v'}$) for all cases, as seen in figure 4.4. The white portion in slopes shows the extreme magnitude of $-\overline{u'v'}$ and display the importance of transverse velocity fluctuations (v') in overall flow in a compound channel. It is also seen that the magnitude of transverse RSS ($-\overline{u'v'}$) is also higher than streamwise RSS ($-\overline{u'w'}$) especially on the slopes, implying the importance of cross-sectional momentum exchange.

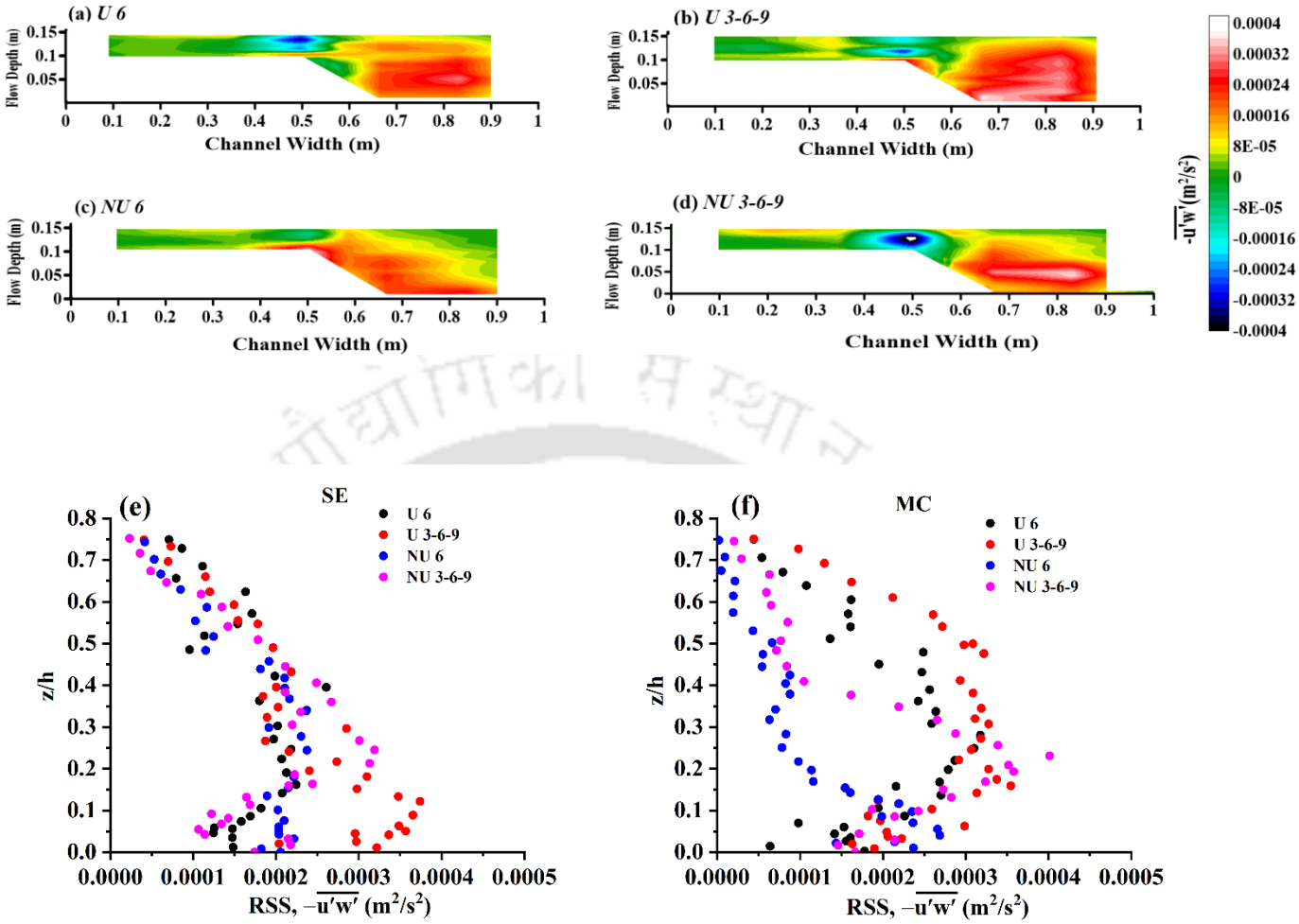

Figure 4.3 (a-d) Contouring of streamwise RSS($\overline{-u'w'}$) and (e, f) pointwise RSS at SE and MC for 35 *lps* at 5.5m cross-section

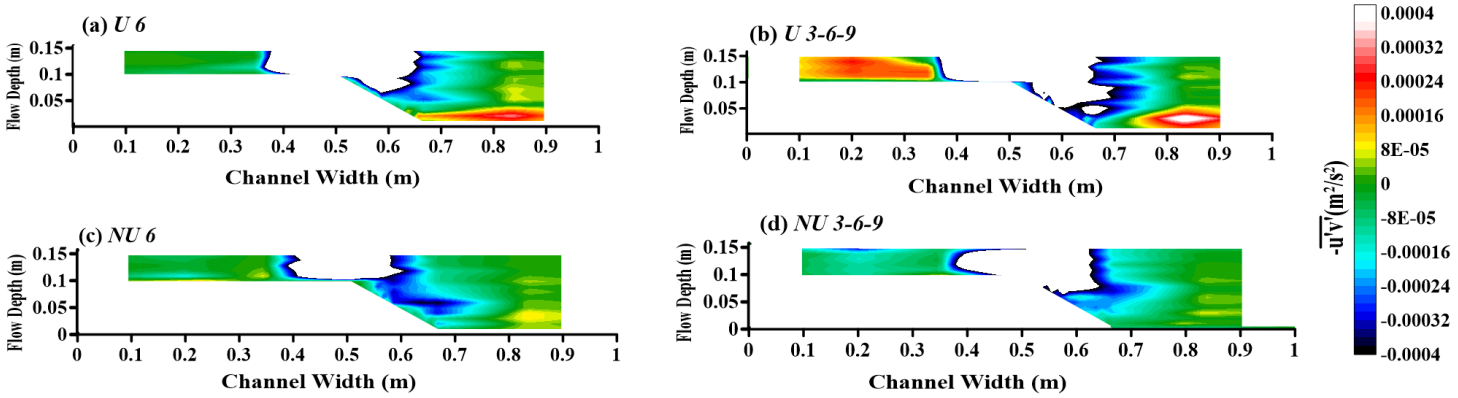

Figure 4.4 Contouring of transverse RSS ($\overline{-u'v'}$) case respectively for 35 lps at 5.5m cross-section

4.4 Turbulent intensities

Figures 4.5 and 4.6 show the streamwise and transverse intensities, respectively at the $5.5m$ cross-section for $35lps$. It is evident from the figures that both intensities are greater in uniform set up at the slopes and main channel sections as compared to non-uniform vegetation setup. The maximum streamwise and transverse intensities in the SE and MC sections are greater than $0.08m/s$ for a uniform setup, whereas it is within $0.08m/s$ for a non-uniform setup (Figures 4.5 (e, f) and 4.6 (e, f)). The magnitude of intensities is also seen to be maximum in the SFPI section as it acts as the boundary where momentum exchange occurs between the floodplain and the main channel. It is also observed that the magnitude of streamwise and transverse intensities of multi-layered vegetation (U 3-6-9 and NU 3-6-9) at SE and MC sections are higher than single-layered vegetation (U 6 and NU 6) throughout the flow depth. However, the percentage increase of depth-averaged intensities is different for uniform and non-uniform vegetation set up. There is a more than 15% increase in averaged streamwise intensities (σ_u) at SE and MC sections in case of NU 3-6-9 to NU 6 whereas it is within 15% for U 3-6-9 compared to U 6. Furthermore, in the case of average transverse intensity (σ_v), it is more than 20% for non-uniform vegetation setup, whereas it is within 20% for uniform vegetation setup. The combined effect of varying height and vegetation density zones could result in greater intensity increase in the case of a non-uniform setup. On the other hand, only vegetation height acts as a variable, whereas vegetation spacing is constant throughout the vegetation zone in the uniform vegetation setup.

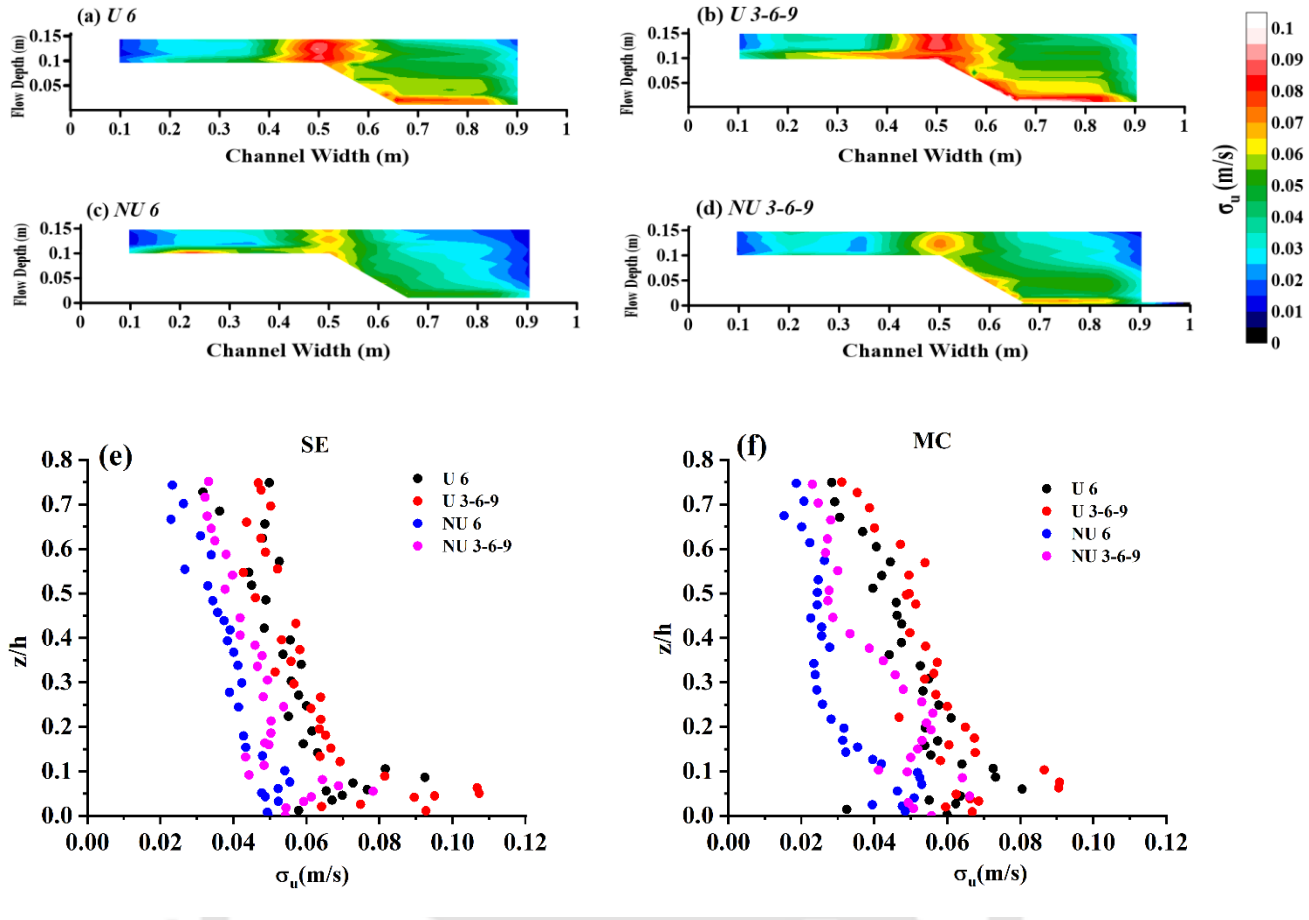

Figure 4.5 (a-d) Contouring of streamwise Intensity σ_u and (e, f) pointwise σ_u at SE and MC for 35 *lps* at 5.5m cross-section

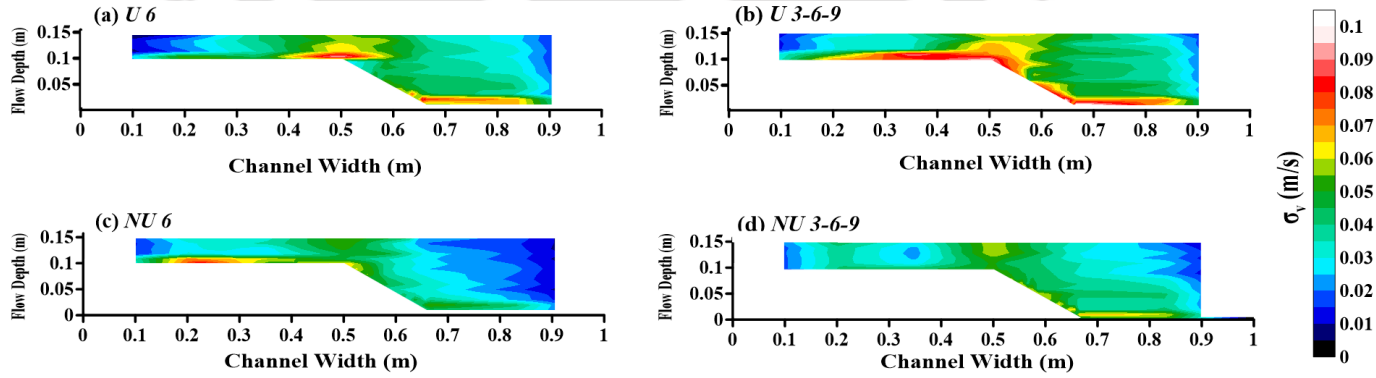

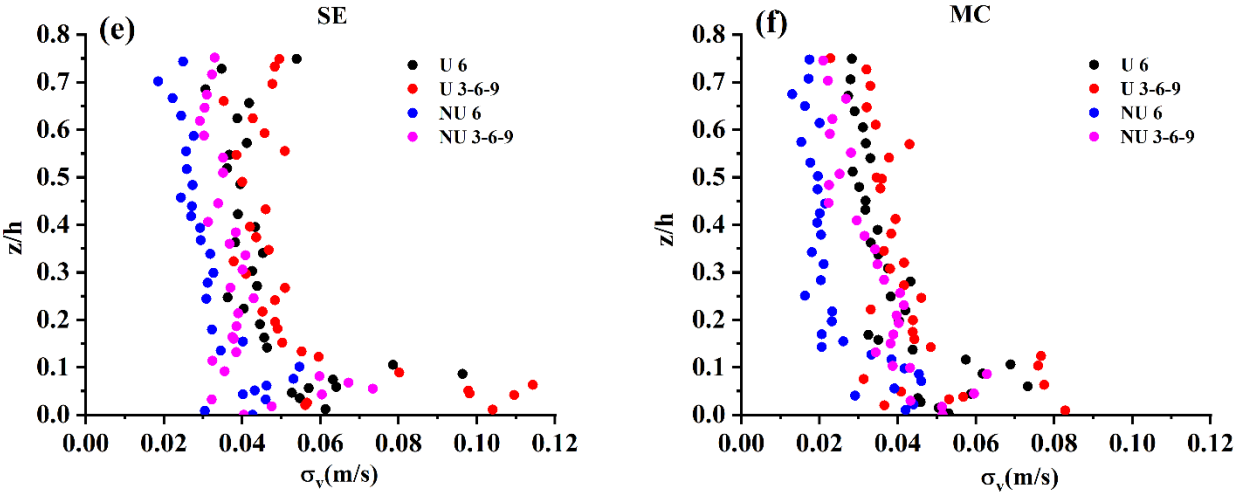

Figure 4.6 (a-d) Contouring of transverse intensity σ_v and (e, f) pointwise σ_v at SE and MC for 35 lps at 5.5m cross-section

4.5 Turbulent Kinetic Energy

The results of TKE resemble turbulent intensities to some extent, as shown in Figures 4.5 and 4.6. The magnitude of TKE is more pronounced in the slopes and main channel sections, irrespective of vegetation setup (Figure 4.7). Like turbulent intensities, the magnitude of TKE in uniform set up is greater than that of non-uniform vegetation throughout the flow depth. The TKE magnitude in multi-layered vegetation cases for both uniform and non-uniform setup is also greater than single or constant vegetation height cases, especially at slope and MC sections. However, there is more than a 30% increase in average TKE magnitude for multi-layered vegetation compared to single-layered vegetation in non-uniform setup, whereas it is within 30% for uniform vegetation setup. It is also observed in figure 4.7 that TKE magnitude in the floodplain sections is comparatively less than in sloping sections. It signifies that the velocity fluctuating components in different directions are more pronounced in the slopes than in the floodplain sections.

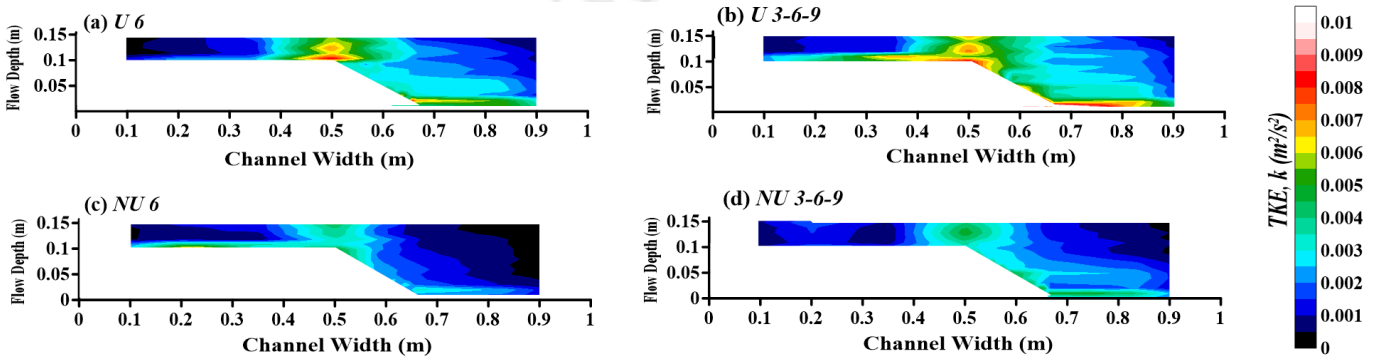

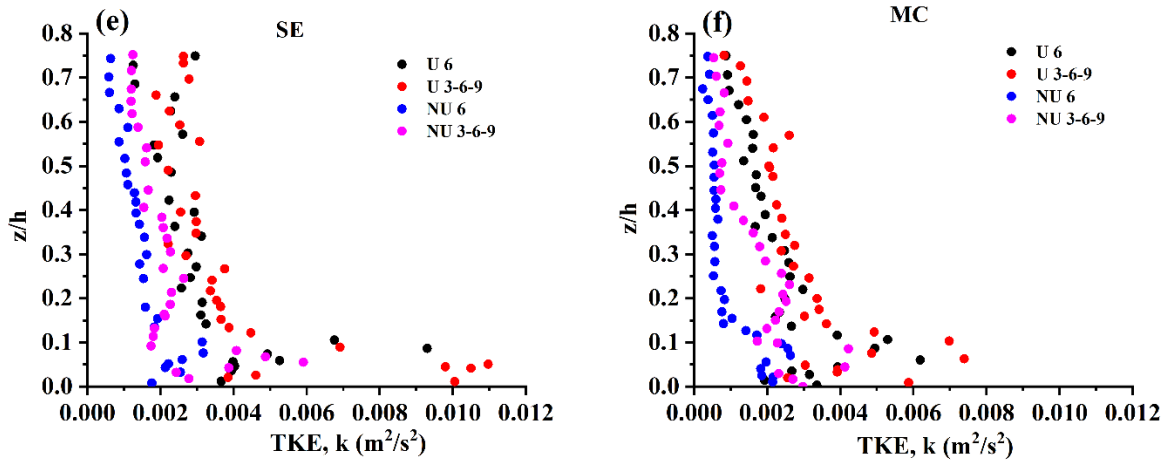

Figure 4.7 (a-d) Contouring of TKE k and (e, f) pointwise TKE at SE and MC for $35lps$ at 5.5m cross-section

4.6 Turbulent Anisotropy

The previous sections (4.1-1.5) from this chapter compared submerged single-layered and multi-layered vegetation in uniform and non-uniform set up in a compound channel. However, the analysis of combined presence of submerged and emergent vegetation for both uniform and non-uniform set up will be performed in this section by using turbulent anisotropy. The Reynolds stress anisotropy is used to observe the deviation and quantify the anisotropy in the flow. Lumley and Newman (1977) expressed the non-dimensional Reynolds anisotropic tensor b_{ij} as:

$$b_{ij} = \frac{\overline{u_i' u_j'}}{2\,k} - \frac{\delta_{ij}}{3} \tag{4.1}$$

where $\overline{u_i' u_j'}$ represents Reynolds stresses in different directions, k represents turbulent kinetic energy (TKE) $=\frac{1}{2}\left(\overline{u_1'^2} + \overline{u_2'^2} + \overline{u_3'^2}\right)$ and δ_{ij}= Kronecker's delta. The b_{ij} is a symmetric and traceless tensor and is bounded by $-\frac{1}{3} \leq b_{ij} \leq \frac{2}{3}$. The b_{ij} tensor is 0 during isotropic turbulence. Physically, the diagonal elements of b_{ij} (b_{11}, b_{22}, b_{33}) represents the relative contribution of Reynolds normal stress or turbulent intensity to turbulent kinetic energy. Furthermore, other components of b_{ij} (b_{13}, b_{12}, b_{23}) represents the Reynolds shear stresses to average turbulent kinetic energy. The eigenvalues $(\lambda_1, \lambda_2, \lambda_3)$ of b_{ij} tensor is found out by solving the characteristic equation $\left|b_{ij} - \lambda\delta_{ij}\right| = 0$, which gives the following polynomial:

$$\lambda^3 - I_1\lambda^2 + I_2\lambda - I_3 = 0 \tag{4.2}$$

Where I_1, I_2 and I_3 represents first, second and third invariants respectively. These invariants are given as follows:

$$I_1 = b_{ii} = 0 \tag{4.3}$$

$$I_2 = -b_{ij}b_{ji}/2 \tag{4.4}$$

$$I_3 = \frac{b_{ij}b_{jk}b_{ki}}{3} = det\,(b_{ij}) \tag{4.5}$$

Since the b_{ij} tensor is a traceless tensor so the first invariant vanishes. Using the 2nd and 3rd invariant (Equation 4.4 and 4.5), an anisotropic invariant map (AIM) was constructed, which gives the deviation of turbulent flow from isotropy (Lumley, 1979). The $-I_2$ and I_3 represents the degree and nature of anisotropy, respectively (Mera *et al.* 2015). However, in this section AIM is constructed using ξ and η where $\xi = (I_3/2)^{1/3}$ and $\eta = (-I_2/3)^{0.5}$ (Choi and Lumley, 2001). The ξ vs η plot shows the turbulent behavior more clearly as compared to $-I_2$ vs I_3 plot. The vertices of the Lumley triangle are: $\xi = 0, \eta = 0$; $\xi = -1/3, \eta = 1/6$ and $\xi = 1/3, \eta = 1/3$. $\xi = \eta = 0$ represents 3D isotropic turbulence where all three components are equal (Simonsen and Krogstad, 2005). The left-hand side vertex of $\xi < 0$ denotes 2D isotropic turbulence and the right vertex where $\xi > 0$ is the 1D turbulence. The expression of the upper boundary which connects the 2D and 1D components is given as: $\eta^2 = \frac{1}{27} + 2\xi^3$ which also represents 2D turbulence. The points on the left margin denote a transformation from 3D to 2D where two components are equal in magnitude and dominant over the third one. When it lies on the right margin, it represents a transformation from 3D to 1D where one component is more dominant than the other two equally distributed components. The transformation from 3D to 2D is given as a pancake-shaped structure, whereas the transformation from 3D to 1D is given as a rod-like or cigar-shaped structure. The pancake-shaped structures formed due to axisymmetric contraction, whereas cigar-shaped forms due to axisymmetric expansion (Lumley and Newman, 1977). The I_2 and I_3 invariants are also used to find the invariant function *F* which is given as: $F = 1 + 9I_2 + 27I_3$ (Lumley and Newman, 1977). This invariant function gives information about the anisotropy level at a particular location. If $F = 0$, it denotes 2D, whereas $F = 1$ implies 3D isotropic turbulence. In AIMs, the two invariants give information about the degree (I_2) and nature (I_3) of anisotropy. However, the invariant function *F* gives an overall scenario of anisotropy at a point.

Figures 4.8-4.11 shows the contouring of b_{ij} stress anisotropy tensor for different vegetation set up at $5.5\,m$ cross-section for $35lps$. Figure 4.8 shows the contouring of b_{11} for uniform and non-uniform vegetation setup. It can be seen that b_{11} dominates in the slope and main channel region irrespective of the vegetation setup. The magnitude is also seen to be more prevalent in the uniform setup (Figure 4.8 (a) and (b)) as compared to the non-uniform setup (Figure 4.8 (c)-(f)). The reason can be attributed to the fact that flow is diverted more towards the main channel in the uniform setup. On the other hand, in the non-uniform setup, less diversion of flow velocity in the main channel region decreases the momentum exchange compared to a uniform setup. The magnitude of b_{11} in the slope and the main channel region is mostly above 0.16, whereas it is within 0.12 in the floodplain region. The situation is a little different in the case of b_{22} anisotropic tensor as shown in figure 4.9. It can be seen that the points in the main channel and slope end section fluctuate in the positive and negative values throughout the flow depth. The magnitude of b_{22} is less than b_{11} in the main channel for all vegetation setup cases. It means that b_{22} component provides less anisotropic turbulence as compared to b_{11} component in the main channel. However, in the floodplain region, the b_{22} tensor is more prevalent as compared to b_{11} tensor. Figures 4.10 and 4.11 shows the contribution of b_{ij} tensor component when $i \neq j$ for different vegetation set up for $35\,lps$. From figure 4.10, it can be seen that b_{13} component heavily dominates the main channel region. However, its contribution in the slope end and main channel section of NU 67E and NU 100E case (Figures 4.10 (e, f)) somewhat consist of both positive and negative values. This behavior of combination of positive and negative values can also be seen for b_{12} component as shown in figure 4.11. It is also seen that the contribution of b_{12} in the slope region is very high as compared to b_{13}. There is also a resemblance of b_{13} and b_{12} contouring with that of $-\overline{u'w'}$ and $-\overline{u'v'}$ contouring respectively because physically, b_{13} and b_{12} are ratio of Reynolds shear stress to the average turbulent kinetic energy.

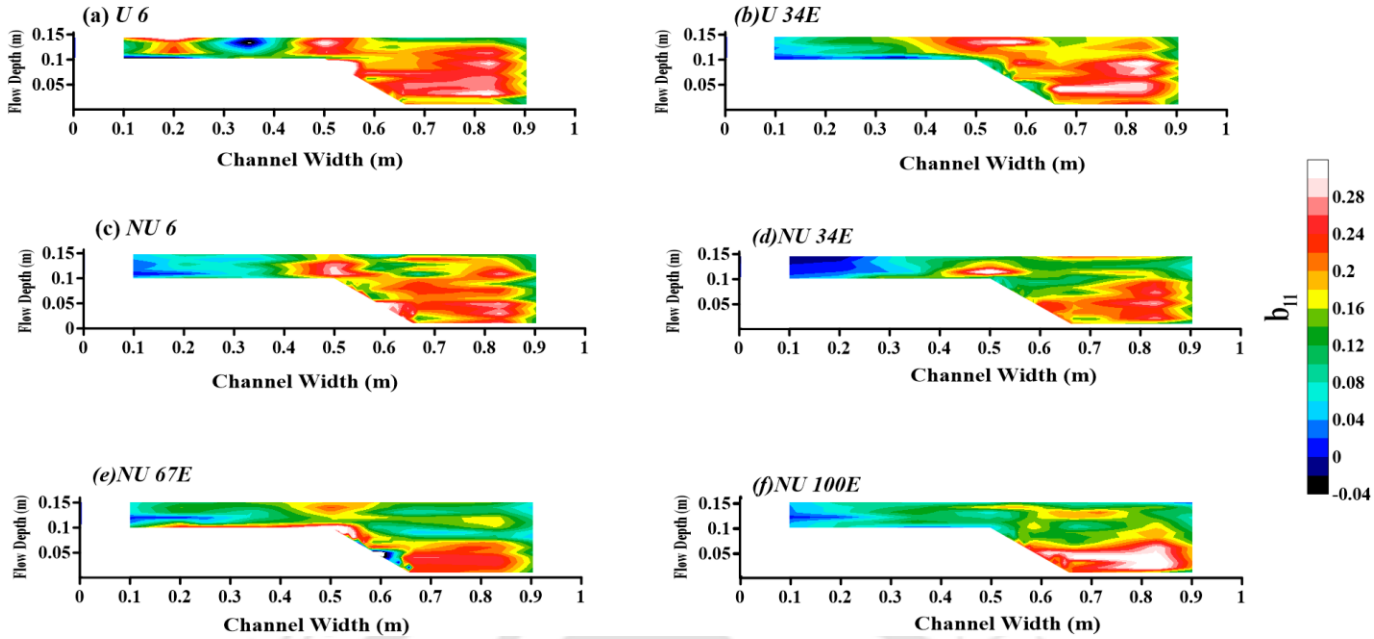

Figure 4.8 Contouring of b_{11} anisotropic stress tensor of uniform and non-uniform cases at 5.5 m cross-section for 35 lps

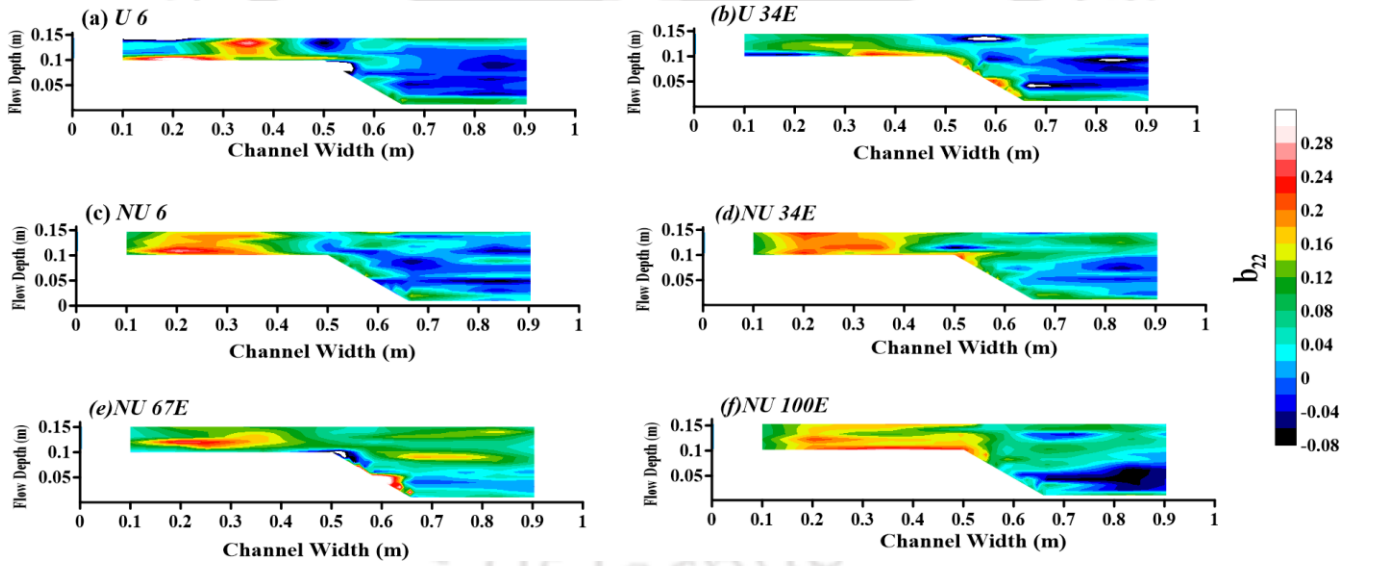

Figure 4.9 Contouring of b_{22} anisotropic stress tensor of uniform and non-uniform cases at 5.5 m cross-section for 35 lps

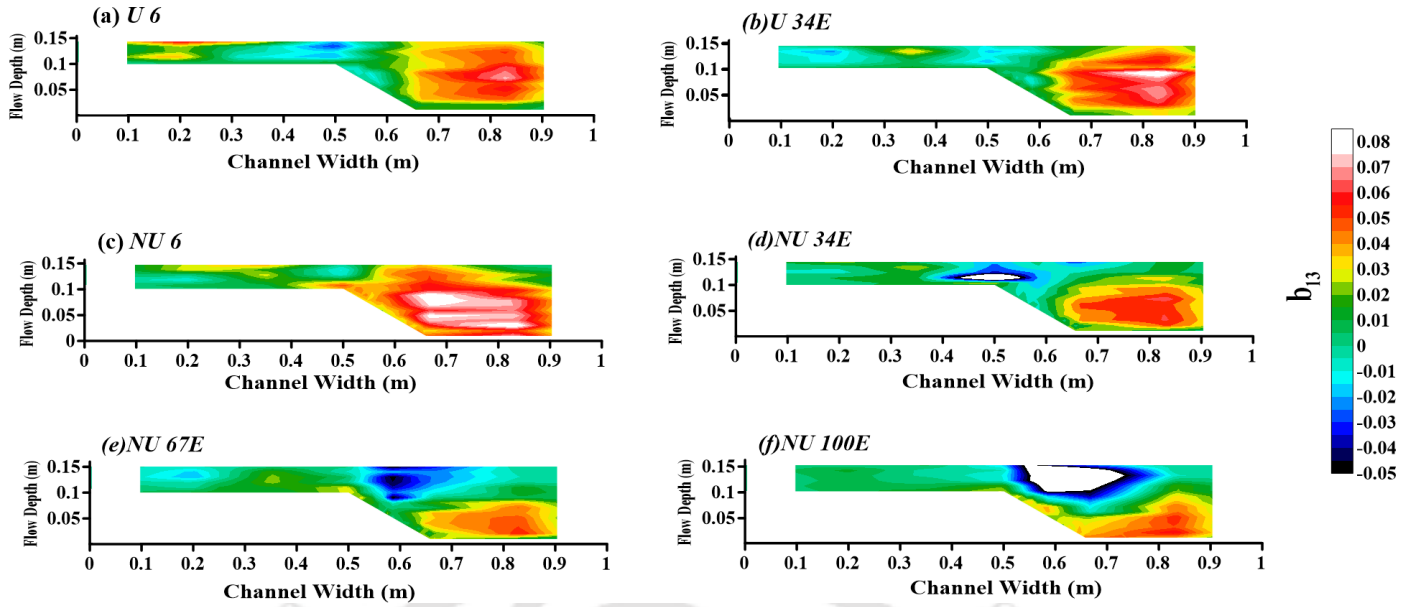

Figure 4.10 Contouring of b_{13} anisotropic stress tensor of uniform and non-uniform cases at 5.5 m cross-section for 35 lps

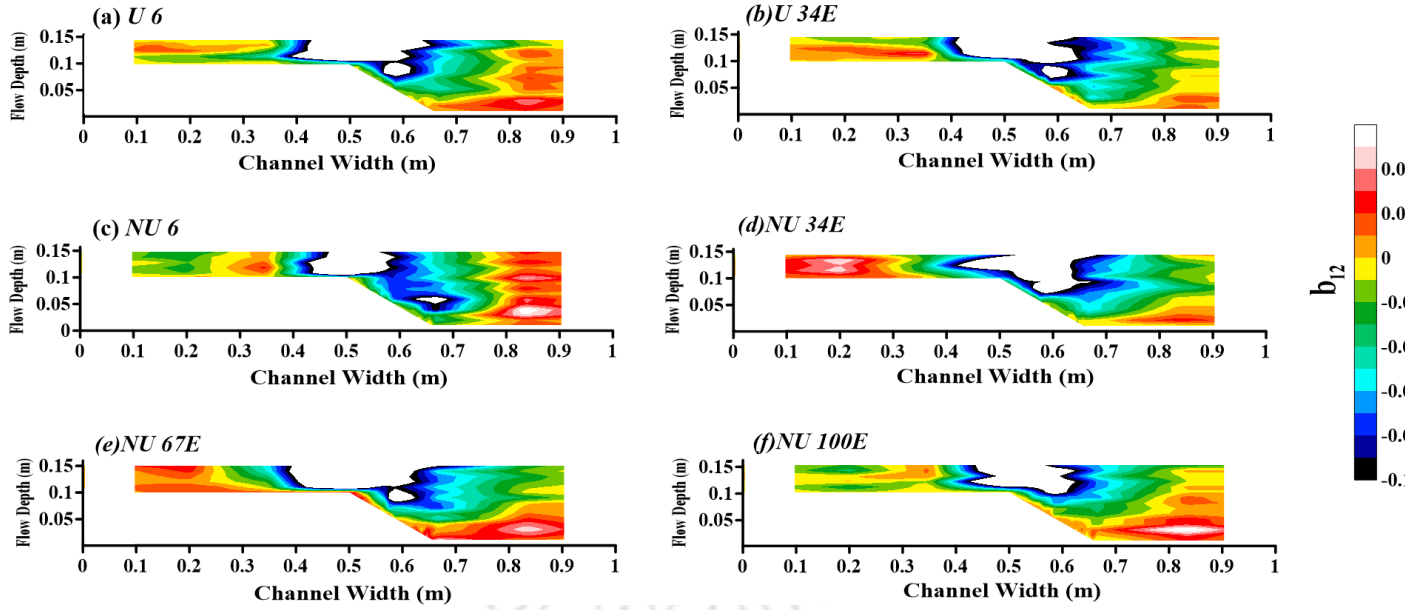

Figure 4.11 Contouring of b_{12} anisotropic stress tensor of uniform and non-uniform cases at 5.5 m cross-section for 35 lps

Though the contribution of different anisotropic tensor component b_{ij} are shown in figures 4.8-4.11, the nature and degree of anisotropy at various points of 5.5 m cross-section for different vegetation setups could be understood more clearly by analyzing the anisotropic invariant map (AIM) as shown in Figure 4.12. The map shows the ξ vs η graph for uniform and non-uniform vegetation setups. From the map, it can be seen that all the points of 5.5m cross-section can be

either classified as pan-caked or cigar-shaped turbulence. The figure shows that most points in the floodplain region (FP 20 and FP 35) for all vegetation setup are pan-caked turbulence anisotropy (Mera *et al.*, 2015). This means that streamwise and spanwise components dominate over the vertical component in the floodplain region. However, it is observed that there is a shift from pancake-shaped turbulence to cigar-shaped turbulence for all vegetation cases as it moves from the floodplain to the SFPI region. This is because SFPI is influenced by high flow velocity from the main channel region as it acts as the boundary where momentum exchange occurs. The nature and degree of approaching the 1D vertex for the SFPI section are different for different vegetation setups. In the non-uniform vegetation setup, the tendency of approaching 1D from 3D is stronger for NU 67E (Figure 4.12 (e)) as compared to NU 34E and NU 100E (Figure 4.12 (d, f)). The reason is that in NU 67E, combined effect of higher frontal area of submerged vegetation (vetiver grass) and 67% of the emergent vegetation (perennial reed) results in higher momentum exchange at SFPI as compared to NU 34E and NU 100E. It is observed from Figure 2.15 (f) that, though 100% of the vegetation is emergent in NU 100E, the frontal area is lesser compared to NU 67E (figure 2.15 (e)). The anisotropy of other sections of the $5.5\ m$ cross-section (SM, SE, and MC) behaves in a diverse set of pancake-shaped and cigar-shaped structures throughout the flow depth. In the SM section, in most of the vegetation cases, it approaches 1D component (cigar-shaped) in the upper flow depth ($z/h > 0.15$) whereas in the lower portion of the flow depth ($z/h < 0.15$) it tends to approach 2D (pancake-shaped) turbulence anisotropy. However, there is an exception for NU 67E and NU 100E where 2D turbulence anisotropy seems to approach at an upper flow depth ($z/h \approx 0.3$) compared to other non-uniform vegetation set-up cases. When it comes to SE and MC, with the addition of lower flow depth influenced by 2D turbulence anisotropy, most vegetation cases also show a 2D approach in the upper region of flow depth. However, all the points in the main channel section of NU 67E approach 2D component (pancake-shaped) turbulence compared to other vegetated cases where a mixed distribution of 2D and 1D components is observed throughout the flow depth.

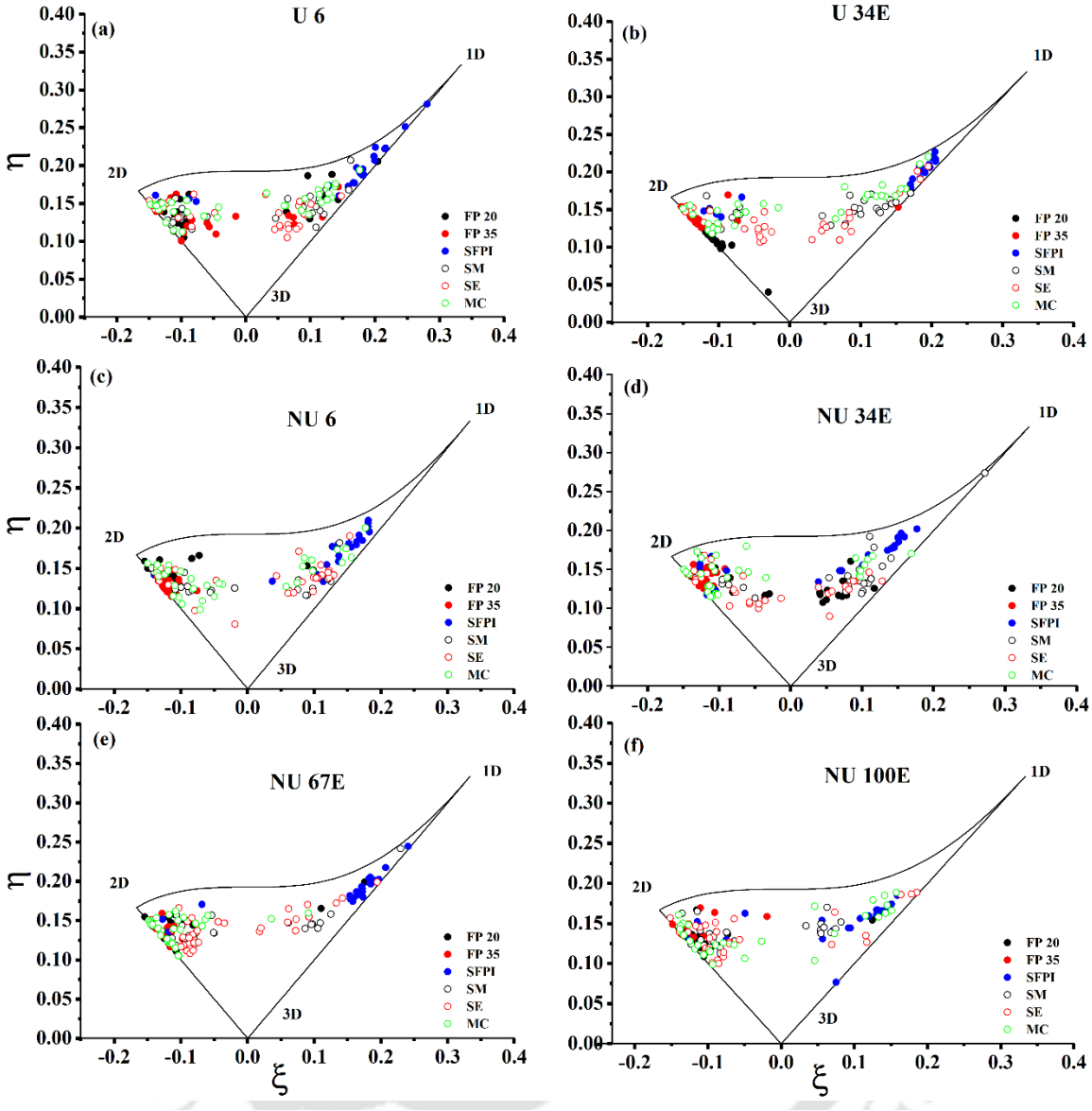

Figure 4.12 Anisotropic invariant map of uniform and non-uniform cases at 5.5m cross-section for 35lps

The turbulence state in the vegetated channel can be further enhanced by studying the invariant function F across the 5.5m cross-section. Figure 4.13 shows the distribution of F across the cross-section of different vegetation setup cases for 35 lps. The value of F is more in most vegetation cases in the upper region of flow depth (>0.08m) in the slope and main channel region. It suggests flow in the sloping and main channel zone has a lesser tendency to approach 2D state than floodplain region. Further, the magnitude of F in the NU 67E case is relatively lower in the slope and main channel region than other non-uniform vegetation setups, suggesting a greater tendency to attain a 2D turbulence state. This point was also seen while analyzing the AIM in Figure 4.12 (e). Figure 4.13 (g, h) show the point distribution of F in the main channel of 6cm uniform and 34E cases. It can be seen that there is a decrease in F for

both cases as it approaches the channel bed. However, the decrease is more in the 34E case than in the 6cm uniform case for both uniform and non-uniform setups, suggesting more anisotropy in the 34E case.

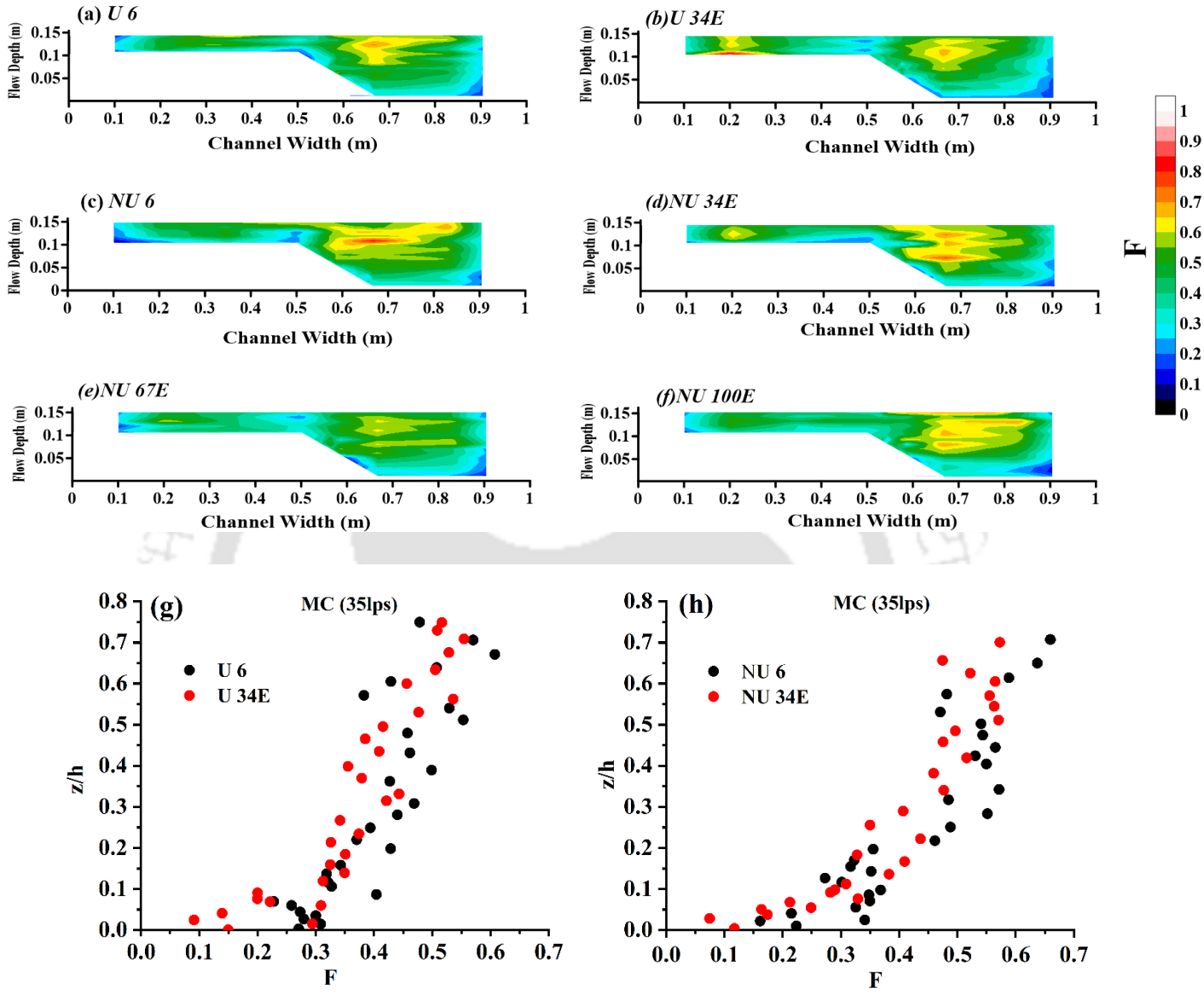

Figure 4.13 (a)-(f) Contouring of evolution of invariant function F and (g)-(h) point distribution of F at main channel of uniform and non-uniform cases at 5.5 m cross-section for 35 lps

4.7 Conclusion

Laboratory experiments were performed to study the flow behavior in multi-layered compound vegetated channels. The multi-layered vegetation in the floodplain of the compound channel was attempted to match the real field situation by using vetiver grass as submerged vegetation and perennial reed as emergent vegetation. It is also observed that there is an increase of more than 20% velocity in the main channel section as the flow progresses from sparsely vegetated

(20cm c/c) to densely vegetated (10cm c/c) region in NU 6. Multi-layered vegetation was considered and compared to single-layered vegetation in compound channels. It was seen that flow characteristics like velocity, streamwise RSS, turbulent intensities and TKE shows higher magnitude for uniform set up (U 6 and U 3-6-9) compared to non-uniform set up (NU 6 and NU 3-6-9) in the SE and MC sections. These findings show that vegetation distribution should preferably be in a non-uniform set up with varying spacing to decrease turbulence and maintain stability of banks. Comparing the multi-layered submerged vegetation (U 3-6-9 and NU 3-6-9) with single-layered submerged vegetation (U 6 and NU 6) showed that flow characteristics like velocity, RSS, and intensity are greater in the multi-layered cases. The flow contrast between U 6 and U 3-6-9 remains consistent, as observed in Chapter 3 for PV 6 and PV 3-6-9. This consistency applies across different vegetation types, where the flow characteristic depends on the resistance offered locally near the SFPI sections.

The different degrees of emergent cases (34%, 67% and 100%) are compared by observing the flow deviation from isotropic behavior by analyzing stress anisotropic tensor for different vegetation cases. The analysis of anisotropic tensor component b_{ij} showed that the main channel is dominated by b_{11} whereas b_{22} mostly dominates the floodplain region of the channel. However, the difference in nature and degree of anisotropy of different vegetation cases could be better understood with the help of an anisotropic invariant map (AIM). The floodplain region of almost all the cases was seen to follow a pancake structure. This means the floodplain region was dominated by 2D component anisotropy. The case differs slightly in the SFPI section, where the points approach from 3D to 1D (cigar-shaped structure). The SFPI section of NU 67E is more inclined to 1D turbulence than NU 34E and NU 100E. The other sections (SM, SE, and MC) offer a mixed distribution of pancake-shaped and cigar-shaped structures for different cases. However, a higher percentage of points in the main channel region in the NU 67E case approaches 2D turbulence than other non-uniform vegetation setups. This was also seen while analyzing the invariant function F where the value of F is less for NU 67E than other cases, which indicates the approach towards 2D turbulence state. Further, the 34E case also seems to have a lower F value than the 6cm uniform case for both vegetation setups.

5 Flow in multi-layered vegetated compound channels with different bank slopes[4]

5.1 Introduction

A variety of factors influence a compound channel's flow. The bank angle is a key factor in determining the flow patterns in the channel, together with the pattern of vegetation distribution on the floodplain. Researchers have attempted studies concerning the bank angle effect on the flow in the compound channel. McBride *et al.* (2007) compared compound channels with different bank slopes (36^0 angled, 90^0 vertical and 144^0 undercut) with rigid emergent vegetation in the floodplain portion. They found that streamwise velocity was higher in the angled banks' main channel than in the vertical and undercut banks. Tominaga *et al.* (1989) and Xiao *et al.* (2018) considered experiments in compound channels with bank slopes varying from 30^0 to 90^0. They found that flow characteristics like Reynolds shear stress and turbulent intensities are correlated with bank slopes. Xiao *et al.* (2018) concluded that lower-value bank slopes are better at maintaining riverbed stability. Yan *et al.* (2020) did a numerical study considering a curved compound channel with different bank slopes. They developed a $k-\varepsilon$ turbulence model and found that flow characteristics change with a change in the channel bank slope. Wang *et al.* (2018) and Xiao *et al.* (2022) studied the hyporheic transport in the transverse direction and biogeochemical reactions in a compound channel. They changed the bank slopes to observe the transport of nutrients in the compound channel. Xiao *et al.* (2022) concluded that a gentle bank slope with protection of the bank slope by large stones and gravels is required for maintaining biogeochemical reactions, which are crucial for streambed ecology. Taye *et al.* (2023) considered meandering channels with side slopes of 90^0 and 35^0 to observe the morphological changes in the presence of seepage. They found that the bank gets more deformed in the presence of seepage as compared to no seepage condition. The studies mentioned focused mainly on the varying bank slopes, and little emphasis was given to the floodplain vegetation. The type of vegetation in the floodplain influences the flow dynamics in the slopes and main channel of the compound channel. When flow encounters flexible

[4] Barman, J., & Kumar, B. (2023). Flow in multi-layered vegetated compound channels with different bank slopes. Physics of Fluids. 35(3), 036601.https://doi.org/10.1063/5.0142400

vegetation as opposed to rigid vegetation, the channel's turbulence changes. A lot of researchers have used flexible vegetation in the laboratory to understand turbulence and roughness in the channel (Nepf and Vivoni, 2000; Carollo *et al.*, 2002; Nepf and Ghisalberti, 2008; Huai *et al.* 2019; Caroppi *et al.* 2021). In the present study, rigid vegetation is considered for experiments as the role of non-uniform height is better displayed using rigid vegetation. Furthermore, rigid vegetation also reduces complexities when flow encounters both submerged and emergent vegetation.

The difference of flow as it encounters single-layered and multi-layered vegetation in partially vegetated and compound channels were discussed in detail in Chapters 3 and 4 respectively. That is why only multi-layered vegetation is considered in the floodplain areas in this chapter. This chapter attempts to understand the impact of vegetation height on the bank slopes of a compound channel. Studies comparing multi-layered vegetated compound channels with different bank slopes have also not been explored previously. The region in and around the slopes will be emphasized in this study as maximum flow interaction occurs in this portion of the compound channel. This study will also help to understand the role of slopes in determining the bank stability of the channel. The experimental setup of different bank angle compound channels was discussed in section 2.9.3.

5.2 Streamwise velocity

Figure 5.1 shows streamwise velocity ($\bar{u}/U$) contours of $45^0$and 90^0 bank slope of compound channel for no-vegetation and multi-layered vegetated cases. The time-averaged velocity ($\bar{u}$) is made non-dimensional by average velocity U in the channel. The velocity contours of NV cases for both sets/bank slopes are shown in Figures 5.1 (a, b). The velocity difference in the floodplain and main channel domain is almost comparable because of the absence of vegetation. The little contrast in velocity between floodplain and main channel in NV cases (figure 5.1 (a, b)) is mainly observed because of the non-uniform cross-section of the channel. However, the velocity magnitude in the main channel of 45^0 compound channel varies compared to 90^0 compound channel. The velocity in the main channel of 45 NV case in Figure 5.1 (a) is larger than the 90 NV case in Figure 5.1 (b). The NV cases show the bank slopes role while determining the channel flow. Previous researchers like Tominaga *et al.* (1989), Tominaga and Nezu (1991), and Xiao *et al.* (2018) also discussed the impact of bank slopes on the flow in compound channels in the absence of vegetation. The inclusion of vegetation in the floodplains gives different flow dynamics as seen in Figures 5.1(c) to 5.1(f). The velocity in

the floodplain for both bank slopes is very less because of vegetation obstruction. With the increase of emergence level (Figure 5.1(e, f)), the average frontal area increases, which provides more restriction to the flow in the floodplain region. Due to the flow obstruction in the floodplain region, flow is shifted to the main channel. However, the magnitude of shifting is different as it also depends on the bank slope and vegetation emergence. The velocity in the main channel region (0.7 m<channel width<0.9 m) of 45 3-6-9 is almost comparable to that of the 90 3-6-9 case. However, with the increase of vegetation emergence in Figures 5.1 (e, f), a more distinguishable difference is observed in the main channel where velocity in 45 34E is more than 90 34E. This increase of velocity in the main channel by lower bank angle (36^0 slope) compared to vertical banks (90^0 slope) was also observed by Mcbride *et al.* (2007). This change in flow dynamics in the main channel is because of the change of bank slopes for both vegetation arrangements (3-6-9 and 34E). Therefore, it is necessary to analyze and compare the velocity profiles in the sloping regions of both $45^0$and 90^0 compound channel, as seen in Figures 5.2 and 5.3.

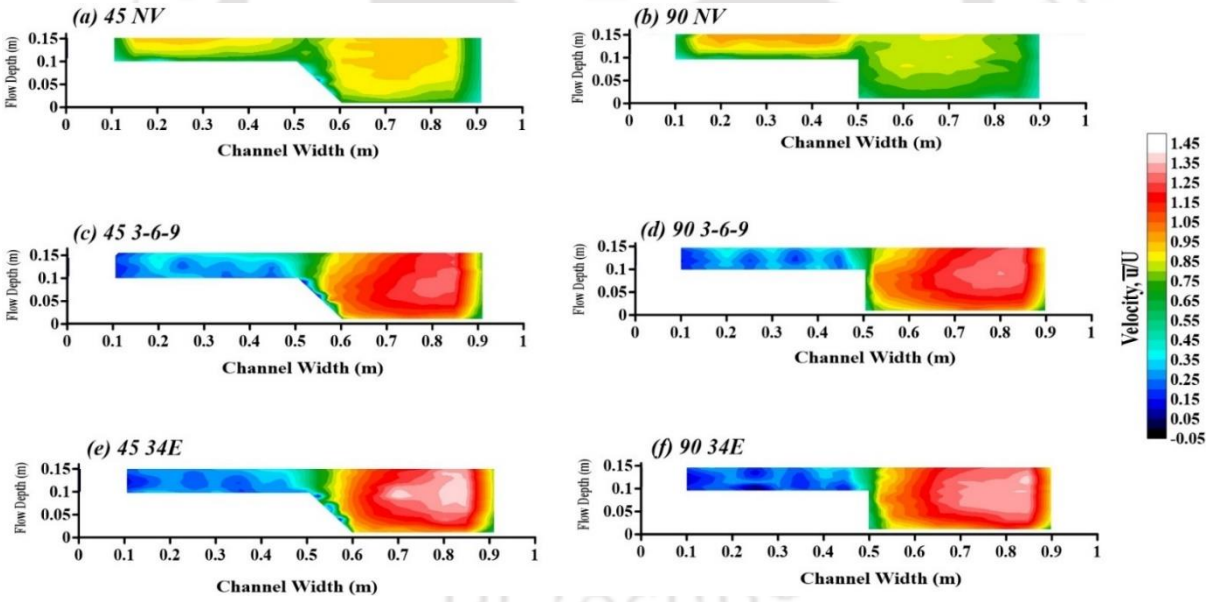

Figure 5.1 Velocity contours of Set 1and Set 2 compound channel for 42 lps

Figure 5.2 depicts the velocity profiles in the sloping and its nearby regions (FP 50, SL 52.5, SL 55, MC 60) of Set 1 and Set 2 compound channels for multi-layered vegetated cases. As shown in Figure 5.1, the velocity on the slopes and nearby also affects the velocity in the main channel. From Figure 5.2, it is seen that the velocity in 90^0 slopes are more compared to 45^0 slopes for both multi-layered vegetation arrangements. However, the magnitude is different for different slope positions. In FP 50 section of Figure 5.2(a), though velocity of 90^0 slopes are

greater than 45^0 slopes, its extent is still less than SL 52.5 and SL 55 sections in Figures 5.2(b) and 5.2(c). The depth-averaged velocity increase of 90^0 slopes in FP 50 section is around $20-30\%$ for both vegetation cases. On the other hand, depth-averaged velocity increase of 90^0 slopes in SL 52.5 and SL 55 sections are more than 50%. The high percentage increase of velocity in the 90^0 slopes can be attributed to the abrupt change of flow depth from FP 50 to SL 52.5 and SL 55 in the case of 90^0 compound channel. On the other hand, the change of flow depth in the case of 45^0 compound channel is very gradual. This means that the energy head gradually increases from FP 50 to MC 60. The slope in 45^0 compound channel acts as an extended part of the floodplain with a gradual increase of flow depth. However, in 90^0 bank slope, SL 52.5 and SL 55 are already part of the main channel and have almost achieved the maximum velocity. The loss of energy from FP 50 to MC 60 is more for 90^0 bank slope as compared to 45^0 bank slope channel. It is also observed from Figure 5.2 (d) that difference in velocity in MC 60 section between 45^0 and 90^0 compound channel is less than SL 52.5 and SL 55 sections. The depth-averaged velocity increase in MC 60 section for 90^0 compound channel is less than 10% compared to 45^0 compound channel. This shows that the velocity difference between different bank slopes is observed to be maximum in and near the slopes, and it decreases as it moves away from the slopes. The compound channel with progressive slopes reaches its maximum velocity gradually relative to slopes with steeper banks. This makes the steeper banks more prone to erosion.

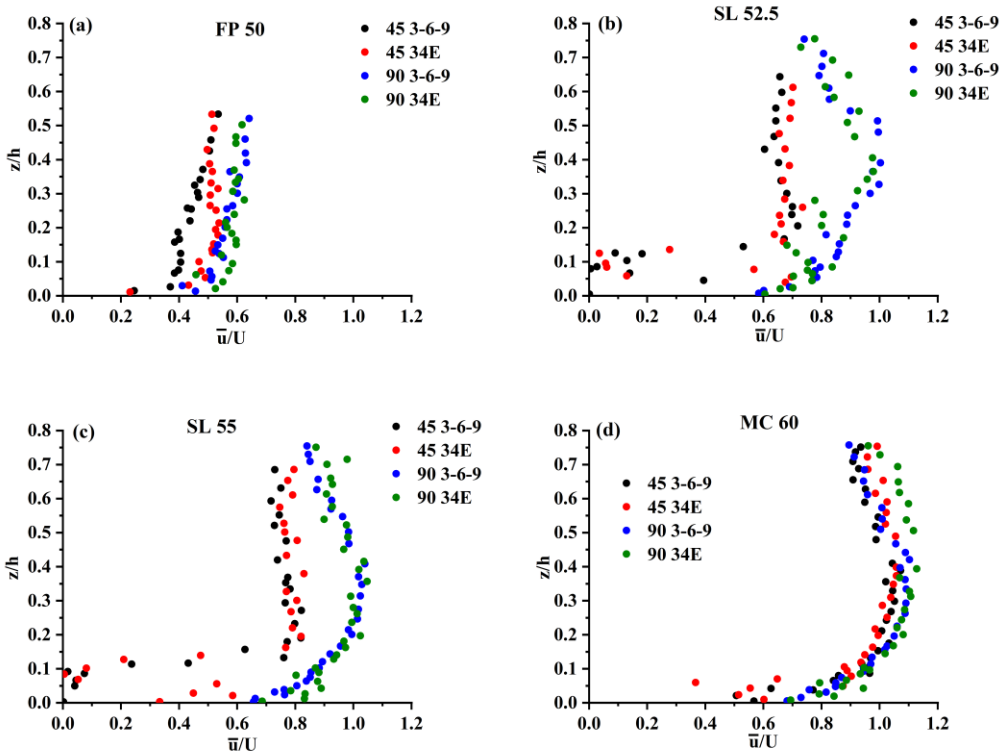

Figure 5.2 Velocity profiles at and near slope region of Set 1 and Set 2 of compound channel for 42 lps

5.3 Reynolds shear stress (RSS)

Figure 5.3 shows RSS contours streamwise ($-\overline{u'w'}/U^2$) direction for NV and multi-layered cases for Set 1 and Set 2 of compound channels. Figures 5.3(a) and 5.3(b) show that streamwise RSS contour has positive values both in the floodplain and main channel areas. The magnitude of $-\overline{u'w'}/U^2$ increases from the surface and attains maximum value in the lower portion of flow depth in the main channel for both NV cases. The multi-layered floodplain vegetation changes RSS throughout the compound channels' cross-sections as seen in Figures 5.3(c) to 5.3(f). The magnitude of $-\overline{u'w'}/U^2$ in the lower region of the main channel (FD<0.1 m) is also higher compared to NV cases. The region in and around slope (0.5 m<channel width<0.6 m) for both the compound channels follow negative streamwise RSS. However, the magnitude varies depending on the compound channel's vegetation emergence and bank angle, as observed in Figure 5.4. It is observed that all the profiles of Figure 5.4 show both positive and negative RSS. This suggests that the region in and around slopes for 45^0 and 90^0 channel is subjected to helical flow or circulation region. However, in the present study, the magnitude is different when the flow is subjected to different bank slopes. From Figures 5.4(b) and 5.4(c),

it is observed that the extent of negative magnitude is observed more in the 45^0 slope channel. However, the magnitude of positive RSS at $z/h < 0.2$ is more for 90^0 channel for both multi-layered vegetation arrangements. This higher magnitude of positive RSS near the channel bed could increase the erosional process for 90^0 compound channel, which might fail the bank. Figure 5.5 demonstrates the distribution of transverse RSS ($-\overline{u'v'}/U^2$) contours for NV cases and multi-layered vegetation cases for both bank slopes. The distribution of $-\overline{u'v'}/U^2$ in absence of vegetation in Figure 5.5(a) and 5.5(b) shows a similar trend as observed in figure 5.3(a) and 5.3(b). The indifference of $-\overline{u'v'}/U^2$ magnitude in the floodplain and main channel is mainly due to the non-uniform cross-section of the channel. However, the inclusion of vegetation primarily affects the region in and around the slopes. The magnitude of transverse RSS (Figure 5.5(c-f)) is more in the sloping region compared to streamwise RSS (figure 5.3(c-f)). Furthermore, an increase in vegetation emergence (Figure 5.5(e, f)) leads to a greater impact of RSS in the sloping region of the channel for both bank slopes. It shows a higher chance of erosion of the banks with higher vegetation emergence in the floodplain areas of the compound channel.

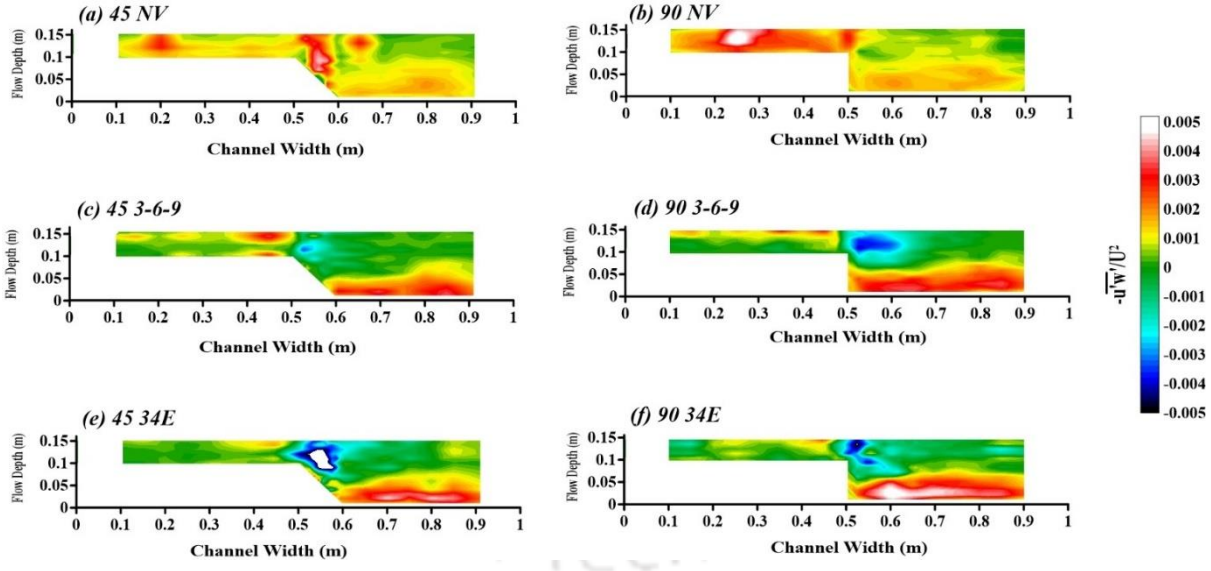

Figure 5.3 Streamwise RSS ($-\overline{u'w'}/U^2$) contours of Set 1 and Set 2 of compound channel for $42\ lps$

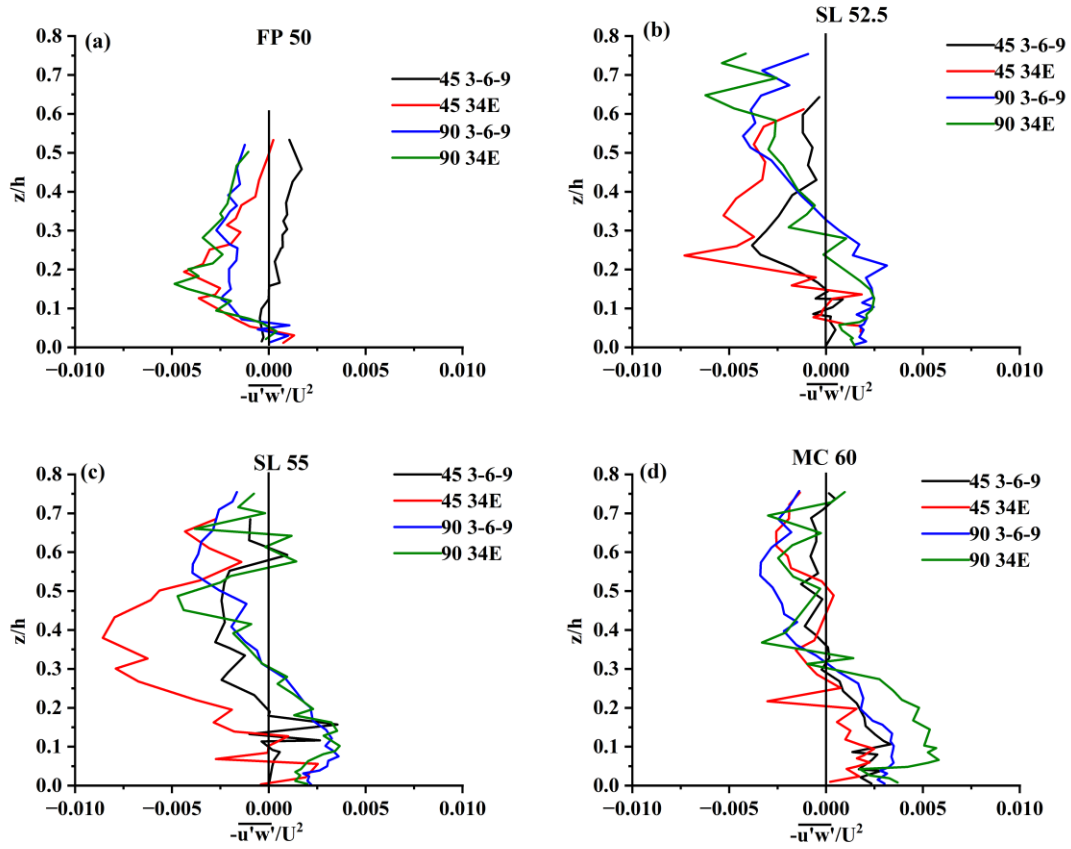

Figure 5.4 Streamwise RSS ($-\overline{u'w'}/U^2$) profiles at and near slope region of Set 1 and Set 2 of compound channel for 42 lps

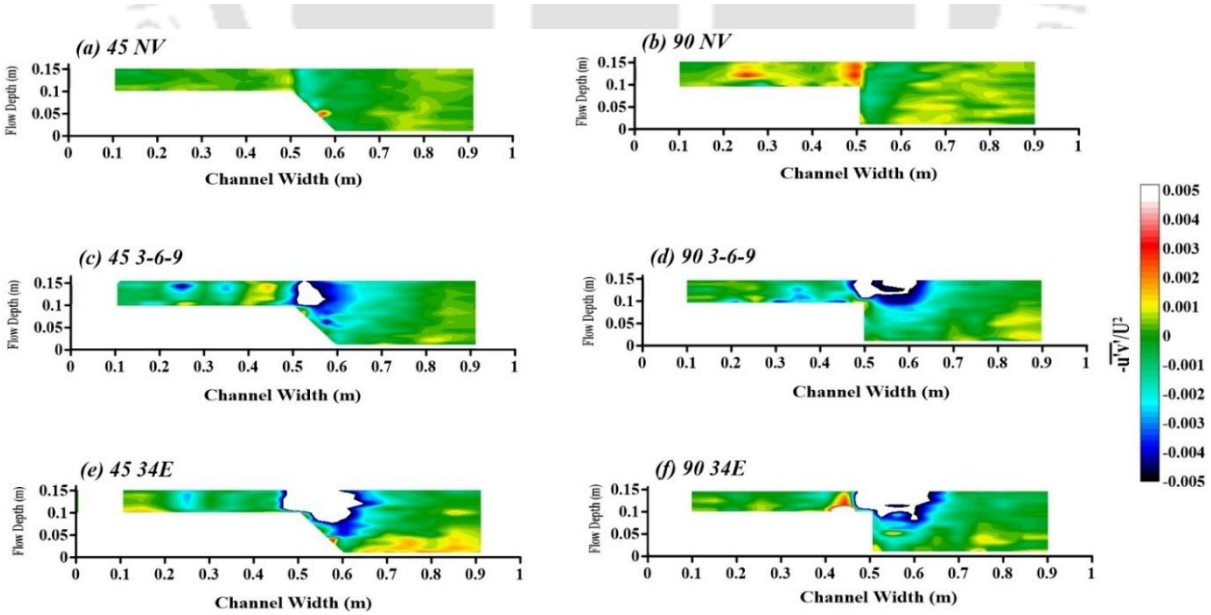

Figure 5.5 Transverse RSS ($-\overline{u'v'}/U^2$) contours of Set 1 and Set 2 of compound channel for 42 lps

5.4 Turbulent Kinetic Energy (TKE)

Figure 5.6 shows the TKE contours of $45^0$and 90^0 bank slopes of compound channels for both NV and multi-layered vegetation arrangement cases. From the NV cases in Figures 5.6(a) and 5.6(b), the TKE is similar in the main channel and floodplain areas. However, the slopes of 45 NV show a higher TKE because of the non-uniform channel cross-section. This increase of TKE in and around slopes is more evident with vegetation in the floodplain, as seen in Figures 5.6(c) to 5.6(f). The TKE is further increased with vegetation emergence for both bank slopes as seen in Figures 5.6(e) and 5.6(f). The 34% vegetation emergence provides greater obstruction in the floodplain, ultimately escalating the momentum exchange between the main channel and the floodplain. This affects the slopes where higher turbulence is observed compared to 3-6-9 multi-layered submerged vegetation. The higher TKE in the slopes of partially emergent vegetation (45 34E and 90 34E) over fully submerged multi-layered vegetation (45 3-6-9 and 90 3-6-9) is observed in Figure 5.7. The TKE in the slope sections (SL 52.5, SL 55, and MC 60) is mostly higher for 34% emergent vegetation over fully submerged vegetation, irrespective of the bank slopes. This shows that the extent of turbulence increases in and around the slopes with a greater obstruction or emergent vegetation in the floodplain. This might increase the chance of erosion in the sloping regions, causing the bank's failure. The TKE profiles in FP 50 section in Figure 5.7(a) show a similar pattern as the velocity profile in Figure 5.2(a). Here, the magnitude of TKE is higher for 90^0 bank slope compared to 45^0 slope channel irrespective of vegetation arrangement. However, the definitive comment cannot be given for other slope sections (SL 52.5, SL 55, and MC 60) for the TKE magnitude as both the profiles of 45^0 and 90^0 bank slopes are almost similar in overall flow depth.

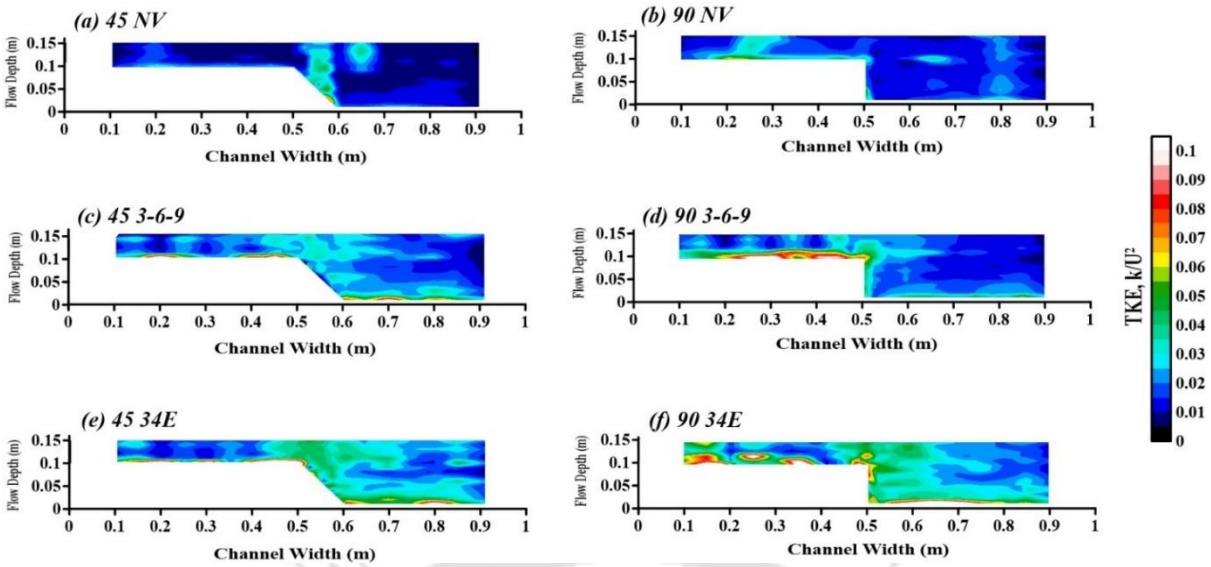

Figure 5.6 TKE (k/U^2) contours of Set 1 and Set 2 of compound channel for 42 lps

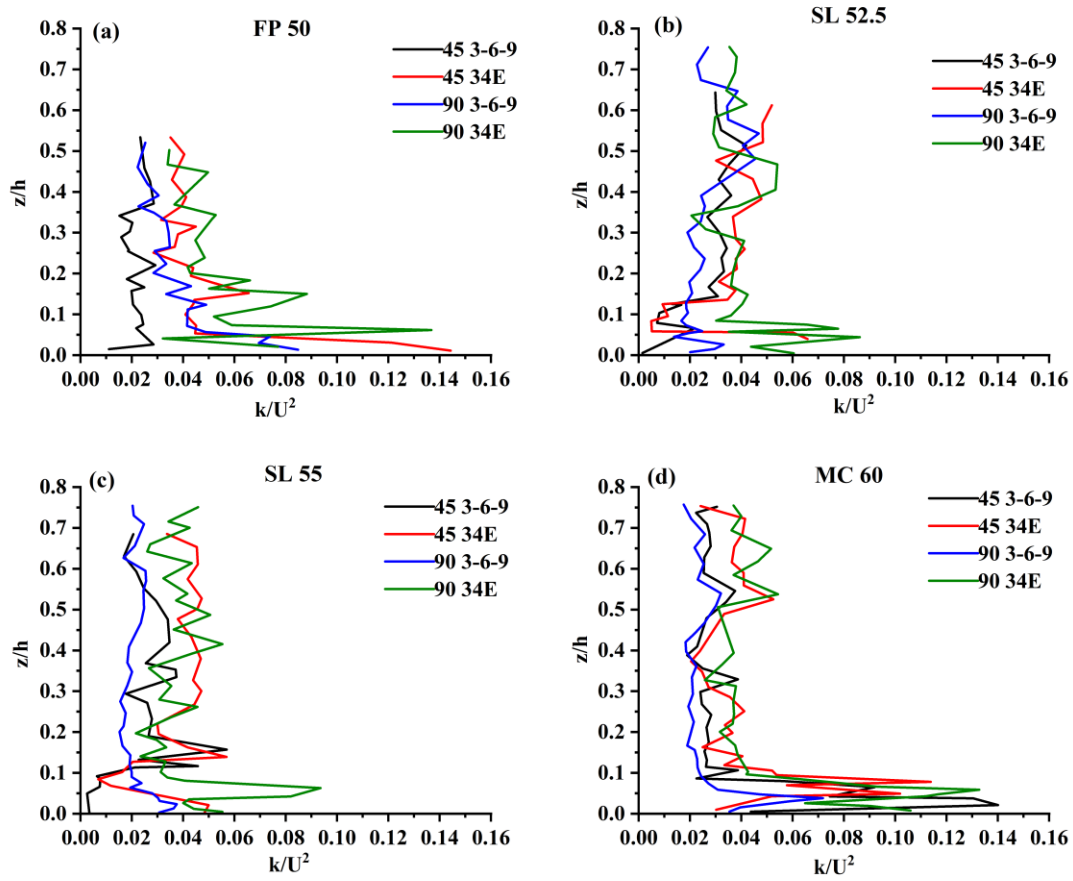

Figure 5.7 TKE profiles at and near slope region of Set 1 and Set 2 of compound channel for 42 lps

5.5 Anisotropic Invariant Map (AIM)

The Anisotropic Invariant Maps (AIMs) are used to observe the degree of anisotropy in this study, particularly in the sloping regions of multi-layered floodplain vegetation at different bank slopes. The AIMs demonstrate turbulent flow that deviates from isotropy (Lumley, 1979). The coordinates of AIMs are ξ and η which denote the nature and degree of anisotropy respectively. Considering the ξ and η coordinates, a Lumley triangle is constructed which decides the nature and degree of anisotropy. The three vertices of the triangle represent 3D ($\xi = 0, \eta = 0$), 2D ($\xi = -{}^{1}/_{3}, \eta = {}^{1}/_{6}$) and 1D ($\xi = {}^{1}/_{3}, \eta = {}^{1}/_{3}$) turbulence as seen in Figures 5.8 and 5.9. The alignment of the points in the Lumley triangle of the AIMs determines whether the transformation of the point is from 3D to 2D or from 3D to 1D. Figures 5.8 and 5.9 show Anisotropic Invariant Maps (AIM) of the floodplain, slopes, and main channel regions of 45 34E and 90 34E, respectively, for 42 lps. It is observed that contrary to floodplain and main channel regions, the higher percentage of points in sloping regions approach 1D turbulence anisotropy for both bank slopes. This shows that since the slopes get affected the highest when momentum exchange occurs between the main channel and floodplain, the transverse component dominates over the other two components (Figure 5.8(b) and 5.9(b)). The dominance of the transverse fluctuating component (v') in the slopes was also observed while analyzing transverse RSS ($-\overline{u'v'}/U^2$) in Figure 5.5. The dominance of 1D turbulence anisotropy in the slopes of 31^0 bank slope comprising of both submerged and emergent vegetation was also observed in Chapter 4. The AIM maps showed the indifferent effect of flow in the slopes compared to the main channel and floodplain, as seen in Figures 5.8(b) and 5.9(b). However, the differentiation between the two bank slopes will be further cleared while analyzing the bursting phenomenon in the next section.

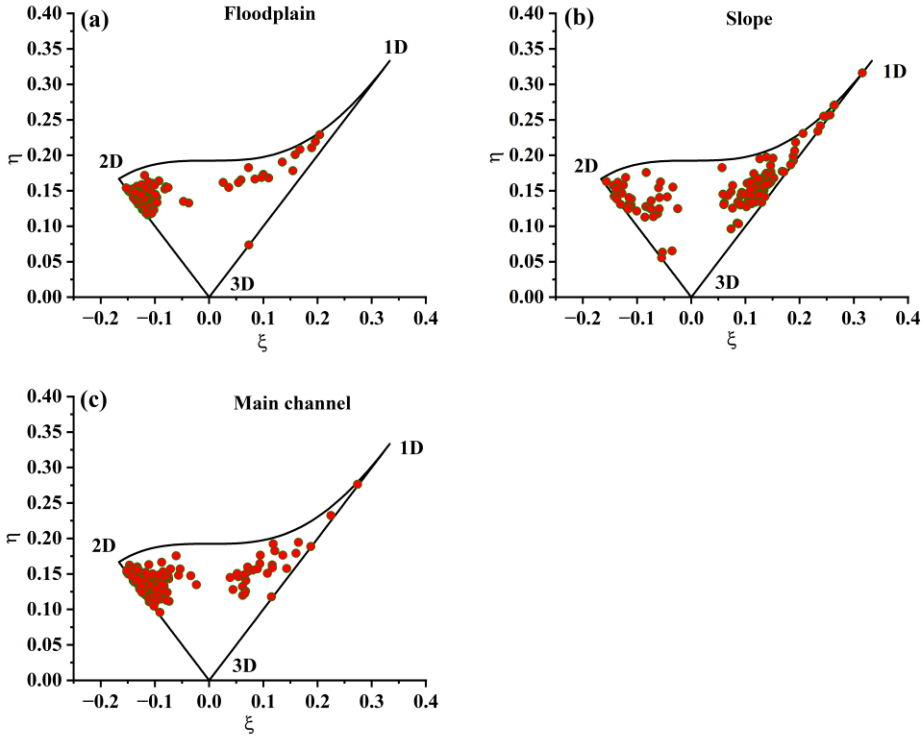

Figure 5.8 Anisotropic Invariant Map (AIM) of 45 34E at 42 *lps* for (a) floodplain, (b) slope and (c) main channel regions

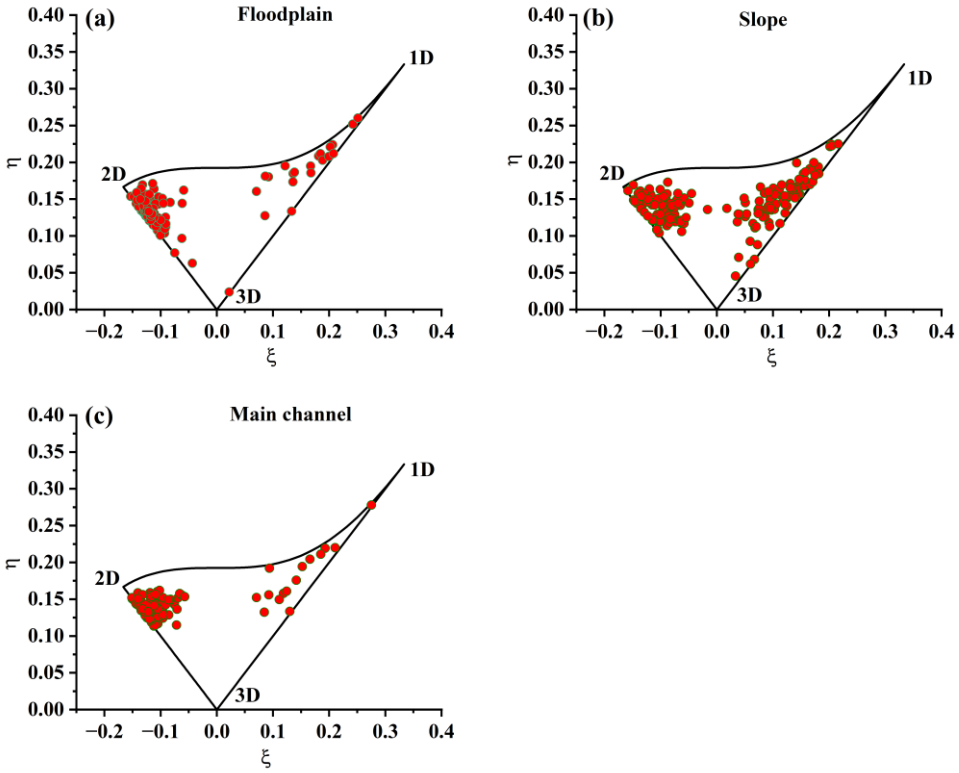

Figure 5.9 Anisotropic Invariant Map (AIM) of 90 34E at 42 *lps* for (a) floodplain, (b) slope and (c) main channel regions

5.6 Bursting Phenomenon

The turbulent structures in the slopes can be further understood by studying the bursting phenomenon of the streamwise RSS. These events can be divided into four quadrants based on the sign of Reynolds shear stress fraction ($S_{i,H}$). The $S_{i,H}$ includes the streamwise Reynolds shear stress ($-\overline{u'w'}$) and the signs of streamwise and vertical velocity fluctuations (u' and w') determine the quadrant event. These events are outward interaction ($u' > 0$, $w' > 0$), ejection ($u' < 0$, $w' > 0$), inward interaction ($u' < 0$, $w' < 0$), and sweep ($u' > 0$, $w' < 0$). The $S_{i,H}$ is defined as: $S_{i,H} = \frac{\langle u'w' \rangle_{i,H}}{\overline{u'w'}}$. The i parameter represents the quadrant and H is the hole size. The increase in hole size H shows that weaker events are eliminated and stronger events are considered. The detailed explanation of quadrant analysis is given in Chapter 3. Figures 5.10 and 5.11 shows conditional Reynolds shear stress ($S_{i,0}$) of 45 3-6-9 and 45 34E respectively at $42\ lps$. It is observed that the region in and around slopes is subjected to higher negative $S_{i,0}$ in the 2nd quadrant (sweep) and 4th quadrant (sweep). The contribution of negative sweep and ejection in the slope region can be credited to the negative streamwise RSS, as observed in Figure 5.3. This means that in the sloping region of 45 3-6-9 and 45 34E, the movement of eddies is in the anticlockwise direction. Furthermore, compared to submerged vegetation (45 3-6-9) in Figure 5.10, the increase in floodplain vegetation emergence (45 34E) in figure 5.11 causes greater negative ejection and sweep, especially in the upper portion (FD>$0.1\ m$) of a sloping region. The extent of this negative ejection and sweep events in the 45 34E cases is also more in the upper portion (FD>$0.1\ m$) of the main channel ($0.65\ m$<channel width<$0.85\ m$) compared to the 45 3-6-9 case. This demonstrates that as vegetation emerges more frequently from the floodplain region's water surface, the compound channel's sloping and main channel experiences more negative ejection and sweep events. The lower region of the main channel where FD<$0.05\ m$, ejection (2nd quadrant), and sweep (4th quadrant) are subjected to positive values as observed in Figures 5.10 and 5.11. The magnitude of this ejection and sweep events in and around slopes shows the probability of sediment mobility in the region observed in Figures 5.14 and 5.15. The contribution of ejection and sweep events on the overall sediment transport was also reported by other researchers like Nelson *et al.* (1995), Garcia *et al.* (1995), Chang *et al.* (2011), Sharma and Kumar (2017), Wu *et al.* (2022), etc.

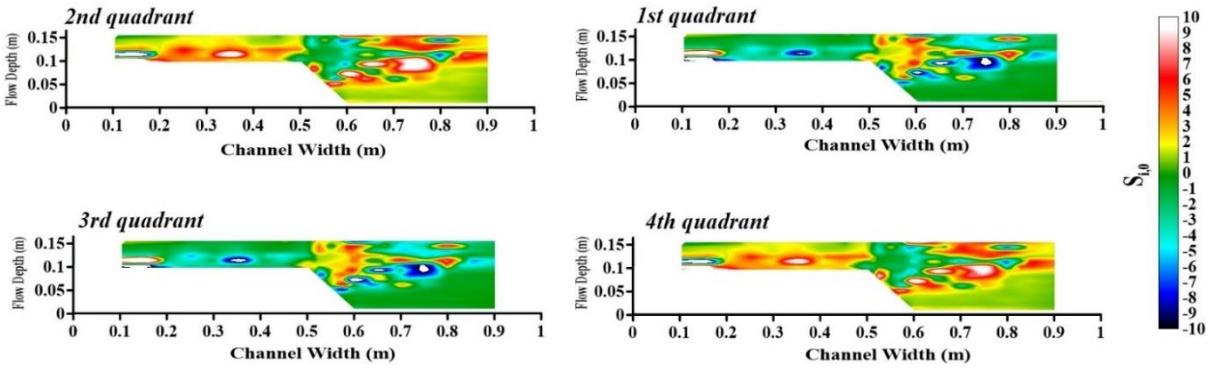

Figure 5.10 Conditional Reynolds stress ($S_{i,0}$) contouring of 45 3-6-9 at 42 lps

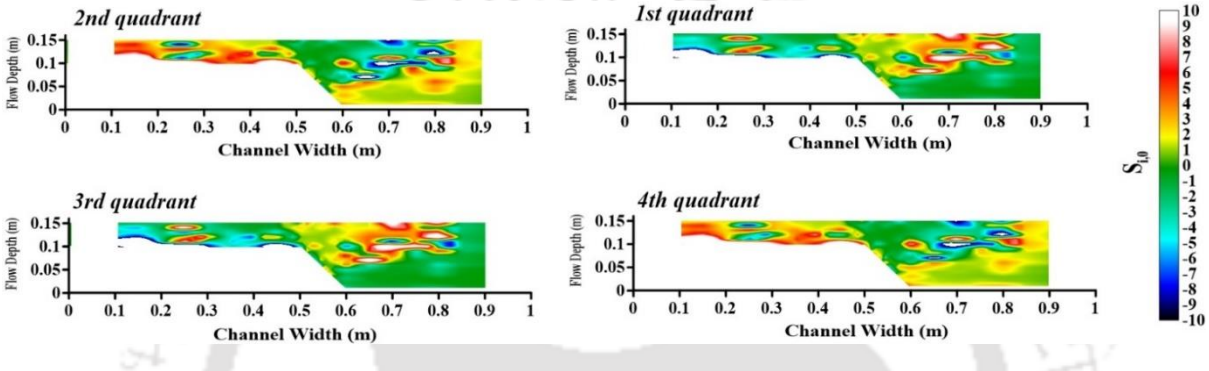

Figure 5.11 Conditional Reynolds stress ($S_{i,0}$) contouring of 45 34E at 42 lps

Figures 5.12 and 5.13 shows the distribution of various bursting events at the cross-section of 90 3-6-9 and 90 34E for 42 lps. The distribution is similar to 45^0 bank slope compound channel from figures 5.10 and 5.11, where negative ejection and sweep events dominate in and around the sloping region. The movement of eddies in this negative ejection and sweep events region is counterclockwise. This shows that irrespective of the bank angle and in the presence of vegetation in the floodplain of the compound channel, the ejection and sweep events follow negative values in and around slopes which provides opposite movement of eddies. However, the magnitude of these events in the slopes is discussed by pointwise comparison, as seen in Figures 5.14 and 5.15.

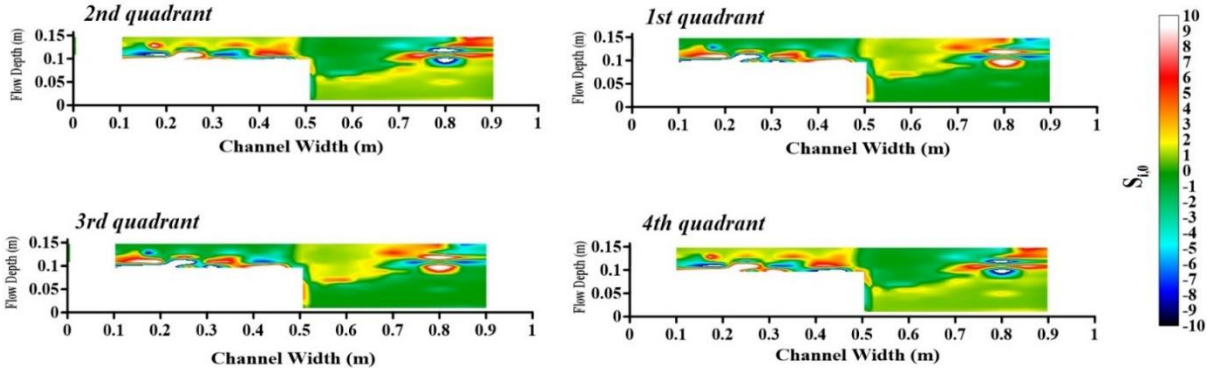

Figure 5.12 Conditional Reynolds stress ($S_{i,0}$) contouring of 90 3-6-9 at 42 lps

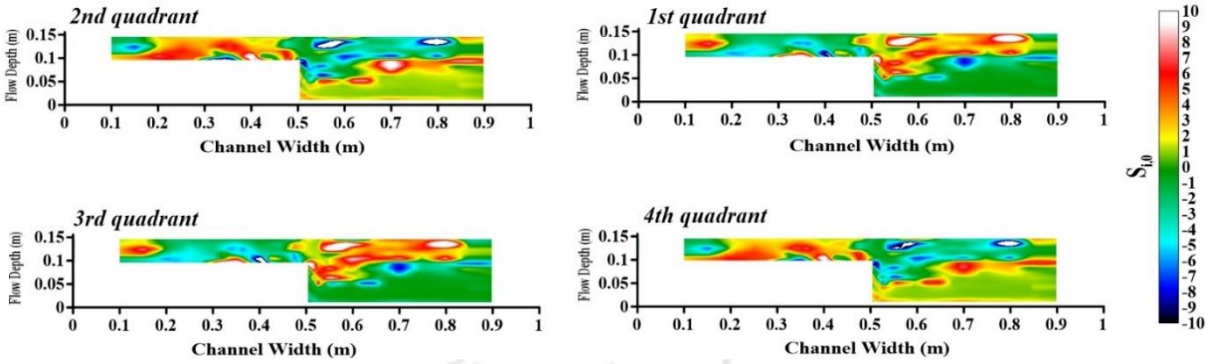

Figure 5.13 Conditional Reynolds stress ($S_{i,0}$) contouring of 90 34E at 42 lps

Figures 5.14 and 5.15 shows the ejection and sweep events at SL 52.5 and SL 55 for 42 lps. This is required to better represent these events at and near the slope region for different multi-layered vegetation arrangements compared to figures 5.10-5.13. In Figures 5.14 and 5.15, H=2 is chosen for analysis so that strong ejection and sweep events are only considered, eliminating the weak events. It is observed that these events follow both positive and negative values, which was also discussed while analyzing bursting event contours from Figures 5.10-5.13. In the 90^0 bank slope for 90 3-6-9 and 90 34E, the positive ejection and sweep are mostly observed in the lower flow region ($z/h < 0.3$), while for $z/h > 0.3$ it follows negative values, as seen in Figures 5.14 and 5.15. However, ejection and sweep events in the 45^0 bank slope mostly follows negative values and only very near the bed ($z/h < 0.1$), some points follow positive values. This shows that for $z/h < 0.3$, the eddies in and around the slopes of 45^0 and 90^0 compound channel moves in the opposite direction. Furthermore, the magnitude of these events as it approaches the channel bed ($z/h < 0.3$) is also observed to be slightly higher for 90^0 bank slope. This means that the process of low-speed fluid parcel near the bed and high-speed fluid towards the bed is higher for 90^0 bank slope in and around the sloping region. This indicates that there is a greater tendency for erosion and deposition processes in and around slopes for 90^0 bank slope compared to 45^0 bank slope compound channel. This study of the bursting events for different bank angles in compound channels can be connected to morphological changes. This can be achieved by extending the present study to include mobile bank slopes with non-uniform sand. The movement of sediment in presence of vegetation has been studied by researchers like Schmeeckle (2015), Salim *et al.* (2017), Yang and Nepf (2019), Huai *et al.* (2021), Wang *et al.* (2023) etc. The quadrant analysis can be used effectively

to understand sediment movement in the presence of multi-layered vegetation in a flexible bank compound channel.

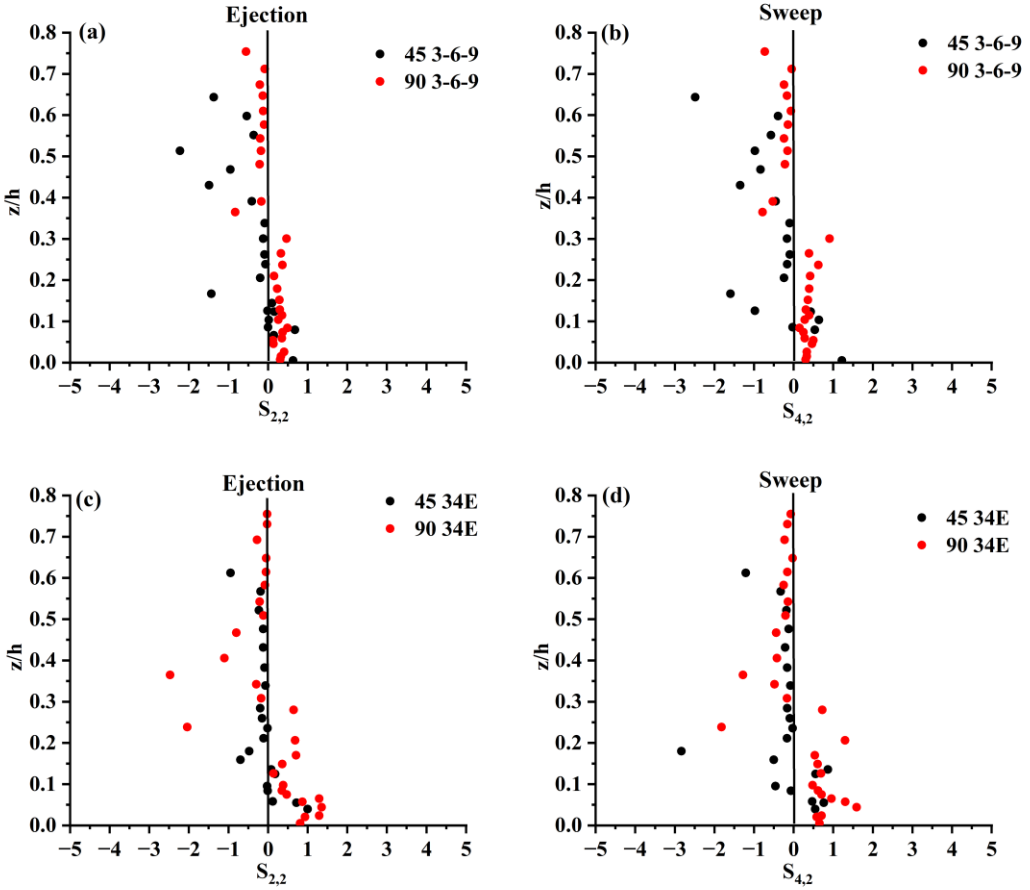

Figure 5.14 Ejection and sweep profiles of Set 1 and Set 2 of compound channel at SL 52.5 for 42 *lps*

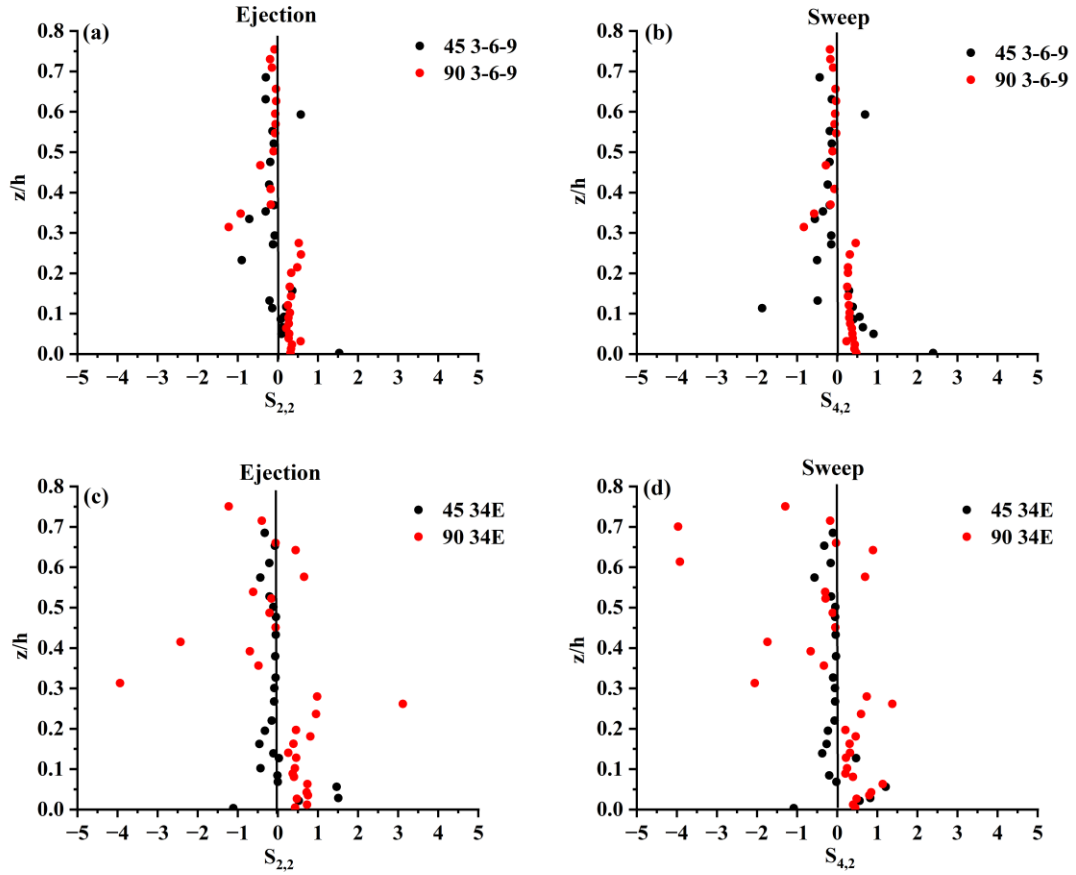

Figure 5.15 Ejection and sweep profiles of Set 1 and Set 2 of compound channel at SL 55 for 42 lps

5.7 Conclusion

Compound channel experiments were employed with multi-layered vegetation height and varying bank slopes. The study emphasized the role of bank slope when the floodplain is covered with multi-layered vegetation to give an actual field perspective. The previous literature did not stress the collective effect of floodplain vegetation and bank slope on the overall flow structure in the compound channel. The study considered two sets of bank angles (45^0 and 90^0) of the compound channel with three cases of floodplain vegetation in each set: no vegetation (NV), multi-layered fully submerged (3-6-9), and multi-layered partially emergent (34% emergent). In the NV cases for both 45° and 90° bank angles, there is little difference in the flow characteristics like velocity, RSS, and TKE over the cross-section. The indifference in flow is mainly observed close to the slopes because of the non-uniformity of the cross-section of the channels. A greater change in flow dynamics in the channel is observed when floodplain vegetation is introduced. The higher flow diversion due to the vegetation obstruction affects the region in and around the slopes. However, the flow magnitude in the

slopes and main channel depend on the bank angle and vegetation emergence in the floodplain. The velocity in and around the slopes of 90^0 bank angle is greater than 45^0 bank angle for both vegetation setups. This shows that a gradual slope (45^0) achieves maximum velocity more gradually than a steeper (90^0) slope channel, making the steeper bank more prone to erosion. Furthermore, for both vegetation settings, the positive streamwise RSS ($-\overline{u'w'}/U^2$) in and around the slopes is likewise higher for 90^0 the channel near the channel bed ($z/h < 0.2$), indicating that the bank is more susceptible to erosion for 90^0 bank slope channels. For both vegetation configurations, the streamwise RSS also revealed negative RSS in the upper flow region close to the slopes, indicating helical flow in that area. The magnitude of streamwise RSS is higher for 34% of emergent vegetation, indicating that the negative streamwise RSS in the slopes will increase with greater floodplain obstruction. The importance of floodplain vegetation was also observed while analyzing TKE where higher floodplain vegetation emergence ensured higher turbulence in and around slopes irrespective of bank angles, increasing the chance of bank failure. The vulnerability of bank slopes in the compound channel is also recognized while analyzing transverse RSS ($-\overline{u'v'}/U^2$) and anisotropic invariant map (AIM). The higher magnitude of transverse RSS in the presence of floodplain vegetation in and around the slopes indicates the chance of bank failure. The AIM analysis shows that slopes, irrespective of the bank angle, have the highest tendency to approach 1D anisotropy compared to the main channel and floodplain. This shows that the transverse component dominates the slopes compared to the other two regions. The quadrant analysis shows the presence of negative ejection and sweep events in the sloping regions irrespective of bank angle, indicating the counterclockwise movement of eddies in the region. However, the magnitude of negative events in and around the slopes is higher with higher floodplain vegetation emergence. The magnitude of these events at $z/h < 0.3$ is also a little higher for 90^0 bank slope, showing that the chance of bank erosion is more for 90^0 compared to 45^0 bank slope channel.

6 Conclusions and Future Recommendations

The present study considers the importance of vegetation height and emergence in partially vegetated and compound channels. The turbulence in river channels depends on vegetation distribution in the floodplain region. Flow characteristics also differ when it interacts with homogeneous and heterogeneous vegetation height. The study helps to understand how crucial it is to replicate multi-layered vegetation in the laboratory to simulate actual field conditions. The study can be helpful while studying soil bioengineering techniques and different nature-based solutions to control excessive erosion and preserve bank stability. Important conclusions regarding hydrodynamics in different channel cross-sections with varying vegetation distribution are given below:

6.1 Hydrodynamics of partially vegetated channel with multi-layered vegetation

- Floodplain with homogeneous/single-layered vegetation height shows similar velocity and streamwise Reynolds shear stress (RSS) distribution in the cross-section of vegetated region, whereas it shows varying flow characteristics with heterogeneous/multi-layered vegetation height.
- The vegetated channel-main channel interaction (VCMCI) and its adjacent region exhibit pronounced changes in flow characteristics because of momentum exchange between the vegetated and main channel regions.
- When the average frontal area of the vegetated zone is same for single-layered and multi-layered vegetation, the flow nature in and around the vegetated channel-main channel interface depends on the local resistance provided by the vegetation elements near the VCMCI section.
- Velocity dip is observed near VCMCI in the main channel for fully emergent cases. The dip phenomenon ensured negative and positive velocity gradients near the water surface and channel bed respectively.
- The dip phenomenon also ensured the presence of negative streamwise RSS in the vicinity of VCMCI near the water surface, whose penetration into the vegetation zone increases with high emergence and density as observed in dense fully emergent case.
- The magnitude of transverse RSS which shows the strength of horizontal vortices is directly proportional to vegetation emergence and density in the floodplain region.

- Bursting phenomenon analysis showed the dominance of outward (Q1) and inward (Q3) interactions near the surface in the main channel for fully emergent cases. The dominance of ejection (Q2) and sweep (Q4) events in the near-bed of main channel with increasing vegetation emergence and density, increases the chance of sediment movement.

6.2 Flow behavior in a multi-layered vegetated floodplain region of a compound channel

- Flow velocity in the main channel increases as it progresses from a sparsely vegetated region to a densely vegetated region in the floodplain region.
- Flow characteristics like velocity, RSS, intensity and TKE are more pronounced for uniform vegetation spacing set up compared to non-uniform vegetation spacing set up in the slopes and main channel of the compound channel. This suggests that for maintaining bank stability and reducing turbulence, it is preferred to have vegetation distributed in a non-uniform setup with varying spacing.
- The flow characteristics like velocity, RSS and intensity showed that its magnitude and impact on the slopes and main channel is greater in case of multi-layered compared to single-layered floodplain vegetation. The reason is that in the present scenario, resistance near the SFPI section is higher for multi-layered submerged vegetation.
- The anisotropy analysis showed that the floodplain region of all vegetated cases follows pancake structure which means the domination of 2D component anisotropy in the floodplain. However, the points in the sloping region mostly approached from the 3D to 1D (cigar-shaped structure). This means the dominance of transverse component is more in the slopes compared to other two components.

6.3 Flow in multi-layered compound channels with different bank slopes

- The study discussed about the role of bank slopes when the floodplain vegetation is covered with multi-layered vegetation.
- The different flow characteristics like velocity, RSS, intensity and TKE have little difference in the cross-section in the absence of vegetation, irrespective of bank angles. The indifference mainly occurs near the slopes because of the non-uniform cross-section of compound channels.
- With the introduction of floodplain vegetation, velocity near the slopes of 90^0 bank angle is greater than 45^0 bank angle. This shows gradual slope achieves maximum

velocity gradually compared to steeper banks making the steeper bank prone to erosion.

- The positive RSS in and around slopes near the channel bed is more for steeper banks making it more susceptible to erosion.
- The magnitude of negative streamwise RSS near the slopes near the surface of compound channels increases with higher vegetation emergence in the floodplain region. The higher emergence of the floodplain also ensures higher TKE near the slopes, increasing the chance of bank failure.
- The quadrant analysis showed that ejection and sweep events are higher near the channel bed for 90^0 bank slope making it more vulnerable to erosion compared to 45^0 bank slope channel.
- The floodplain vegetation should be extended to the slopes and their nearby region to decrease the flow turbulence and maintain stability.

6.4 Recommendations for Future Research

- This study could be further extended to study sediment transport in the presence of highly dense heterogeneous floodplain vegetation. It will help to understand the mechanism of erosion in regions of both emergent and submerged vegetation and use the knowledge to control excessive erosion and preserve bank stability.
- The stability of the flexible banks will also be checked by changing the roughness of the slopes by different vegetation elements.
- The morphology change in compound channels could also be studied by considering flexible bank slopes.
- Non-uniform bed material replicates the real field scenario in alluvial rivers. Thus, its use in laboratory setup can be explored further to study the flow-vegetation interactions in partially vegetated and compound channels.
- The vegetation distribution in the study can be made more random to replicate a field situation. Scaled experiments in the laboratory can be performed by replicating vegetation distribution near the river channels.

References

Afzalimehr, H., Moghbel, R., Gallichand, J., & Sui, J. (2011). Investigation of turbulence characteristics in channel with dense vegetation. *International Journal of Sediment Research*, *26*(3), 269–282. https://doi.org/10.1016/S1001-6279(11)60093-0

Ahmad, M., Ghani, U., Anjum, N., Pasha, G. A., Ullah, M. K., and Ahmed, A. (2020). Investigating the flow hydrodynamics in a compound channel with layered vegetated floodplains. *Civil Engineering Journal (Iran)*, *6*(5), 860–876. https://doi.org/10.28991/cej-2020-03091513

Allmendinger, N. E., Pizzuto, J. E., Potter Jr, N., Johnson, T. E., & Hession, W. C. (2005). The influence of riparian vegetation on stream width, eastern Pennsylvania, USA. *Geological Society of America Bulletin*, *117*(1-2), 229-243.

Anjum, N., & Tanaka, N. (2020). Study on the flow structure around discontinued vertically layered vegetation in an open channel. *Journal of Hydrodynamics*, *32*, 454-467.

Baptist, M. J., Babovic, V., Rodríguez Uthurburu, J., Keijzer, M., Uittenbogaard, R. E., Mynett, A., & Verwey, A. (2007). On inducing equations for vegetation resistance. *Journal of Hydraulic Research*, *45*(4), 435-450.

Bertoldi, W., Welber, M., Gurnell, A. M., Mao, L., Comiti, F., & Tal, M. (2015). Physical modelling of the combined effect of vegetation and wood on river morphology. *Geomorphology*, *246*, 178–187. https://doi.org/10.1016/j.geomorph.2015.05.038

Blanckaert, K. (2010). Topographic steering, flow recirculation, velocity redistribution, and bed topography in sharp meander bends. *Water resources research*, 46(9).

Bos, A. R., Bouma, T. J., de Kort, G. L., & van Katwijk, M. M. (2007). Ecosystem engineering by annual intertidal seagrass beds: sediment accretion and modification. *Estuarine, Coastal and Shelf Science*, *74*(1), 344-348.

Box, W., Järvelä, J., & Västilä, K. (2021). Flow resistance of floodplain vegetation mixtures for modelling river flows. *Journal of Hydrology*, *601*, 126593.

Cao, T. E., Ni, L., Xie, P., Xu, J. U. N., & Zhang, M. (2011). Effects of moderate ammonium enrichment on three submersed macrophytes under contrasting light availability. *Freshwater Biology*, *56*(8), 1620-1629.

Carollo, F. G., Ferro, V., and Termini, D. (2002). Flow velocity measurements in vegetated channels. *Journal of Hydraulic Engineering*, *128*(7), 664-673.

Carollo, F. G., Ferro, V. I. T. O., & Termini, D. (2005). Flow resistance law in channels with flexible submerged vegetation. *Journal of Hydraulic Engineering*, *131*(7), 554-564.

Carollo, F. G., Ferro, V. I. T. O., & Termini, D. (2007). Analysing Longitudinal Turbulence intensity in Vegetated Channels. *Journal of Agriculture Engineering, Riv. di Ing. Agr.* (2007), **4**, 25-35.

Caroppi, G., Västilä, K., Gualtieri, P., Järvelä, J., Giugni, M., and Rowiński, P. M. (2021). Comparison of Flexible and Rigid Vegetation Induced Shear Layers in Partly Vegetated Channels. *Water Resources Research*, *57*(3). https://doi.org/10.1029/2020WR028243

Caroppi, G., Västilä, K., Järvelä, J., Lee, C., Ji, U., Kim, H. S., & Kim, S. (2022). Flow and wake characteristics associated with riparian vegetation patches: Results from field-scale experiments. *Hydrological Processes*, *36*(2), e14506.

Carpenter, S. R., & Lodge, D. M. (1986). Effects of submersed macrophytes on ecosystem processes. *Aquatic botany*, *26*, 341-370.

Cassan, L., Belaud, G., Baume, J. P., Dejean, C., & Moulin, F. (2015). Velocity profiles in a real vegetated channel. *Environmental Fluid Mechanics*, 15, 1263-1279.

Cea, L., Puertas, J., and Pena, L. (2007). "Velocity measurements on highly turbulent free surface flow using ADV." *Exp. Fluids*, 42(3), 333–348.

Chang, W. Y., Constantinescu, G., Tsai, W. F., & Lien, H. C. (2011). Coherent structure dynamics and sediment erosion mechanisms around an in-stream rectangular cylinder at low and moderate angles of attack. *Water Resources Research*, *47*(12).

Chembolu, V., Kakati, R., & Dutta, S. (2019). A laboratory study of flow characteristics in natural heterogeneous vegetation patches under submerged conditions. *Advances in Water Resources*, *133*(September). https://doi.org/10.1016/j.advwatres.2019.103418

Chen, X., & Chiew, Y. M. (2004). Velocity distribution of turbulent open-channel flow with bed suction. *Journal of Hydraulic Engineering*, *130*(2), 140-148.

Chen, S. C., Kuo, Y. M., & Li, Y. H. (2011). Flow characteristics within different configurations of submerged flexible vegetation. *Journal of Hydrology*, *398*(1), 124-134.

Choi, S. U., & Kang, H. (2006). Numerical investigations of mean flow and turbulence structures of partly-vegetated open-channel flows using the Reynolds stress model. *Journal of Hydraulic Research*, 44(2), 203-217.

Choi, K. S., and Lumley, J. L., 2001, The Return to Isotropy of Homogeneous Turbulence, *J Fluid Mech*, 436, pp. 59–84.

Cui, H., Felder, S., & Kramer, M. (2023). Predicting flow resistance in open-channel flows with submerged vegetation. *Environmental Fluid Mechanics*, 1-22.

Devi, T. B., & Kumar, B. (2016). Channel Hydrodynamics of Submerged, Flexible Vegetation with Seepage. *Journal of Hydraulic Engineering*, *142*(11). https://doi.org/10.1061/(asce)hy.1943-7900.0001180

Devi, Thokchom Bebina, and Kumar, B. (2016). "Flow Characteristics in an Alluvial Channel Covered Partially with Submerged Vegetation." *Ecological Engineering* 94: 478–92. http://dx.doi.org/10.1016/j.ecoleng.2016.06.018.

Devi, T. B., Daga, R., Mahto, S. K., & Kumar, B. (2016). Drag and turbulent characteristics of mobile bed channel with mixed vegetation densities under downward seepage. *Journal of Fluids Engineering*, *138*(7), 071104.

Devi,B. et al. (2019). " Flow Characteristics in a Partly Vegetated Channel with Emergent Vegetation and Seepage." *Ecohydrology & Hydrobiology* 19(1): 93–108. http://dx.doi.org/10.1016/j.ecohyd.2018.07.006.

D'Ippolito, A., Lauria, A., Alfonsi, G., & Calomino, F. (2019). Investigation of flow resistance exerted by rigid emergent vegetation in open channel. *Acta Geophysica*, *67*, 971-986.

Dupuis, V., Proust, S., Berni, C., and Paquier, A. (2017). Mixing layer development in compound channel flows with submerged and emergent rigid vegetation over the

floodplains. *Experiments in Fluids*, *58*(4), 1–18. https://doi.org/10.1007/s00348-017-2319-9

Edgar, G. J. (1990). The influence of plant structure on the species richness, biomass and secondary production of macrofaunal assemblages associated with Western Australian seagrass beds. *Journal of Experimental Marine Biology and Ecology*, *137*(3), 215-240.

Fairbanks, J. D. (1998). Velocity and turbulence characteristics in flows through rigid vegetation (*Doctoral dissertation, Virginia Polytechnic Institute & State University*).

Ferro, V. (2019). Assessing flow resistance law in vegetated channels by dimensional analysis and self-similarity. *Flow Measurement and Instrumentation*, *69*, 101610.

Ferro, V. (2006). *La sistemazione dei bacini idrografici-seconda edizione* (Vol. 1, pp. 1-848). McGraw-Hill.

Finnigan, J. J. (1985, March). Turbulent transport in flexible plant canopies. In *The Forest-Atmosphere Interaction: Proceedings of the Forest Environmental Measurements Conference held at Oak Ridge, Tennessee, October 23–28, 1983* (pp. 443-480). Dordrecht: Springer Netherlands.

Follett, E. M., & Nepf, H. M. (2012). Sediment patterns near a model patch of reedy emergent vegetation. *Geomorphology*, *179*, 141-151.

Fu, S., Mu, H., Liu, B., Yu, X., Zhang, G., & Liu, Y. (2020). Effects on the plant stem arrangement onsediment transport capacity of croplands. *Land Degradation & Development*, *31*(11), 1325-1334.

Garcia, M., Lopez, F., & Nino, Y. (1995). Characterization of near-bed coherent structures in turbulent open channel flow using synchronized high-speed video and hot-film measurements. *Experiments in fluids*, *19*(1), 16-28.

García, C. M., Cantero, M. I., Niño, Y., & García, M. H. (2005). Turbulence measurements with acoustic Doppler velocimeters. *Journal of Hydraulic Engineering*, *131*(12), 1062-1073.

Ghisalberti, M., & Nepf, H. (2009). Shallow flows over a permeable medium: the hydrodynamics of submerged aquatic canopies. *Transport in porous media*, *78*(2), 309-326.

Ghisalberti, M., & Nepf, H. (2006). The structure of the shear layer in flows over rigid and flexible canopies. *Environmental Fluid Mechanics*, *6*(3), 277-301.

Gholami, V., & Khalegi, M. R. (2013). The impact of vegetation on the bank erosion (case study: the Haraz river). *Soil and Water Research*, *8*(4), 158-164.

Goring, D. G., and Nikora, V. I. (2002). Despiking Acoustic Doppler Velocimeter Data. *Journal of Hydraulic Engineering*, *128*(1), 117–126. https://doi.org/10.1061/(asce)0733-9429(2002)128:1(117)

Grinvald D.I., Nikora V.I. 1988. The turbulence of rivers (in Russian). Hydrometeoizdat, Leningrad, Rosja.

Hamed, A. M., Sadowski, M. J., Nepf, H. M., & Chamorro, L. P. (2017). Impact of height heterogeneity on canopy turbulence. *Journal of Fluid Mechanics*, *813*, 1176–1196. https://doi.org/10.1017/jfm.2017.22

Hamidifar, H., Keshavarzi, A., & Truong, P. (2018). Enhancement of river bank shear strength parameters using Vetiver grass root system. *Arabian Journal of Geosciences*, *11*, 1-11.

Horstman, E. M., Bryan, K. R., Mullarney, J. C., Pilditch, C. A., and Eager, C. A. (2018). Are flow-vegetation interactions well represented by mimics? A case study of mangrove pneumatophores. *Advances in Water Resources*, *111*(June 2017), 360–371. https://doi.org/10.1016/j.advwatres.2017.11.018

Hu, R., & Zhang, J. (2022). Modeling velocity in a compound channel with co-existing emergent and submerged vegetation. *Physics of Fluids*, *34*(10). https://doi.org/10.1063/5.0121264

Huai, W., Wang, W., Hu, Y., Zeng, Y., and Yang, Z. (2014). Analytical model of the mean velocity distribution in an open channel with double-layered rigid vegetation. *Advances in Water Resources*, *69*, 106–113. https://doi.org/10.1016/j.advwatres.2014.04.001

Huai, W. xin, Zhang, J., Katul, G. G., Cheng, Y. guang, Tang, X., and Wang, W. jie. (2019). The structure of turbulent flow through submerged flexible vegetation. *Journal of Hydrodynamics*, *31*(2), 274–292. https://doi.org/10.1007/s42241-019-0023-3

Huai, W. X., Li, S., Katul, G. G., Liu, M. Y., & Yang, Z. H. (2021). Flow dynamics and sediment transport in vegetated rivers: A review. *Journal of Hydrodynamics*, *33*(3), 400-420.

Hurther, D. (2001) 3-D acoustic Doppler velocimetry and turbulence in open channel flow, PhD thesis, Ecole Polytechnique Fédérale Lausanne, Switzerland.

Ikeda, S., & Kanazawa, M. (1996). Three-dimensional organized vortices above flexible water plants. *Journal of Hydraulic Engineering*, *122*(11), 634-640.

Ishikawa, Y., Mizuhara, K., & Ashida, M. (2000). Drag force on multiple rows of cylinders in an open channel. *Grant-in-aid research project report, Kyushu Univ, Fukuoka, Japan*.

Islam, M. S., Arifuzzaman, Md. Shahin, H., & Nasrin, S. (2013). Effectiveness of vetiver root in embankment slope protection: Bangladesh perspective. *International Journal of Geotechnical Engineering*, *7*(2), 136-148.

Islam, M. R., and Zhu, D. Z. (2013). Kernel Density–Based Algorithm for Despiking ADV Data. *Journal of Hydraulic Engineering*, *139*(7), 785–793. https://doi.org/10.1061/(asce)hy.1943-7900.0000734

Järvelä, J. (2002). Flow resistance of flexible and stiff vegetation: a flume study with natural plants. *Journal of hydrology*, *269*(1-2), 44-54.

Järvelä, J. (2004). Determination of flow resistance caused by non-submerged woody vegetation. *International Journal of River Basin Management*, *2*(1), 61-70.

Järvelä, J. (2005). Effect of submerged flexible vegetation on flow structure and resistance. *Journal of hydrology*, *307*(1-4), 233-241.

Jaspers-Focks, D. J., & Algera, A. (2006, October). Vetiver grass for river bank protection. In *Proc. 4th Vetiver Int. Conf., Caracas, Venezuela*.

Kirkgöz, M. S., & Ardiçlioğlu, M. (1997). Velocity profiles of developing and developed open channel flow. *Journal of hydraulic engineering*, *123*(12), 1099-1105.

Kitsikoudis, V., Yagci, O., & Kirca, V. O. (2020). Experimental analysis of flow and turbulence in the wake of neighboring emergent vegetation patches with different densities. *Environmental fluid mechanics*, *20*(6), 1417-1439.

Koken, M., & Constantinescu, G. (2021). Flow structure inside and around a rectangular array of rigid emerged cylinders located at the sidewall of an open channel. *Journal of Fluid Mechanics*. https://doi.org/10.1017/jfm.2020.900

Kothyari, U. C., Hayashi, K., & Hashimoto, H. (2009b). "Drag coefficient of unsubmerged rigid vegetation stems in open channel flows". *Journal of Hydraulic Research*, *47*(6), 691-699.

Kouwen, N., Unny, T. E., & Hill, H. M. (1969). Flow retardance in vegetated channels. Journal of the Irrigation and Drainage Division, 95(2), 329-344.

Kouwen, N. (1988). Field estimation of the biomechanical properties of grass. *Journal of Hydraulic Research*, *26*(5), 559-568.

Kouwen, N. (1992). "Modern approach to design of grassed channels." *J. Irrigation and Drain. Engg*., 118(5), 733-743.

Kowobari, T. S., Rice, C. E., & Garton, J. E. (1972). Effect of roughness elements on hydraulic resistance for overland flow. Transactions of the ASAE, 15(5), 979-0984.

Koziol, A. P. (2011). Turbulent kinetic energy of water in a compound channel. Annals of Warsaw University of Life Sciences-SGGW. Land Reclamation, 43(2).

Kemp, J. L., Harper, D. M., & Crosa, G. A. (2000). The habitat-scale ecohydraulics of rivers. *Ecological Engineering*, *16*(1), 17–29. https://doi.org/10.1016/S0925-8574(00)00073-2

Knight, D. W., & Shiono, K. (1990). Turbulence measurements in a shear layer region of a compound channel. *Journal of hydraulic research*, *28*(2), 175-196.

Lacy, J. R., & Wyllie-Echeverria, S. (2011). The influence of current speed and vegetation density on flow structure in two macrotidal eelgrass canopies. *Limnology and Oceanography: Fluids and Environments*, *1*(1), 38-55.

Le Bouteiller, C., & Venditti, J. G. (2015). Sediment transport and shear stress partitioning in a vegetated flow. *Water Resources Research*, *51*(4), 2901-2922.

Lee, H. Y., & Shih, S. S. (2004). Impacts of vegetation changes on the hydraulic and sediment transport characteristics in Guandu mangrove wetland. *Ecological Engineering*, *23*(2), 85-94.

Li, Y., Anim, D. O., Wang, Y., Tang, C., Du, W., and Yu, Z. (2014). An open-channel flume study of flow characteristics through a combined layer of submerged and emerged flexible vegetation. *Ecohydrology. 7*, 633–647. https://doi.org/10.1002/eco.1384

Li, D., Huai, W. xin, & Liu, M. yang. (2020). Investigation of the flow characteristics with one-line emergent canopy patches in open channel. *Journal of Hydrology*, *590*(June), 125248. https://doi.org/10.1016/j.jhydrol.2020.125248

Li, F., Shan, Y., Huang, S., Liu, C., & Liu, X. (2021). Flow depth, velocity, and sediment motions in a straight widened channel with vegetated floodplains. *Environmental Fluid Mechanics*, *21*, 483-501.

Li, D., Liu, M., & Huai, W. (2022). Modeling transverse momentum exchange in partially vegetated flow. *Physics of Fluids*, *34*(2), 025124. https://doi.org/10.1063/5.0081202

Li, D., Huai, W., Guo, Y., & Liu, M. (2022). Flow characteristics in partially vegetated channel with homogeneous and heterogeneous layouts. *Environmental Science and Pollution Research*, 29(25), 38186-38197.

Lightbody, A. F., & Nepf, H. M. (2006). Prediction of near-field shear dispersion in an emergent canopy with heterogeneous morphology. *Environmental Fluid Mechanics*, 6, 477-488.

Liu, D., Diplas, P., Fairbanks, J. D., & Hodges, C. C. (2008). An experimental study of flow through rigid vegetation. *Journal of Geophysical Research: Earth Surface*, *113*(F4).

Liu, D., Diplas, P., Hodges, C. C., and Fairbanks, J. D. (2010). Geomorphology Hydrodynamics of flow through double layer rigid vegetation. *Geomorphology*, *116*(3–4), 286–296. https://doi.org/10.1016/j.geomorph.2009.11.024

Liu, C., & Nepf, H. (2016). Sediment deposition within and around a finite patch of model vegetation over a range of channel velocity. *Water Resources Research*, *52*(1), 600-612.

Liu, C., Shan, Y., & Nepf, H. (2021). Impact of Stem Size on Turbulence and Sediment Resuspension Under Unidirectional Flow. *Water Resources Research*, *57*(3). https://doi.org/10.1029/2020WR028620

López, F., & García, M. H. (2001). Mean flow and turbulence structure of open-channel flow through non-emergent vegetation. *Journal of Hydraulic Engineering*, *127*(5), 392-402.

Lu, S. S., & Wilmarth, W. W. (1973). Measurements of the structure of the Reynolds stress in a turbulent boundary layer. J. Fluid Mech., 60(3), 481–511.

Lumley, J. L. (1979). Computational modeling of turbulent flows. In *Advances in applied mechanics* (Vol. 18, pp. 123-176). Elsevier.

Lumley, J. L., & Newman, G. R. (1977). The return to isotropy of homogeneous turbulence. J. Fluid Mech. 82(1), 161–178.

Marsh, N. A., Western, A. W., & Grayson, R. B. (2004). Comparison of methods for predicting incipient motion for sand beds. Journal of hydraulic engineering, 130(7), 616-621.

Masterman, R., and Thorne, C.R., (1992). "Predicting influence of bank vegetation on channel capacity." *Journal of Hydraulic Engineering*, 118(7), 1052-1058.

McBride, M., Hession, W. C., Rizzo, D. M., & Thompson, D. M. (2007). The influence of riparian vegetation on near-bank turbulence: A flume experiment. *Earth Surface Processes and Landforms: The Journal of the British Geomorphological Research Group*, *32*(13), 2019-2037.

Mehrabani, V., F., Mohammadi, M., Ayyoubzadeh, S. A., Fernandes, J. N., and Ferreira, R. M. L. (2020). Turbulent flow structure in a vegetated non-prismatic compound channel. *River Research and Applications*, *36*(9), 1868–1878. https://doi.org/10.1002/rra.3723

Meijer, D. G., & Van Velzen, E. H. (1999, August). Prototype-scale flume experiments on hydraulic roughness of submerged vegetation. In *Conference Proceedings of the 28th International IAHR Conference, Graz*.

Meire, D. W., Kondziolka, J. M., & Nepf, H. M. (2014). "Interaction between neighbouring vegetation patches: Impact on flow and deposition." *Water Resources Research*, *50*(5), 3809-3825.

Mera, I., Franca, M. J., Anta, J., & Peña, E. (2015). Turbulence anisotropy in a compound meandering channel with different submergence conditions. *Advances in water resources*, *81*, 142-151.

Modalavalasa, S., Chembolu, V., Dutta, S., & Kulkarni, V. (2023). Laboratory investigation on flow structure and turbulent characteristics in low sinuous compound channels with vegetated floodplains. *Journal of Hydrology*, 618, 129178.

Mohan, B. S., & Hosetti, B. B. (1999). Aquatic plants for toxicity assessment. *Environmental research*, *81*(4), 259-274.

Moltchanov, S., Bohbot-Raviv, Y., & Shavit, U. (2011). Dispersive stresses at the canopy upstream edge. *Boundary-layer meteorology*, 139, 333-351.

Mu, H., Yu, X., Fu, S., Yu, B., Liu, Y., & Zhang, G. (2019). Effect of stem basal cover on the sediment transport capacity of overland flows. *Geoderma*, *337*, 384-393.

Naden, P., P. Rameshwaran, O. Mountford, and C. Robertson (2006). The influence of macrophyte growth, typical of eutrophic conditions, on river flow velocities and turbulence production, *Hydrol. Processes, 20(18), 3915–3938.*

Naghavi, M., Mohammadi, M., & Mahtabi, G. (2022). An experimental evaluation of the blocks in floodplain on hydraulic characteristics of flow in a meandering compound channel. *Journal of Hydrology*, 612, 127976.

Naot, D., Nezu, I., & Nakagawa, H. (1996a). Hydrodynamic behavior of partly vegetated open channels. *Journal of Hydraulic Engineering*, 122(11), 625-633.

Nelson, J. M., Shreve, R. L., McLean, S. R., & Drake, T. G. (1995). Role of near-bed turbulence structure in bed load transport and bed form mechanics. *Water resources research*, *31*(8), 2071-2086.

Nepf, H. M. (1999). Drag, turbulence, and diffusion in flow through emergent vegetation. *Water resources research*, *35*(2), 479-489.

Nepf, H. M., & Vivoni, E. R. (2000). Flow structure in depth-limited, vegetated flow. *Journal of Geophysical Research: Oceans*, *105*(C12), 28547-28557.

Nepf, H., & Ghisalberti, M. (2008). Flow and transport in channels with submerged vegetation. *Acta Geophysica 56*(3), 753–777. https://doi.org/10.2478/s11600-008-0017-y

Nepf, H. M. (2011). Flow and transport in regions with aquatic vegetation. *Annual Review of Fluid Mechanics*, 44, 123–142. https://doi.org/10.1146/annurev-fluid-120710-101048

Nepf, H. M. (2012). Hydrodynamics of vegetated channels. *Journal of Hydraulic Research*, *50*(3), 262-279.

Nezu I., Nakagawa H. 1993. Turbulence in Open-channel Flows. IAHR Monograph, Balkema, Rotterdam.

Nezu, I., & Onitsuka, K. (2001). Turbulent structures in partly vegetated open-channel flows with LDA and PIV measurements. *Journal of Hydraulic Research*, *39*(6), 629–642. https://doi.org/10.1080/00221686.2001.9628292

Nezu, I., & Sanjou, M. (2008). Turburence structure and coherent motion in vegetated canopy open-channel flows. *Journal of hydro-environment research*, *2*(2), 62-90.

Nicosia, A., & Ferro, V. (2023). Flow resistance due to shrubs and woody vegetation. *Flow Measurement and Instrumentation*, *89*, 102308.

Okamoto, T. A., Nezu, I., & Ikeda, H. (2012). Vertical mass and momentum transport in open-channel flows with submerged vegetations. *Journal of Hydro-environment Research*, *6*(4), 287-297.

Pierobon, E., Castaldelli, G., Mantovani, S., Vincenzi, F., & Fano, E. A. (2013). Nitrogen removal in vegetated and unvegetated drainage ditches impacted by diffuse and point sources of pollution. *CLEAN–Soil, Air, Water*, *41*(1), 24-31. 54: 879-889.

Poggi, D., Porporato, A., Ridolfi, L., Albertson, J. D., & Katul, G. G. (2004). The effect of vegetation density on canopy sub-layer turbulence. *Boundary-Layer Meteorology*, *111*, 565-587.

Proust, S., & Nikora, V. I. (2019). Compound open-channel flows: Effects of transverse currents on the flow structure. *Journal of Fluid Mechanics*, *885*. https://doi.org/10.1017/jfm.2019.973

Pu, J. H. (2019). Turbulent rectangular compound open channel flow study using multi-zonal approach. *Environmental Fluid Mechanics*, *19*(3), 785-800.

Pu, J. H., Pandey, M., & Hanmaiahgari, P. R. (2020). Analytical modelling of sidewall turbulence effect on streamwise velocity profile using 2D approach: A comparison of rectangular and trapezoidal open channel flows. *Journal of Hydro-Environment Research*, *32*, 17-25.

Przyborowski, Ł., & Łoboda, A. M. (2021). Identification of coherent structures downstream of patches of aquatic vegetation in a natural environment. *Journal of Hydrology*, *596*, 126123.

Rao, P. L., Prasad, B. S. S., Sharma, A., & Khatua, K. K. (2022). Experimental and numerical analysis of velocity distribution in a compound meandering channel with double layered rigid vegetated flood plains. *Flow Measurement and Instrumentation*, *83*, 102111.

Rauch, H. P., von der Thannen, M., Raymond, P., Mira, E., & Evette, A. (2022). Ecological challenges* for the use of soil and water bioengineering techniques in river and coastal engineering projects. *Ecological Engineering*, *176*, 106539.

Raupach, M. R. (1981). "Conditional statistics of Reynolds stress in rough-wall and smooth-wall turbulent boundary layers." J. Fluid Mech., 108, 363–382.

Raupach, M. R., & Shaw, R. H. (1982). Averaging procedures for flow within vegetation canopies. *Boundary-layer meteorology*, *22*(1), 79-90.

Rolland, T. (1994) Développement d'une instrumentation Doppler ultrasonore adaptée à l'étude hydraulique de la turbulence dans les canaux, PhD Thesis, EPFL, Lausanne, Switzerland.

Rominger, J. T., & Nepf, H. M. (2011). Flow adjustment and interior flow associated with a rectangular porous obstruction. *Journal of Fluid Mechanics*, 680, 636-659.

Rowiński, P. M., Czernuszenko, W., Kozioł, A. P., & Kubrak, J. (2002). Properties of a streamwise turbulent flow field in an open two-stage channel. Archives of Hydro-Engineering and Environmental Mechanics, 49(2), 37-57.

Rowiński, P. M., Västilä, K., Aberle, J., Järvelä, J., & Kalinowska, M. B. (2018). How vegetation can aid in coping with river management challenges: A brief review. *Ecohydrology & Hydrobiology*, *18*(4), 345-354.

Ricardo, A. M., Koll, K., Franca, M. J., Schleiss, A. J., & Ferreira, R. M. (2014). The terms of turbulent kinetic energy budget within random arrays of emergent cylinders. *Water resources research*, *50*(5), 4131-4148.

Righetti, M., & Armanini, A. (2002). Flow resistance in open channel flows with sparsely distributed bushes. *Journal of Hydrology*, *269*(1), 55-64.

Righetti, M. (2008). Flow analysis in a channel with flexible vegetation using double-averaging method. *Acta Geophysica*, 56(3), 801-823.

Salim, S., Pattiaratchi, C., Tinoco, R., Coco, G., Hetzel, Y., Wijeratne, S., & Jayaratne, R. (2017). The influence of turbulent bursting on sediment resuspension under unidirectional currents. *Earth Surface Dynamics*, *5*(3), 399-415.

Schmeeckle, M. W. (2015). The role of velocity, pressure, and bed stress fluctuations in bed load transport over bed forms: numerical simulation downstream of a backward-facing step. *Earth Surface Dynamics*, *3*(1), 105-112.

Shan, Y., Huang, S., Liu, C., Guo, Y., & Yang, K. (2018). Prediction of the depth-averaged two-dimensional flow direction along a meander in compound channels. *Journal of hydrology*, *565*, 318-330.

Sharma, A., & Kumar, B. (2017). Structure of turbulence over non uniform sand bed channel with downward seepage. *European Journal of Mechanics-B/Fluids*, *65*, 530-551.

Sharpe, R. G., & James, C. S. (2006). Deposition of sediment from suspension in emergent vegetation. *Water Sa*, *32*(2), 211-218.

Shucksmith, J. D., Boxall, J. B., and Guymer, I. (2010). Effects of emergent and submerged natural vegetation on longitudinal mixing in open channel flow. *Water Resources Research, VOL. 46*, 1–14. https://doi.org/10.1029/2008WR007657

Shi, Z., Pethick, J. S., Burd, F., & Murphy, B. (1996). Velocity profiles in a salt marsh canopy. *Geo-Marine Letters*, *16*(4), 319-323.

Shi, H., Zhang, J., & Huai, W. (2023). Experimental study on velocity distributions, secondary currents, and coherent structures in open channel flow with submerged riparian vegetation. *Advances in Water Resources*, *173*, 104406.

Shiono, K., & Knight, D. W. (1991). Turbulent open-channel flows with variable depth across the channel. *Journal of fluid mechanics*, *222*, 617-646.

Shimizu,Y. and Tsujimoto, T. (1994). Numerical Analysis of Turbulent Open Channel Flow: Vegetation Layer Using a k–ε turbulence model. J. Hydrosci. Hydraul. Engng. 11(2), 57–67.

Simonsen, A. J., & Krogstad, P. Å. (2005). Turbulent stress invariant analysis: Clarification of existing terminology. *Physics of Fluids*, *17*(8), 088103.

Soana, E., Fano, E. A., & Castaldelli, G. (2021). The achievement of Water Framework Directive goals through the restoration of vegetation in agricultural canals. *Journal of Environmental Management*, *294*(May), 113016. https://doi.org/10.1016/j.jenvman.2021.113016

Stamati, F. E., Chalkias, N., Moraetis, D., & Nikolaidis, N. P. (2010). Natural attenuation of nutrients in a mediterranean drainage canal. *Journal of Environmental Monitoring*, *12*(1), 164–171. https://doi.org/10.1039/b913083g

Stephan, U., & Gutknecht, D. (2002). Hydraulic resistance of submerged flexible vegetation. *Journal of Hydrology*, *269*(1), 27-43.

Stone, B. M., & Shen, H. T. (2002). Hydraulic resistance of flow in channels with cylindrical roughness. *Journal of hydraulic engineering*, *128*(5), 500-506.

Sukhodolov, A., & Sukhodolova, T. (2010). Case study: Effect of submerged aquatic plants on turbulence structure in a lowland river. *Journal of Hydraulic Engineering*, *136*, 434–446.

Sukhodolov, A., Sukhodolova, T., Krick, J. (2016). Effects of vegetation on turbulent flow structure in groyne fields. *Journal of Hydraulic Research*, ISSN: 0022-1686 (Print) 1814-2079 (Online) Journal homepage: http://www.tandfonline.com/loi/tjhr20.

Taborda, C., Fael, C., Ricardo, A. M., & Ferreira, R. M. L. (2022). Wave-like motion and secondary currents in arrays of emergent cylinders induced by large scale eddying motion. *Environmental Fluid Mechanics*, *22*(2–3), 403–428. https://doi.org/10.1007/s10652-022-09863-4

Tang, X., & Knight, D. W. (2008). A general model of lateral depth-averaged velocity distributions for open channel flows. *Advances in Water Resources*, *31*(5), 846-857.

Tang, X., Rahimi, H., Guan, Y., and Wang, Y. (2021). Hydraulic characteristics of open-channel flow with partially-placed double layer rigid vegetation. *Environmental Fluid Mechanics*, *21*(2), 317–342. https://doi.org/10.1007/s10652-020-09775-1

Tang, C., Yi, Y., & Zhang, S. (2023). Flow and turbulence in unevenly obstructed channels with rigid and flexible vegetation. *Journal of Environmental Management*, *326*, 116736.

Tanino, Y., and Nepf, H. (2008). "Lateral dispersion in random cylinder arrays at high Reynolds number." *J. Fluid Mech.* 600, 339-371.

Taye, J., Sharma, A., & Kumar, B. (2023). Effect of downward seepage on turbulence and morphology in mobile boundary sinuous channel. *Physics of Fluids*, *35*(1).

Termini, D. (2015). Flexible vegetation behaviour and effects on flow conveyance: experimental observations. *International Journal of River Basin Management*, *13*(4), 401-411.

Termini, D. (2019). Turbulent mixing and dispersion mechanisms over flexible and dense vegetation. *Acta Geophysica*, *67*(3), 961–970. https://doi.org/10.1007/s11600-019-00272-8.

Tisserant, M., Bourgeois, B., González, E., Evette, A., & Poulin, M. (2021). Controlling erosion while fostering plant biodiversity: A comparison of riverbank stabilization techniques. *Ecological Engineering*, *172*, 106387.

Tominaga, A., Nezu, I., Ezaki, K., & Nakagawa, H. (1989). Three-dimensional turbulent structure in straight open channel flows. *Journal of Hydraulic Research*, *27*(1), 149–173. https://doi.org/10.1080/00221688909499249

Tominaga, A. and Nezu, L. (1991) Turbulent structure in compound open-channel flows. *Journal of Hydraulic Engineering, ASCE, 117*(1), 21–41.

Truong, S. H., & Uijttewaal, W. S. J. (2019). Transverse Momentum Exchange Induced by Large Coherent Structures in a Vegetated Compound Channel. Water Resources Research, 55(1), 589–612. https://doi.org/10.1029/2018WR023273

Truong, S. H., Uijttewaal, W. S. J., & Stive, M. J. F. (2019). Exchange processes induced by large horizontal coherent structures in floodplain vegetated channels. Water Resources Research, 55(3), 2014-2032.

Tsujimoto, T., Shimizu, Y., Kitamura, T., & Okada, T. (1992). Turbulent open-channel flow over bed covered by rigid vegetation. *Journal of Hydroscience and Hydraulic Engineering*, *10*(2), 13-25.

Turker, U., Yagci, O., and Kabdasli, M. (2006). Analysis of coastal damage of a beach profile under the protection of emergent vegetation. *Ocean Engineering*, 33, 810-828.

Türker, U., Yagci, O., & Kabdasli, M. S. (2019). Impact of nearshore vegetation on coastal dune erosion: assessment through laboratory experiments. *Environmental Earth Sciences*, *78*(19), 1–14. https://doi.org/10.1007/s12665-019-8602-8

Urantinon, A. (2017). Study of accumulated fine particulate in water hyacinth root in open channel: Laboratory scale. In *Proceedings of the 6th International Symposium on the Fusion of Science and Technologies (ISFT), Jeju, South Korea*.

Vandenbruwaene, W., Temmerman, S., Bouma, T. J., Klaassen, P. C., De Vries, M. B., Callaghan, D. P., Van Steeg, P., Dekker, F., Van Duren, L. A., Martini, E., Balke, T., Biermans, G., Schoelynck, J., & Meire, P. (2011). Flow interaction with dynamic

vegetation patches: Implications for biogeomorphic evolution of a tidal landscape. *Journal of Geophysical Research: Earth Surface*, *116*(1), 1–13. https://doi.org/10.1029/2010JF001788

Velasco, D., Bateman, A., Redondo, J. M., & DeMedina, V. (2003). An open channel flow experimental and theoretical study of resistance and turbulent characterization over flexible vegetated linings. *Flow, turbulence and combustion*, *70*(1-4), 69-88.

Verschoren, V., Schoelynck, J., Cox, T., Schoutens, K., Temmerman, S., & Meire, P. (2017). Opposing effects of aquatic vegetation on hydraulic functioning and transport of dissolved and organic particulate matter in a lowland river: a field experiment. *Ecological Engineering*, *105*, 221-230.

Vincent, C. D., Lawlor, A. J., & Tipping, E. (2001). Accumulation of Al, Mn, Fe, Cu, Zn, Cd and Pb by the bryophyte Scapania undulata in three upland waters of different pH. *Environmental Pollution*, *114*(1), 93-100.

Wahl, T. L. (2003). "Discussion of 'Despiking acoustic Doppler velocimeter data' by Derek G. Goring and Vladimir I. Nikora." J. Hydraul. Eng., 129(6), 484–487.

Wang, W. C., & Freemark, K. (1995). The use of plants for environmental monitoring and assessment. *Ecotoxicology and environmental safety*, *30*(3), 289-301.

Wang, C., Wang, C., & Wang, Z. (2010). Effects of submerged macrophytes on sediment suspension and NH sub (4)-N release under hydrodynamic conditions. *Journal of hydrodynamics*, *22*(6), 810-815.

Wang, H., Tang, H. W., Zhao, H. Q., Zhao, X. Y., & Lü, S. Q. (2015). Incipient motion of sediment in presence of submerged flexible vegetation. *Water Science and Engineering*, *8*(1), 63-67.

Wang, N., Zhang, C., Xiao, Y., Jin, G., & Li, L. (2018). Transverse hyporheic flow in the cross-section of a compound river system. *Advances in Water Resources*, *122*(1), 263–277. https://doi.org/10.1016/j.advwatres.2018.10.006

Wang, J., Liu, X., Min, F., Dai, J., & Jiang, X. (2022). Turbulence structure and longitudinal velocity distribution of open channel flows with reedy emergent vegetation. *Ecohydrology*, *15*(1), e2352.

Wang, X., Gualtieri, C., & Huai, W. (2023). Grain shear stress and bed-load transport in open channel flow with emergent vegetation. *Journal of Hydrology*, *618*, 129204.

Wilcock, R. J., Champion, P. D., Nagels, J. W., & Croker, G. F. (1999). The influence of aquatic macrophytes on the hydraulic and physico-chemical properties of a New Zealand lowland stream. *Hydrobiologia*, *416*, 203-214.

Wilson, N. R., & Shaw, R. H. 1977. A higher order closure model for canopy flow. Journal of 787 Applied Meteorology, 16(11), 1197-1205.

Wilson, C. A. M. E., Stoesser, T., Bates, P. D., & Pinzen, A. B. (2003). Open channel flow through different forms of submerged flexible vegetation. *Journal of Hydraulic Engineering*, *129*(11), 847-853.

Wu, F. C., Shen, H. W., & Chou, Y. J. (1999). Variation of roughness coefficients for unsubmerged and submerged vegetation. *Journal of Hydraulic Engineering*, *125*(9), 934-942.

Wu, K. T., Tsai, C. W., & Wu, M. J. (2022). Probabilistic characterization of sweep and ejection events in turbulent flows and its implications on sediment transport. *Water Resources Research*, *58*(5), e2021WR030417.

Wu, W., Chen, G., Meng, T., Li, C., Feng, H., Si, B., & Siddique, K. H. (2023). Effect of different vegetation restoration on soil properties in the semi-arid Loess Plateau of China. *Catena*, *220*, 106630.

Xiao, Y., Wang, N., Liang, D., & Liu, J. (2018). Flow Structures in Trapezoidal Compound Channels with Different Side Slopes of Main Channel. *International Journal of Civil Engineering*, *16*(7), 823–835. https://doi.org/10.1007/s40999-017-0212-9

Xiao, Y., Zhang, T., Liu, J., Wang, N., Gualtieri, C., & Zhou, J. (2022). Numerical simulation of overbank hyporheic transport and biogeochemical reactions in a compound channel. *Hydrological Processes, 2022; 36; e14670.* https://doi.org/10.1002/hyp.14670

Xu, Y., & Nepf, H. (2020). Measured and Predicted Turbulent Kinetic Energy in Flow Through Emergent Vegetation with Real Plant Morphology. Water Resources Research, 56(12), 1–20. https://doi.org/10.1029/2020WR027892

Yamasaki, T. N., Jiang, B., Janzen, J. G., & Nepf, H. M. (2021). Feedback between vegetation, flow, and deposition: A study of artificial vegetation patch development. *Journal of Hydrology*, *598*(March), 126232. https://doi.org/10.1016/j.jhydrol.2021.126232

Yan, X. F., Wai, W. H. O., & Li, C. W. (2016). Characteristics of flow structure of free-surface flow in a partly obstructed open channel with vegetation patch. *Environmental fluid mechanics*, 16, 807-832.

Yan, X., Rennie, C. D., & Mohammadian, A. (2020). A three - dimensional numerical study of flow characteristics in strongly curved channel bends with different side slopes. *Environmental Fluid Mechanics*, *20*(6), 1491–1510. https://doi.org/10.1007/s10652-020-09751-9

Yan, X. F., Duan, H. F., Wai, W. H. O., Li, C. W., & Wang, X. K. (2022). Spatial Flow Pattern, Multi-Dimensional Vortices, and Junction Momentum Exchange in a Partially Covered Submerged Canopy Flume. *Water Resources Research*, *58*(3). https://doi.org/10.1029/2020WR029494

Yang, K., Cao, S., & Knight, D. W. (2007). Flow patterns in compound channels with vegetated floodplains. *Journal of hydraulic engineering*, *133*(2), 148-159.

Yang, J. Q., & Nepf, H. M. (2019). Impact of vegetation on bed load transport rate and bedform characteristics. *Water Resources Research*, *55*(7), 6109-6124.

Zarkami, R., Esfandi, J., & Sadeghi, R. (2021). Modelling occurrence of invasive water hyacinth (Eichhornia crassipes) in Wetlands. *Wetlands*, *41*, 1-13.

Zayed, A., Lytle, C. M., Qian, J. H., & Terry, N. (1998). Chromium accumulation, translocation and chemical speciation in vegetable crops. *Planta*, *206*, 293-299.

Zeng, C., & Li, C. W. (2014). Measurements and modeling of open-channel flows with finite semi-rigid vegetation patches. *Environmental Fluid Mechanics*, *14*, 113-134.

Zhang, Y., Lai, X., Zhang, L., Song, K., Yao, X., Gu, L., Pang, C. (2020) The influence of aquatic vegetation on flow structure and sediment deposition: A field study in Dongting Lake, China. *Journal of Hydrology*, 584 (2020) 124644.

Zhu, T., Cao, T., Ni, L., He, L., Yi, C., Yuan, C., & Xie, P. (2016). Improvement of water quality by sediment capping and re-vegetation with Vallisneria natans L.: A short-term investigation using an in situ enclosure experiment in Lake Erhai, China. *Ecological Engg*., *86*, 113-119.

Appendix A

Velocity estimation in compound channels with different bank slopes using Renyi and Tsallis entropy[5]

1 Introduction

Understanding the velocity profile in any aquatic system is important for modeling and studying flow discharge, pollutant transport, erosional processes, and sediment transport. As an example, knowledge of velocity is required to find shear stress while calculating sediment concentration. Velocity information is required before solving various hydraulic and turbulence parameters like Reynolds shear stress (RSS), turbulent intensity, turbulent kinetic energy, etc. Velocity distribution in natural river channels and laboratory flumes differs in such a way that the velocity profile in natural rivers is influenced by vegetation, bends, roughness, and channel geometry. On the other hand, velocity distribution in laboratory flumes can be controlled as per the requirement. That is why velocity estimation is difficult, and many researchers and scientists have attempted it since last century. The first theoretical method was provided by Chezy, followed by Mannings, which is widely used in the problems of hydraulics. Several other laws, like the power law and the Prandtl-von Karman universal velocity profile laws were used to describe the velocity profile in open channels. Though the power law method is simple, its exactness with the observed value is less (Cui and Singh 2014). Furthermore, the velocity obtained using the Prandtl von Karman equation is not accurate, especially close to the bed and at the free surface. The velocity profile estimation with these methods is also limited for wide open channels and does not explain the dip phenomenon properly.

Experimental and deterministic hydrodynamic approaches were utilized to determine velocity distributions by various researchers (Utami and Ueno, 1987; Fatima *et al.*, 2009; Liu *et al.*, 2012; Wang *et al.*, 2022). However, irregularities in the geometry and hydraulics of the open channels add uncertainty to the flow velocity. Entropy is a system characteristic that quantifies

[5] Barman, J., Roy, M. & Kumar, B. (2023). Velocity estimation in compound channels with different bank slopes using Renyi and Tsallis entropy. Stochastic Environmental Research and Risk Assessment. https://doi.org/10.1007/s00477-023-02423-2

the system's randomness or chaos. There are usually uncertainties connected with variables like flow velocity, silt content, and shear strength in hydraulic research (Kumbhakar and Ghosal, 2016). Chiu (1987) used the concept of Shannon entropy to find the one-dimensional velocity profile by assuming the time average velocity as a random variable. Later Chiu (1988) developed a velocity profile equation that reasonably explains the effect of velocity in both directions, that is, longitudinal and transverse directions. However, one of the primary flaws of this velocity profile is that it has an excessive number of empirical parameters with no physical relevance. Chin and Murray (1992) used a graphical technique to illustrate velocity profile estimate parameters and describe the fluctuation in velocity profile over a nonuniform open channel flow. Marini *et al.* (2011) proposed a new technique for characterizing 2D velocity distributions based on Shannon entropy, in which the cumulative distribution function (CDF) was theorized using x and y-coordinates. The Tsallis entropy (Tsallis, 1988), a generalization of the Shannon entropy, is another type of entropy approach used to estimate velocity profile. Researchers like Luo and Singh (2011) and Cui and Singh (2013) used Tsallis entropy to generate a unique velocity profile. Since the Tsallis index parameter is accessible, it has been shown that the velocity profiles derived using Tsallis entropy are accurate. Renyi entropy, a generalized form of Shannon entropy, was used by Kumbhakar and Ghoshal (2016, 2017) to create 1D and 2D velocity profiles. Kumbhakar and Ghoshal (2016) found that Renyi entropy-based velocity profile performs better than Shannon and Tsallis for laboratory and field data. Kumbhakar and Ghosal (2017) found that the resulting velocity profile changes with the parameter α, which lies in (0,1). Sharma *et al.* (2022 (a, b)) used all three entropies (Shannon, Tsallis, and Renyi) to estimate the velocities in the seepage-affected channel. Ahamed and Kundu (2022) used the faction-based entropy equation to fully comprehend the impact of non-local mixing caused by turbulent bursting to foresee the one-dimensional velocity profile with the dip phenomenon.

The literature discussed to predict velocities by entropy methods are either rectangular channels or the cross-section is uniform. However, the floodplain submerges during peak flood season, and it becomes a compound channel with floodplain, bank slope, and main channel regions. The compound channel cross-section is not uniform, and it becomes difficult to predict velocity distribution because of the continuous exchange momentum between the floodplain and main channel domains. The momentum exchange in compound channels has been discussed in detail in Chapters 4 and 5. Researchers have previously predicted the velocity profile in compound channel by various methods like the Shiono and Knight Method (SKM). The SKM provides an

analytical solution for the lateral distributions of depth-averaged velocity. The SKM has been applied to different channels by various researchers like Knight and Shiono (1990), Knight and Shiono (1996), Abril and Knight (2004), and Knight *et al.* (2007). Bousmar and Zech (2004) used the method of Lateral Distribution Method (LDM) which is obtained from Navier–Stokes streamwise momentum equation. Patra *et al.* (2004) estimated the velocity in meandering compound channel using the power law. Other researchers tried to predict the velocity distribution by numerical modeling on the basis of the k-ε turbulence model (Keller and Rodi, 1988) and on the basis of algebraic stress models, adopting the complete three-dimensional form of the equations (Krishnappan and Lau, 1986; Kawahara and Tamai, 1989; Prinos, 1990; Naot *et al.*, 1993). Furthermore, the floodplain region is generally covered with vegetation which adds to the complexity. Researchers have previously predicted the velocity profile in the presence of vegetation in the laboratory (Kouwen *et al.*,1969; Carollo *et al.*, 2002; Nepf and Ghisalberti, 2008). Furthermore, compound channel research was also conducted to study the flow structure (Dupuis *et al.*,2017; Proust and Nikora, 2019; Mehrabani *et al.*, 2020). However, the prediction of velocity distribution by entropy method in compound channels has not been explored.

The study focuses on estimating the velocity profile in the compound channel by considering two bank slopes of 45^0 and 90^0 in the laboratory. This study does not consider floodplain vegetation as it will only focus on the effect of nonuniform cross-section while estimating velocity profile. The study will consider the Renyi and Tsallis entropy method to estimate velocity distribution in the cross-section of the compound channels and will make an effort to assess the methods' accuracy with experimental findings.

2 Methodology

Experiments were performed in a laboratory flume whose length, breadth and height are 17.2 m, 1 m and 0.72 m respectively which was explained in detail in section 2.1. A compound channel consisting of floodplain, slope and main channel of 9 m length is constructed in the flume. Experiments were conducted considering two compound channels of 45^0 and 90^0 bank angles whose construction was explained in section 2.4 (Figure 1(a, b)). Experiments were conducted for two discharges of 35 lps and 42 lps for each bank angle of 45^0 and 90^0 compound channels. The floodplain and main channel depth for all experiment cases were 10 cm and 20 cm respectively. The detailed description of the experimental cases in this section is explained in Section 2.9.3. The floodplain region of the compound channels is not

vegetated in this section as shown in Figure 1(a, b). This was done to completely focus on velocity distribution using the entropy technique, only considering the effects of asymmetrical cross-sections and disregarding any effects from vegetation obstruction. Velocity data was collected using the ADV in the downstream cross-sectional region from 17 different sections, as shown in Figure 1(c, d). The location of velocity reading is the same which was explained in section 2.9.3. After filtering the velocity data, it is compared with the velocity distribution found by Renyi and Tsallis entropy method, which is discussed in detail in the next section.

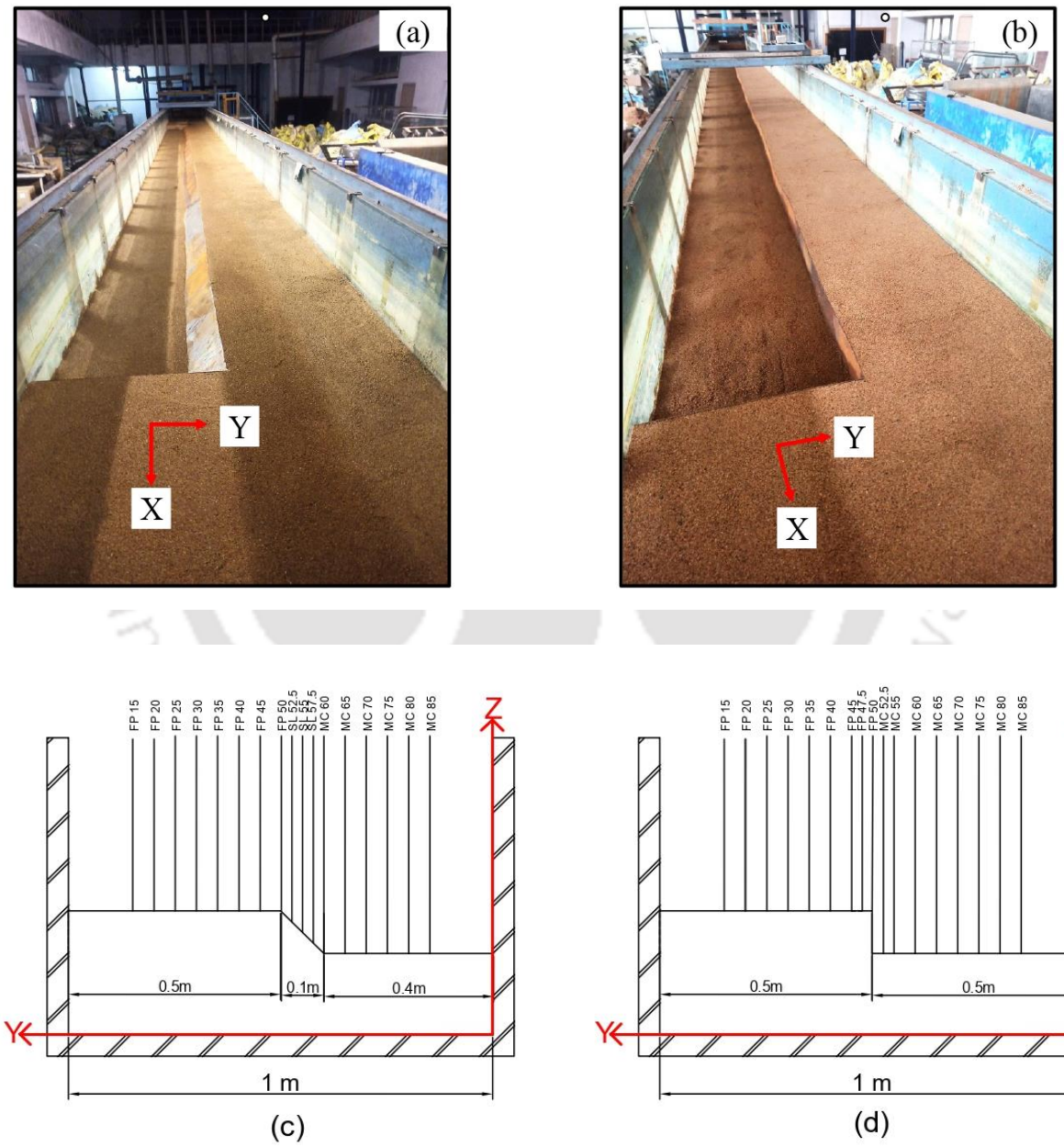

Figure 1 Snapshots of (a) 45^0 and (b) 90^0 compound channels from downstream section of the flume. Position of ADV data sections at (a) 45^0 and (b) 90^0 bank angle compound channels in the 5.5m cross-section.

3 Theoretical backgrounds

The different steps involved in deriving the velocity distribution in the present study are given as follows:

3.1 Renyi entropy velocity distributions derivation

3.1.1 Defining Renyi entropy

Renyi (1961) proposed Renyi entropy of order α which was defined by Xu and Erdogmuns (2010) in continuous form as

$$H_\alpha(\hat{U}) = \frac{1}{1-\alpha} log_2 \left\{ \int_0^1 [f(\hat{u})]^\alpha d\hat{u} \right\} \quad (1)$$

where $f(\hat{u})$ is defined as a probability density function (PDF) and $\hat{u}$ denotes the dimensionless velocity given by $\hat{u} = \left(\frac{u}{u_{max}}\right)$. Velocity at particular height *y* from the channel bed to the top surface distance *D* is denoted as *u*, and the maximum velocity is specified as u_{max}.

According to the maximum entropy principle, equation (1) is maximized within the first two constraints to provide the unbiased PDF $f(u)$ (Jaynes, 1957). The constraints give the information that measurements may provide and can be expressed in terms of statistical moments. The total probability is stated as the first constraint.

$$\int_0^1 f(\hat{u}) d\hat{u} = 1 \quad (2)$$

The mean value can be used to describe the second constraint:

$$\int_0^1 \hat{u} f(\hat{u}) d\hat{u} = \hat{u}_m \quad (3)$$

The Lagrange multiplier approach may be used to maximize entropy. The final equation is obtained for PDF $f(\hat{u})$ by Kumbhakar and Ghoshal (2016) after applying the method of Lagrange multiplier approach as follows:

$$f(\hat{u}) = \left(\frac{-\lambda_0 - \lambda_1 \hat{u}}{\alpha}\right)^{\frac{1}{\alpha-1}} \quad (4)$$

Where λ_0 and λ_1 denotes the Lagrange multipliers.

The CDF $F(\hat{u})$ may be constructed by integrating the PDF $f(\hat{u})$ from equation (4) as follows:

$$F(\hat{u}) = \int_0^{\hat{u}} f(\hat{u}) d\hat{u}$$

$$= \int_0^{\hat{u}} \left(\frac{-\lambda_0 - \lambda_1 \hat{u}}{\alpha}\right)^{\frac{1}{\alpha-1}} d\hat{u} \quad (5)$$

For the derivation of cumulative distribution function (CDF), Chiu (1988) used the illustration of isovels to show the connection between vertical (Y) and transverse (Z) (line linking points of equal velocity) directions, as illustrated in Figure 3, to account for the influence of the channel's two sides as

$$\psi = Y(1-X)^{N_i} \exp\left(N_i X + 1 - Y\right) \quad (6)$$

where $Y = \frac{y+\delta_y}{D+h+\delta_y}$

and $X = \frac{|x|}{B_i+\delta_i}$

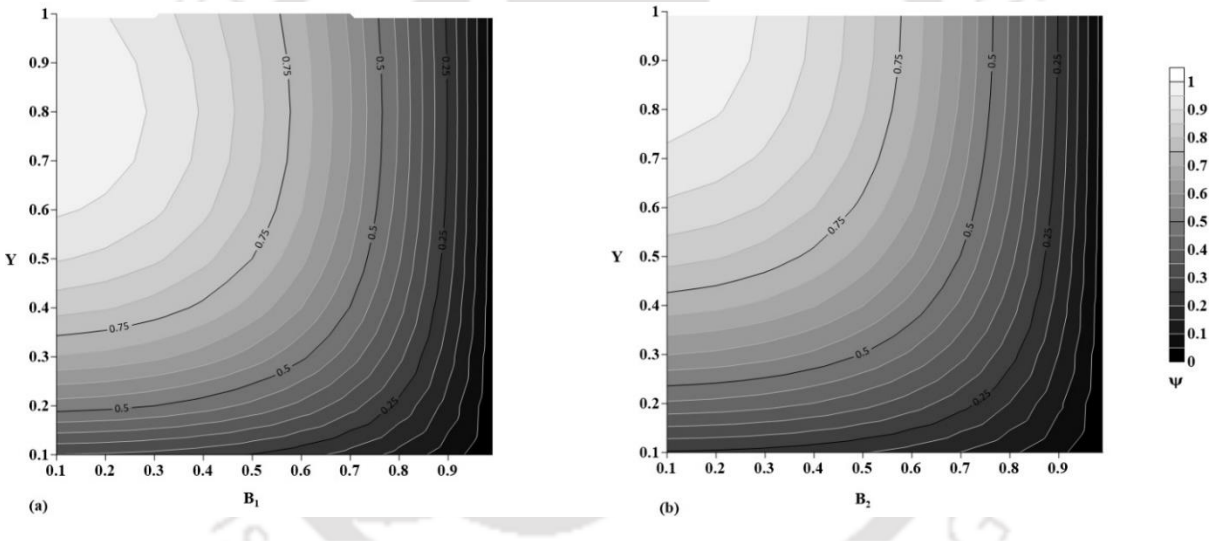

Figure 3 ψ-equation for the case (a) h<0 and (b) h=0.

Detailed explanation of equation (6) is provided in Sharma *et al.* (2022). Therefore, if $\hat{u}$ is chosen at random, the probability that the velocity is less than or equal to $\hat{u}$ is (Chiu 1988):

$$F(\hat{u}) = \frac{\psi}{\psi_{max}} = \int_0^1 f(\hat{u})\ d\hat{u} \quad (7)$$

The expression $\frac{\psi}{\psi_{max}}$ in equation (7) reflects the ratio of the area between the channel bed and isovel ψ to the total area of the channel cross-section. Equation (7) may be differentiated to obtain the value of $f(\hat{u})$:

$$f(\hat{u}) = \frac{dF(\hat{u})}{d\hat{u}} = \frac{dF(\hat{u})}{d\psi}\frac{d\psi}{d\hat{u}} = \frac{1}{\psi_{max}}\frac{d\psi}{d\hat{u}} \quad (8)$$

3.1.2 Formulation of velocity distribution

Eqs. (4) and (8), when equated, yield the dimensionless velocity as

$$\hat{u} = \frac{u}{u_{max}} = \frac{1}{\lambda_1}\left\{-\lambda_0 - \left[(-\lambda_0)^{\frac{\alpha}{\alpha-1}} - \frac{\alpha^{\frac{\alpha}{\alpha-1}}}{\alpha-1}\lambda_1 \frac{\psi}{\psi_{max}}\right]^{\frac{\alpha-1}{\alpha}}\right\} \quad (9)$$

When $x = 0$, Eq. (6) can be expressed as,

$$\psi = \frac{y}{D+h}\exp\left(1 - \frac{y}{D+h}\right) \quad (10)$$

when the maximum velocity is below the water surface that is $h < 0$ and ψ_{max} occurs at some depth y which is defined as $y = D + h$

$$\frac{\psi}{\psi_{max}} = \frac{y}{D+h}\exp\left(1 - \frac{y}{D+h}\right) \quad (11)$$

When the maximum velocity is at the water surface that is $h \geq 0$ and ψ_{max} occurs at depth y and is define as $y = D$

$$\frac{\psi}{\psi_{max}} = \frac{y}{D}\exp\left(1 - \frac{1-\frac{y}{D}}{1+\frac{h}{D}}\right) \quad (12)$$

As a result, the final expression for the dimensionless velocity profile is provided for $h < 0$ as

$$\hat{u} = \frac{u}{u_{max}} = \frac{1}{\lambda_1}\left\{-\lambda_0 - \left[(-\lambda_0)^{\frac{\alpha}{\alpha-1}} - \frac{\alpha^{\frac{\alpha}{\alpha-1}}}{\alpha-1}\lambda_1 \frac{y}{D+h}\exp\left(1 - \frac{y}{D+h}\right)\right]^{\frac{\alpha-1}{\alpha}}\right\} \quad (13)$$

For $h \geq 0$

$$\hat{u} = \frac{u}{u_{max}} = \frac{1}{\lambda_1}\left\{-\lambda_0 - \left[(-\lambda_0)^{\frac{\alpha}{\alpha-1}} - \frac{\alpha^{\frac{\alpha}{\alpha-1}}}{\alpha-1}\lambda_1 \frac{y}{D}\exp\left(1 - \frac{1-\frac{y}{D}}{1+\frac{h}{D}}\right)\right]^{\frac{\alpha-1}{\alpha}}\right\} \quad (14)$$

3.2 Derivation of Tsallis velocity distributions

3.2.1 Defining Tsallis entropy

Tsallis (1988) presented a generalised form of entropy, which is expressed in continuous form as follows:

$$H(U) = \frac{1}{m-1}\left\{1 - \int_0^{u_{max}} [f(u)]^m du\right\}$$

$$H(U) = \frac{1}{m-1}\left\{\int_0^{u_{max}} f(u)\{1-[f(u)]^{m-1}\}du\right\} \quad (15)$$

where u = velocity at a given position, u_{max} = maximum velocity in the cross section, $f(u)$= PDF, and m = real number. For $m > 0$, $H(U)$ takes a convex shape.

The maximum entropy principle (Jaynes (1957 I), (1957 II)) will be applied to derive the Tsallis-based velocity profile in a similar way to that of the Renyi entropy velocity distribution. The constraints give the information that measurements may provide and can be expressed in terms of statistical moments. The total probability is stated as the first constraint.

$$\int_0^{u_{max}} f(u)du = 1 \quad (16)$$

The mean value can be used to describe the second constraint

$$\int_0^{u_{max}} uf(u)du = \bar{u} \quad (17)$$

where $\bar{u}$ = mean velocity in the cross-section = Q/A for 1D velocity distribution. However, for 2D velocity distribution the $\bar{u}$ is represented as $\bar{u} = \frac{1}{D}\int_0^D udy$ given by Marini and Fontana (2020).

Now, by approach of Lagrange multipliers is used to maximize the result which is expressed as:

$$L = \int_0^{u_{max}} \frac{f(u)}{m-1}\{1-[f(u)]^{m-1}\}du + \lambda_1\left[\int_0^{u_{max}} f(u)du - 1\right] + \lambda_2\left[\int_0^{u_{max}} uf(u)du - \bar{u}\right] \quad (18)$$

where, λ_1 and λ_2 are the Lagrange multipliers. Eq. (18) is differentiated with respect to $f(u)$ and the derivative is equated to zero to maximise entropy.

$$f(u) = \left[\frac{m-1}{m}\left(\frac{1}{m-1} + \lambda_1 + \lambda_2 u\right)\right]^{1/m-1} \quad (19)$$

For simplified version of Eq. (19), let $\lambda_f = \frac{1}{m-1} + \lambda_1$, and replacing $\frac{1}{m-1} + \lambda_1$ with λ_f, it simplifies to

$$f(u) = \left[\frac{m-1}{m}\left(\lambda_f + \lambda_2 u\right)\right]^{1/m-1} \quad (20)$$

Entropy-based probability distribution (Eq. (20)) should be coupled to the space domain to represent the velocity profile over the entire cross-section. To achieve that goal, it is necessary

to theorize the CDF, which could represent the channel's geometry. Cui and Singh (2012) demonstrated that this kind of nonlinear cumulative distribution function.

$$F(u) = \left[1 - \left(\frac{x}{B}\right)^2\right]^b \left(\frac{y}{D}\right)^a \tag{21}$$

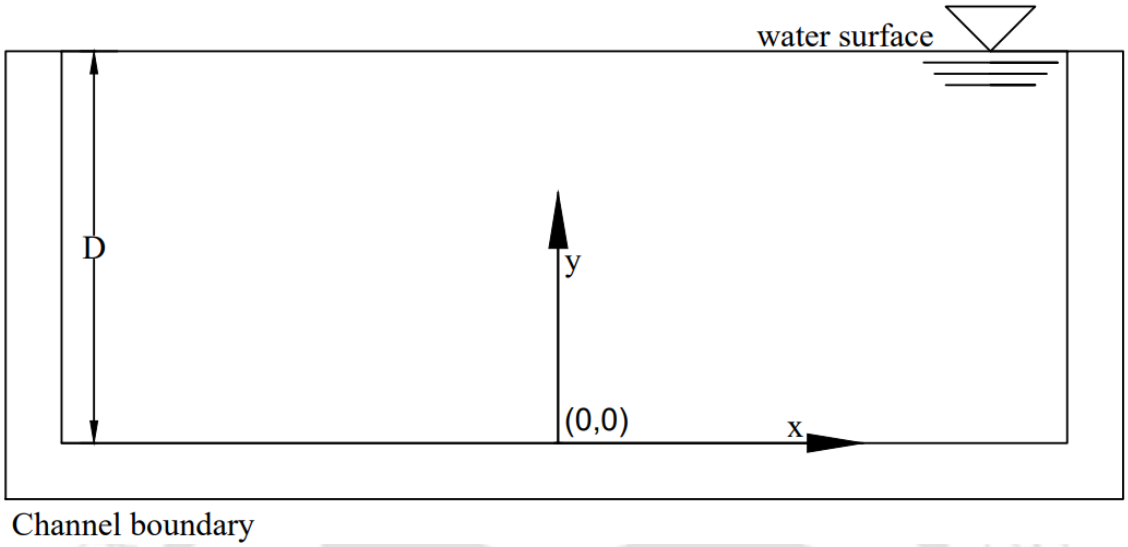

Figure 4 Idealized Rectangular cross section channel.

Considering a rectangular cross section, with the co-ordinate of the center as (0, 0), i.e., at the middle of the rectangular section. Here, y= flow depth and x = distance from center. The term $\left[1 - \left(\frac{x}{B}\right)^2\right]^b$ explains the variation of the CDF function across the width as it moves away from the center towards the boundary and the term $\left(\frac{y}{D}\right)^a$ explains how the CDF function varies along the depth. a and b are shape parameters which are associated to the width-depth ratio. For further reference, detailed explanation is provided by Cui *et al.* (2013).

Therefore Cui *et al.* (2013) derived the velocity based on Tallis entropy theory as:

$$u = \frac{\lambda_f}{\lambda_2} + \frac{1}{\lambda_2}\frac{m}{m-1}\left[\lambda_2 F(u) + \left[\frac{m-1}{m}\ \lambda_f\right]^{\frac{1}{m-1}}\right]^{m/m-1} \tag{22}$$

Furthermore, the dimensionless entropy parameter G is discussed in relation to the one-dimensional velocity profile (Cui and Singh (2013)), is given as

$$G = \frac{\lambda_2 u_{max}}{\lambda_2 u_{max} + \lambda_f} \tag{23}$$

According to Chiu and Said (1995) and Chiu and Tung (2002), the ratio of mean to maximum velocity was shown to represent a relationship between parameter G. Using the recorded mean and maximum values of velocity a quadratic relation is obtained (Cui and Singh, 2013)

$$\frac{\bar{u}}{u_{max}} = 0.554G^2 - 0.077G + 0.568 \tag{24}$$

Consequently, the velocity profile may be expressed as follows in terms of G:

$$\frac{u}{u_{max}} = 1 - \frac{1}{G}\left(1 - \left\{(1-G)^{m/m-1} + \left[1 - (1-G)^{m/m-1}\right]F(u)\right\}^{m-1/m}\right) \tag{25}$$

When $x = 0$, Eq. (42) changes to,

$$\frac{u}{u_{max}} = 1 - \frac{1}{G}\left(1 - \left\{(1-G)^{m/m-1} + \left[1 - (1-G)^{m/m-1}\right]\left(\frac{y}{D}\right)^{a}\right\}^{m-1/m}\right) \tag{26}$$

3.3 Renyi and Tsallis entropy in compound channels

3.3.1 Parameter estimation

For the calculation of velocity using Renyi entropy in compound channels, the unknown terms are λ_1, λ_0 and α. Detailed calculation of λ_1, λ_0 and α are provided by (Kumbhakar *et al.*, 2016; Sharma *et al.*, 2022b). The unknown term in Eq. (6) is N_i which is calculated from a graph given in Figure 8 of Chiu and Hsu (2006) from the calculated value of M. Chiu (1988) derived an equation for the calculation of M which is given by.

$$\frac{u_m}{u_{max}} = \frac{e^M}{e^M - 1} - \frac{1}{M} \tag{27}$$

Table1 Calculated values of λ_0 and λ_1 for various flow condition

Channel type	u_{max} (m/s)	u_m (m/s)	α	λ_0	λ_1	M
45° Slope angle compound channel	0.2575	0.2107	0.99	-1.025	0.055	5.35
90° Slope angle compound channel	0.2601	0.2076	0.99	-1.022	0.048	`4.74

For the calculation of velocity using Tsallis entropy, the unknown terms are G and m. The value of G is calculated using Eq. (24) from the observed values of u_{max} and u_m. The velocity profile variation with different value of m shows that $m = 3$ gives the best results as the change in velocity profile for m value greater than 3 is significantly less. Cui and Singh (2013) also supported this assertion. For the value of 'a' and 'b' in Eq. (21), the entire cross section for the 45° slope angle is divided into 3 parts i.e, floodplain portion, sloping portion and the main channel portion. Similarly, for the 90° slope angle, it is divided into two parts i.e., flood plain portion and the main channel portion. As mentioned above, the location of maximum velocity for 45° and 90° slope angle is located at FP 15 and FP 40 respectively. For the calculation of velocities at different verticals, the value of 'a' and 'b' at different portion of the cross section are shown in Table 2.

Table 2 Calculated values of a and b for various flow condition

Channel type		a	b	G	u_{max} (m/s)	u_m (m/s)
45° Slope angle compound channel	Flood plain region	0.1	0.3	0.752	0.2575	0.2107
	Sloping region	0.1	0.2			
	Main channel region	0.1	0.1			
90° Slope angle compound channel	Flood plain region	0.09	0.01	0.725	0.2601	0.2076
	Main channel region	0.085	0.15			

3.3.2 Selection of maximum velocity location

In order to apply the developed velocity equations, the location of Z_y axis in the compound channel of 45^0 and 90^0 bank angle must be known, i.e., the position where maximum velocity occurs. In a natural channel, the location of Z_y axis can be anywhere within the cross section. In a rectangular cross-section, the Z_y axis is located as shown in Figure 4. Velocity data are collected in different sections (Figure 2) to determine the Z_y axis in 45^0 and 90^0 compound channel. An isoval is plotted from the velocity data. For a given discharge and if the bed of the channel does not change rapidly, Z_y axis is found to be stable and invariant with time (Chen and Chiew, 2004). In the present study, a compound channel's Z_y-axis is chosen at the location where the channel's maximum velocity occurs. Eqs. (13), (14) and (26) provide the necessary velocity profile for a certain vertical line along the y-axis when x = 0, depending on whether the maximum velocity occurs below or on the water surface. Aside from the velocities along the Z_y-axis, velocities at various verticals throughout the section are determined using Eq. (9)

and Eq. (25) derived from Renyi entropy and Tsallis entropy respectively. Figure 5 (a) shows that the position of maximum velocity for 45° compound channel was found at the FP 15 i.e., the Z_y-axis. Therefore, the co-ordinate of X is considered as 0. Since, there were no points of velocity measurements on the left side of the Z_y axis, so the variation of velocity profile on the right side of the cross sections are simulated at different verticals. Therefore $B_1 = 85\ cm$ and x varies from $0\ to\ 85$. Figure 5 (b) shows that the Z_y-axis for 90° compound channel was located at FP 40. The co-ordinate of X is considered as 0. As a result, $B_1 = 60\ cm$ with x ranging from 0 to 60 cm on the right-hand side of the cross-section and $B_2 = 40\ cm$ with x ranging from 0 to 40 cm on the left-hand side of the cross-section. The Z_y-axis and steps involved in the calculation of velocity distribution are the same for both 45^0 and 90^0 bank angle compound channel. Figure 6 shows velocity estimation by Renyi method for 45^0 and 90^0 bank angle compound channel. It is observed that velocities begin to decrease as the points move away from the point of maximum velocity (Z_y-axis) for both the bank angles.

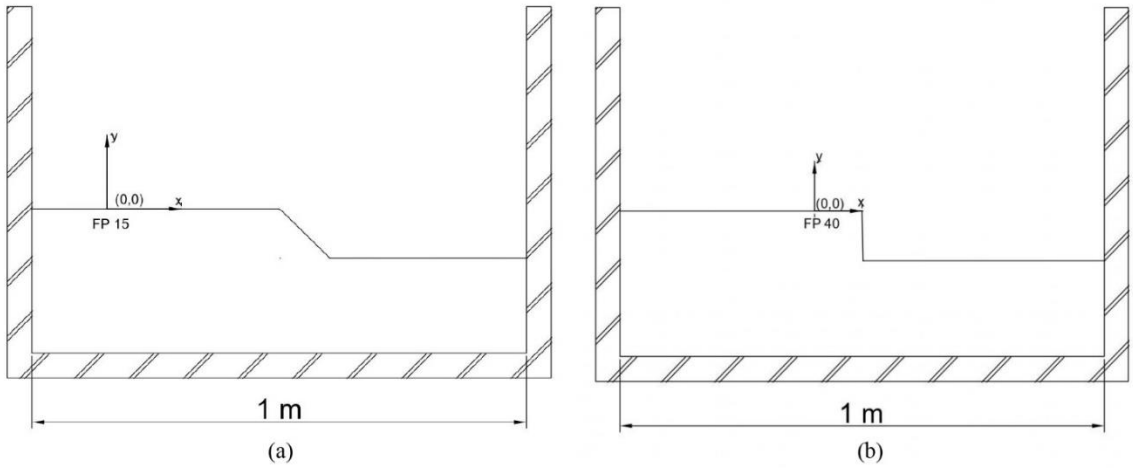

Figure 5 Point of maximum velocity in (a) 45^0 compound channel and (b) 90^0 compound

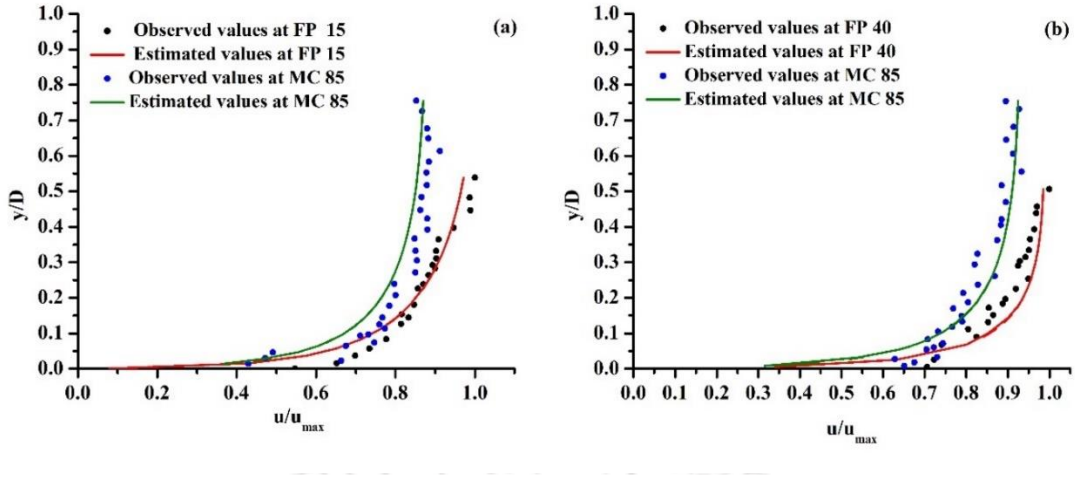

Figure 6 Variation of velocity profile estimated by Renyi entropy-based equation towards the main channel at (a) 45^0 compound channel (b) 90^0 compound channel.

3.3.3 Estimating errors

The error measurement method described below is used to measure the effectiveness of the created entropy-based velocity profile against experimental data. The error between calculated and observed values is determined as

$$\epsilon = \frac{|u_{obs} - u_{est}|}{u_{obs}} \tag{28}$$

Where u_{est} is the calculated velocity values obtained from entropry equations and u_{obs} is the experimental values.

4 Results and Discussion

4.1 Velocity distribution from Renyi entropy

Figure 7 depicts the predicted and observed velocity contour for 45^0 and 90^0 bank angle across the entire cross-section of the compound channel. Figures 7(a) and 7(b) shows velocity distribution in the downstream of 45^0 compound channel by Renyi entropy method and observed experimental values respectively. The velocity is observed to be higher near the sloping region of the channel for both computed and observed velocity distribution. However, the estimated velocity by Renyi method is observed to be more uniformly distributed than the experimental values. This is because the velocity profile determined by the entropy approach has the highest entropy, which under the given constraints tends toward uniform distribution (Cui and Singh, 2013). The velocity magnitude of 90^0 compound channel in Figures 7(c) and

7(d) near the sloping portion is more compared to 45^0 compound channel for both computed and observed distribution. However, the velocity contour of 90^0 compound channel by Renyi entropy in Figure 7(c) is smoother and uniform compared to experimental values in Figure 7(d) which was also observed for 45^0 compound channel. These contour diagrams provide a general view of how flow velocity behaves in the compound channel. The difference in velocity distribution between Renyi and experimental values will be clearer by analyzing velocity profiles in floodplain, slope and main channel regions.

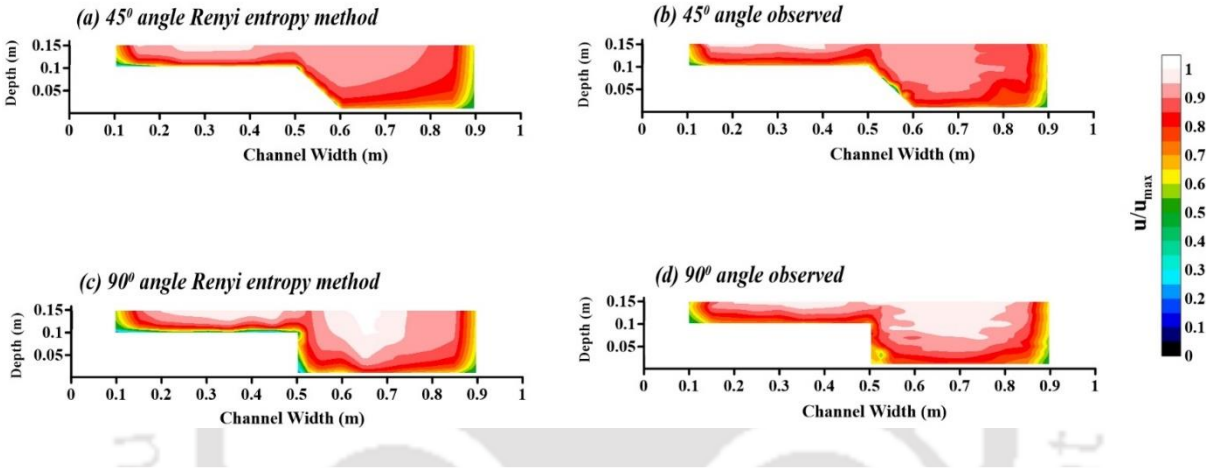

Figure 7 Velocity contours for (a, b) 45° and (c, d) 90° angle compound channel by Renyi entropy method and observed values.

Figure 8 depicts the predicted velocity profile at various crucial locations of floodplain, slope and main channel regions of a 45° compound channel. It is observed that the velocity profile calculated by the Renyi entropy method and observed experimental values are almost similar in the floodplain (Figure 8(a)) and main channel regions (Figure 8(d, e)). However, there is a deviation between the calculated and observed value at FP 50 as seen in Figure 8(b). This might be because FP 50 serves as a border where momentum exchange between the main channel domain and the floodplain zone is dominant. Another reason for this deviation could also be the involvement of secondary currents because of the nonuniform cross-section of the compound channel. Shiono and Knight (1991) and Ervine *et al.* (2000) also suggested that the secondary currents play a crucial role in affecting the velocity profiles in the compound channel. This is because of the mass transfer between sub-sections due to the non-prismatic nature of the channel. The shear stress at the intersection of the floodplains and the main channel also significantly impacts both conveyance and velocity distribution at the sloping

portions (Bousmar and Zech, 2004; Patra *et al.*, 2004). Table 3 shows the mean percentage error range between calculated values by the Renyi entropy method and observed experimental values for floodplain, slope and main channel regions of 45° and 90° compound channel. The portions that were considered for floodplain, slope and main channel regions in Table 3 are from $0.15 - 0.45\,m$, $0.5 - 0.6\,m$ and $0.65 - 0.85\,m$ channel width respectively. The mean percentage error range in the floodplain domain and main channel domain for 45° compound channel is less compared to the sloping region as seen in table 3. The percentage range in sloping region is within 8% whereas floodplain and main channel error is within 6%. This shows that Renyi entropy method is suitable for predicting in the floodplain and main channel regions as compared to the sloping portion.

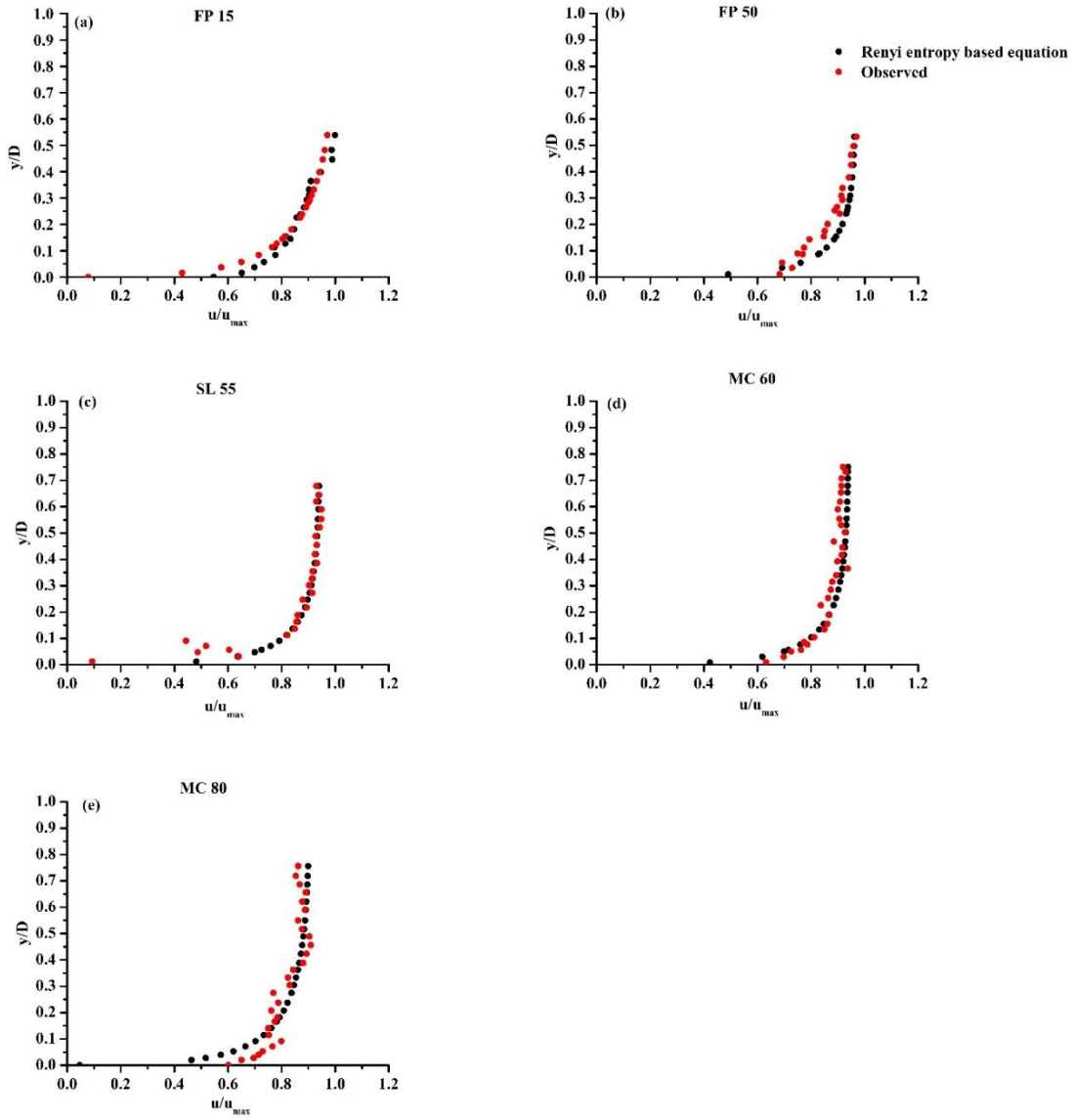

Figure 8. Velocity profiles by Renyi entropy method and observed values for 45° slope angle compound channel at (a) FP 15 (b) FP 50 (c) SL 55 (d) MC 60 (e) MC 80.

Figure 9 shows the calculated values by Renyi entropy and observed experimental values of 90° compound channel. Different crucial locations in the floodplain and main channel regions are shown in Figure 9. The FP 40 section in Figure 9(a) is crucial as the Z_y-axis is located at FP 40 of the floodplain region. It is observed that computed and observed values are almost similar throughout the flow depth. It is observed in Figure 9 that the calculated and observed values mostly deviates at lower flow depth of $z/h < 0.2$ for all the velocity profiles. The reason for this could be the sediment interaction near the channel bed. The percentage error in Table 3 also shows that it is higher near the sloping portion ($0.5 - 0.6\,m$ channel width) compared

to floodplain region and main channel region. The percentage error in the sloping region is within 10%, whereas it is within 8% in the floodplain and main channel.

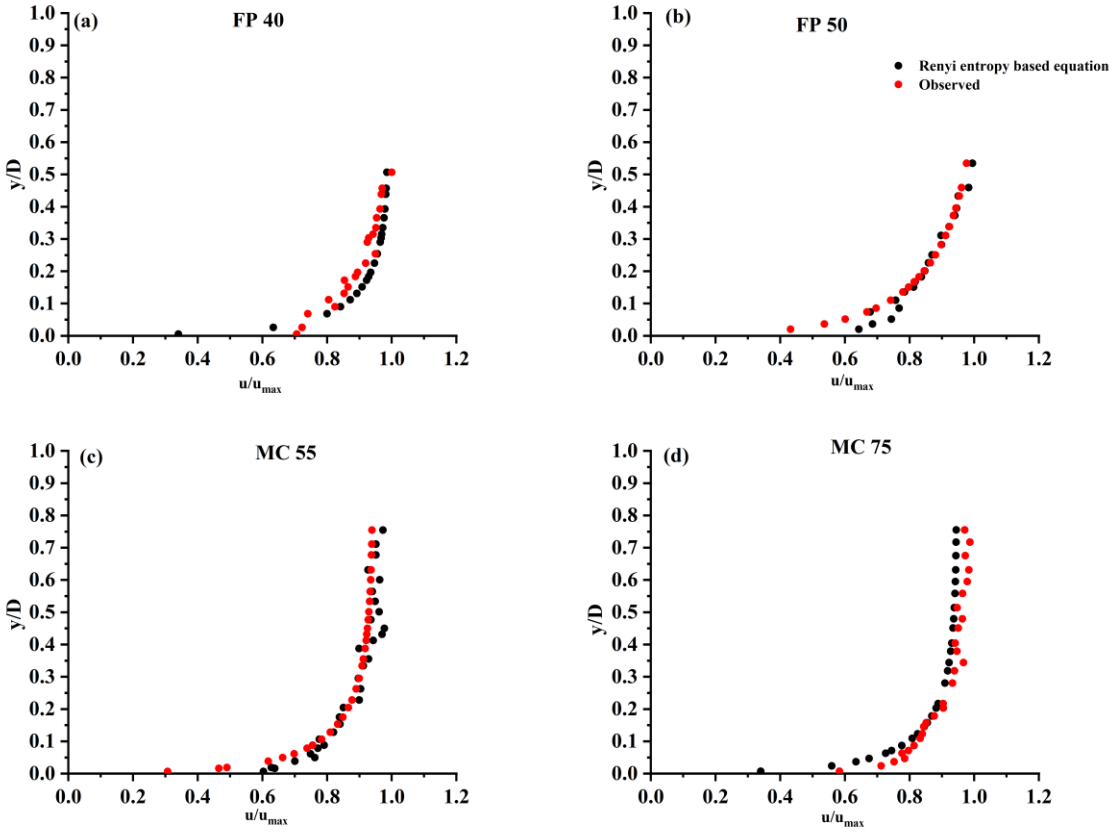

Figure 9 Velocity profiles by Renyi entropy method and observed values for 90° slope angle compound channel at (a) FP 40 (b) FP 50 (c) MC 55 (d) MC 75.

Table 3 Mean percentage error range between calculated values by Renyi entropy and experimental observed values at various regions of compound channel

Location	Mean % error range	
	45^0 bank slope	90^0 bank slope
Floodplain	3-6	3.6-7.7
Slope	4-8	5-10
Main channel	3.5-6	4-7

4.2 Velocity distribution from Tsallis entropy

Figure 10 shows velocity contours of 45^0 and 90^0 compound channel by Tsallis entropy method and experimental observed values. It is observed that the position of high velocity near the sloping region by experimental values (Figure 10(b, d)) is almost accurately predicted by Tsallis entropy method in Figure 10(a, c). However, it is also observed from the figure that the calculated and observed values mainly deviates in the lower flow depth ($< 0.1\ m$) in the main channel region. This behavior was also observed while predicting velocity contour by Renyi entropy method in Figure 7. This point is clearly observed in Figures 11 and 12 where calculated and observed values are compared at different locations of the compound channel.

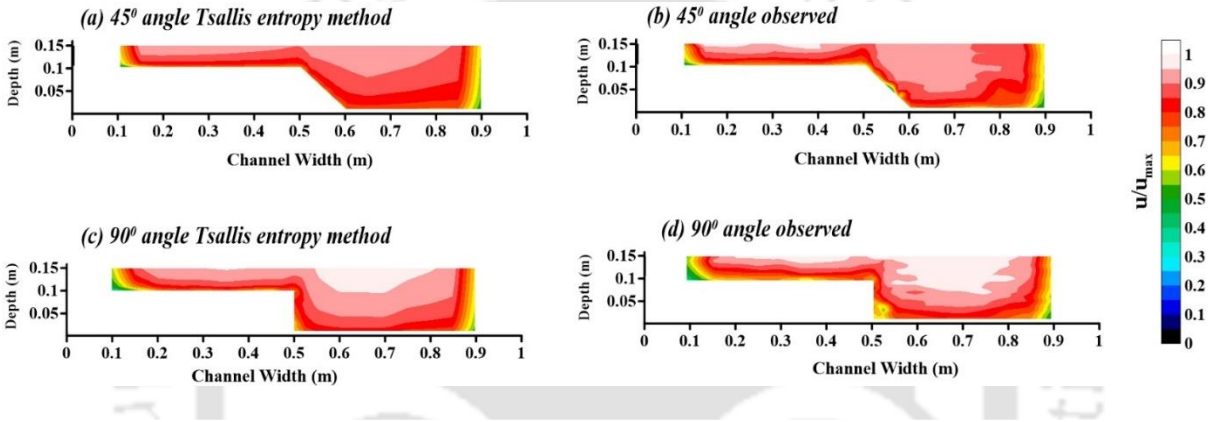

Figure 10 Velocity contours for (a, b) 45° and (c, d) 90° angle compound channel by Tsallis entropy method and observed values.

Figure 11 shows velocity comparison between Tsallis entropy and observed values of 45° compound channel at floodplain, slope and main channel regions. It is observed that the calculated and observed values are almost similar in the floodplain (Figure 11(a)) and main channel (Figure 11(d, e)) for $z/h > 0.2$. However, there is a deviation between calculated and observed values in the lower flow depth ($z/h < 0.2$) because of sediment and channel bed interaction. This deviation was also observed while analyzing the velocity profile by Renyi method in Figure 8. Furthermore, velocity deviation is mostly prominent in FP 50 and SL 55 from Figure 11(b, c) due to the exchange of momentum between floodplain and main channel. This point is also confirmed by Table 4 where the mean percentage error range in the sloping region is within 9%, whereas it is within 5% for floodplain and main channel regions. This shows that just like Reyni entropy method, Tsallis method can also predict velocity distribution in the upper flow depth of floodplain and main channel. However, prediction in the sloping region by Tsallis method gives more error compared to the floodplain and main channel.

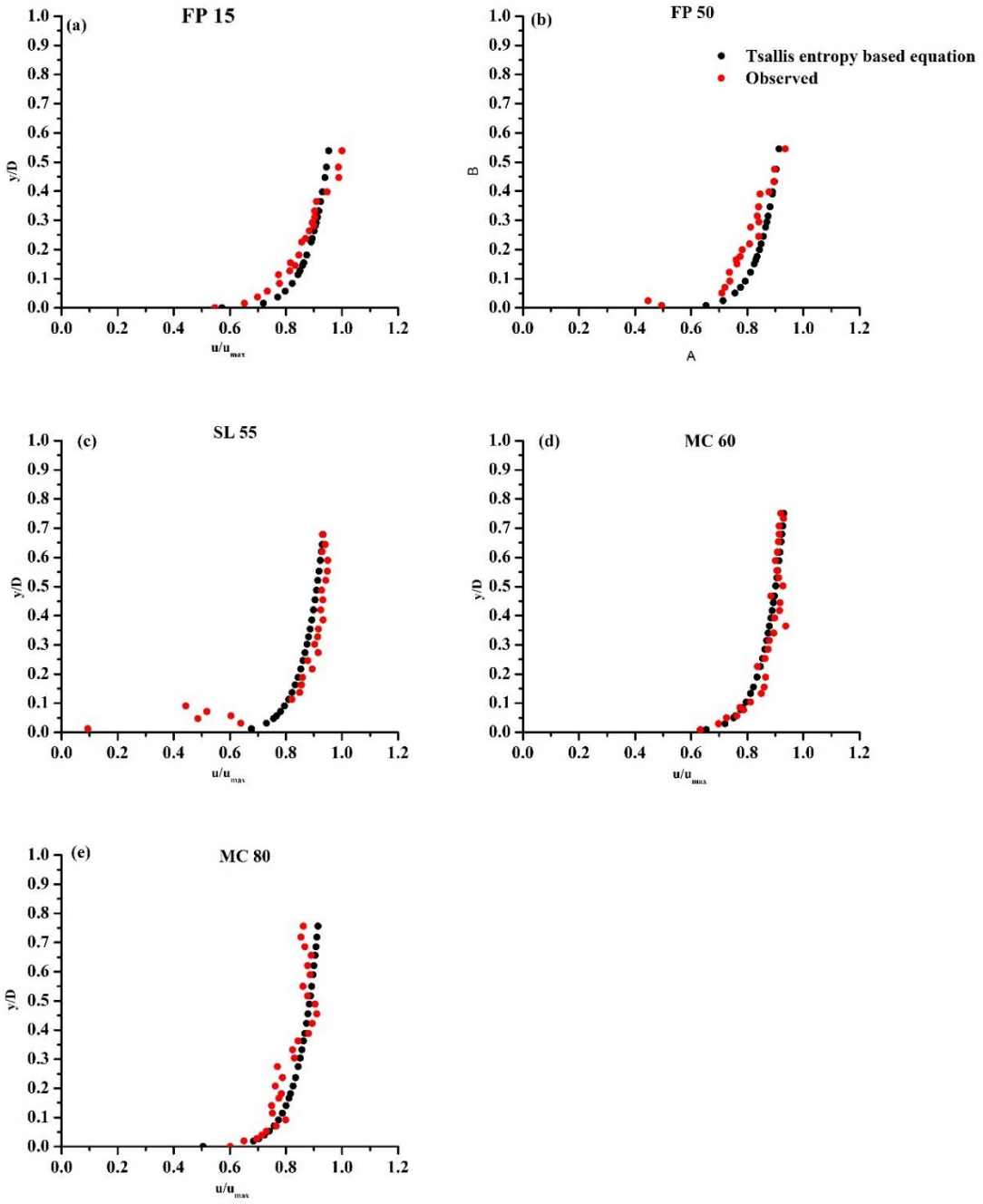

Figure 11 Velocity profiles by Tsallis entropy method and observed values for 45° slope angle compound channel at (a) FP 15 (b) FP 50 (c) Slope 55 (d) MC 60 (e) MC 80.

Figure 12 shows velocity comparison between predicted velocity by Tsallis entropy and observed experimental values at crucial locations of floodplain and main channel regions of 90° compound channel. The velocity prediction gives almost accurate results in FP 40 and MC 75 locations from Figure 12(a, d). However, at the floodplain-main channel interaction section

of FP 50 in Figure 12(b), velocity prediction is not accurate and the percentage of error is also high. Furthermore, experimental observation at MC 55 of Figure 12(c) also does not follow proper logarithmic trend at $z/h > 0.2$. This point is also evident from Table 4 where mean percentage error in and near sloping region (FP 50, MC 55) is higher and within 9% whereas it is lower in the case of floodplain and main channel, which is within 5%. It demonstrates that, similarly to 45°compound channel, velocity predictions near floodplain-main channel interactions in 90° compound channel by Tsallis and Renyi entropy method is more error prone compared to floodplain and main channel.

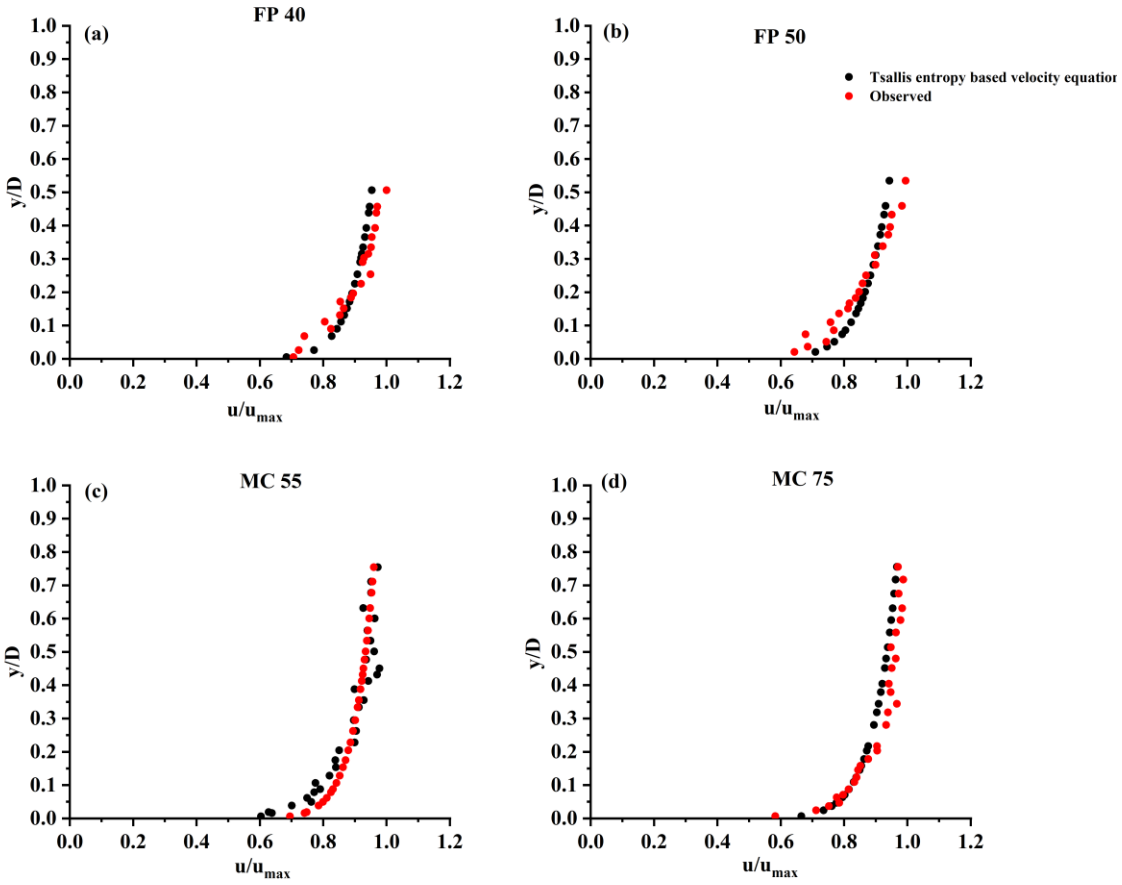

Figure 12 Velocity profiles by Tsallis entropy method and observed values for 90° slope angle compound channel at (a) FP 40 (b) FP 50 (c) MC 55 (d) MC 75.

Table 4 Mean percentage error range between calculated values by Tsallis entropy and experimental observed values at various regions of compound channel

Location	Mean % error range	
	45^0 bank slope	90^0 bank slope
Floodplain	2-5	3-5
Slope	2-9	5-9
Main channel	3-5	2.4-4

Conclusion

This study demonstrated the entropy method for velocity estimation in compound channels, in addition to previous methods like the Prandtl-von Karman universal velocity profile law and the power law. The present work focusses on using Renyi and Tsallis entropy in a compound channel and comparing its accuracy with experimental findings. Two bank angles of 45^0 and 90^0 were considered and velocity readings were taken at 17 different sections in the downstream of the channel cross-section. The parameters λ_0 and λ_1 for the case of Renyi entropy and G for the case of Tsallis entropy are dimensionless, since all these parameters are calculated by using the quotient of mean to that maximum velocity. The value of $m > 3$, the velocity does not change significantly. In Renyi's entropy equation, only two parameters i.e., the average and the maximum velocities and the location of maximum velocity is required for predicting the velocities over the entire cross-section. On the other hand, in case of Tsallis based entropy equation, the value of a and b takes different value at different portion of the cross-section. It was found that the created velocity Tsallis and Renyi entropy model for both 45^0 and 90^0 compound channels correlate well with experimental findings. This accuracy between the entropy and experimental findings is more in the floodplain and main channel domains with less error percentage. However, the error percentage is higher and less accurate in and near the sloping region than in the floodplain and main channel. It could be because of a nonuniform cross-section, which increases the role of secondary currents ultimately affecting the streamwise velocity profile. The velocity profile near the channel boundary ($z/h < 0.2$) is also found to be less accurate compared to away from the channel boundary ($z/h > 0.2$) because of sediment interaction near the channel bed.

The present work can be extended to analyse Shannon entropy which was first used by Chiu (1987) to find the one-dimensional velocity profile by assuming the time average velocity as a random variable. The future study also includes the comparison of different entropy studies (Renyi, Tsallis and Shannon) in compound channels by considering a wide range of bank angles and flow discharges. Furthermore, the addition of floodplain with high density and emergence of vegetation gives rise to dip phenomenon near the vegetated-main channel interface which was discussed in detail in Chapter 3. The entropy method could be used to explain this dip phenomenon and analyse the accuracy of velocity profiles in the slopes and main channel.

References

Abril, J. B., & Knight, D. W. (2004). Stage-discharge prediction for rivers in flood applying a depth-averaged model. *Journal of Hydraulic Research, 42*(6), 616-629.

Ahamed, N., and Kundu, S. (2022). Application of the fractional entropy for one-dimensional velocity distribution with dip-phenomenon in open-channel turbulent flows. *Stochastic Environmental Research and Risk Assessment, 36*(5), 1289–1312.

Barman, J., and Kumar, B. (2022a). Turbulence in a compound channel with the combination of submerged and emergent vegetation. *Physics of Fluids, 34*(4), 045114.

Barman, J., and Kumar, B. (2022b). Flow behavior in a multi-layered vegetated floodplain region of a compound channel. *Ecohydrology, 15(4), e2427.*

Bousmar, D., & Zech, Y. (2004, June). Velocity distribution in non-prismatic compound channels. In *Proceedings of the Institution of Civil Engineers-water management* (Vol. 157, No. 2, pp. 99-108). Thomas Telford Ltd.

Carollo, F. G., Ferro, V., and Termini, D. (2002). Flow velocity measurements in vegetated channels. *Journal of Hydraulic Engineering, 128*(7), 664-673.

Cea, L., Puertas, J., and Pena, L. (2007). "Velocity measurements on highly turbulent free surface flow using ADV." Exp. Fluids, 42(3), 333–348.

Chen X, and Chiew YM (2004) Velocity distribution of turbulent open-channel flow with bed suction. J Hydraul Eng 130(2):140–148

Chin, C. L., and Murray, D.W. (1992). Variation of velocity distribution along nonuniform open-channel flow. J. Hydraul. Eng. 118 (7): 989– 1001.

Chiu, C. L. (1987) Entropy and probability concepts in hydraulics. J. Hydraulic Eng. 113 (5): 583–599.

Chiu, CL (1988) Entropy and 2-D velocity distribution in open channels. J Hydraul Eng. 114(7):738–756.

Chiu, C. L., & Tung, N. C. (2002). Maximum velocity and regularities in open-channel flow. *Journal of hydraulic engineering*, *128*(4), 390-398.

Chiu, CL, and Said, CAA (1995) Maximum and mean velocities and entropy in open-channel flow. J Hydraul Eng 121(1):26–35

Chiu, C. L., and Hsu, S. M. (2006). Probabilistic approach to modeling of velocity distributions in fluid flows. *Journal of Hydrology*, *316*(1–4), 28–42.

Cui, H, and Singh, V.P. (2012). On the cumulative distribution function for entropy-based hydrologic modeling. Trans. ASABE 55 (2): 429–438.

Cui, H, and Singh, V.P. (2013) Two-dimensional velocity distribution in open channels using the Tsallis entropy. J Hydrol Eng 18(3):331–339.

Cui, H., and Singh, V. P. (2014) One-Dimensional Velocity Distribution in Open Channels Using Tsallis Entropy. *Journal of Hydrologic Engineering*, *19*(2), 290–298.

Dupuis, V., Proust, S., Berni, C., and Paquier, A. (2017). Mixing layer development in compound channel flows with submerged and emergent rigid vegetation over the floodplains. *Experiments in Fluids*, *58*(4), 1–18.

Ervine, D. A., Babaeyan-Koopaei, K., & Sellin, R. H. (2000). Two-dimensional solution for straight and meandering overbank flows. *Journal of Hydraulic Engineering*, *126*(9), 653-669.

Fatima, J., Yamamoto, H., Tsubaki, R., & Kawahara, Y. (2009). Experimental study of mean velocity distributions in open channels with emergent and submerged vegetation. *Journal of Applied Mechanics*, *12*, 663-672.

Goring, D. G., and Nikora, V. I. (2002). Despiking Acoustic Doppler Velocimeter Data. *Journal of Hydraulic Engineering*, *128*(1), 117–126.

Islam, M. R., and Zhu, D. Z. (2013). Kernel Density–Based Algorithm for Despiking ADV Data. *Journal of Hydraulic Engineering*, *139*(7), 785–793.

Jaynes, E. T. (1957a). Information theory and statistical mechanics. I. Phys. Rev. 106(4): 620.

Jaynes, E. T. (1957b). Information theory and statistical mechanics. II. Phys. Rev. 108 (2): 171.

Kawahara, Y., & Tamai, N. (1989). Mechanism of lateral momentum transfer in compound open channel flow. In *Proceeding of the 23rd IAHR congress, Ottawa, Canada, B463–B470*.

Knight, D. W., & Shiono, K. (1990). Turbulence measurements in a shear layer region of a compound channel. *Journal of hydraulic research*, *28*(2), 175-196.

Knight, D. W., and Shiono, K. 1996. "River channel and floodplain hydraulics." Floodplain processes, M. G. Anderson, D. E. Walling, and P. D. Bates, eds., Chap. 5, Wiley, Chichester, U.K., 139–181

Knight, D. W., Omran, M., & Tang, X. (2007). Modeling depth-averaged velocity and boundary shear in trapezoidal channels with secondary flows. *Journal of Hydraulic Engineering*, *133*(1), 39-47.

Keller, R. J., & Rodi, W. (1988). Prediction of flow characteristics in main channel/flood plain flows. *Journal of Hydraulic research*, *26*(4), 425-441.

Kouwen, N., Unny, T. E., and Hill, H. M. (1969). Flow retardance in vegetated channels. *Journal of the Irrigation and Drainage Division*, *95*(2), 329-344.

Krishnappan, B. G., & Lau, Y. L. (1986). Turbulence modeling of flood plain flows. *Journal of hydraulic engineering*, *112*(4), 251-266.

Kumbhakar, M., and Ghoshal, K. 2016 Two dimensional velocity distribution in open channels using Renyi entropy. Physica A 450 (May): 546–559.

Kumbhakar, M., Kundu, S., Ghoshal, K. and Singh, V. P. 2016. Entropy-based modeling of velocity lag in sediment-laden open channel turbulent flow." Entropy (Basel) 18 (9): 318.

Kumbhakar, M., and Ghoshal, K. 2017 One-dimensional velocity distribution in open channels using Renyi entropy. Stochastic Environ. Res. Risk Assess. 31 (4): 949–959.

Liu, T. H., Li, C. H. E. N., & Fan, B. L. (2012). Experimental study on flow pattern and sediment transportation at a 90 open-channel confluence. *International Journal of Sediment Research*, *27*(2), 178-187.

Luo H, and Singh VP (2011) Entropy theory for two-dimensional velocity distribution. J Hydrol Eng 16(4):303–315.

Marini, G, De Martino G, Fontana, N, Fiorentino, M, and Singh, VP (2011) Entropy approach for 2D velocity distribution in open-channel flow. J Hydraul Res 49(6):784–790.

Marini, G., & Fontana, N. (2020). Mean Velocity and Entropy in Wide Channel Flows. *Journal of Hydrologic Engineering*, *25*(1), 06019009.

Mehrabani, V., F., Mohammadi, M., Ayyoubzadeh, S. A., Fernandes, J. N., and Ferreira, R. M. L. (2020). Turbulent flow structure in a vegetated non-prismatic compound channel. *River Research and Applications*, *36*(9), 1868–1878.

Naot, D., Nezu, I., & Nakagawa, H. (1993). Hydrodynamic behavior of compound rectangular open channels. *Journal of Hydraulic Engineering*, *119*(3), 390-408.

Nepf, H., and Ghisalberti, M. (2008). Flow and transport in channels with submerged vegetation. *Acta Geophysica 56*(3), 753–777.

Patra, K. C., Kar, S. K., & Bhattacharya, A. K. (2004). Flow and velocity distribution in meandering compound channels. *Journal of Hydraulic Engineering*, *130*(5), 398-411.

Prinos, P. (1990, September). Turbulence modeling of main channel-floodplain flows with an algebraic stress model. In *Proc. Conf. River Flood Hydraulics* (pp. 173-185).

Proust, S., and Nikora, V. I. (2019). Compound open-channel flows: Effects of transverse currents on the flow structure. *Journal of Fluid Mechanics*, *885*.

Rényi, A. (1961, January). On measures of entropy and information. In *Proceedings of the Fourth Berkeley Symposium on Mathematical Statistics and Probability, Volume 1: Contributions to the Theory of Statistics* (Vol. 4, pp. 547-562). University of California Press.

Sharma, A., Jha, V., Roy, M., and Kumar, B. (2022a). One-dimensional velocity distribution in seepage channel using Tsallis and Shannon entropy. *Stochastic Environmental Research and Risk Assessment*, *36*(10), 3255–3264.

Sharma, A., Roy, M., Jha, V., Kumar, B., and Singh, V. P. (2022b). Velocity Distribution in Seepage-Affected Alluvial Channels Using Renyi Entropy. *Journal of Hydrologic Engineering*, *27*(6), 1–12.

Shiono, K., & Knight, D. W. (1991). Turbulent open-channel flows with variable depth across the channel. *Journal of fluid mechanics*, *222*, 617-646.

Tsallis, C. 1988. Possible generalization of Boltzmann-Gibbs statistics. J. Stat. Phys. 52 (1): 479–487.

Utami, T., & Ueno, T. (1987). Experimental study on the coherent structure of turbulent open-channel flow using visualization and picture processing. *Journal of Fluid Mechanics*, *174*, 399-440.

Wahl, T. L. (2003). Discussion of 'Despiking acoustic Doppler velocimeter data by Derek G. Goring and Vladimir I. Nikora." J. Hydraul. Eng., 129(6), 484–487.

Wang, J., Liu, X., Min, F., Dai, J., & Jiang, X. (2022). Turbulence structure and longitudinal velocity distribution of open channel flows with reedy emergent vegetation. *Ecohydrology*, *15*(1), e2352

Xu, D., and D. Erdogmuns. (2010). “Renyi’s entropy, divergence and their nonparametric estimators.” In Information theoretic learning, 47–102. New York: Springer.